Luminescence Study of Dolomite Mineral

A Thesis Submitted to

The Saurashtra University, Rajkot

For the award of the Degree of

Doctor of Philosophy

In

Physics

By

Mr. Pushparaj P. Zala

Under the Guidance of

Dr. R. U. Purohit

Joint Commissionner,

Commissionner of Higher Education

Government of Gujarat, Gandhinagar- 382010

May, 2012

Certificate

This is to certify that the thesis entitled **"LUMINESCENCE STUDY OF DOLOMITE MINERAL"** which is being submitted by **Mr.Pushparaj P. Zala,** in fulfillment of the degree of "**Doctor of Philosophy"** in **Physics** to the Saurashtra University, Rajkot has been carried out by him under my guidance. The matter present in this thesis incorporates the results of independent investigations carried out by the candidate himself. The matter presented in this thesis has not been submitted elsewhere for the award of any other degree or diploma.

Dr. R.U. Purohit

(Research Gide)

(Recognition No.: 1892)

Declaration

This is to declare that thesis entitled **"LUMINESCENCE STUDY OF DOLOMITE MINERAL"** which is being submitted by me in fulfillment for the degree of **"Doctor of Philosophy"** in **Physics** to the Saurashtra University, Rajkot has been carried out by me under the guidance of Dr.R.U.Purhit. The matter presented in this thesis incorporate the results of my independent investigations carried out since last four year. The matter presented in this thesis has not been submitted elsewhere for the award of any other degree or diploma.

Date :

Place :

(Pushparaj P. Zala)

(Registration No.: 3880)

Acknowledgment

I express to my sincere thanks to **my guide Dr.R.U.Purohit** whose able guidance, important suggestions, encouragement and discussion has led me through the entire course of this work.

I would like to thank the key person behind this research work **Dr.K.V.R.Murthy,** applied physics department, Faculty of Technology & Engineering, M.S. University of Baroda to provide me research, and experimental facilities in his laboratory at Baroda.

I would like to thank **Prof.D.R.Joshi,** Head and all the faculty members of Applied Physics Department, M.S.University of Baroda to provide me research facilities in the department.

I heartily thankful to **Shri Virendra Education Society,** Dr. V.M. Patel, The Principal and Mr.Aniruddh C. Dave, Head of the Physics department, Shri Natwarsinhji Arts & Science College and Shri S.G. Patel Commerce College, Chhotaudepur, Gujarat to encourage me and promote for this research.

I express my thanks to my friend Mr. Jitubhai Bhut, Mr.Dharmeshbhai Shah, Mahavir minerals, Yamunaji Enterprise and Aashray Enterprise to provide me the necessary information regarding economical data, application field of dolomite.

I would like to express my thanks to Mr. Ashok Singh and Mr. Prafulbhai for giving me the information related to the mines of Chhotaudepur, Gujarat. And also helped me in the collection of minerals.

I would like to thank all the **Staff members** of Shri Natwarsinhji Arts & Science College and Shri S.G. Patel Commerce College, Chhotaudepur, Gujarat for encouragement and their co-operation throughout the work.

I express to my sincere thanks to **Prof.H.H.Joshi,** Head & all the faculty members of

department of Physics, Saurashtra Universty Rajkot, and all the staff members of Department of Physics, Bhavnagar University, Bhavnagar to provide me necessary guidance.

I would like to express my thanks to Dr.R.V.Upadhyay, The Principal of P.D.Patel Institute of Applied Sciences and Dr.T.K.Chaudhari, Head, Dr.K.C.Patel R & D Centre, CHARUSAT, Changa, Gujarat for providing me the XRD and FTIR characterization facility at their laboratories, CSMCRI for providing me the TGA facility.

I would like to express my thanks to Dr.Vanarajsinh A. Jadeja, Mr. Pratipalsinh Rayjada (Scientist, FCIPT, Gandhinagar), Mr.Vimalsinh P.Gohil (Asst.Professor, Govt.Eng.College, Bhavnagar) for encouraging and motivating me.

I must thanks to my parents, *Didi*, Brother, wife and all my friends who not only encourage me but also participated indirectly in this work.

At last all this work is not possible without ***blessing of God;*** I express my heartily ***Vandan*** to them.

Pushparaj P. Zala

Preface

The town, **Chhotaudepur** is situated in the east of Baroda, Gujarat, India. This town is in the Eastern tribal belt of Gujarat, famous for the Rathwa tribal community, the forest of this area and the resources for the natural minerals. As we know the minerals are also basic needs of human being as well as also drawn the vast industrial applications. The town is rich by the mineral dolomite, and near by the Chhotaudepur 'Amba Dungar', near Kadipani, the hilly area is famous for the mineral Fluorspar. Well known Kadipanai Fluorspar project is drawn by the GMDC (Gujarat Minerals Development Corporation Ltd.)- An agency of Gujarat government. While the Dolomite mining activity is on the lease base, but under the observation of GMDC. There are 25 working mines and 150 dolomite factories involved in this business. About 2000 labors are employed through this business. About 350 people are involved in the administration and trading work. The average turnover is around 3000 metric ton per day. Due to these reasons, these mining activity and business of dolomite is the backbone of the Chhotaudepur's economy.

Among different practical and industrial application, dolomite is commonly used as a refractory material as well as in the magnesium metal production. Dolomite is a fluxing agent in metallurgical, glass and ceramic industry, filling material in paper, rubber and plastic production. Large amounts of dolomite are also used in building industry and agriculture (dolomite fertilizer). In chemical industry dolomite is first of all a source of magnesium compounds. Dolomite has a large amount of MgO and is an important raw material for refractory industry.

The term luminescence implies luminous emission which is not purely thermal in origin i.e. luminescence is 'cold light', light from other sources of energy, which takes place at normal and lower temperature. In luminescence, some energy sources kicks an electron of an atom of its ground state (lowest energy) into an exited state (highest energy) by supplying extra energy, then as this excited state is not stable electron jumps back to its ground state by giving out this energy in form of light. We can observe the luminescence phenomenon in nature like during lightening, in glowworms, fireflies, and in certain sea bacteria and deep-sea animals. This

phenomenon have been used in various fields by different scientist all over the world like, Archaeology, Geology, Biomedical, Engineering, Chemistry, Physics, and various Industrial Application for Quality Control, Research and Developments.

The purpose of the present work is to study the Thermoluminescence characteristics, dosimetric study in the case of radiation accidents and environmental dosimetry of the mineral dolomite collected from various mines of Chhotaudepur, District-Vadodara, Gujarat, India and also subjected to quality control in the industrial applications.

The **General Introduction** chapter includes the socioeconomic condition of Chhotaudepur and shows how the dolomite industries are economic backbone of the town. Also includes the various applications of dolomite origin of problem. The dolomite is sedimentary rock; hence it is also important to know the formation of these sedimentary rocks in the earth crust.

The **second chapter** deals with the basics of luminescence, and particularly the phenomenon of thermoluminescence followed by the historical background of thermoluminescence. The trapping and detrapping of charge careers are also explains with the mathematical description. Also explains the procedure to find the different parameters of thermally stimulated luminescence. Second part of this chapter is giving the short introduction of the minerals under the study. This part contains the history, mineral group, chemistry and some other physical properties like; crystal system, color, luster, cleavage, fracture, specific gravity, hardness etc.

The **Instrumentation** chapter presents the different experimental techniques used to characterize the samples which were under the study. The eighteen samples were collected from different mines of Chhotaudepur and one was collected from Madhya Pradesh. Fluorspar was collected from the Amba dungar, Kadipani, Gujarat. Seven other samples were collected from the different genesis of Maharshtra. The instruments used for characterization techniques are TL reader system, X-Ray Diffractometer (XRD), Fourier Transform Infrared Spectroscopy (FT-IR), Particle size Analyzer, Scanning Electron Microscope (SEM) and Thermo Gravimetric Analysis (TGA).

The **Fourth chapter** presents the Natural Thermoluminescence and artificial thermoluminescence of as received samples. All the samples were also annealed and quenched from different temperatures and irradiated using Sr-90 beta source of 25Gy and TL recorded for these samples. Some of the samples were characterized by XRD, FTIR, SEM, and Particle size analysis for better understanding. Results of TL and characterization study are also discussed at the end of the chapter and some of the samples which showed good TL were selected for Thermoluminescence dosimetric study.

The **Thermoluminescence Dosimetric Study** of Dolomite minerals represents the dosimetric study of some selected samples which showed good TL. The first part leads to the Thermoluminescence growth study in which the selected samples was irradiated different amount of beta doses 15Gy, 25Gy, 50Gy, 100Gy, 150Gy and 250Gy using Sr-90 beta source and TL was recorded. The second part deals with the Thermoluminescence decay study in which all the samples was irradiated by 25Gy dose using Sr-90 beta source and TL was recorded immediately and after 24hr, 48hr, 75hr, 100hr, 150hr and 300hr.

Chapter six provides over all view of the results and general conclusions of the study followed by suggestions for future studies.

Pushparaj P. Zala

Index

Chapter # 1

General Introduction

1.1 The Town Chhotaudepur:

The Chhotaudepur is a well planed town, situated in Gujarat (Dist- Baroda, 100km from the east of Baroda), India, surrounded by the hills, on the bank of river 'Orsang'. This town was established by the Khichi Chauhan Rajputs. This princely state was ruled by the rajputs before the freedom, whose ancestral origin was from the great Rajput King Prithviraj Chauhan. This area is rich from the cultural variety, specially Rathwa tribal community, heritage places, forest and centuries, and natural minerals. The people from the surround places comes the town to buy things of their daily needs on Saturday, which is known as 'Haat'. Holi and Dasahara is main festival of this area. On those days all the community from the surround places gathered with their weapons (aero and bow) and musical instruments (Like 'Dhol', 'Piho'-) at Haat places and celebrates the festival. These are the main attraction for the foreign tourists. The town is also surrounded by the forest, which is rich from the ayurveda and herbal plants. This forest has one century for the black Beer-'Jambughoda Black Beer century'. Rarer of the rare Indian Flying Squirrel is also protected in the Kevdi forest range. Some of the area in the forest has also dolomite mines.

This region is also rich from the natural minerals like Dolomite, Limestone and Fluorspar. The mines are running on lease base, under the observation of GMDC (Gujarat Mineral Development Corporation Ltd. – A Agency of Gujarat government). Due to this natural gift, the mining, mineral factory, transportation business is developed in the surrounded area, which is the backbone of the town's economy. Many people get employed through this business. Due to the tribal area there is no problem of labor, the labor is cheap also. About 25 mines are extracting the dolomite, which is then supplied to the factories where the rocks are pulverized and converted in the powder form of different particle size. About 150 dolomite factory is involving in this business. About 2000 labors are employed through this business. About 350 people are involved in the administration and trading work. The average turnover is around 3000 metric ton per day. The mineral fluorspar is excavates from the 'Amba dungar'-the hilly area near Kadipani village, nearby Chhotaudepur, Taluka-Kawant, Dist- Baroda. Fluorspar project is also one of the important projects under GMDC.

1.2 Rocks and Minerals

The earth can be physically described as a ball of rock (the crust or lithosphere), partly covered by water (the hydrosphere) and wrapped in an envelope of air (the atmosphere). To these three physical zones one may add the biological zone (the biosphere). The crust or lithosphere is made up of a great variety of rocks containing only a handful of elements. Rocks are the aggregate of minerals and are the individuals units constituting the crust of the earth or the lithosphere. Some of them were formed during consolidation of molten silicates (magma) and are describing as the igneous rocks (granite, basalt etc.). During later periods, the primary rocks suffered erosion by wind, water, ice, etc. and the products of such decay were carried away by the natural forces and deposited as loose sediments. Later on, they were subjected to compaction and the resulting products are known as the sedimentary rocks (e.g. sandstones and shales). The rocks occurring in any region may suffer physico-chemical change and accordingly, develop remarkable changes in their mineral compositions or texture or both. The processes which bring about such changes are known as metamorphism and the resulting products are the metamorphic rocks.

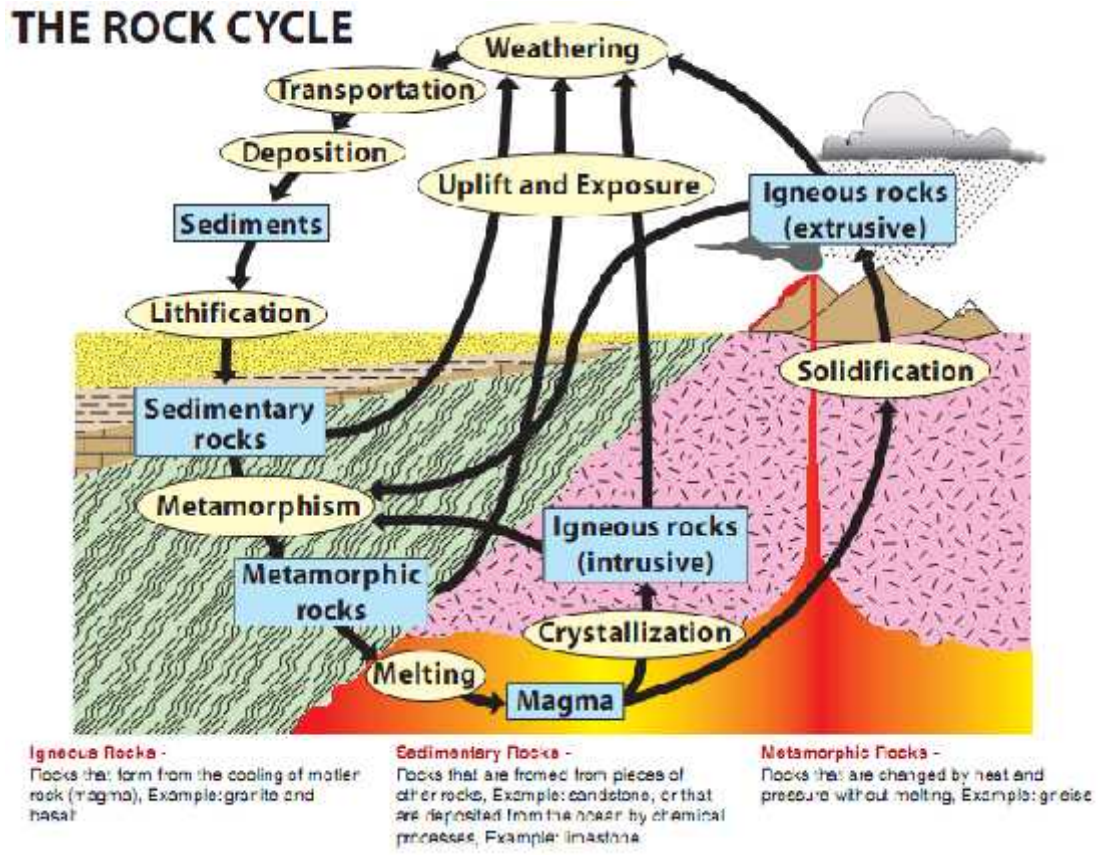

Fig. 1.1: The Rock cycle

1.3 Origin of the problem

Due to the vast applications of dolomite listed below, the dolomite mining, factory and transportation business developed in the Chhotaudepur town, and is the backbone of the town's economy.

- Dolomite used in the paint as filler material, in ceramic tiles as base mineral, and also uses in the glass. So the quality of powder should be an important.
- Dolomite contains the magnesium carbonate; it is used to make the milk of magnesia.
- It is also used in raw fertilizer material, as agricultural lime-'aglime', to reduce the soil acidity and also to reduce the magnesium deficiencies. This is the only mineral that can fulfill both the requirement.
- It is also used in cattle field as source of calcium.
- It is used in the making of refractory bricks.
- Fluxing agent in the steel making factory.
- The production cost of the dolomite powder is as low as the eatable salt, we are using in the daily life. So there are possibilities to be misuse also. Plastic industries mix this mineral with the raw material to save the production cost, which affects the quality of plastic.

Nowadays people are talking about globalization, it is also important to stand in the global market, with the quality product and also according to the production rate of the world market. Due to these reasons this area attracts and challenges to be better.

- The quality of mineral is checked on base of appearance and particle size. There is no chemical or any other tests done on the mineral. And also there is also unavailability of such scientific laboratories.
- There is also need of a R&D section.
- There are many mines located in different areas having different calcium to magnesium ratio, without taken care about this point some material or product gets rejected.
- Also the impurity level is also not considered, which also changes from mines to mines.
- The application of this mineral is on commercial base, there is lake of scientific view.

- Due to dolomite factories, the environment is also polluted with the dolomite powder.

Due to the above factors, I have decided to study the mineral though the thermoluminescence, because thermoluminescence is a very sensitive tool for the impurities and imperfections. It will also help to study, how geology as well as mineralogy differs from one mines to other mines.

Around 22 samples are collected from the different mines of the dolomite, around the Chhotaudepur town. Out of these 22 samples, 10 samples are selected for the TL (thermoluminescence), XRD, TGA, FT-IR. And few of them are selected for SEM and particle size analysis. Also approximately seven samples are collected from the different places of Maharashtra, India. They are Appophyllite, Heulandite, Prehnite, and Stilbite.

The present TL study is intended to suggest quality of dolomite, calcium to magnesium ratio, and also about the impurity. TL dosimetry study can be done if any accident or radiation damage occurs, as they are used in paint, ceramics.

1.4 Geology of Sedimentary Rocks

The record of Earth's history preserved in sedimentary rocks is truly remarkable. Each bedding plane is a remnant of what was once the surface of Earth. Each rock layer is the product of a previous period of erosion and deposition. In addition, details of texture, composition, and fossils are important records of global change, showing how Earth evolved in the past and how it may change in the future. To interpret the sedimentary record correctly, we must first understand something about modern sedimentary systems, the sources of sediment, transportation pathways, and places where sediment is accumulating today, such as deltas, beaches, and rivers. The study of how modern sediment originates and is deposited provides insight into how ancient sedimentary rocks formed. Fossils preserved in sedimentary rocks not only reveal the environment of deposition but also the pace and course of evolution through Earth's long life.

Apart from their scientific significance, the sedimentary rocks have been a controlling factor in the development of industry, society, and culture. Humans have used materials from sedimentary rocks since the Neolithic Age; flint and chert played an important role in the development of tools, arrowheads, and axes. The great cathedrals of Europe are made from sedimentary rock, and the statues made by the artists of ancient Greece and Rome and during the Renaissance would have been impossible without limestone. Fully 85% to 90% of mineral products used by our society come from sedimentary rocks. Virtually our entire store of petroleum, natural gas, coal, and fertilizer come from sedimentary rocks. Sand, gravel, and limestone are the raw materials for cement. Sedimentary rocks are also important reservoirs for groundwater, and host important deposits of copper, uranium, lead, zinc, as well as gold and diamonds.

1.4.1 What is Sedimentary rock?

Sedimentary rocks are probably more familiar than the other major rock types. The constituents of sedimentary rocks are derived from the mechanical breakdown and chemical decay of preexisting rocks. This **sediment** is compacted and cemented to form solid rock bodies. The original sediment can be composed of various substances:

1. Fragments of other rocks and minerals, such as gravel in a river channel, sand on a beach, or mud in the ocean
2. Chemical precipitates, such as salt in a saline lake or gypsum in a shallow sea.
3. Organic materials formed by biochemical processes, such as vegetation in a swamp, coral reefs, and calcium carbonate precipitated by in the ocean.

1.4.2 Importance of Sedimentary Rocks

Apart from the industrial and inn daily uses, Sedimentary rocks are important because they preserve a record of ancient landscapes, climates, and mountain ranges, as well as the history of the erosion of Earth. Animal and plant **fossils** are common in most of the rock units and can be preserved in great detail (Fig.:1.2). In addition, fossils are found in abundance in sedimentary rocks younger than 600 million years and provide evidence of the evolution of life through time. Earth's geologic time scale was worked out using this record of sedimentary rocks and fossils. Fossils often reveal much about

the past environment, giving us hints about whether a deposit is marine or continental, what the water depth was when the sediment was deposited, and about temperature and salinity of the water. Beyond that, however, fossils in sedimentary rocks reveal the history of the evolution of life. Although the record is far from complete, everything we know about past life comes from reconstructions based on ancient fossils.

Tracks, trails, and borings of animals are typically associated with ripple marks and mud cracks and can provide additional important clues about the environment in which the sediment accumulated.

As can be seen, primary sedimentary structures and fossils are the clues or the tools used by geologists to interpret the conditions and environment at the site where the sediment is deposited. The texture of most sedimentary rocks consists of mineral grains or rock fragments that show evidence of abrasion (Fig.1.3) or consist of interlocking grains of the minerals calcite or dolomite. In addition, many layers show ripple marks (Fig.1.4), mud cracks (Fig.:1.5), and other evidence of water deposition preserved in the bedding planes. All of these features show that sedimentary rocks form at Earth's surface in environments similar to those of present-day deltas, streams, beaches, tidal flats, lagoons, and shallow seas.

Fig.1.2: Fossils found in sedimentary rocks include representatives of most types of marine animals.

Fig.1.3: A microscopic view of sand grains in sediment shows the effects of transportation by running water. The grains are rounded and sorted to approximately the same size.

Fig.1.4: Ripple marks preserved in sandstone suggest that the sediment was deposited by the current action of wind or water.

Fig.1.5: Mud cracks form where sediment dries while it is temporarily exposed to the air. This structure is common on tidal flats, in shallow lake beds, and on stream banks.

1.4.3 Types of sedimentary rocks

Sedimentary rocks are classified on the basis of the texture and composition of their constituent particles. Two main groups are recognized:

(1) Clastic (also called detrital) rocks, formed from fragments of other rocks, and

(2) Chemical rocks and biochemical rocks.

Group: 1 Clastic Sedimentary Rock

One important category of sedimentary rock consists of particles of gravel, sand, or mud. Rocks made up of such fragmental material are called Clastic rocks. The term **clastic** comes from the Greek word *klastos,* meaning "broken" and describes the broken and worn particles of rock and minerals that were carried to the sites of deposition by streams, wind, glaciers, and marine currents.

In general, clastic rocks are subdivided according to grain size. From the largest grain size to the smallest; the types of clastic rocks are conglomerate sandstone, and mudrock.

Conglomerate consists of consolidated deposits of gravel (fragments larger than 2 mm in diameter) with various amounts of sand and mud in the spaces between the larger grains.

Sandstone is probably the most familiar, though not the most abundant, sedimentary rock because it is well exposed, easily recognized, and generally resistant to weathering. The sand grains range from 0.0625 to 2 mm in diameter and can be composed of almost any material, so sandstones can be almost any color. Quartz grains, however, are usually most abundant because quartz is a common constituent in many other rock types and because it is resistant to abrasion or chemical breakdown as the sediment particles are transported. The particles of sand in most sandstone are cemented by calcite, quartz, or iron oxide. Other grains maybe feldspar (in a rock called arkose), pieces of chert, or small rock fragments.

The composition of sandstone provides an important clue to its history. During prolonged transportation, small rock fragments and minerals that readily decompose such as olivine, feldspar, and mica break down into finer particles and are winnowed out, leaving only the stable quartz. Clean, well-sorted sandstone composed of well-rounded quartz grains indicates prolonged transportation, or even several cycles of erosion and deposition.

Mud rocks are fine-grained clastic rocks with grains less than 1/16 mm (0.0625 mm) across. Mud rocks are the most abundant sedimentary rocks. They are usually soft and weather rapidly to form slopes, so relatively few fresh, unweathered exposures are found. They are frequently deposited in river floodplains and deltas and other shallow marine settings. Many mud rocks also show evidence of burrowing by organisms.

There are several important varieties of mud rocks. **Siltstone** is a fine-grained clastic rock coarser than **claystone.** A mud rock that contains very thin layers (**laminae**) is called **shale**. Shales split easily along these layers to form small paper -thin sheets or flakes.

Group: 2 Biochemical and Chemical Sedimentary Rocks

The other major category of sedimentary rocks form when chemical processes remove ions dissolved in water to make solid particles. Some are **biochemical rocks** with sediment formed during the growth of organisms such as algae, coral, or swamp vegetation. Others are inorganic **chemical precipitates** from lakes or shallow seas.

Limestone is by far the most abundant chemically precipitated rock. It is composed principally of calcium carbonate ($CaCO_3$—dominantly calcite) and originates by both inorganic chemical and biochemical processes. Indeed, the distinction between biochemical and chemical rocks is rarely clear cut. Limestones have a great variety of rock textures, and many different types have been classified. Three important examples are described here: skeletal limestone, oolitic limestone, and microcrystalline limestone.

Some marine invertebrate animals construct their shells or hard parts by ex-tracting calcium and carbonate ions from seawater. Corals, clams, algae, snails, and many other marine organisms construct their skeletons of calcium carbonate. After the organisms die, the shells accumulate on the seafloor. Over a long period of time, they build up a deposit of limestone with a texture consisting of shells and shell fragments. These particles may then be cemented together as more calcite precipitates between the grains. This type of limestone, composed mostly of skeletal debris, can be several hundred meters thick and can extend over thousands of square kilometers. **Chalk**, for example, is a skeletal limestone in which the skeletal fragments are remains of microscopic plants and animals.

Other limestones are composed of small semispherical grains of calcium carbonate known as **oolites.** Oolites form where small fragments of shells or other tiny grains become coated with successive thin layers of $CaCO_3$as they are rolled along the seafloor by waves and currents.

A third important type of limestone forms in quiet waters where calcium carbonate is precipitated by algae as tiny, needle like crystals that accumulate on the seafloor as limy mud. Soon after deposition, the grains commonly are modified by compaction and recrystallization. This modification produces microcrystalline limestone (or

micrite), a rock with a dense, very fine-grained texture. Other types of carbonate grains may be cemented together by microcrystalline limestone.

Inorganic limestone also is precipitated from springs and from the dripping water in caves to form beautifully layered rocks called travertine.
Most limestone forms on the shallow continental shelves where waters are warm and organic production is high. In contrast, carbonate sediments are rare in deep water and do not accumulate on the abyssal plains. In fact, calcite is not stable at the low temperatures and high pressures found on the deep seafloor. Calcite shells formed in surface waters fall toward the seafloor when the organism dies; but in deep water, calcite shells dissolve before they reach the bottom. Near the equator, calcite is not stable at depths below about 4,500 m, where the seafloor is shallower than this, as on oceanic ridges, carbonate sediment will accumulate.

Dolostone is a carbonate rock composed of the mineral dolomite, a calcium magnesium carbonate $CaMg(CO_3)_2$. It is similar to limestone in general appearance, but reacts with acid only when powdered. Dolostone is commonly dull brownish yellow or light gray. It can develop by direct precipitation from seawater, but such environments are extremely rare. Instead, dolostone may form by the reaction of magnesium-bearing groundwater with calcium carbonate in limestone. The recrystallization generally destroys the original texture of the rock. In a fashion, dolostones are chemical precipitates formed from biochemical rocks.

Chert is a common rock composed of microcrystalline quartz. In a hand specimen, it is hard, dense, and typically breaks like glass, but under a high-power microscope, it has a fibrous or granular texture. Chert is usually white or shades of gray, tan, green, or red. Because it fractures to make sharp edges, it has been shaped by many ancient people to make arrowheads, spear points, and tools. Chert commonly occurs as irregular nodules in limestone or as distinct thin layers in marine sedimentary rocks. Some nodular chert precipitates from pore fluids, particularly in carbonate rocks. However, most chert probably forms biochemically.

Another important biochemical component of many sedimentary rocks is hydrocarbons or organic compounds derived from living things. The decay of these materials at in deeply buried sedimentary rocks produces oil, natural gas, and coal.

Only a few important rock types form strictly by inorganic processes. **Rock salt** is made of the mineral halite (NaCl). It crystallizes when evaporation concentrates sodium and chlorine ions to the point that salt is stable in the residual brine. Strong evaporation creates saline lakes in closed desert basins (for example, the Great Salt Lake and the Dead Sea).Enhanced evaporation also occurs in restricted bays along the shore of the ocean.**Gypsum,** $CaSO_4 \cdot 2H_2O$, also originates from evaporation. It collects in layers as calcium sulfate is precipitated from water. Because **evaporites** (rocks formed by evaporation) accumulate only in restricted basins subjected to prolonged evaporation, they are important indicators of ancient climatic and geographic conditions.

1.4.4 Sedimentary structures

Sedimentary rocks commonly show layering and other structures that form as sediment is transported. The most important sedimentary structures are stratification, cross-bedding, graded bedding, ripple marks, and mud cracks. Primary sedimentary structures provide key information about the conditions under which the sediment accumulated.

Stratification

One of the most obvious characteristics of sedimentary rocks is that they occur in distinct layers expressed by changes in color, texture, and the way the different rock units weather and erode. These layers are termed strata, or simply **beds.** The planes separating the layers are planes of stratification, or bedding planes. **Stratification** occurs on many scales and reflects the changes that occur during the formation of a sedimentary rock. Large-scale stratification is expressed by major changes in rock types (**formations**) (Figure 4.5).For example, cliffs of limestone or sandstone can alternate with slopes of weaker shale .

The origin of stratification is quite simple. Different layers form because of some change that occurs during the process of deposition. But there are many types of changes that occur and operate on many different scales, so the construction of a

detailed history of sedimentary rocks presents a real challenge to geologists. Changes in weather, changes in the seasons, and changes in climate all can produce stratification in a sedimentary basin. Tectonic changes such as uplift and subsidence of the continental platform, mountain building, and volcanism all produce changes in material transported to the sea, and all can produce different layers of sedimentary rock.

Fig. 1.6: Dolomite beds in the dolomite mines Situated at Chhotaudepur

Cross-Bedding

Cross-bedding is a type of stratification in which the layers within a bed are inclined at an angle to the upper and lower surfaces of the bed. As sand grains are moved by wind or water, they form small ripples or large **dunes.** These **sand waves** range in scale from small ripples less than a centimeter high to giant sand dunes several hundred meters high. Typically, they are asymmetrical, with the gentle slope facing the moving current. As the particles migrate up and over the sand wave, they accumulate on the steep down current face and form inclined layers. The direction of flow of the ancient currents that formed a given set of cross-strata can be determined by measuring the direction in which the strata are inclined. We can determine the

patterns of ancient current systems by mapping the direction of cross-bedding in sedimentary rocks. Moreover, the style of cross-bedding changes with the sediment supply and with the flow conditions at the depositional site. Thus, the details of an ancient environment can be interpreted from careful study of the type of cross-bedding.

Graded Bedding

Another distinctive type of stratification, called **graded bedding,** displays a progressive decrease in grain size upward through a bed. This type of stratification commonly is produced on the deep-ocean floor by **turbidity currents,** which transport sediment from the continental slope to adjacent deep ocean forming bodies of rock called **turbidites.**

Sedimentary systems

Weathering of preexisting rocks, transportation, and deposition, followed by compaction and cementation, are the major steps in the formation of sedimentary rocks. The major sedimentary systems are (1) fluvial, (2) alluvial-fan, (3) eolian, (4) glacial, (5) delta, (6) shoreline, (7) organic reef, (8) shallow-marine, and (9) deep-marine. Each of these systems has a specific set of physical, chemical, and biological conditions and therefore develops distinctive rock types and fossil assemblages.

Sedimentary systems operate at Earth's surface through interactions of the hydrologic system and the crust. As a result of the transfer of energy between the various parts of a sedimentary system, new landforms and new bodies of sedimentary rock are created. Most the energy that drives these systems ultimately comes from the Sun; gravitational and chemical potential energy are also transferred in various parts of the sedimentary system. It is useful to visualize a hypothetical sedimentary system as consisting of a source of sediment (weathering), a transport path for the sediment, a site of deposition, and the processes that compact and cement the sediment together to form a solid rock. Fortunately, many of these sedimentary processes operate today, and geologists actively study rivers, deltas, and oceans and other sedimentary systems in an effort to understand the characteristics of rocks formed in these environments.

Weathering

Weathering is the interaction between the elements in the atmosphere and the rocks exposed at Earth's surface. The atmosphere can mechanically break down the rock through processes such as ice wedging, and it can chemically decompose the rock by a variety of reactions. Note that weathering is the first step in the genesis of sedimentary rock. The atmosphere breaks down and decomposes preexisting solid rock and forms a layer of loose, decayed rock debris, or soil. This unconsolidated material can then be transported easily by water, wind, and glacial ice.

Transportation

Running water is the most effective form of sediment transport. All rivers carry large quantities of sediment toward the sea. This fact is readily appreciated if you consider the great deltas of the world, each formed from sediment transported by a river. Indeed, sediment is so abundant in most rivers that a river might best be thought of as a system of water and sediment rather than simply a channel of flowing water.

As clastic sediment is transported by a river, it is sorted and separated according to grain size and composition. Large particles accumulate in high-energy environments as gravel, medium-sized grains are concentrated as sand, and finer material settles out as mud. The grain size of the sediment correlates with the energy of the transporting medium. Thus, large particles are carried by rapidly moving streams with high amounts of kinetic energy; only small particles are transported by slowly moving streams. Wind, glaciers, and shoreline currents also transport sediment, but their activity is somewhat restricted to special climate zones. Components from dissolved minerals are carried in solution and are ultimately precipitated to form limestone or salt, for example.

Deposition

Probably the most significant factor in the genesis of sedimentary rocks is the place where the sediment is deposited. The idealized diagram in Figure 1.7shows the major depositional systems. The most important continental systems are river (**fluvial**) systems, **alluvial fans,** desert dunes, and margins of **glaciers.**

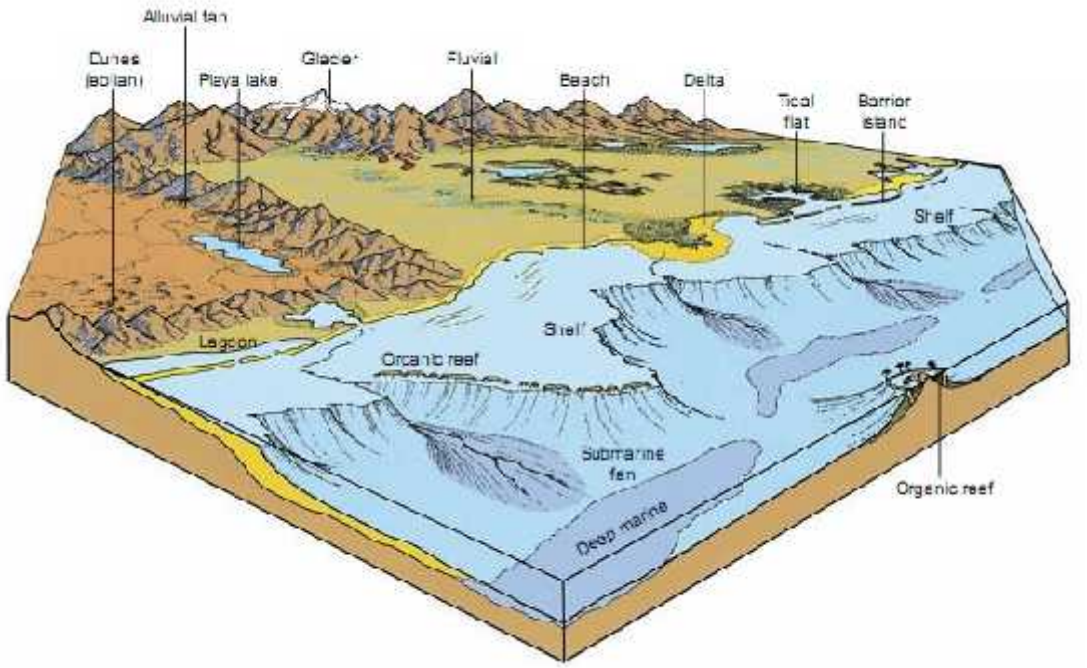

Fig. 1.7: The major sedimentary systems are represented in this idealized diagram.

Most sediment moves down slope from continental highlands toward the oceans, so the most important sedimentary systems are found along the shores and in the shallow seas beyond. Sedimentary systems can be categorized in three groups: continental, shoreline (transitional), and marine.

Systems include the shallow marine, which cover parts of the continental platform, reefs, submarine fans, and the floors of the deep-ocean basins. Between continental areas and marine areas are the transitional, or mixed, environments that occur along the coasts and are influenced by both marine and non marine processes. These include deltas, beaches, barrier islands, tidal flats, and lagoons.

Each depositional system imprints specific characteristics on the rocks formed within it. A small depositional area within a system creates a **facies**—a body of rock with distinct chemical, physical, and biological characteristics created by the environment. Thus, a delta system produces many different facies, for example, sediment deposited in channels, between channels, and at the mouths of channels. Distinctive textures, compositions, sedimentary structures, and fossil assemblages develop in each facies.

Compaction and Cementation

The final stage in the formation of sedimentary rocks is the transformation of loose, unconsolidated sediment into solid rock. **Compaction** occurs when the weight of overlying material, which continually accumulates in a sedimentary environment, compresses the sediment buried beneath into a tight, coherent mass. Wet mud consists of 60 to 80% water, most of which is driven out during compaction. **Cementation** occurs when dissolved ions, carried by water seeping through pores, are precipitated. Common cementing minerals are calcite, quartz, and iron oxides. This post depositional crystallization of cement holds the grains of sediment together and is a fundamental process in transforming sediment into solid rock.

Table- 1: Classification of sedimentary rocks

CLASTIC SEDIMENTARY ROCKS			
Texture	**Sediment particle size**	**Other characteristics**	**Sedimentary rock**
Clastic	Gravel (> 2 mm)	Rounded rock fragments, Poorly-sorted	Conglomerate
		Angular rock fragments, Poorly-sorted	Breccia
	Sand (0.0625 mm – 2 mm)	Quartz (>50%), Moderate – well sorted	Quartz sandstone
		Quartz with Feldspar, Moderate – Well sorted	Arkose
		Quartz, Feldspar, Clays, Rocky Fragments, Well-sorted	Gray wacke
	Mud (< 0.0625 mm)	Fine, thin layers, or cohesive clumps, Well-sorted	Shale, Siltstone, and Mudstone
CHEMICAL SEDIMENTARY ROCKS (INORGANIC AND BIOCHEMICAL)			
Group	**Texture**	**Chemical composition**	**Sedimentary rock**
Inorganic	clastic or non-clastic	Calcite, $CaCO_3$	Limestone
	non-clastic	Dolomite, $CaMg(CO_3)_2$	Dolostone
	non-clastic	Microcrystalline quartz, SiO_2	Chert
	non-clastic	Halite NaCl	Rock salt
	non-clastic	Gypsum, CaSO4 $2H_2O$	Rock Gypsum
Biochemical	clastic or non-clastic	Calcite, $CaCO_3$	Limestone
	non-clastic	Microcrystalline quartz, SiO_2	Chert
	non-clastic	Altered plant remains Coal	coal

1.5 The Mineral Dolomite

1.5.1 History

Diedonnè-Silvain-Guy-Tancrede de Gvalet de Dolomieu, born June 23, 1750 in the village of Dolomieu, was a typical naturalist of his time. With 26 years he travelled trough half Europe, he got interested in the mines of the Bretagne and the basaltic plateau in Portugal, and he visited South Italy to study the aftermath of an earthquake in Sicily and observed an eruption of the Aetna.

In 1789 during a voyage to Italy with his student fellow Fleuriau de Bellevue he also travelled trough Tyrol. In the Brenner Pass area and between the cities of Bozen und Trento he noted a rock similar to limestone, but which showed no appreciable effervescences with acids. He published these observations in July 1791 in a letter to the "*Journal of Physique*". Nicolas de Saussure, son of the Alpinist/naturalist Horace Benedict de Saussure requested some samples to analyze it. After some tentative denominations like "*Tyrolit*" or "*Saussurit*" in 1792 de Saussure published the "*Analyse de la Dolomie*" in the "*Journal of Physique*". Even if the rock itself was not completely unknown, in fact called "*Spat*" or "*Perlspat*" by miners, it was not realized until the publication of Dolomieu that the rock was composed of a peculiar Ca-Mg carbonate. The Italian naturalist Giovanni Arduino (1713-1795) published in 1779 his observations about a peculiar limestone, found in the mountains surrounding Verona, but he didn't delve further into the subject and consider the idea of a new mineral. So the name "*Dolomite*" became soon established, and in 1794 Richard Kirman introduced the Dolomite as a new mineral; the name from there became used to name the dolostone rocks and finally gave the Dolomites their actual name.

In the 19th century the genesis of both the Dolomite Mountains as the rock forming them became a major problem in geology. One of the most important achievements' was the recognition that the outstanding peaks and mountain groups are remains of ancient carbonate platforms and coral reefs.
In early days of geology less was known about the bottom of the sea and sedimentation occurring in oceans, only in 1842 Darwin formulated a first hypothesis dealing with the formations of tropic reefs.

Influenced by this model, intensive field mapping was carried out, and in 1860 the German geologist Ferdinand von Richthofen (1833-1905) recognized as first the Schlern Mountain as a slope of an ancient reef and other peaks as the remnants of large carbonate platforms.

1.4.2 Dolomite Problem

After geologists could answer how the most spectacular rock walls and peaks in the Dolomites formed, the next urgent questions was if dolomite was a primary product of marine deposition or a secondary product of alteration of common limestone.
An insight to the problem came from the study of a characteristic geological formation in the Dolomites and its depositional environment: The appropriately denominated *Hauptdolomit*, the "main dolostone" formation, was defined in the Bavarian Alps by VON GUEMBEL 1857, and introduced in the stratigraphic nomenclature of the Alps in 1876 by LEPSIUS.

During the Upper Carnian and the Norian stage (216, 5 - 203,6Ma) the Tethyan Sea experienced various regression and transgression phases. The changing sea level resulted in the development of large water covered carbonate platforms or emerged tidal flats, on which a sequence of homogenous, meter thick carbonate muds with rare fossils (subtidal facies) and laminated bacterial mats and dolomite marls (peritidal facies) were deposited.

These deposits are widely distributed in the Eastern Alps, they can be found in the Southalpine unit (here denominated *Hauptdolomit/Dolomia Principale Formation*), as well as in a very similar development in the entire Austroalpine unit (*Hauptdolomit-Gruppe* in the Northern Calcareous Alps, Ortles nappe, S-charl nappe etc.) and in the Apennines and Dinarides, and therefore points at an enormous extension of this tidal sea.

During sea level low stand the muddy flats were colonized by algae and a species-poor faunal community, dominated by gastropods (*Worthenia confabulate*) and bivalves (*Megalodus)*. Dinosaurs roved through the tidal flat, their tracks have been preserved at some locations. In times of emersion only thin mud layers were deposited

by storms, which themselves were colonized by algae and bacterial mats, and which dried out repeatedly.

The extreme shallow water conditions continued uninterrupted throughout the whole Norian. The uniform and slow subsidence of the basement led to deposition of an up to 1.000 meters thick succession of homogeneous cycles of the two facies. The top of the Hauptdolomite, and the end of the platform succession, is characterized by the development of polycyclic paleosols up to 30m thick, reflecting a major eustatic sea-level fall. One of the most intriguing differences of the Southalpine Hauptdolomite to other corresponding formations is the lack of intraplattform basins, with a succession of dark dolo- and limestone's, found for example in Lombardy and Austria. This fact is explained by missing tectonic activity during the Triassic in the area of the future Dolomite-mountains.

With this proposed reconstruction, geologists tried to find an actual and comparable environment to understand the deposition of dolostone: the large carbonate platform of the Bahamas Bank seemed to fit perfectly the prerequisites: a vast area covered with a shallow, tropical sea, with sparse islands and coral reefs surrounded by large tidal flats - there was only one problem: no or only a limited formation of dolomite is today observed in this environment.

References

1. Alien M. Alper, High temperature Oxides-part -1 – academic press , new York, 70
2. Kirk – Othmer, Encyclopedia of chemical technology – 3rd Edn Vols 3, 12, 14, 15, 19, 22, & 24 Wiley – Inter – Science Publication, John, Wilely & sons, New York
3. D.K. Banerjee, Mineral Resources of India, - The World press Pvt. Ltd, Kolkatta,1992.
4. Indian Minerals Hand Book,- Indian Bureau of Mines , 1998 &1999.
5. Nina – Keegan – Industrial Mineral Directory, - 4th Edition, Industrial minerals information Ltd, U.K. 1999.
6. A.V Sankaran, K.S.V Nambi & C.M Sunta – progress of Thermonluminescence reasearch on Geological Materials – 7th September, 1982.
7. Amin, Y.M Bull R.K. & Durrani, S.A. (1982) Effect of radiation damage on TL properties of crystals, Third specialities Meeting on T.L & ESR dating, Helslinger Counc, Eur, PACt J,9
8. J.P Patel G.H. Upadhaya – Material Science, Atul Parakashan, 2006-07.
9. Material Science – S.L Kakani – New Age Int. Pub. 2006
10. Saxena Gupta – Solid State Physics – 1985
11. H.V Keer – Solid State Physics – Wilay Eastern Ltd. 1993
12. Azaroff – Introduction to Solid, 1977
13. Skoog , Holler, Nieman – Principles of Instrumental Analysis, 5th Edition 2005
14. M.J Aitken – Thermo. Lumi. Dating, 1985.
15. P.L Soni . Mohan Katyal – Text Book of Inorganic Chemistry, 2007.
16. D. J Mc Dougall – Thermo. Lumi. of Geological Materials, Academic press, London & New York , 1984.
17. Hurlbut, Cornelius S.; Klein, Cornelis, 1985, Manual of Mineralogy, 20th ed., Pearse, Roger (2002-09-16). Stwertka, Albert (1996).
18. A Guide to the Elements. Oxford University Press. pp. 117–119.
19. http://www.etymonline.com/index.php
20. John W. Valley, William H. Peck, Elizabeth M. King, Simon A. Wilde (2002).
21. "A Cool Early Earth". Geology 30: 351–354. Retrieved 20050411.

22. Ehlers, Ernest G. and Blatt, Harvey (1982). 'Petrology, Igneous, Sedimentary, and Metamorphic' San Francisco: W.H. Freeman and Company. ISBN 0-7167-1279-2.
23. Hillier S. (2003) Clay Mineralogy. pp 139–142 In: Middleton G.V., Church M.J., Coniglio M., Hardie L.A. and Longstaffe F.J.(Editors) Encyclopedia of sediments and sedimentary rocks. Kluwer Academic Publishers, Dordrecht.
24. Dictionary of Ceramics (3rd Edition) Edited by Dodd, A. Murfin, D.Institute of Materials. 1994.
25. T. Pradell et al. 2006, Physical Processes Involved in Production of the Ancient Pigment, Egyptian Blue, Journal of the American Ceramic Society 89.4: 1431.
26. L. Lee and S. Quirke 2000, Painting Materials, In: P.T. Nicholson and I. Shaw (eds.), Ancient Egyptian Materials and Technology, Cambridge: Cambridge University Press.
27. 'Potter and Ceramics. Rosethal E. Pelican Books. 1949.
28. O.R. Lazutkina et al. 2006, Glass Enamel for Steel Based on Diatomite Material, Glass and Ceramics 63.5-6: 170.
29. Nickel, Ernest H. (June 1995). "The definition of a mineral". The Canadian Mineralogist 33 (3): 689–690.
30. M.E.Tucker, An Introduction to the origin of Sedimentary rocks, Blackwell, 1991, p.228.
31. “Dolomite”- Mineral Planning factsheet, British Geological Survey, Office of the Deputy Prime minister, 2006. Adams, A. D., W. S. MacKenzie, and C. Guilford, 1984. Atlas of Sedimentary Rocks under the Microscope. New York: Wiley.
32. Blatt H., and R.J. Tracy. 1996. Petrology: Igneous, Sedimentary, and Metamorphic. New York: Freeman.
33. Boggs S. 2001. Principles of Sedimentology and Stratigraphy. Upper Saddle River, NJ: Prentice Hall.
34. Carozzi A. V. 1993. Sedimentary Petrography. Englewood Cliffs, N.J.: Prentice Hall.
35. Open University. 1998. The Ocean Basins: Their Structure and Evolution. Oxford: Butterworth and Heinemann.
36. Prothero D.R., and F. Schwab. 1996. Sedimentary Geology. New York:

Freeman.
37. Reading, H. G. 1996. Sedimentary Environments: Processes, Facies and Stratigraphy. Oxford: Blackwell.
38. http://www.handbookofmineralogy.org/pdfs/

Chapter # 2

Basic theory of Thermoluminescence and Introduction to the Minerals

2.1 Luminescence

The term luminescence implies luminous emission which is not purely thermal in origin i.e. luminescence is 'cold light', light from other sources of energy, which takes place at normal and lower temperature. In luminescence, some energy sources kicks an electron of an atom of its ground state (lowest energy) into an exited state (highest energy) by supplying extra energy, then as this excited state is not stable electron jumps back to its ground state by giving out this energy in form of light. We can observe the luminescence phenomenon in nature like during lightening, in glowworms, fireflies, and in certain sea bacteria and deep-sea animals. This phenomenon have been used in various fields by different scientist all over the world like, Archaeology, Geology, Biomedical, Engineering, Chemistry, Physics, and various Industrial Application for Quality Control, Research and Developments.

Luminescence is a rare phenomenon among inorganic compounds. This is due to the predominance of nonradiative relaxation processes. An electronic excitation of a complex or a metal center in a crystal usually ends up as vibrational energy and eventually as heat. In those cases where spontaneous light emission does occur, its spectral and temporal characteristics carry a lot of important information about the metastable emitting state and its relation to the ground state. Luminescence spectroscopy is thus a valuable tool to explore these properties. By studying the luminescence properties we can gain insight not only into the light emission process itself, but also into the competing nonradiative photophysical and photochemical processes.

Luminescence is the emission of optical radiation (infrared, visible, or ultraviolet light) by matter. This phenomenon is to be distinguished incandescence, which is the emission of radiation by a substance by virtue of its being at a high temperature (>5000^{o}C) (Black body radiation). Luminescence can in occur in a wide variety of matter and under many different circumstances. Thus, atoms, polymers, inorganic, organic or Organo metallic molecules, organic or inorganic crystals, and amorphous substances all emit luminescence under appropriate conditions. The various

luminescence phenomena are given their names, which reflect the type of radiation used to excite and to get the emission.

2.1.1 Luminescence and Stokes law:

When radiation is incident on a material some of its energy is absorbed and re-emitted as a light of a longer wavelength (stokes law). This is the process of luminescence. Wavelength of light emitted is characteristics of a luminescent substance and not on the incident radiation. The light emitted could be visible light, ultra-violet, or infrared light. This cold emission i.e. luminescence, that does not include the emission of black body radiation thus involve two steps.

1) The excitation of electronic system of a solid material to higher energy state and
2) Subsequent emission of photons or simply light.

The emission of light takes place at characteristics time 'τ_c' after absorption of the radiation, this parameter allows us to sub classify the process of luminescence into fluorescence and phosphorescence. Thus, if the characteristic time'τ_c'is less than 10^{-8} sec, then it are known as Fluorescence & If the characteristics time 'τ_c' is greater than that of 10^{-8}sec, them it is known as Phosphorescence.

A large number of substances both organic and inorganic show the property of luminescence, but principal materials used in various applications of luminescence, involves inorganic solid insulating materials such as alkali and alkaline earth halides, Quartz(SiO_2),Phosphates,Borates,and Sulphates etc. Luminescence solids are usually referred to as Phosphors.

2.1.2 Types of Luminescence

The various luminescence phenomena are given their names, which reflect the type of radiation used to excite the emission.

Radio luminescence (or scintillation) is produced by ionizing radiations. Some polymers contains organic molecules which emit visible light when exposed to such radiations as X-rays, gamma rays or cosmic rays, and thus act as detectors for high energy radiations.

Cathodoluminescence is due to emission of light during electron irradiation (CRO & TV Screen Phosphors).

Chemiluminescence is produced as a result of a chemical reaction usually involving an oxidation-reduction process. The most common mechanism for such an emission is the conversion of chemical energy, released in a highly exothermic reaction, into light energy.

Electroluminescence is the efficient generation of light in a non-metallic solid or gas by an applied electric field or plasmas.

Mechanoluminescence (triboluminescence or piezoluminescence) is due to the emission of light on applying an external mechanical energy. It could be excited by cutting cleaving, grinding, rubbing, and compressing or by impulsive deformation of solids.

Sonoluminescence is the emission of light due to the excitation by Sound waves including ultrasonic waves.

Thermoluminescence (TL) or more specifically Thermally Stimulated Luminescence (TSL) is activated thermally after initial irradiation by some other means. ($\propto$- rays, β -rays, γ - rays and UV rays and X-rays).

Bioluminescence is luminescence caused by chemical reactions in living things; it is a form of chemiluminescences. Fireflies glow by bioluminescence.

Electro luminescence is luminescence caused by electric current.

Triboluminescence is phosphorescence that is triggered by mechanical action or electroluminescence excited by electricity generated by mechanical action. Some minerals glow when hit or scratched, as you can see by banging two quartz pebbles together in the dark.

Optically stimulated luminescence is phosphorescence triggered by visible light or infrared. In this case red or infrared light is only a trigger for release of previously stored energy.

2.2 Introduction to Thermoluminescence:

TL or more specifically Thermally Stimulated Luminescence (TSL) is stimulated thermally after initial irradiation given to a phosphor by some other means (a- rays, γ - rays, ß- rays, UV- rays and X-rays). Thermally stimulated luminescence (TSL) is the phenomenon of emission of light from a solid which has been previously exposed to ionizing radiation under conditions of increasing temperature. Unlike other luminescence process such as Electroluminescence, Chemiluminescence, here heat is

not an exciting agent, but it acts only as a stimulant. Hence, it is better known as thermally stimulated luminescence (TSL). Excitation is achieved by any conventional, sources like ionizing radiation, a rays, ß-rays, γ- rays and UV rays and X-rays. TSL is exhibited by a host of materials, glasses, ceramics, plastics and some organic solids. By far insulating solids doped with suitable chemical impurities, termed as activator, are the most sensitive TL materials. The band theory of solid is normally used to explain this phenomenon. When a solid is irradiated, electrons and holes are produced. The defects in the solid results in the presence of localized energy level within the forbidden gap. On irradiation, electron and holes can be trapped at these sites. When the solid is heated, these trapped electrons/holes get enough thermal energy to escape from the trap to the conduction band (or valence band). From here they may get retrapped again or may recombine with trapped holes/electrons. The site of recombination is called recombination center. If this recombination is radiative, then center is called luminescence center. Alternatively a trapped hole can be released by heating which can recombine with a trapped electron resulting in luminescence.

2.3 Historical Background of Thermoluminescence phenomenon:

Historically, thermoluminescence (TL), or more appropriately Thermally Stimulated Luminescence (TSL) may be said to have its beginning in 1663 with Robert Boyle who reported to the Royal Society of London (Boyle, 1664) his observation "Eleventhely, I also brought it some kind of glimmering light by taking it (natural diamond) into bed with me and holding it a good while upon a warm part of my naked body." Not much later Elsholtz (1676) observed similar effect in fluorspar (Encyclopedia Britannica). However, experimental and radiation induced TSL under its modern name in a wide variety of natural and synthetic materials was probably first reported by Wiedemann and Schmidt (1895) of Germany in an article entitled "On Luminescence" in a then widely read and highly regarded scientific journal. Wiedemann and Schmidt were probably the first to report the TSL of at least two of the modern materials widely used viz. fluorite and CaF_2: Mn. They also spoke of the possibilities of TSL of glasses and borates. Then in 1904 Marie Curie's dissertation was perhaps the first dissertation on TSL, viz. in rocks, minerals and synthetic crystals has been studied by an ever increasing number of workers. But the real boost can be said to have been given in the late 1940s and early 1950s by the pioneering work of Farrington Daniels and his group at the Universities of

Wisconsin (USA).

Farrington Daniels and his group first suggested the use of TSL as a technique in radiation dosimetry (Daniels et al., 1953) through studies on LiF as a TSL material. Lithium fluoride was used to measure radiation dose after a bomb test. Soon the idea of using TSL in dosimetry caught on and many groups started working in the field of thermoluminescent dosimetry (TLD). It became evident that in LiF the desirable properties of the material were the result of the interplay between the complex defects present within the material resulting from the presence of the Mg and Ti. This realization emerged from the work of Cameron and colleagues (Cameron et al., 1963, 1968) and this work led eventually to the patenting of TLD-100 by the Harshaw Chemical Company in 1963. In last few decades there has been tremendous research in this field. Thermoluminescence (TL), as an experiment technique, find application in diverse scientific disciplines, such as radiation dosimetry, archaeology, geology, medicine, solid state physics, biology and organic chemistry. In the last four decades, many new and dosimetrically useful TLD materials were reported. $Li_2BV_4O_7$:Mn (Schulman et al., 1965), CaF_2:Dy (Binder et al.,1968), $CaSO_4$:Dy and $CaSO_4$:Tm (Yamashita et al., 1968,1971), BeO (Tochilin et al., 1969), Al_2O_3:Mg,Y(Janas et al., 1976) and Al_2O_3:Si,Ti (Mehta et al., 1976), CaF_2:Tm (Lucas et al., 1977), LiF:Mg, Cu, P (Nakajima et al., 1978), $Li_2B_4O_7$:Cu (Takenaga et al., 1980) and MgB_4O_7:Dy or Tm (Prokic, 1980), Al_2O_3:C (Akselrod et al., 1990a, 1990b). Subsequently, a large number of laboratories have also been successful in preparing LiF:Mg,Cu,P, BeO, $CaSO_4$:Dy or Tm and some other TLD phosphors.

With the progress in crystal growing techniques, artificially doped samples were grown in the laboratory. Wiedemann developed the first artificially activated $CaSO_4$:Mn phosphor. Extensive work of Cameron et al. (1963, 1968) of LiF powder supplied by Harshaw Chemical Co., U.S.A., has led to development of now well-known dosimetric phosphor LiF: Mg, Ti. This phosphor is being manufactured by Harshaw Chemical Co. under the trade names of TLD-100, TLD-600 and TLD-700. These phosphors have been extensively studied for its thermoluminescent properties relevant to radiation dosimetry. The presence of rare-earth ions in the natural fluorite (CaF_2) as efficient emission centers, led to the development and study of rare earth doped phosphors such as CaF_2:Dy, CaF_2:Tm, $CaSO_4$:Dy, $CaSO_4$:Tm and Mg_2SiO_2:Tb. These phosphors have

proved to be more sensitive in comparison to LiF:Mg,Ti phosphor. Many of these phosphors have now become commercially available.

In the case of Phosphor development, it started with the development of $CaSO_4$:Mn, which was used, by Wiedemann and Schmidt (1895) in late nineteenth century, for TSL studies and for radiation detection. In early 1950s Farrington Daniels successfully used LiF for radiation dosimetry during atomic bomb testing. The late nineteenth-early twentieth century was dominated by studies on natural minerals. Natural CaF_2 was used by Marie Curie to detect radiations from radium source. X-ray induced TSL was examined by many workers like Lind and Bardwell (1923). The study of the TSL properties of synthetic materials also gained momentum at this time with $CaSO_4$:Mn phosphor being the particular interest. The use of TSL in UV dosimetry using $CaSO_4$:Mn was actively being examined during this period. Even though, TSL studies on $CaSO_4$:Mn were carried out by Wiedemann and Schmidt (1895), its use as a possible TSL dosimeter was demonstrated by Watanabe in 1951. Search for new materials for specific applications started in early 1950s. Outcome of efforts of Daniels et al. (1950, 1953) in this direction was development of promising material LiF. But the study of complex behavior of this material by Cameron and colleagues (1963,1968) led to the patenting of TLD-100 by the Harshaw Chemical Company in 1963. Despaired with unpredictable properties of LiF, Daniels group turned their attention to the next material, Al_2O_3 (Rieke and Daniels, 1957). Al_2O_3 in the form of sapphire, was high grade optical material, but due to lack of sensitivity, lost its credibility. In 1957, two new materials BeO (Moore, 1957) and CaF_2:Mn (Ginther and Kirk, 1957) made their appearance. CaF_2:Mn had major impact in this field due to its excellent sensitivity and simple glow curve structure. It is the first TLD material in this field and still never went back seat any time (McKeever et al., 1995).

In 1960s several new materials like $CaSO_4$: Sm (Kraysnaya et al., 1961), $Li_2B_4O_7$: Mn (Schulman, et al., 1965), CaF_2: Tm and $CaSO_4$: Dy (Binder, et al., 1968), $CaSO_4$: Dy (Yamashita, et al., 1968) entered into the field. Natural CaF_2 (Kozlowitz et al., 1965) made its appearance again along with tissue equivalent and promising material, LiF: Mg, Ti (Cameron et al., 1963 and 1968). Thomas and Houstan's (1964) MgO was another addition to this family. In 1970s,

Al_2O_3 reappeared in new form as Al_2O_3: Mg, Y (Janas et al., 1976) and Al_2O_3: Si, Ti (Mehta et al., 1976). Another form of CaF_2, namely, CaF_2: Tm (Lucas et al., 1977) was reported during this period. Two new materials, namely, $Li_2B_4O_7$: Cu (Takenaga et al.., 1980) and MgB_4O_7: Dy or Tm (Prokic, 1980), were reported during 6th International Conference on Luminescence at Toulouse, France, MgB_4O_7: Mn (Prokic, 1993) was latter addition to this group. Another remarkable newcomer was LiF: Mg, Cu, P (Nakajima et al., 1978), but remained unnoticed until the group at Solid Dosimetric and Detector Laboratory in Beijing reported the manufacture of a LiF: Mg, Cu, P TLD material (Wang et al.., 1986), known as GR-200, in 1986. This is reported as an ultra sensitive material with sensitivity as high as 50 times that of TLD-100. This is followed by even more sensitive material, Al_2O_3: C (Akselrod et al., 1990). These two materials are now dominating the field of TLD material research. At the 12th International Conference on Solid State Dosimetry, it was reported (Nam et al., 1999) that LiF:Mg,Cu,Na,Si has a similar glow curve shape to that of LiF:Mg,Cu,P but the relative TSL sensitivity is about 2 times that of LiF:Mg,Cu,P.

Around 1940s clear picture of general processes involved in TSL had been developed. Randall and Wilkins (1945a, 1945b) and Garlick and Gibson (1948) gave a theoretical basis to this phenomenon. The TSL was used for the first time by Daniels (1950) to make quantitative measurements of radiation exposure. Their main interest was in TSL of geological specimen and in TSL properties of alkali halides. Since that time TSL dosimetry has found wide application particularly in radiation dosimetry. Daniels et al. (1953) suggested some more possible applications of TSL in archeological and geological dating, including radiation dosimetry. A lot of progress has taken place during 1960s and 1970s in this field and now TSL phenomenon is used in many fields with improved sophisticated techniques.

Thermally Stimulated Luminescence (TSL) is the emission of light (in excess of thermal radiation) from an insulator (or semiconductor) when the TSL material is heated (stimulation), following an initial irradiation (excitation) of the TSL material. This latter component (i.e. radiation absorption) is an essential feature of TSL phenomenon. The light emitted from the TSL material is proportional to the amount of radiation absorbed by the TSL material and hence this process can be used to estimate the dose (energy absorbed per unit mass of the material) absorbed in the material. The TSL phenomenon

has a very high sensitivity of detecting the presence of defect centers which are responsible for the TL process. Townsend and Kelly (1993) estimated that the technique is capable of detecting as few as 10 defects levels in the material.

This high sensitivity of the process allows the determination of very low radiation doses. On the other hand this high sensitivity hampers the investigation of the relation between the TSL and the defects involved the TSL process. This is because a very small change in the defect concentration responsible for TSL will give rise to an appreciable change in TSL output and this small variation in the defect concentrations is very difficult to detect by other techniques such as Optical Absorption (OA) and Electron Spin Resonance (ESR). TSL is one of a family of processes collectively known as thermally stimulated phenomenon. Other members of the family are thermally stimulated conductivity (TSC), thermally stimulated capacitance (TSCap), thermally stimulated polarization (TSPC) and depolarization currents (TSDC); including ionic thermocurrents (ITC), deep level transient spectroscopy (DLTS), thermo gravimetry (TG), and several more (Chen and Kirsh, 1981). Each of these phenomenons may be described by two fundamental stages: Stage I, the perturbation of the system from equilibrium into a metastable state; and stage II, the thermally stimulated relaxation of the system back to equilibrium. In each of the above techniques one monitors the no isothermal change of a particular property of the material (e.g., luminescence, conductivity, capacitance, etc) as the system returns to equilibrium during stage II.

In the case of TSL, stage I necessitates the absorption of energy, normally from ionizing radiation, in order to perturb the material into a nonequilibrium state. Energy storage occurs through the processes of electron-hole pair production, exciton creation, and/or direct displacement damage, followed by charge localization (trapping) at defects within the host lattice of the irradiation material.

During stage II, the stored energy is released as the temperature of the sample is increases, and a fraction of the released energy is in the form of luminescence. The luminescence originates from electron-hole recombination or vacancy-interstitial recombination. In either case, electrons undergo deexcitation from metastable excited states to the ground state, thereby restoring equilibrium. The simplest manner in which this can be achieved is via electron – hole recombination of thermally freed charges

(although the discussion could just as well proceed on the basis that it is holes that are thermally liberated). The process is initiated when phonon coupling between the trapped electron and the lattice results in the absorption of an amount of thermal energy by the electron. The probability per second that the amount of energy is enough to release the trapped electron from its localized state (i.e.to overcome the energy barrier E and undergo a transition into the conduction band is given by

$$P = s \exp\left(\frac{-E}{kT}\right)$$

where, 's' is frequency factor and is related to the local lattice vibration
frequency and the entropy change associated with the charge release. Thus, once the temperature is high enough, the electron will be released into conduction band and will then be free either to get retrapped (either in same or different localized states) or to recombine with trapped holes. The recombination process results in the emission of phonons (nonradiative recombination) or photons (radiative recombination). It is the latter that are monitored when recording the emission. Thus, we have the thermally stimulated return of the system from its metastable state to equilibrium, with a portion of the excess energy being liberated as light (McKeever, 1997).

2.4 Basic Phenomenon of Thermally Stimulated Luminescence:

The phenomenon underlying the TSL process is usually explained on the basis of band structure of electronic transition in an insulating material exhibiting TSL. The figure shows the simplest process one can visualize that can occur in the phosphor during and after exposure of ionizing radiation.

TL is usually observed by heating a sample at a constant rate to some temperature (e.g. 500C) and recording the luminescence emitted as function of temperature. The TL signal is characterized by a so-called "glow curve", with distinct peaks occurring at different temperatures, which relate to the electron traps present in the sample. Defects in the lattice structure are responsible for these traps. A typical defect may be created by the dislocation of a negative ion, providing a negative ion vacancy that acts as an electron trap. Once trapped, an electron will eventually be evicted by thermal vibrations of the lattice. As the temperature is raised these vibrations get stronger, and the

probability of eviction increases so rapidly that within a narrow temperature range trapped electrons are quickly liberated. Some electrons then give rise to radiative recombinations with trapped "holes", resulting in emission of light (TL). Although a TL glow curve may look like a smooth continuum, it is composed of a number of overlapping peaks derived from the thermal release of electrons from traps of different stabilities.

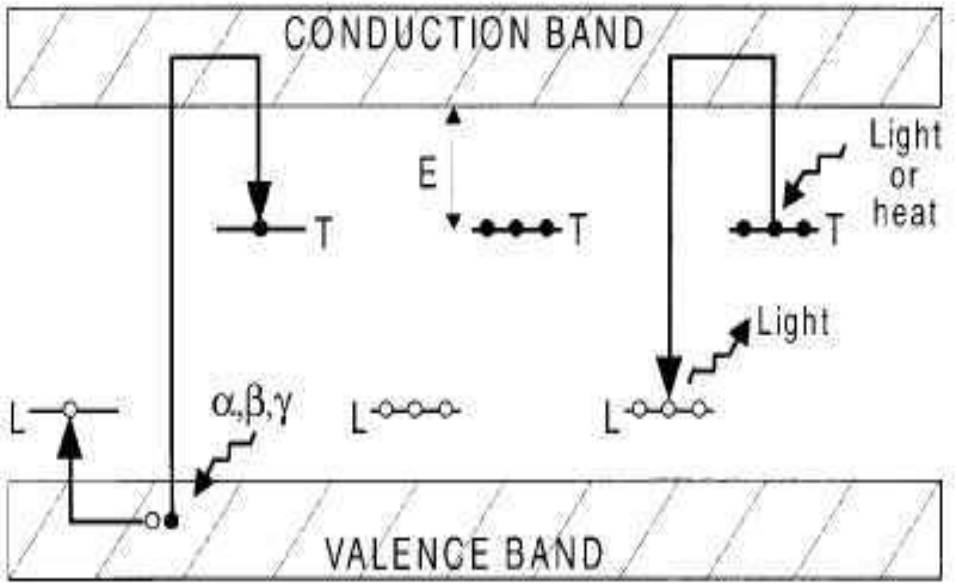

Fig. 2.1: The Energy-level representation of TL process

(I) Ionization (II) Storage (III) Eviction

Where, T = Electron Trap, L = Luminescence Center

(I) Ionization due to exposure to nuclear radiation with trapping of electrons and holes at defects T and L, respectively.

(II) Storage of radiation energy during time; if leakage is negligible the lifetime of the electrons in the traps needs to be much longer than the storage time of the sample. This lifetime is dependent on the energy depth E of the trap below the conduction band.

(III) By heating the sample, electrons are evicted from the electron traps and some of these reach luminescence centres (L); if so, light (i.e. TL) is emitted as a result of the process of recombining into these centres.

2.5 Dynamics of Detrapping (Trap Emptying Process):

Release of the charge carrier, i.e., the trapped electron or the hole from its trapped position is the most important step in the emission of TL. The release of the charge carrier can be achieved in two ways:

- Optical stimulation
- Thermal stimulation

In optical stimulation, an optical photon of energy greater than the binding energy of the charge carrier can knock out it from its trap by direct hit. In contrast to this the thermal stimulation process consists of multiple hits. The energy required for the release of the charge carrier is called the thermal activation energy. It is observed that thermal activation energy is always smaller than the optical activation energy. This arises due to the change in the configuration co-ordinates of the trap in the excited state than in the normal state.

An electron trapped at a depth of 1 eV get free at a temperature barely 100^0-200^0C, this is because the average thermal energy available at 200^0C is= 3/2 (273+200) = 0.04 eV, only, which is much smaller compared to 1eV (the activation energy). The Maxwell-Boaltzmann distribution for a system in equilibrium at temperature T tells that the fraction of the particles having thermal energy of 1eV above the ground level is $N/No= e^{-E/kT}$. For E=1eV and sample temperature, T=200^0C, this fraction would be about 10^{-13}. It is only this fraction which is capable of escaping from the trap. This however, is an incredibly small fraction to make an impact on the total population of the charge carriers in the traps. Yet the traps get emptied in 'no time' when the sample temperature is raised quickly to the peak temperature of the glow curve.

Two factors are reasonable for this: The few energetic electrons ($E \geq 1$ eV) make an attempt to escape into the conduction band at an incredibly fast rate. The attempt frequency is as high as 10^{13} second (vibrational frequency) this is called 'frequency factor' or more precisely 'attempt to escape frequency'. How does an electron or a hole make an attempt? –It is by jumping and knocking around randomly. Some knocks may push it backward from the 'mouth' of the trap.

Probability for escaping from the traps is given as

$$P = s\,\frac{N}{N_0}$$

$$P = s \exp\left(\frac{-E}{kT}\right)$$

Where, s=frequency factor.

If $s=10^{13}$ and $N/N_0=10^{-13}$, then P=1 per second. This means, 100 % probability for escaping from the traps. Apparently only an insignificant fraction i.e., 10^{-13}, is able to escape at any point of time when the glow peak is being emitted.

The second factor which helps to empty the traps quickly is the rapidness with which thermal equilibrium (Maxwell-Boltzmann distribution) is re-established after the charge carriers with E=1eV (i.e. 10^{-13} fraction) have escaped. To visualize the rapines with which equilibrium is re-established, we need to remember that the particles in equilibrium at room temperature have a velocity of 2000 ms^{-1}, which is approximately equivalent to 2×10^{13} lattice distances. This means that in 1 second 2×10^{13} knocks are exchanged by a single particle. Due to such a high frequency of collisions, the equilibrium is reestablished quickly. Thus once again we have particles with energy E=1eV. The process of re-establishing equilibrium and escaping (de-trapping) thus sustains (the phonon relaxation time is 10^{-13}second).

2.6 Mathematical description

2.6.1 First Order Kinetics

The most simplified mathematical model which describes the above process was first given by Randall and Wilkins (1945 a,b).

Consider a material containing defects which give rise to a single electron trap level, having trap depth or activation energy E containing n electrons at time r and at temperature T (in kelvin). The energy distribution of electrons within the trap will be

described by Boltzmann distribution, and hence the probability p of release of an electron from the trap is given by the Arrhenius equation,

$$P = s \exp\left(\frac{-E}{kT}\right) \quad \text{---------- (1)}$$

Where, k is Boltzmann's constant and s is a frequency factor or attempt to escape factor having value in the order of the lattice vibration frequency, namely 10^{12}-10^{14} s^{-1}. The rate of release of electrons from the trap is

$$-\frac{dn}{dt} = n\, s \exp\left(\frac{-E}{kT}\right) \quad \text{----------(2)}$$

Randall and Wilkins assumed that all electrons released from traps undergo TSL transitions, i.e., there is no retrapping. This leads to the concept that the rate of release is proportional to the trapped charge concentration, and thus termed a "first-order" reaction. The intensity of the TSL glow, I (t) depends on the rate of release of electrons from traps and their rate of arrival at luminescence centers:

$$I(t) = -C\left(\frac{dn}{dt}\right) = C\, ns \exp\left(\frac{-E}{kT}\right) \quad \text{\_\_\_\_\_ (3)}$$

Where C is a constant related to luminescence efficiency.

$$\text{Heating rate,} \quad \beta = \frac{dT}{dt} \quad \text{\_\_\_\_\_(4)}$$

Equation (2) becomes

$$\frac{dn}{dT} = -\left(1/\beta\right) n\, s \exp\left(\frac{-E}{kT}\right) \quad \text{\_\_\_\_\_(5)}$$

Integrating above equation we get,

$$\ln\left(\frac{n}{n_0}\right) = -\int \left(\frac{1}{\beta}\right) s \exp\left(\frac{-E}{kT}\right) dT \quad \text{\_\_\_\_\_(6)}$$

Where, n_0 is the number of electrons present in the trap at time t_0 and temperature T_0. Finally, substituting for n in equation (3),

$$I(T) = n_0 \, s \exp\left(\frac{-E}{kT}\right) \exp\left\{\frac{-s}{\beta} \int_{T_0}^{T} \exp\left(\frac{-E}{kT}\right) dT\right\} \quad \text{___(7)}$$

This is the expression for the glow intensity I from electrons trap at a single trapping level E. It is a Randall and Wilkins expression for first order (monomolecular) kinetics. The plot of I against T is termed as glow curve. The glow curve has a characteristics asymmetric shape being wider on the low temperature side than on the high temperature side. The condition of maximum intensity can be found by differentiating equation (7) with respect to T and equating the derivative to zero (i.e. $\left(\frac{dI}{dT}\right)_{T=T_m} = 0$ which yields,

$$\frac{\beta E}{kT_m^2} = s \exp\left(\frac{-E}{kT_m}\right) \quad \text{_____(8)}$$

where, Tm is glow peak temperature.

From equation (1) and (8) it is concluded that greater the value of E andsmaller the value of s, the greater is the thermal stability of the trapped electrons and hence the higher is the temperature of the glow peak.

2.6.2 Second Order Kinetics

A modification of this view was presented by Garlick and Gibson (1948), who used this same one-trap, one-recombination center model but who included the concept of significant retrapping of the released charges. This leads to the rate of the reaction being proportional to the square of the trapped charge concentration, and thus, we have a "second-order" reaction. Here we have

$$\frac{dn}{dt} = -n^2 \, s' \exp\left(\frac{-E}{kT}\right) \quad \text{_____(9)}$$

where, s' = s/N, and N is the total concentration of available electron traps. This leads to the Garlick-Gibson equation for TSL under second-order kinetics,

$$I(t) = \frac{n_0^2 s' \exp\left(\frac{-E}{kT}\right)}{\left[1+\frac{n_0 s'}{\beta}\int_{T_0}^{T} \exp\left(\frac{-E}{kT}\right) dT\right]} \quad \text{(10)}$$

The main feature of this equations is that the glow is nearly symmetric, with the high temperature half of the curve slightly broader than the low temperature half. This can be understood from the consideration of the fact that in the second order reaction, significant concentrations of released electrons are retrapped before they recombine in this way giving rise to a delay in the TSL and spreading out of the emission over a wider temperature range (Bos, 2001).

2.6.3 General Order Kinetics

The Randall-Wilkins and Garlick-Gibson forms of TSL equation have been derived with the use of specific assumptions concerning the relative values of the retrapping and recombination probabilities. However, when these simplifying assumptions do not hold, the TSL peak will fit neither first- nor the second order kinetics. May and Partridge (1964) gave the following empirical expression for general order TSL kinetics

$$I(t) = -\frac{dn}{dt} = n^b s' \exp\left(\frac{-E}{kT}\right) \quad \text{(11)}$$

Where, s' has the dimension of $m^{3(b-1)}s^{-1}$ and b is defined as the general-order parameter and is not necessarily 1 or 2. Integration of the above equation for $b \neq 1$ yields,

$$I(t) = s' n_0 \exp\left(\frac{-E}{kT}\right) \times \left[1 + (b-1)\frac{s'}{\beta}\int_{T_0}^{T} \exp\left(\frac{-E}{kT}\right) dT\right]^{\frac{-b}{b-1}} \quad \text{(12)}$$

Where, $s'' = s' n_0^{b-1}$ with units s^{-1}. The above equation includes the second order case (b=2) and reduces to equation (7) when $b \rightarrow 1$. It should be noted that the dimensions of s' is $m^{3(b-1)}$ s^{-1}which means that the dimension changes with the order of kinetics b. Thus, it is difficult to interpret physically.

The theoretical mechanism discussed above is related only to electrons trapped at a single trapping level. In real phosphors many different trapping levels will be present,

each one due to a particular lattice defect or complex of defects. Each trapping level will give rise to an associated glow peak maximum, which may or may not be resolved during readout. The area and peak height of each glow peak depends on number of associated electron traps present. This in turn depends on the number of lattice defects and, for real phosphors, on the type and amount of impurity atoms present, as well as on the thermal history and treatment of the material.

2.7 Determination of Thermally Stimulated Luminescence (TSL) parameters:

During the process of TSL, part of energy, absorbed by the phosphor crystals, is re-emitted during subsequent heating, in the form of light. The plot of the TSL intensity (light output) as a function of rising temperature (at a constant rate of increase in temperature i.e. ß = dT/dt = constant) exhibits one or more peaks and is called a glow curve.

The glow curve provides a useful tool for studying the traps and trapping parameters (such as trap depth E, kinetic order b and frequency factors, etc.). Number of methods based on different models that explain the TSL behavior of different phosphor systems, have been developed (Braunlich, 1968, Chen 1969 a, b) for determination of trapping parameters utilizing the glow curve technique. All the models are statistical in nature and describe the distribution of electron traps over the level in the forbidden band, which takes place during the warming up of the phosphor. Based on these models different expressions have been derived for calculation of electron or hole trap depths from conduction or valence band respectively, using different experimental methods such as shape of the glow curve, glow peak maxima and change in the maximum peak temperature and different heating rate and isothermal decay method. Hoogenstraten (1958), Nicholas and Woods (1964), Braunlich (1968), Chen and Krish (1981), Shalgaonkar and Narlikar (1972), Nambi (1977), Kivits and Hagebeuk (1977), McKeever (1985), Mahesh et al. (1989) and Azorin and Nito (1990) have made a critical review of all these methods.

The values of trap depths for the same material by different methods are found to be somewhat different and also discrepancies in the results are observed when the same material is used by different workers for the calculation of trapping parameters (Kelly, 1970). These discrepancies are because of different approximations and models used

by different workers, different levels of impurities present in the sample and various experimental conditions employed. However, the study of trapping parameters gives definite information regarding the order of kinetics, trap (energy) distribution and frequency factor. These methods can broadly be divided in the following categories.

1. Empirical method (Urbach's method) (Urbach, 1930)
2. Initial rise method (Garlic and Gibson, 1948)
3. Variable heating rate method (Bohum, 1954, Booth, 1954, Parfianovitvh, 1954, Halperin and Braner, 1960, Chem 1969a)
4. Isothermal decay method (Randall and Wilkins, 1945b, May and Partrigdge, 1964)
5. Peak shape methods (Grossweiner, 1953, Halperin and Braner, 1960, Chen, 1969a, b)
6. Numerical curve fitting method (Mohan & Chen 1970)

All these methods require reliable temperature control and separation of glow peaks is a necessity in most of the glow curves as these methods mainly use peak resolution technique. However, in complex glow curves it may not be that easy.

The isothermal decay method, for determination of thermal activation energy, is the only method, which is not affected by temperature and emission spectra and allows estimation of the order of kinetics b for general order case. For the first-order kinetics, the TSL will decay exponentially with time and a plot of $\ln\left(I/I_0\right) \rightarrow t$ will give a straight line of slope m = s exp (-E/kT). If the decay is monitored at several different temperatures a plot of ln(m) vs. 1/T will give a straight line of slope E/k from which E can be calculated. The intercept will give ln(s). The general order feature of the isothermal decay of TSL can be demonstrated if a plot of $I^{(1-b)/b}$ vs. t yields a straight line. Since the value of b is not known before hand, a straight line will only be obtained when correct value of b is inserted.

The initial rise method is a widely used method for calculating trapping parameters (E & s) and is independent of order of kinetics. However, it is affected by satellite peaks and by thermal quenching (McKeever, 1985).

2.8 Applications:

The applications of the phenomenon of TSL to the measurement of dose have progressed a great deal since the initial work by Daniels and Colleagues (1953). Several thermoluminescent phosphors are now used routinely in many dosimetric applications for environmental monitoring, personnel dosimetry and medical applications. For dosimetric applications, it is always desirable to use TLD phosphors in various physical forms, as routine measurements with loose powder are quite cumbersome due to associated weighing of individual powder samples. A large number of dosimetry phosphors are now available in various physical forms such as single crystals, extruded ribbons (chips) in different thickness (0.15 to 0.8mm), micro rods, and sintered pellets and as thin substrates for beta and charged particle dosimetry.

However, among the large number of thermoluminescent materials investigated and described in the literature (Prokic and Botter-Jensen, 1993), only a few have been found to be attractive for dosimetry purposes, especially for applications in connection with personnel and environmental dosimetry.

2.8.1 TSL Dosimetry

In TSL dosimetry the relationship between the TSL signal and the absorbed dose to be measured must be determined by an appropriate calibration. Thermoluminescent Dosimeters (TLDs) have found increasing application with the progress made in the development of solid thermoluminescent dosimeters and instrumentation for reading them. Many TLD based systems are now commercially available, and are widely used in routine personal dosimetry, environmental monitoring and clinical radiation dosimetry. The extreme sensitivity of TSL for detecting the presence of defects, as few as 10^9 within a specimen is beneficial for detecting low radiation levels which are encountered in personal and environmental monitoring. Thermoluminescent Dosimeters (TLDs) are increasingly accepted for radiation dosimetry for the following reasons:

a. The existence of nearly tissue equivalent thermoluminescent materials;
b Sufficiently high sensitivity and accuracy for both personal and environmental monitoring;

c. Commercial availabitility as small sized solid detectors adaptable for both manual and automatic processing;
d. Suitability for skin and extremity dosimetry;
e. Availability of materials with excellent long-term stability under varying environmental conditions;
f. Ease of processing; g. Reusability;
h. Linearity of response with dose and dose rate over a large range.

2.8.2 Personnel Dosimetry

The primary objective of personnel dosimetry is the monitoring of radiation dose delivered to personnel during routine occupational exposure. Examples include workers in nuclear industry, hospital medical physicist and radiotherapy technicians, workers in industrial radiography and high intensity gamma irradiators and naval personnel on nuclear powered vessels. By means of such monitoring it is hoped to limit the exposure of such personnel to within prescribed safety limits, which are based on recommendations of the International Commission of Radiological Protection, publication 60 (ICRP 60).

Clearly, a major requirement of any TLD to be used in these applications is that it is tissue equivalent. The dose equivalent range of interest in this field is from 10^{-5}Sv to 10^{-1}Sv, with a required uncertainty in the calculated dose of ± 10-20% (McKeever, 1985).

2.8.3 Environmental Dosimetry

In recent years regulatory authorities in many countries have become more acutely aware of the increasing concern demonstrated by the public with regard to the potential environmental impact of "man-made" radiation exposure, controlled releases of gaseous radionuclides from nuclear power stations during day-to-day operations, low-level waste disposal, nuclear fuels reprocessing, incidents of nuclear power station accidents and activities connected with nuclear power industry have led to widespread public concern about possible detrimental effects to the public.

In many countries TLD systems are in place near nuclear installations for the purpose of monitoring pre-operational levels (background levels) as well as levels above the natural background, which can be linked with the operation of these facilities. Tissue equivalence is not an issue. However, since exposure levels are low (with a dose equivalent of typically, 10^{-2} mSv) long exposure times are required, and thus, long-term stability becomes vitally important, along with extreme sensitivity. Gamma emitters are the main radiation sources of interest (McKeever, 1985).

2.8.4 Clinical Dosimetry

The small size of TLD materials has long been exploited in clinical studies by inserting the TLDs (with proper covering and encapsulations) into appropriate openings on the human body before exposing the patient to ionizing radiations during diagnosis and/or therapy. The exposed TLDs are then retrieved and analyzed. In this way physicians are able to determine actual doses delivered to critical internal organs during these procedures and from such information are able to prescribe necessary additional treatments. Such utility is generally not possible with any other form of radiation dosimeter/detector.

The two areas of use for clinical radiation exposure of humans are diagnosis's radiology (e.g. X-ray exposure in mammography, dentistry and general health screening) and radiotherapy. Radiation types include X rays (as low as 10 keV), gamma rays (from Cs ^{137}or Co^{60}), high energy photon beams up to 25 MeV, electrons (up to 40 MeV), heavy charges particle and neutrons. Range of doses varies from 10^{-5} to 10^{-2} Gy in radiology, and up to 20-60 Gy in radiotherapy. For radiation therapy dose estimation accuracy of better than ±3% is aimed for since errors greater than this can adversely affect the outcome of the treatment.

Clearly, the foremost, requirement of a TLD material to be used in this fashion is tissue equivalency. High sensitivity is desirable so that TLD sizes can be kept as small as possible for *in vivo* measurements. Furthermore, since the doses used can be quite in radiotherapy a linear dose response over a wide dose range is an advantageous property (McKeever, 1985).

2.8.4 High Dose

The use of TLDs in monitoring high dose radiation (for example, from 10^2 Gy up to 10^6 Gy) is a further example of one of the mainstream uses of the technology. Such high doses may be found, for example, inside nuclear reactors, or during food sterilization and materials testing. The use of conventional TLDs in these dose regimes can be somewhat limited, however, due to the onset of sublinearity (saturation) of the TLD response. Some high temperature peaks in some TLD material (e.g. $CaSO_4$:Dy and LiF:Mg,Ti) have been used for these purposes since these appear to saturate at higher dose levels (McKeever, 1985).

2.8.5 Retrospective Dosimetry

Worldwide, interest is growing in the development of new and improved methods for retrospectively assessing the radiation dose in accidentally contaminated areas. For a number of years TSL techniques have been used with some success in this application. Examples include Chernobyl (Byelorussia and Ukraine) and the Techa River (Russia), along with similar efforts at Hiroshima and Nagasaki (Japan) and the Nevada bomb test (United States). The thrust has been to use commonly available materials, located at the actual sites. Example TSL materials that are proving to be useful in this context are pottery, the porcelain, and other ceramic objects. From these materials quartz and feldspar can extract, and the absorbed dose to these components is determined by TSL dosimetry techniques (McKeever, 1997).

2.8.6 Archeological Dating

The accumulated dose absorbed by ceramic artifacts over their archeological or geological lifetime can be appreciable, and this dose lends itself to determination of its age using TSL. The materials of interest are ceramics containing luminescent materials – particularly quartz and feldspar that, when heated after irradiation exposure, emit TSL proportional to the time of their exposure. The radiation originates from cosmic rays and from gamma, beta and alpha irradiation from the local surroundings (due to traces of uranium, thorium and potassium). The "natural" signal is thus related to the age of the specimen by

$$Age = \frac{Natural\ TSL}{TSL\ per\ unit\ dose} \times natural\ dose\ rate$$

Thus, age assessment consists of measurement of the natural TSL, calibrating the TSL signal from the material to determine the TSL per unit dose, and measurement of the natural dose rate in the location of the find(Aitken, 1974). Strictly, the "age" being determined is the time since the TSL signal was last reset to zero. Thus, a "zeroing" event – such as high temperature heating (e.g. in the manufacture of pottery) or optical bleaching (e.g., during the deposition of sediments) – must have occurred in order for the method to be applicable. Otherwise, a TSL signal related to the geological age of the component mineral will be determined instead (McKeever, 1985).

2.8.7 Other Applications

Age determination and radiation dosimetry are the two most extensive applications of TSL. It is also used in solid state physics as a tool for detecting the presence of defects and for establishing such parameters as the trap depth and capture cross sections, along with information regarding the dynamics of the various charge recombination kinetics (McKeever, 1997). The TSL has also found use in both terrestrial and extraterrestrial geology for mineral identification and for determining the classification and the irradiation and thermal histories of meteorites, source identification for various minerals, radioactive ore, and oil and gas well prospecting (McKeever, 1985).

APPLICATIONS OF THERMOLUMINESCENCE

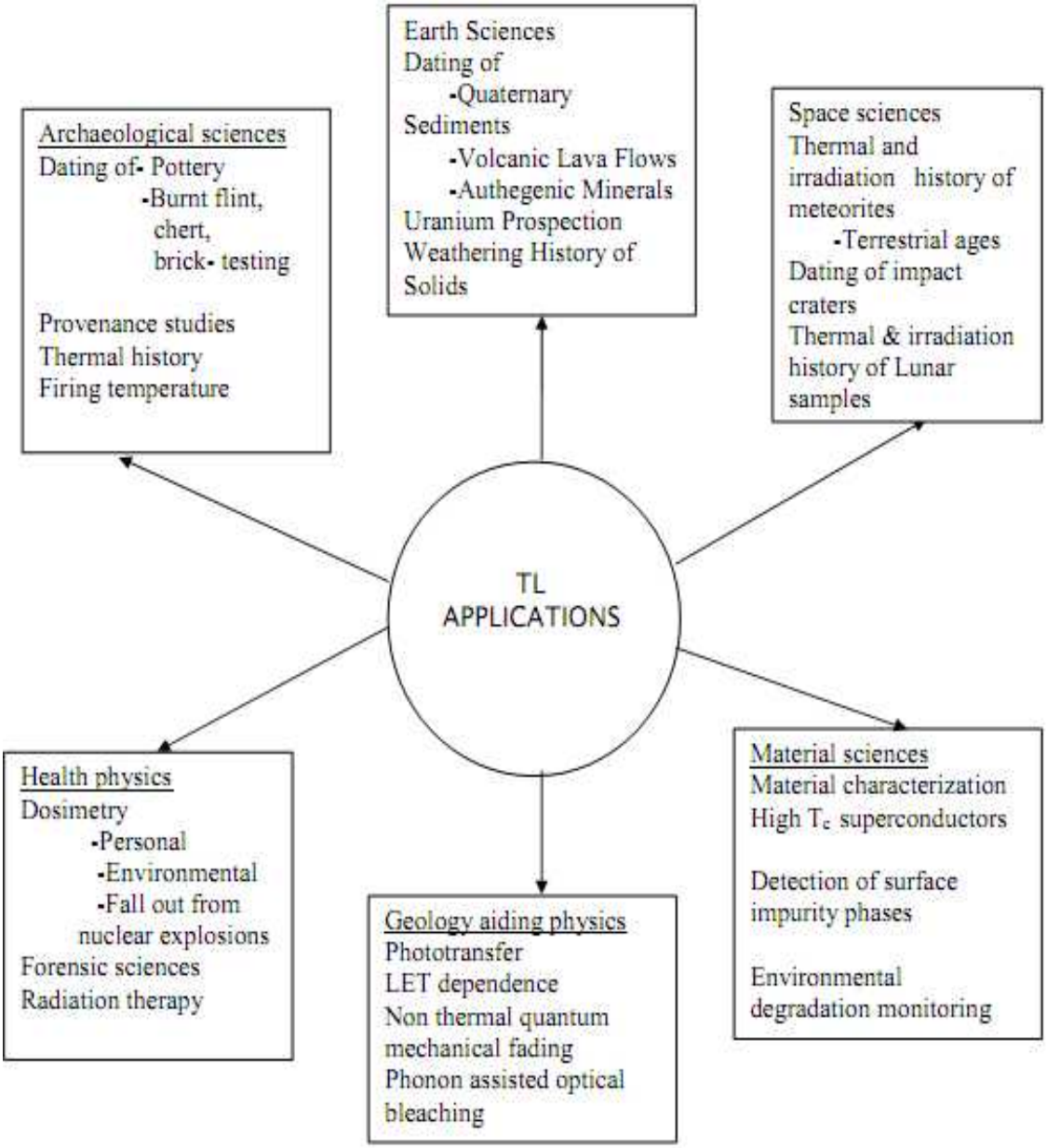

Fig. 2.2: Schematic representation of Applications of TL

2.9 Minerals

This section contains some introduction of the minerals selected for the research, like origin, classification, crystal system, physical properties etc.

2.9.1 Dolomite

- Chemistry: $CaMg(CO_3)_2$, Calcium Magnesium Carbonate
- Class: Carbonates
- Group: Dolomite

Dolomite, which is named for the French mineralogist Deodat de Dolomieu, is a common sedimentary rock-forming mineral that can be found in massive beds several hundred feet thick. They are found all over the world and are quite common in sedimentary rock sequences. These rocks are called appropriately enough dolomite or dolomitic limestone. Disputes have arisen as to how these dolomite beds formed and the debate has been called the "Dolomite Problem". Dolomite at present time, does not form on the surface of the earth; yet massive layers of dolomite can be found in ancient rocks. That is quite a problem for sedimentologists who see sandstones, shales and lime stones formed today almost before their eyes. Why no dolomite? Well there are no good simple answers, but it appears that dolomite rock is one of the few sedimentary rocks that undergo a significant mineralogical change after it is deposited. They are originally deposited as calcite/aragonite rich limes tones, but during a process call diagenesis the calcite and/or aragonite is altered to dolomite. The process is not metamorphism, but something just short of that. Magnesium rich ground waters that have a significant amount of salinity are probably crucial and warm, tropical near ocean environments are probably the best source of dolomite formation.

Dolomite in addition to the sedimentary beds is also found in metamorphic marbles, hydrothermal veins and replacement deposits. Except in its pink, curved crystal habit dolomite is hard to distinguish from its second cousin, calcite. But calcite is far more common and effervesces easily when acid is applied to it. But this is not the case with dolomite which only weakly bubbles with acid and only when the acid is warm or the dolomite is powdered. Dolomite is also slightly harder, denser and never forms scalenohedrons (calcite's most typical habit).

Dolomite differs from calcite, $CaCO_3$, in the addition of magnesium ions to make the formula, $CaMg(CO_3)_2$. The magnesium ions are not the same size as calcium and the two ions seem incompatible in the same layer. In calcite the structure is composed of alternating layers of carbonate ions, CO_3, and calcium ions. In dolomite, the magnesium occupy one layer by themselves followed by a carbonate layer which is followed by an exclusively calcite layer and so forth. Why the alternating layers? It is probably the significant size difference between calcium and magnesium and it is more stable to group the differing sized ions into same sized layers. Other carbonate minerals that have this alternating layered structure belong to the Dolomite Group. Dolomite is the principle member of the Dolomite Group of minerals which includes ankerite, the only other somewhat common member.

Dolomite forms rhombohedrons as its typical crystal habit. But for some reason, possibly twinning, some crystals curve into saddle-shaped crystals. These crystals represent a unique crystal habit that is well known as classical dolomite. Not all crystals of dolomite are curved and some impressive specimens show well formed, sharp rhombohedrons. The luster of dolomite is unique as well and is probably the best illustration of a pearly luster. The pearl-like effect is best seen on the curved crystals as a sheen of light can sweep across the curved surface. Dolomite can be several different colors, but colorless and white are very common. However it is dolomite's pink color that sets another unique characteristic for dolomite. Crystals of dolomite are well known for their typical beautiful pink color, pearly luster and unusual crystal habit and it is these clusters that make very attractive specimens.

Physical characteristics:

- **Color** is often pink or pinkish and can be colorless, white, yellow, gray or even brown or black when iron is present in the crystal.
- **Luster** is pearly to vitreous to dull.
- **Transparency** crystals are transparent to translucent.
- **Crystal System** is trigonal; bar 3
- **Crystal Habits** include saddle shaped rhombohedral twins and simple rhombs some with slightly curved faces, also prismatic, massive, granular and rock forming. Never found in scalenohedrons.
- **Cleavage** is perfect in three directions forming rhombohedrons.

- **Fracture** is conchoidal.
- **Hardness** is 3.5-4
- **Specific Gravity** is 2.86 (average)
- **Streak** is white.
- **Other Characteristics:** Unlike calcite, effervesces weakly with warm acid or when first powdered with cold HCl.
- **Associated Minerals:** include calcite, sulfide ore minerals, fluorite, barite, quartz and occasionally with gold**.**
- **Best Field Indicators** are typical pink color, crystal habit, hardness, slow reaction to acid, density and luster.

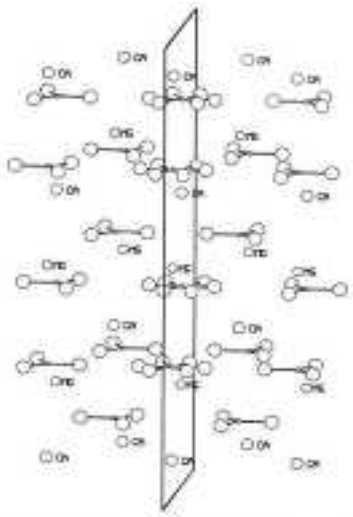

Fig. 2.3: Twinned structure of dolomite.

The c axis is nearly vertical and a_2 is nearly horizontal. The mirror is perpendicular to a_2. Anion disorder occurs only for the CO_3^{-2} groups lying in the composition plane.

2.9.2 Fluorspar

- Chemistry: CaF2, Calcium Fluoride
- Class: Halides

When found in nature, fluorspar is known by the mineral name *fluorite*. Fluorspar (fluorite) is calcium fluoride (CaF_2). It is found in a variety of geologic environments. Fluorspar is found in granite (igneous rock), it fills cracks and holes in sandstone, and it is found in large deposits in limestone (sedimentary rock). The term fluorspar, when

used as a commodity name, also refers to calcium fluoride formed as a by-product of industrial processes.

Fluorspar is relatively soft, number 4 on Moh's scale of hardness. Pure fluorspar is colorless, but a variety of impurities give fluorite a rainbow of different colors, including green, purple, blue, yellow, pink, brown, and black. It has a pronounced cleavage, which means it breaks on flat planes. Fluorite crystals can be well formed, beautiful and highly prized by collectors. Despite its beauty and physical properties, fluorspar is primarily valuable for its fluorine content.

Name

Even though fluorite contains the element fluorine, its name is not derived from its chemical composition. The name was given by Georg Agricola in 1546 and was derived from the Latin verb *fluere* which means *to flow* because it melts easily. *Spar* is a generic name used by mineralogists to refer to any non-metallic mineral that breaks easily to produce flat surfaces and which has a glassy luster. A miner's name used long ago for fluorite was *Blue John*.

Fluorite is a mineral with a veritable bouquet of brilliant colors. Fluorite is well known and prized for its glassy luster and rich variety of colors. The range of common colors for fluorite starting from the hallmark color purple, then blue, green, yellow, colorless, brown, pink, black and reddish orange is amazing and is only rivaled in color range by quartz. Intermediate pastels between the previously mentioned colors are also possible. It is easy to see why fluorite earns the reputation as *"The Most Colorful Mineral in the World"*.

The many colors of fluorite are truly wonderful. The rich purple color is by far fluorite's most famous and popular color. It easily competes with the beautiful purple of amethyst. Often specimens of fluorite and amethyst with similar shades of purple are used in mineral identification classes to illustrate the folly of using color as the sole means to identify minerals.

The blue, green and yellow varieties of fluorite are also deeply colored, popular and attractive. The colorless variety is not as well received as the colored varieties, but their rarity still makes them sought after by collectors. A brown variety found in Ohio and elsewhere has a distinctive iridescence that improves an otherwise poor color for fluorite. The rarer colors of pink, reddish orange (rose) and even black are usually very attractive and in demand.

Most specimens of fluorite have a single color, but a significant percentage of fluorites have multiple colors and the colors are arranged in bands or zones that correspond to the shapes of fluorite's crystals. In other words, the typical habit of fluorite is a cube and the color zones are often in cubic arrangement. The effect is similar to phantomed crystals that appear to have crystals within crystals that are of differing colors. A fluorite crystal could have a clear outer zone allowing a cube of purple fluorite to be seen inside. Sometimes the less common habits such as a colored octahedron are seen inside of a colorless cube. One crystal of fluorite could potentially have four or five different color zones or bands.

To top it all off, fluorite is frequently fluorescent and, like its *normal light* colors, its fluorescent colors are extremely variable. Typically it fluoresces blue but other fluorescent colors include yellow, green, red, white and purple. Some specimens have the added effect of simultaneously having a different color under long wave UV light from its color under shortwave UV light. And some will even demonstrate phosphorescence in a third color! That's four possible color luminescence in one specimen! If you count the normal light color too. The blue fluorescence has been attributed to the presence of europium ions (Eu +2). Yttrium is the activator for the yellow fluorescence. Green and red fluorescent activation is not exactly pinned down as of yet, but may be due to the elements already mentioned as well as other rare earth metals; also manganese, uranium or a combination of these. Even unbounded fluorine trapped in the structure has been suggested. The word fluorescent was derived from fluorite since specimens of fluorite were some of the first fluorescent specimens ever studied. The naming followed the naming precedence set by *opalescence* from opal; ergo *fluorescence* from fluorite.

Another unique luminescent property of fluorite is its thermoluminescence. Thermoluminescence is the ability to glow when heated. Not all fluorites do this; in

fact it is quite a rare phenomenon. A variety of fluorite known as *"chlorophane"* can demonstrate this property very well and will even thermoluminescence while the specimen is held in a person's hand activated by the person's own body heat (of course in a dark room, as it is not bright enough to be seen in daylight). The thermoluminescence is green to blue-green and can be produced on the coils of a heater or electric stove top. Once seen, the glow will fade away and can no longer by seen in the same specimen again. It is a one shot deal. Chlorophane (which means *to show green*) is found in very limited quantities at Amelia Court House, Virginia; Franklin, New Jersey and the Bluebird Mine, Arizona, USA; Gilgit, Pakistan; Mont Saint-Hilaire, Quebec, Canada and at Nerchinsk in the Ural Mountains, Russia.

Fluorite has other qualities besides its great color assortments that make it a popular mineral. It has several different crystal habits that always produce well formed, good, clean crystals. The cube is by far the most recognized habit of fluorite followed by the octahedron which is believed to form at higher temperatures than the cube. Although the cleavage of fluorite can produce an octahedral shape and these cleaved octahedrons are popular in rock shops the world over, the natural (e.g. uncleaved) octahedrons are harder to find.

A rarer habit variety is the twelve sided dodecahedron however it is never seen by itself and usually modifies the cubic crystals by replacing the edges of the cube with one flat face of a dodecahedron. The tetra hexahedron is a twenty four sided habit that is also seen modifying the cubic habit. But instead of one face replacing each cubic edge, two faces modify the cube's edges. Occasionally combinations of a cube, dodecahedron and tetra hexahedron are seen producing an overall cubic crystal with no less than three minor parallel faces replacing each cubic edge. A fifth form is the hex octahedron which modifies the cube by placing six very minor faces at each corner of the cube. Twinning is also common in fluorite and symmetrical penetration twins, especially from Cumberland England are much sought after by collectors.

Fluorite, as mention above, has octahedral cleavage. This means that it has four identical directions of cleavage and when cleaved in the right ways can produce a perfect octahedral shape. Many thousands of octahedrons are produced from massive or large undesirable crystals of fluorite (hopefully!) and are sold in rock shops and museum gift shops at a small cost. Fluorite mine workers are reported to sit down at

lunch breaks and cleave the octahedrons for the extra cash. The octahedrons are very popular due to their attractive colors, clarity, "*diamond-shaped*" and low costs, but to a serious collector they are nothing more than "*cleavage fragments*".

Fluorite not only is attractive in its own right but is often associated with other attractive minerals. Fluorite crystals will frequently accompany specimens of silver gray galena, brassy yellow pyrite, chalcopyrite or marcasite, golden barite, black sparkling sphalerite, intricately crystallized calcite and crystal clear quartz, even amethyst.

The origin of the word fluorite comes from the use of fluorite as a flux in steel and aluminum processing. It was originally referred to as *fluorospar* by miners and is still called that today. Fluorite is also used as a source of fluorine for hydrofluoric acid and fluorinated water. The element fluorine also gets its name from fluorite, fluorines only common mineral. Other uses of fluorite include an uncommon use as a gemstone (low hardness and good cleavage reduce its desirability as a gemstone), ornamental carvings (sometimes misleadingly called *Green Quartz*) and special optical uses.

Fluorite is the most popular mineral for mineral collectors in the world, second only to quartz. Every mineral collection owned by even the newest and youngest of mineral collectors must have a specimen of fluorite. Fluorite is by far one of the most beautiful and interesting minerals available on the mineral markets.

Physical characteristics:

- **Color** is extremely variable and many times can be an intense purple, blue, green or yellow; also colorless (Pure), reddish orange, pink, white and brown. A single crystal can be multi-colored.
- **Luster** is vitreous.
- **Transparency:** Crystals are transparent to translucent.
- **Crystal System:** Isometric; 4/m bar 3 2/m
- **Crystal Habits** include the typical cube and to a lesser extent, the octahedron as well as combinations of these two and other rarer isometric habits. Always with equant crystals; less common are crusts and botryoidal forms. Twinning also produces penetration twins that look like two cubes grown together.

- **Cleavage** is perfect in 4 directions forming octahedrons.
- **Fracture** is irregular and brittle.
- **Hardness** is 4
- **Specific Gravity** is 3.1+ (average)
- **Streak** is white.
- **Other Characteristics:** Often fluorescent blue or more rarely green, white, red or violet and may be thermoluminescent, phosphorescent and triboluminescent.
- **Associated Minerals** are many and include calcite, quartz, willemite, barite, witherite, apatite, chalcopyrite, galena, sphalerite, pyrite and other sulfides.
- **Best Field Indicators** are crystal habit, color zoning, hardness (harder than calcite, but softer than quartz or apatite), fluorescence and especially the octahedral cleavage.

Uses

Fluorite (fluorspar*)* used in production of hydrofluoric acid, which is used in the electroplating, stainless steel, refrigerant, and plastics industries; in production of aluminum fluoride, which is used in aluminum smelting; as a flux in ceramics and glass, and in steel furnaces; and in emery wheels, optics, and welding rods.

The majority of the United States' annual consumption of fluorspar is for the production of hydrofluoric acid (HF) and aluminum fluoride (AlF3). HF is a key ingredient for the production of all organic and non-organic chemicals that contain the element fluorine. It is also used in the manufacture of uranium. AlF3 is used in the production of aluminum. The remainder of fluorspar consumption is as a flux in making steel, glass, enamel, and other products. A flux is a substance that lowers the melting temperature of a material.

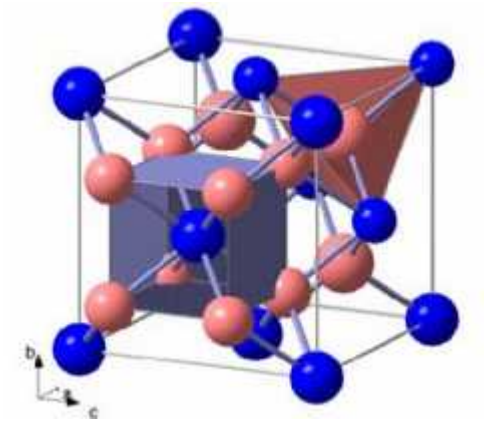

Fig.2.4: Crystal structure of fluorspar

2.9.3 APOPHYLLITE:

The mineral Hydrated Potassium Calcium Silicate Fluoride Hydroxide [$KFCa_4(SiO_5)_4$ $8H_2O$], which is generally known as Apophyllite classified as under.

Class: Silicate (Subclass : Phyllosilicate)

Group: Apophyllite.

Apophyllite, whose name roughly means "*to leaf apart*" in Greek, is a mineral classic. It was given its name because crystals tend to peel or flake apart when they are heated due to the loss of water molecules. Although not that well-known by the general public, apophyllite is quite popular among mineral collectors. It is probably the first exotic mineral that a young collector will own after filling up on specimens of calcite, quartz, pyrite, galena, mica, fluorite, gypsum, apatite, etc, etc. After these common minerals, apophyllite seems like a real rarity and it offers so much to the collector. It has beauty, pastel colors, a bright luster, interesting well formed habits, unusual associations with other exotic minerals and recently large amounts of quality specimens have become available at amazingly low prices compared to twenty years ago.

Apophyllite is a general term for three *official* minerals that are similar in their chemistry and physical properties. Below is a comparison of the three official apophyllite minerals.

Table- 2.1 The official apophyllites

MINERAL:	FORMULA:	SYMMETRY:	COLOR RANGE:
FLUOR-APOPHYLLITE	$(K,Na)Ca_4Si_8O_{20}(F, OH) - 8H_2O$	Tetragonal; 4/m 2/m 2/m	White, colorless, green, yellow or violet
HYDROXY-APOPHYLLITE	$KCa_4Si_8O_{20}(OH, F) - 8H_2O$	Tetragonal; 4/m 2/m 2/m	White or colorless
NATRO-APOPHYLLITE	$NaCa_4Si_8O_{20}F - 8H_2O$	Orthorhombic; 2/m 2/m 2/m (pseudo-tetragonal)	brown, brownish yellow, yellow or colorless

Fluorapophyllite is by far the most abundant and colorful of the three and is usually what is referred to when a specimen is just labeled apophyllite. Hydroxyapophyllite is also relatively common, but specimens typically lack any color and are limited to pseudo-cubic crystal habits. The natroapophyllite is quite rare and is found at only a few localities. Its typical brown color can help distinguish it from its close cousins. Natroapophyllite, by virtue of its more significant chemical and symmetrical difference, is truly a distinct mineral. Fluorapophyllite and hydroxyapophyllite however are a different story. The two are different minerals only because of the difference in the percentage of fluorine to hydroxyl ions. They represent the end members of a series that could be called the apophyllite series. The name apophyllite persists however and its usage is widespread, especially when distinguishing the true identity of specimens is difficult. Most mineral guide books list apophyllite as a single mineral and the rest of this discussion will deal with apophyllite in general.

Apophyllite is often thought of as a Zeolite Group mineral. But this would be wrong ! Zeolites are network silicates belonging to the Tectosilicate Subclass whereas apophyllite is a layered Phyllosilicate.The structural differences aside, apophyllite does have a lot of similar properties to many of the zeolite minerals. Chief among them is its low specific gravity, environment of formation and ability to lose water when heated (although it does not have the ability to re-absorb the water like zeolites). What confuses the issue is that frequently apophyllite and zeolites are associated together in low temperature/low pressure metamorphic environments. This is

fortunate for mineral collectors as there are few mineral combinations that can beat the awesome apophyllite, stilbite, heulandite and natrolite specimens for sheer aesthetic beauty!

Another typically associated mineral is the green translucent prehnite that forms a rolling carpet on top of which are scattered sparkling clear pseudo-cubic apophyllite crystals, making very attractive specimens. Kinoite from the Christmas Mine in Arizona is a beautiful blue color and is often coated in tiny sparkling apophyllite crystals. Apophyllite is commonly associated with exceptional quartz and calcite crystals as well.

What makes apophyllite so popular among collectors is its fantastic crystals with their gem-like vitreous to pearly luster. Apophyllite almost always forms good crystals of two major types. The favorite crystal habit is the rectangular prism capped by a steep four sided pyramid (*tetragonal dipyramid*). A doubly terminated crystal is exceptionally special. The faces of the pyramids are rotated 45 degrees with respect to the prism faces and so plunge down into the prism edges. This produces a diamond-shaped pyramidal face instead of a typical triangular pyramid face such as on quartz. The shape is an extraordinary example of tetragonal crystal form. Although normally colorless or white, colored examples of apophyllite are always treasured. By far its most impressive color is the pastel green color that augments specimens from Poona, India. Some crystals of apophyllite are cut as gems, but mostly just for collectors.

The other common crystal habit is a pseudo-cubic crystal that occurs when there is no pyramid and the prism is ended by a flat termination (*a pinacoid*). The pinacoid is a crystal form that is perpendicular to the length of the crystal and so can abruptly terminate the prism. It is often seen as simply truncating the pyramids by cutting off the points of the crystal. When the prism is short and blocky and there is no pyramidal face, then the pinacoid face can make the crystal appear cube shaped. However the prism faces are commonly striated and all in one direction while the pinacoid is smooth, giving its true symmetry away. Conversely, if the pyramid faces are the only dominant form then the crystal can fool someone in to thinking it is octahedral!

Apophyllite specimens are found in ancient lava and basalt flows. The crystals grow in the now solid cavities, called amygdules or vesicles, formed by air bubbles when

the rock was molten. Apophyllite is also found in the voids in the contact metamorphic zone limes tones that surround intrusive rocks.

Apophyllite lends it name to a small group of minerals called the Apophyllite Group which includes, in addition to fluorapophyllite, hydroxyapophyllite and natroapophyllite, the mineral carletonite with a formula of $KNa_4Ca_4(CO_3)_4Si_8O_{18}$ (F, OH) - H_2O. The Apophyllite Group is structurally very interesting. Like other members of the Phyllosilicates Subclass, the Apophyllite Group's structure is layered with alternating silicate sheets and the potassium, sodium, calcium, fluorine and water layers. But unlike other phyllosilicates, the Apophyllite Group silicate sheets are composed of interconnected four and eight-member rings. The sheets can be thought of as being like chicken wire with alternating octagon and square shaped holes. Both octagons and squares have fourfold symmetry and this is what gives these minerals their typical tetragonal or pseudo-tetragonal symmetry. Only Apophyllite Group members have this unique interconnected four and eight-member ring structure.

The physical characteristics of apophyllite:

- **Color** is clear, white, green, yellow, pink, violet or rarely brown.
- **Luster** is vitreous to pearly on cleavage surfaces.
- **Transparency:** Crystals are transparent to translucent.
- **Crystal System:** Tetragonal; 4/m 2/m 2/m; natroapophyllite is orthorhombic, 2/m 2/m 2/m.
- **Crystal Habits** include four sided prisms (with a square cross-section) truncated with either a steep four sided pyramid or a pinacoid termination or both. If the pyramids are missing, the crystals can look cubic. Rarely are the prisms missing, but if they are, crystals could appear octahedral because of the four sided pyramids. The faces of the pyramids do not lineup with the prism faces but with their edges, therefore the pyramid faces have four edges and appear diamond shaped instead of triangular like the pyramid faces of quartz. Rare tabular hydroxyapophyllite crystals are also known.
- **Cleavage**: perfect in one direction (basal).
- **Fracture**: uneven.
- **Hardness** is 4.5 - 5.
- **Specific Gravity:** 2.3 - 2.4 (lighter than most translucent minerals).

- **Streak:** white.
- **Other Characteristics:** Prism faces are striated lengthwise, some specimens are fluorescent and crystals will flake when heated.
- **Associated Minerals**: prehnite, quartz, heulandite, stilbite, natrolite, analcime, datolite, babingtonite, cavansite, calcite, idocrase, wollastonite, kinoite, gyrolite and many other zeolites.
- **Best Field Indicators** are crystal habit, striations, associations, environment of formation, cleavage and luster on cleavage surfaces.
- 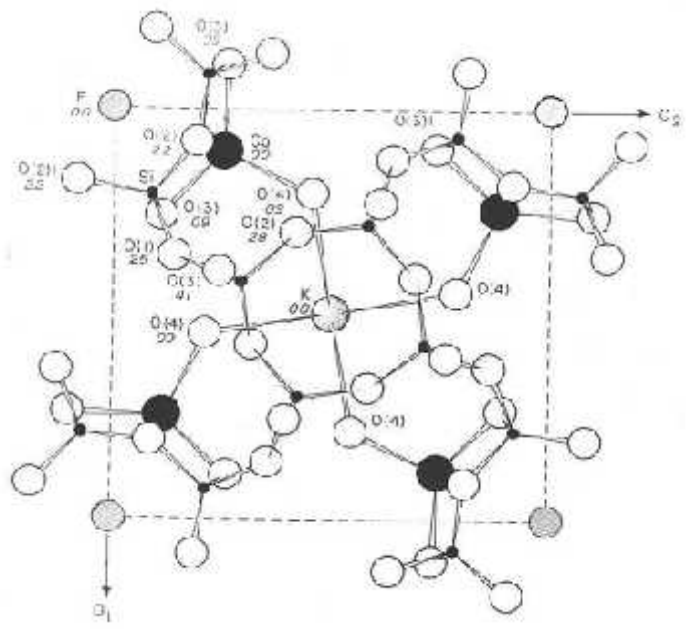

Fig. 2.5: Crystal Structure of apophyllite viewed along [001]

2.9.4 Heulandite

- Chemistry: $(Ca, Na)_{2-3}Al_3(Al, Si)_2Si_{13}O_{36} \cdot 12H_2O$, Hydrated Calcium Sodium Aluminum Silicate
- Class: Silicates
- Subclass: Tectosilicates
- Group: Zeolites
- Zeolite Family: Heulandite

Heulandite is the name of a series of tecto-silicate minerals of the zeolite group. Prior to 1997, heulandite was recognized as a mineral species, but a reclassification in 1997

by the International Mineralogical Association changed it to a series name, with the mineral species being named heulandite-Ca, heulandite-Na, heulandite-K, and heulandite-Sr. Heulandite-Ca, the most common of these, is a hydrous hydrous calcium and aluminium silicate, $(Ca,Na)_{2-3}Al_3(Al,Si)_2Si_{13}O_{36}\cdot 12H_2O$. Small amounts of sodium and potassium are usually present replacing part of the calcium. Strontium replaces calcium in the heulandite-Sr variety. The appropriate species name depends on the dominant element. The species are visually indistinguishable, and the series name heulandite is still used whenever testing has not been performed.

Crystals are monoclinic. They may have a characteristic coffin-shaped habit, but may also form simple rhombic prisms. Frequently, a crust of fine crystals will form with only the ends of the rhombs visible, making the crystals look like wedges. They have a perfect cleavage parallel to the plane of symmetry, on which the luster is markedly pearly; on other faces the luster is of the vitreous type. The mineral is usually colorless or white, but may be orange, brown, yellow, brick-red, or green due to inclusions of celadonite. It varies from transparent to translucent. Isomorphous with heulandite is the strontium and barium zeolite brewsterite.

The Mohs' hardness is 3-4, and the specific gravity 2.2. Heulandite is similar to stilbite. The two minerals may, however, be readily distinguished by the fact that in heulandite the acute positive bisectrix of the optic axes emerges perpendicular to the cleavage.

Heulandite was first separated from stilbite by August Breithaupt in 1818, and named by him "euzeolite" (meaning beautiful zeolite); independently, in 1822, H. J. Brooke arrived at the same result, giving the name heulandite, after the mineral collector, Henry Heuland (1778-1856).

Heulandite occurs with stilbite and other zeolites in the amygdaloidal cavities of basaltic volcanic rocks, and occasionally in gneiss and hydrothermal veins.
The best specimens are from the basalts of Berufjord, near Djupivogr, in Iceland and the Faroe Islands, and the Deccan traps of the Sahyadri Mountains near Bombay. Crystals of a brick-red colour are from Campsie Fells in Stirlingshire and

the Fassathal in Tirol. A variety known as beaumontite occurs as small yellow crystals on syenitic schist near Baltimore in Maryland.

Physical characteristics:

- **Color**: colorless, white, gray, green, pink, yellow, red, brown and black.
- **Luster:** vitreous to pearly on the most prominent pinacoid face and on cleavage surfaces.
- **Transparency:** Crystals are transparent but most commonly translucent.
- **Crystal System**: monoclinic; 2/m
- **Crystal Habits** include blocky crystals described as diamond-shaped, trapezoidal and old fashioned coffin shape with the two faces of a pinacoid usually prominent. Crystals are often modified by secondary faces with pairs of triangular faces very common. Prismatic and acicular forms are also known and are difficult to identify as heulandite. In aggregate specimens this face can be oriented upward producing a crust of curved pearly faces or it can be oriented to the side where the tops of the crystals jut out like the roof tops of a suburban community. Crystals can be simple or complexly modified by a variety of prism and pinacoid faces.
- **Cleavage:** perfect in one direction parallel to the prominent pinacoid face.
- **Fracture**: uneven.
- **Hardness:** 3.5 - 4, maybe softer on cleavage surfaces.
- **Specific Gravity**: approximately 2.1 - 2.3 (very light due to the open channels and high water content).
- **Streak**: white.
- **Associated Minerals** are extensive and include quartz, calcite, apophyllite, barite, pyrite, prehnite, pollucite, tourmaline, scolecite, analcime, chabazite, ferrierite, mordenite, laumontite, natrolite, stilbite and other zeolites.

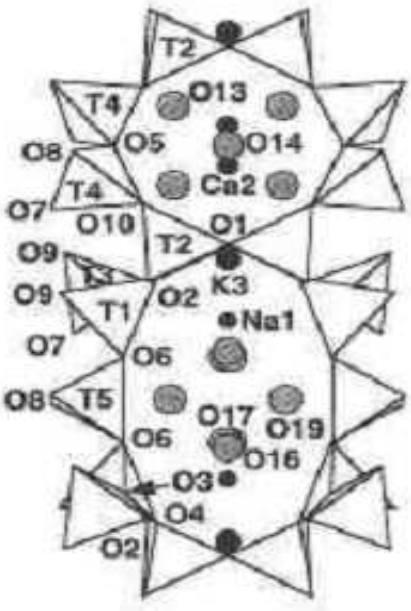

Fig. 2.6(A): Projections along [00l] displaying the larger A channel confined by ten tetrahedral and the B channel confined by eight tetrahedra.

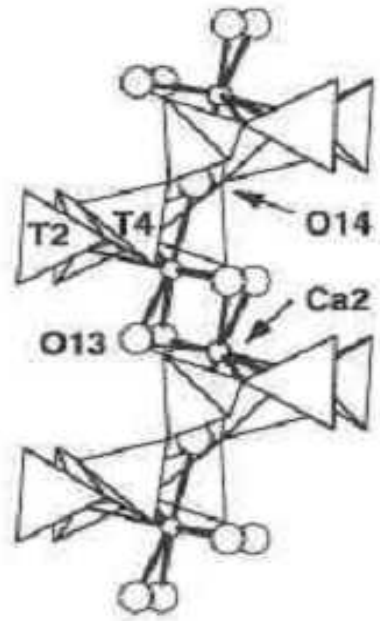

Fig. 2.6(B): Cation bonding in the B channel with c vertical and a rotated 13^0out of t he page.

2.9.5 PREHNITE:

Calcium aluminum silicate hydroxide [$Ca_2 Al_2 Si_3 O_{10}(OH)_2$] which is known as Prehnite is classified as under.

Class: Silicates

Subclass: Phyllosilicates

Prehnite is a common hydrothermal mineral in veins or cavities in igneous rocks. Often occurring as a mass of small radiating crystals in the form of rosettes. It is also found in some skarns and as a product of low-grade regional metamorphism. Often associated with pumpellyite.

Its color is usually a pleasant green and is at times quite unique to prehnite. Typical prehnite forms rather thick crusts with a rough or crystalline texture. Epimorphosis (crystal growth over the surface of another mineral) over laumontite crystals are

interesting and attractive. Usually the laumontite has dissolved away leaving the hollow crust of prehnite behind.

Prehnite is often found with zeolites and is sometimes thought of as a zeolite. But zeolites are actually tectosilicates and prehnite is a member the Phyllosilicates Subclass. However, like zeolites, prehnite can give off water when heated, but cannot gain the water back like they can. Like most zeolites, prehnite is formed as a result of low grade metamorphism usually from hydrothermal solutions. Crystals can be found in cavities of mafic igneous rocks.

Minerals that can be confused with prehnite include gyrolite, smithsonite and hemimorphite. Prehnite is harder than all of these and lacks smithsonite's unusual luster. Hemimorphite is usually blue and gyrolite is not as glassy. Prehnite can be associated with many beautiful minerals and can make a fine specimen on its own.

Physical characteristics:

- **Color** is usually a pale green to a yellowish grass green, also gray, white or colorless.
- **Luster** is vitreous to waxy or pearly.
- **Transparency:** Crystals are transparent to mostly translucent.
- **Crystal System** is orthorhombic; **2 m m.**
- **Crystal Habits** include nodular, concretionary, radial, encrusting and stalactitic formations among other similar types. Tabular or pyramidal individual crystals are rare but some nodular specimens show tabular crystal protrusions. Epimorphs (crystal growth over the surface of another mineral) over laumontite are usual, but available (see above).
- **Cleavage** is good in one direction (pinacoidal).
- **Fracture** is uneven.
- **Hardness** is 6 - 6.5.
- **Specific Gravity** is approximately 2.9+ (average).
- **Streak** is white.
- **Other Characteristics:** Lacks the luster of smithsonite and cleavage surfaces is curved and pearly.

- **Associated Minerals** include datolite, gyrolite, fluorapophyllite, quartz, calcite, copper, pectolite, stilbite and other zeolites.

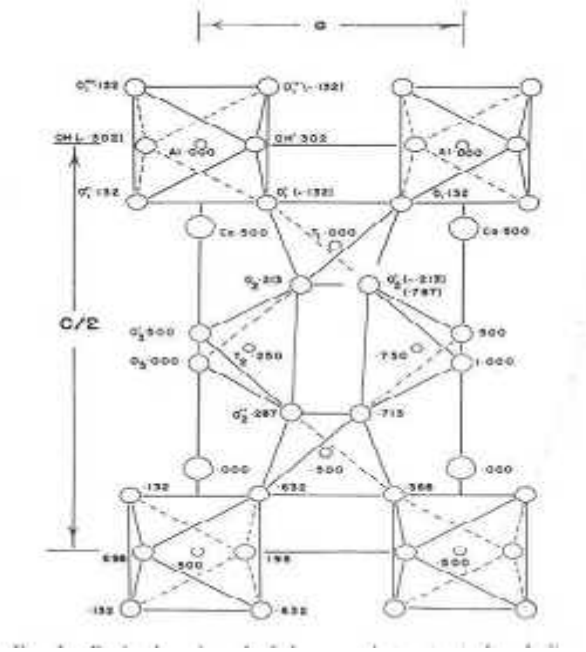

Fig. 2.7: The Projection along b of the crystal structure of prehnite.

2.9.6 STILBITE:

Hydrated sodium calcium aluminum silicate (Ca, Na_2) $Al_2Si_7O_{18}$ $6H_2O$, which is known as Stilbite is classified as under.

Class: Silicates

Subclass: Tektosilicates

Group: Zeolites

Uses: mineral specimen and chemical filter

Stilbite is a common and perhaps the most popular zeolite mineral for collectors. Stilbite crystals can aggregate together to form a structure resembling wheat sheafs. This hourglass structure looks like several crystals stacked parallel to each other with the tops and bottoms of this structure fanning out while the middle remains thin. Stilbite's hallmark crystal habit is unique to stilbite and a rarer but related zeolite called stellerite. Whether in the wheat sheafs or not, stilbite can be a handsome specimen with its pearly luster and often colorful pink tints. Stilbite commonly forms

nice crystals inside the petrified bubbles (called vesicles) of volcanic rocks that have undergone a small amount of metamorphism.

Stilbite's structure has a typical zeolite openness about it that allows large ions and molecules to reside and actually move around inside the overall framework. The structure contains open channels that allow water and large ions to travel into and out of the crystal structure. The size of these channels controls the size of the molecules or ions and therefore a zeolite like stilbite can act as a chemical sieve. Stilbite's structure contains rings of alumino-silicate tetrahedrons oriented in one direction and this produces the prominent pinacoid faces, the perfect cleavage and the unique luster on those faces.

Physical characteristics:

- **Color** is pink or white; also tinted yellow and red.
- **Luster** is vitreous to pearly especially on the prominent pinacoid and cleavage surfaces.
- **Transparency:** crystals are transparent to mostly translucent.
- **Crystal System** is monoclinic; 2/m
- **Crystal Habits** include platy often thin crystals that can aggregate together into a wheat sheaf like structure. The prominent pinacoid is sometimes but rarely modified by other pinacoid and prism faces. Cruciform (cross-like) twins can also be found. Also forms radiating nodules.
- **Cleavage** is perfect in one direction parallel to the prominent pinacoid.
- **Fracture** is uneven.
- **Hardness** is 3.5 - 4.
- **Specific Gravity** is approximately 2.2 (very light)
- **Streak** is white.
- **Associated Minerals** are quartz, calcite, babingtonite, apophyllite, heulandite, natrolite and other zeolites.
- **Notable Occurrences** include Poona, India; Scotland; Iceland; New Jersey and Nova Scotia, Canada.
- **Best Field Indicators** are crystal habit, luster, density and associations.

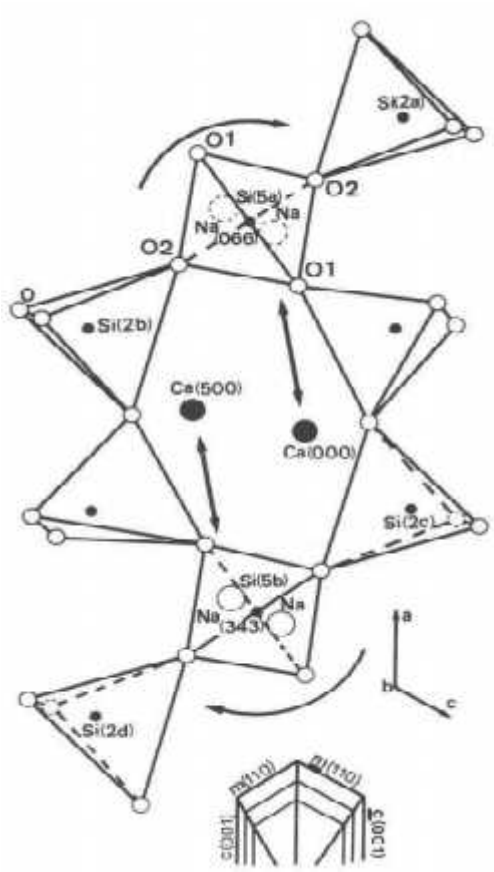

Fig. 2.8(A): Part of the structure of stilbite projected along the b axis.

Numbers adjacent to calcium and sodium give the heights of the atoms in thousandths of a cell edge. Rotations of the tetra hedra and sodium atoms are shown by curved arrows. Repulsion between sodium and calcium ions is shown by straight arrows. Also, schematic internal texture is shown below. The m and -m(l 10) are inclined to the plane of the figure, whereas c and -c(001) are normal to the plane of figure.

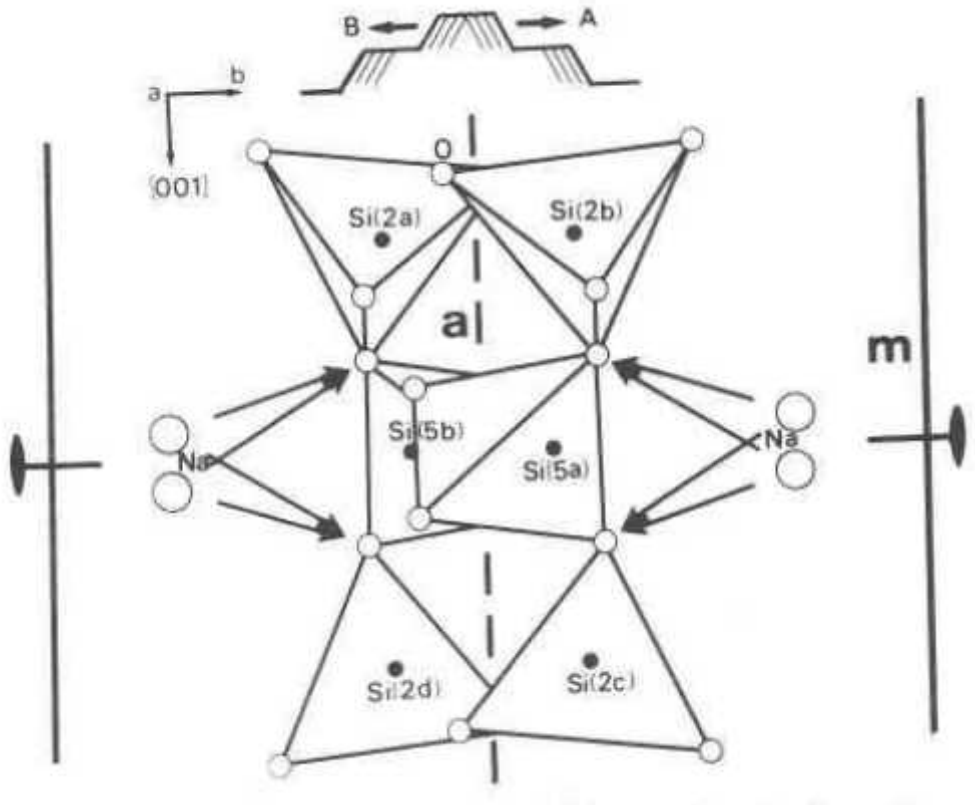

Fig.2.8 (B): Part of the structure of stilbite projected along the a-axis.
Two graph steps (A and B) move on vicinal faces normal to the plane of the figure in the direction shown by small arrows. Oxygen atoms bonded to sodium are shown by four large arrows. Mirror planes are vertical and diad axes are horizontal.

References:

1. Harvey E.: A History of Luminescence: From the Earliest Times Until 1900. Dover Phoenix Editions, USA (2005)
2. McKeever S.W.S., Moscovitch M., Townsend P.: Thermoluminescence Dosimetry Materials: Properties and Uses. Nuclear Technology Publishing, England (1995)
3. Harvey E.: A History of Luminescence: From the Earliest Times Until 1900. Dover Phoenix Editions, USA (2005)
4. Chen R., McKeever S.W.S.: Theory of Thermoluminescence and Related Phenomena. World Scientific Publishing Co. Pte. Ltd., Singapore (1997)
5. Furetta C.: Handbook of Thermoluminescence. World Scientific Publishing Co. Pte. Ltd., Singapore (2003)
6. Pekpak E.: Synthesis and Characterization of Lithium Tetraborate Doped with Metals. MS Thesis, METU, Ankara (2009)
7. Schauer D., Brodsky A., Sayeg J.: Handbook of Radioactivity Analysis, Second Edition. Academic Press, Great Britan (2003)
8. McKeever S. W. S.: Thermoluminescence of solids, Cambridge University Press, Cambridge (1983)
9. Kortov V., Materials for thermoluminescent dosimetry: Current status and future needs. Radiation Measurements(42), 576-581 (2007)
10. Cameron J.R., Suntharalingam N., Kenney G.K., Thermoluminescent Dosimetry, University of Wisconsin Press, Madison, WI (1968).
11. Attix F.H., Introduction to Radiological Physics and Radiation Dosimetry, Wiley, New York (1986).
12. Horton J.,Handbook of Radiation Therapy Physics, Prentice Hall, New York, (1987).
13. Gad Shani, Radiation dosimetry Instrumention and Methods, Second Edition, CRC Press, New York, 2000.
14. Palache C., H. Berman, and C. Frondel (1951) Dana's system of mineralogy, (7th edition), v. II, 208–217
15. Chang L.L.Y., R.A. Howie, and J. Zussman (1996) Rock-forming minerals, (2nd edition), v. 5B, non-silicates, 189–218.

16. Effenberger H., K. Mereiter and J. Zemann (1981) Crystal structure refinements of magnesite, calcite, rhodochrosite, siderite, smithsonite, and dolomite, with discussion of some aspects of the stereochemistry of calcite type carbonates. Zeits. Krist., 156, 233–243.
17. Howie R.A. and F.M. Broadhurst (1958) X-ray data for dolomite and ankerite, Amer. Mineral., 43, 1210–1214.
18. Hazen,R.M., and Finger,L.W.(1982) Comparative crystal chemistry. John Wiley, New York.
19. Higgs, D.V., and Handin, J.W. (1959) Experimental deformation of dolomite single crystals. Geological Society of America Bulletin, 70, 245-278.
20. Chao G. Y. (1971) The refinement of the crystal structure of apophyllite. II. Determination of The hydrogen positions by X-ray diffraction. American Mineralogist, 56, 123+1242.
21. Colville A.A., Anderson C.P., And Black P. M. (1971) Refinement Of the crystal structure of apophyllite. I. X-ray diffraction and physical properties. American Mineralogist 56, 1222-1233.
22. Dunn P. J. and Wilsor W. E. (1978) Nomenclature revisions in the apophyllite group: hydroxyapophyllite, apophyllite, fluorapophyllite. Mineralogical Record, 3, 95-98.
23. Dunn P. J., Rouse R. C. and Norberg J. A. (1978) Hydroxyapophyllite, A new mineral, and a redefinition of the apophyllite group. L Description, occurrences and nomenclature. American Mineralogist, 63, 196-199.
24. E. Prince, Refinement Of the crystal Structure Of Apophyllite III. Determination Of The hydrogen Positions By Neutron Diffraction, The American mineralogist, vol 56, July-august, 1971
25. Palache, C., H. Berman, and C. Frondel (1951) Dana's system of mineralogy (7th edition), v. II, 29–37.
26. Deer, W.A., R.A. Howie, and J. Zussman (1962) Rock-forming minerals, v. 5, non-silicates, 348–356.
27. Westbrook, J.H. and P.J. Jorgensen (1968) Effects of water desorption on indentation microhardness anisotropy in minerals. Amer. Mineral., 53, 1899–1909.
28. (1953) NBS Circ. 539, 1, 69.
29. Dana E.S. (1892) Dana's system of mineralogy, (6th edition), 573-576.

30. Deer W.A., R.A. Howie, and J. Zussman (1963) Rock-forming minerals, v. 4, framework silicates, 377-384.
31. Alietti A. (1972) Polymorphism and crystal chemistry of heulandites and clinoptilolites. Amer. Mineral., 57, 1448-1462.
32. Alberti A. (1972) On the crystal structure of the zeolite heulandite. Tschermaks Mineral. Petrog. Mitt., 18, 129-146.
33. Hambley T.W. and J.C. Taylor (1984) Neutron diffraction studies on natural heulandite and partially dehydrated heulandite. J. Solid State Chem., 54, 1-9.
34. Merkle A.B. and M. Slaughter (1968) Determination and refinement of the structure of heulandite (1968) Amer. Mineral., 53, 1120-1138.
35. J. J.Papike ORDERING OF TETRAHEDRAL ALUMINUM IN PREHNITE, The American Mineralogist, Vol.52, July-August,1967.
36. http://www.galleries.com/Minerals
37. http://www.mindat.org
38. http://webmineral.com/data/
39. Rosemarie Szostak, Handbook of molecular sieves
40. Mizuhiko Akizuki and HIroshi Koono Order disorder structure and the internal texture of stilbite, American Mineralogist, Volume 70, 814-821, 1985.

Chapter # 3

Instrumentation

3.1 Introduction:

This chapter describes the experimental technique used for the work. A brief description of collection of minerals and preparation technique of samples for TL study is given in first stage of this chapter then after a brief description of high temperature furnace, and brief description of the TL glow curve recorder, the Sr^{90} beta source, XRD and TGA (Thermal Gravimetric Analysis) also given with photographs of instruments and procedure.

3.2 Collection of the samples:

The required samples for TL studies for this work are collected from the different mines, of different villages of Chhotaudepur region, Baroda district, Gujarat. The samples are collected in the evening or morning, after the blasting in the mines. All the fresh samples are then collected and put in the plastic zip bag, and given the name of mine, location, and village. This plastic gag is also kept safe in the black box. There are twenty two samples are collected for study point of view and out of them twelve samples selected for TL characteristics study. Following twelve samples are selected for TL study. These all the samples are natural dolomite mineral and one sample of fluorspar is collected from the 'Amba Dungar', at Kadipani, GMDC's fluorspar project, Taluka-Kawant, District Baroda. Seven more samples are collected from Maharashtra, India.

Fig. 3.1: Mining activity at Chhotaudepur

Fig. 3.2: The collection of dolomite samples for present study.

Fig. 3.3: Dolomite samples collected for the TL study from the mines of Chhotaudepur

Fig. 3.4: Dolomite stones used in the construction of building.

Table: 3.1 Sample Codes:

Codes are given to the as received samples are as given below.

S. No.	Sample Name	Location/ Name of mines	Code
1	Dolomite	Khanij Mining-1 (Kanawat)	Z03
2	Dolomite	Khanij Mining-2 (Kanawat)	Z04
3	Dolomite	Jalaram Mining (Kanawat)	Z05
4	Dolomite	Shreeji Mining (Kanawat)	Z06
5	Dolomite	Bharat Mining (Kanawat)	Z07
6	Dolomite	Chamunda Mining (Kanawat)	Z08
7	Dolomite	Aaras Mining (Dadigaam)	Z09
8	Dolomite	Noor Mining (Dadigaam)	Z10
9	Dolomite	Mala Mining (Zair)	Z11
10	Dolomite	Alirajpur (M.P.)	Z12
11	Dolomite	Bachubhai (Bedvi)	Z13
12	Dolomite	Mala Mining (Bedvi)	Z14
13	Dolomite	R.C.Mistry (Bedvi)	Z15
14	Dolomite	Mine in the Centre of Bedvi	Z16
15	Dolomite	Kishanbhai (Bedvi)	Z17
16	Dolomite	Silver Mining (Bedvi)	Z18
17	Dolomite	Nazru sheth (Bedvi)	Z19
18	Dolomite	Madhav (Dhamodi)	Z20
19	Dolomite	Padaliya	Z21
20	Fluorspar	Amba dungar	Z22
21	Appophyllite	Jalgaon (M.S.)	Z23
22	Appophyllite	Nasik (M.S.)	Z24
23	Appophyllite	Mahod (M.S.)	Z25
24	Heulandite	Nasik (M.S.)	Z26
25	Prehnite	Mumbai (M.S.)	Z27
26	Stilbite	Mahad (M.S.)	Z28
27	Stilbite	Poona (M.S.)	Z29

3.3 Preparation of the samples:

Fig. 3.5: Hand Grinder (Agate: Mortar & pestle)

Fig. 3.6: Samples Ready for experiment

All the selected samples are filled into plastic zip bag after making powder to each material then after code are given to each sample as given bellow.

The above codes are quoted in each plastic bag of the sample. Then after high Alumina crucibles are taken and filled 30gram of each samples into the different crucibles these crucibles have high temperature stability against temperature. Then after all these crucibles are put in to the high temperature auto control furnace for heat treatment of annealing and quenching temperature for 200^0C, 400^0C, 600^0C and 800^0C step by step.

Fig. 3.7: High Alumina Crucibles

Fig. 3.8: Experiment Kit for Furnace

Thermal Annealing Treatment:

Thermal annealing for the specimen was carried out in the muffle furnace. The laboratory muffle furnace has temperature range up to 1200^0C and the size of chamber for sample heating was 22cm × 10cm × 10cm. The temperature was maintained with $\pm 1^0$C accuracy using a temperature controller, which supplied required current to the furnace. Power supply of 230V was provided to the furnace. A silica crucible containing a powdered form of virgin specimens was kept in the furnace at required annealing temperature for desired time. After completion of annealing duration the specimens were rapidly air-quenched to room temperature by withdrawing the silica crucible on to a ceramic block. Such material or specimens are called "annealed and quenched" or "thermally pre-treated specimen".

Fig. 3.9: High temperature Furnace

After the heat treatment all the samples are recollected into the particular zip bag indicating their code, Then after 5mg sample are collected from the each zip bag and irradiated it with beta source of 25Gy by Sr^{90}, after irradiation of the sample immediately TL is measured by TL recorder.

3.4 Radioactive Sources for Irradiation:

Strontium-90

β- Irradiation Sr^{90} source is used for the TL study. Strontium-90 (Sr^{90}) is a radioactive isotope of strontium, with a half life of 28.8 years

Natural strontium is nonradioactive and nontoxic, but Sr^{90} is a radioactivity hazard. Sr^{90}undergoes β decay with decay energy of 0.546 MeV to an electron and the yttrium

isotope Y^{90}, which in turn undergoes β- decay with half life of 64 hours and decay energy 2.28 MeV for beta particles to an electron and Zr^{90} (zirconium), which is stable. Note that $^{90}Sr/Y$ is almost a perfectly pure beta source; the gamma photon emission from the decay of Y^{90} is so weak that it can normally be ignored.

Fig. 3.10: Irradiation process by Sr^{90} beta source

Strontium-90	
General	
Name, symbol	Strontium-90, ^{90}Sr
Neutrons	52
Protons	38
Nuclide data	
Half-life	28.8 years
Decay products	^{90}Y
Decay mode	Beta decay
Decay energy	0.546 MeV

Sr^{90} finds extensive use in medicine and industry, as a radioactive source for thickness gauges and for superficial radiotherapy of some cancers. Controlled amounts of Sr^{90} and Sr^{89} can be used in treatment of bone cancer. As the radioactive decay of strontium-90 generates significant amount of heat, and is cheaper than the alternative Pu^{238}, it is used as a heat source in many Russian/Soviet radioisotope thermoelectric generators, usually in the form of strontium fluoride. It is also used as a radioactive tracer in medicine and agriculture.

Sr^{90} is a product of nuclear fission. It is present in significant amount in spent nuclear fuel and in radioactive waste from nuclear reactors and in nuclear fallout from nuclear tests. For thermal neutron fission as in today's nuclear power plants, the fission product yield from U^{235} is 5.8%, from U^{233} 6.8%, but from Pu^{239} only 2.1%. Together with cesium isotopes Cs^{134}, Cs^{137}, and iodine isotope I^{131} it was among the most important isotopes regarding health impacts after the Chernobyl disaster.

Strontium-90 is a "bone seeker" that exhibits biochemical behavior similar to calcium, the next lighter Group 2 element. After entering the organism, most often by ingestion with contaminated food or water, about 70-80% of the dose gets excreted. Virtually all remaining strontium-90 is deposited in bones and bone marrow, with the remaining 1% remaining in blood and soft tissues. Its presence in bones can cause bone cancer, cancer of nearby tissues, and leukemia. Exposure to Sr^{90} can be tested by a bioassay, most commonly by urinalysis.

Accidental mixing of radioactive sources containing strontium with metal scrap can result in production of radioactive steel. Discarded radioisotope thermoelectric generators are a major source of Sr^{90} contamination in the area of the former Soviet Union.

3.5 Units of radiation:

Rad (unit):

The **rad** is a largely obsolete unit of absorbed radiation dose, equal to 10 milliGray. The rad was first proposed in 1918 as "that quantity of X rays which when absorbed will cause the destruction of the [malignant mammalian] cells in question..."

It was defined in CGS units in 1953 as the dose causing 100 ergs of energy to be absorbed by one gram of matter. It was restated in SI units in 1970 as the dose causing 0.01 joule of energy to be absorbed per kilogram of matter.

The United States Nuclear Regulatory Commission requires the use of the units curie, rad, and rem as part of the Code of Federal Regulations 10CFR20.

However, it is now superseded in the SI by the gray; 1 rad is equal to 10 milligray, and 100 rads are equal to 1 Gy. The continued use of the rad is "strongly discouraged" by the author style guide of the U.S. National Institute of Standards and Technology.

Gray (unit)

The **gray** (symbol: Gy) is the SI unit of absorbed radiation dose of ionizing radiation (for example, X-rays), and is defined as the absorption of one joule of ionizing

radiation by one kilogram of matter (usually human tissue). It supersedes the old cgs unit, the rad (10 mGy), which is now "strongly discouraged."

"One gray is the absorption of one joule of energy, in the form of ionizing radiation, by one kilogram of matter."

$$1\text{Gy} = 1\frac{\text{J}}{\text{kg}} = 1\ \text{m}^2\ \text{s}^{-1}$$

For X-rays and gamma rays, these are the same units as the sievert (Sv). To avoid any risk of confusion between the absorbed dose (by matter) and the equivalent dose (by biological tissues), one must use the corresponding special units, namely the *gray* instead of the joule per kilogram for absorbed dose and the sievert instead of the joule per kilogram for the dose equivalent. The unit *gray* spells out the same in both the singular and the plural.

This SI unit is named after Louis Harold Gray. As with every SI unit whose name is derived from the proper name of a person, the first letter of its symbol is uppercase (**Gy**). When an SI unit is spelled out in English, it should always begin with a lowercase letter (**gray**), except where *any* word would be capitalized, such as at the beginning of a sentence or in capitalized material such as a title. Note that "degree Celsius" conforms to this rule because the "d" is lowercase. Based on the International System of Units.

Origin :

The gray was defined in 1975 in honor of Louis Harold Gray (1905–1965), who used a similar concept, "that amount of neutron radiation which produces an increment of energy in unit volume of tissue equal to the increment of energy produced in unit volume of water by one röntgen of radiation," in 1940.

Explanation:

The gray measures the deposited energy of radiation. The biological effects vary by the type and energy of the radiation and the organism and tissues involved. The sievert attempts to account for these variations. A whole-body exposure to 5 or more

gray of high-energy radiation at one time usually leads to death within 14 days (see Radiation poisoning for details). This dosage represents 375 joules for a 75 kg adult (equivalent to the chemical energy in 20 mg of sugar). Since gray are such large amounts of radiation, medical use of radiation is typically measured in milligrays (mGy).

The average radiation dose from an abdominal x-ray is 1.4 mGy, that from an abdominal CT scan is 8.0 mGy, that from a pelvic CT scan is 25 mGy, and that from a selective spiral CT scan of the abdomen and the pelvis is 30 mGy.

Conversions

1 rad is equal to 1 centi**gray**, and 300 krad are equal to 3 kGy.

The röntgen is defined as the radiation exposure equal to the quantity of ionizing radiation that will produce one esu of electricity in one cubic centimeter of dry air at 0°C and a standard atmosphere, and is conventionally taken to be worth 0.258 mC/kg (using a conventional air density of about 1.293 kg/m^3). Using air ionization energy of about 36.161 J/C, we have 1 Gy ˜ 115 R.

3.6 Thermoluminescence (TL) Set-up:

The specimen is spread uniformly (5mg weighed) over a metallic strip of Kanthal (Fe-72%, Ce-23%, Al–3%, and Co–2%). The strip is narrow and has a circular depression of 15 mm at its center. A chromel-alumel thermocouple is spot welded to record the temperature of the specimen. The uniform heating rate that is controlled by the temperature programmer maintains a linear relationship between the rises in temperature versus time. The photomultiplier tube is housed in a light-tight cylinder and a high voltage is applied to it. When the kanthal strip is loaded with the irradiated specimen which is placed in front of the photomultiplier window, the light emitted by the specimen during heating is recorded through the photomultiplier window.

Fig. 3.11: TL Reader set-up

Fig. 3.12: Kanthal Strip and TL detection head

The light emitted by the specimen during heating is detected by a photomultiplier tube and is recorded through auto ranging D.C. amplifier by the output device. In the present study, the thermoluminescence glow curves of the samples were taken on a Nucleonix make Windows Based thermoluminescence reader. The system consists of

a PMT housing with drawer assembly, high voltage module, AM576 TL data acquisition module with auto ranging facility, Temperature programmer controller unit, power supply unit, AD-DA card and a personal computer system along with required hardware and software. Block diagram is given bellow.

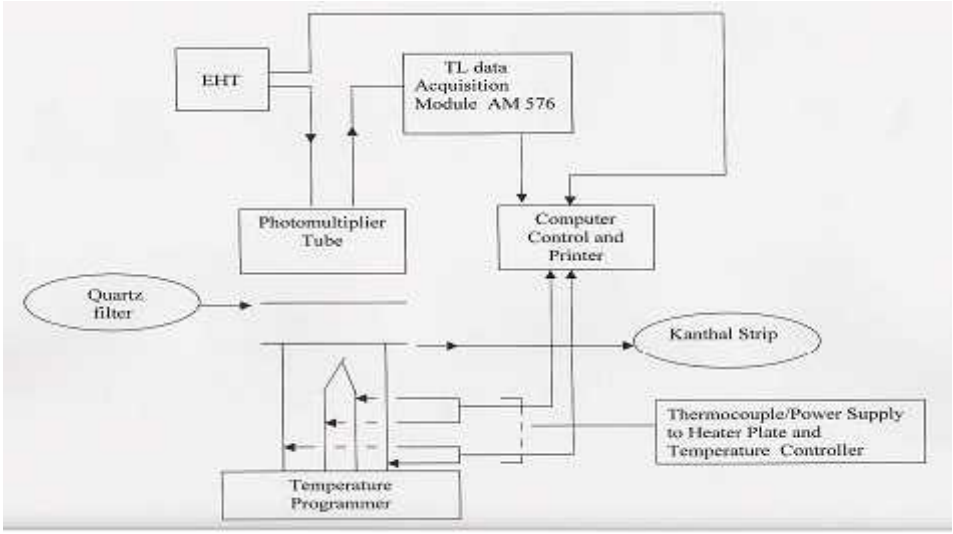

Fig. 3.13: Block Diagram of TL Set-up

The power supply provides four different outputs with a ripple and noise better than 3mV at full load for all the supplies. The TL data acquisition module AM 576 is a two bit module which converts the PMT current into a proportional voltage signal which is in built auto ranging facility. Due to this facility one can record TL intensity as a digitized signal and can be transferred to the computer. The temperature controller TC575 works in PC programmable mode as well as ISO mode. The temperature range is from room temperature to 500^0C, with an accuracy of $\pm 2^0$C. Temperature is increased by resistive heating and is measured by a thermocouple sensor. Various type of heating profiles, temperature in different regions, time heating rates, etc. can be set through the windows program specially developed for TL acquisition. The controller accepts DAC output signal from the AD – DA card to make up for the various functions. The high voltage unit, HV 501 generates EHT in the range of 0-1500V, 1mA, which is used for biasing the PMT. The ripple and noise is better than 15 mV. The PMT (type EMI 9924 B) and heater drawer assembly is a compact, light leakage free housing with PMT mounted inside. There is a IR cut-off, i.e. heat absorbing filter provided just below the PMT window. The housing has a kanthal strip with a circular depression of 15 mm diameter for loading of TL materials.

Among the computer components are, an IBM compatible Pentium-III 750 MHz or above with 64 MB RAM, 1.44 MB mini FDD, 40 GB Hard disc drive, SVGA color monitor and mouse and A4 size Inkjet printer, with color cartridge. The window-based software is developed in Visual C++ 4.0. The following is the procedure for making the TL measurements.

3.7 Procedure to Measure TL more accurately using NUCLEONIX PC based TL Reader System:

❖ Precautions to be observed for measurements with TL materials in powder form:

a. It is very important to measure the powder accurately and place it into the kanthal strip.
b. Accuracy depends mainly on the accurate weight measurement.
c. Powder should not be placed on the kanthal strip as a heap but should be spread uniformly. This ensures that while heating takes place all the particles in the powder get heated up to the same temperature.
d. While disposing from the kanthal strip, it should be gently brushed aside, so that powder particles fall on to the collection tray.
e. Any particle left out may contribute to the next measurement as a residual TL adding to the next sample, measurement being inaccurate to that extent.

❖ Choosing appropriate heating profile :

a. Depending on the type of TL material ($CaSO_4$, LiF or other material) and the form in which it is used (disc, rod, chip, powder crystals, pellets etc.) the heating profile is to be chosen.
b. The purpose of choosing most appropriate heating profile is primarily to maximize TL output and leave minimum residual TL in it. Also to minimize the contributions due to thermal and IR emissions.
c. Most commonly used heating profiles are:
    1. Linear
    2. Linear with cooling region included into total run time
    3. Linear clamped (Single plateau),

4. Linear clamped with cooling region included in run time.

d. For Teflon coated disc, it is desirable to choose either linear clamped or linear clamped with cooling region. Longer clamped duration may be required to ensure that TL emission is complete and residual TL is completely removed.
e. Clamping temperature around 300^0C is more than is enough in majority of cases for normal TL materials (other than pottery, sand and geological samples)
f. Thermal emission starts above 300^0C on wards hence it is important that we restrict heating to set temperatures up to maximum of 300^0C up to 350^0, in some cases provided there is good IR cut-off filtering done.
g. For low-level TL measurements if it is provided it helps in any spurious signal due to oxidation and other effects.
h. For low-level TL measurements it is better to choose a heating profile of "Linear clamped with cooling region included". Because some TL curve may extend in to this region. Also restrict clamping to 300^0C to restrict thermal contribution. Some time it may be better to clamp at 300^0C for certain time say 5 to 10 sec or even more to ensure that no residual TL is left. In which choose profile "C(4)" . For powder clamping for 5 to 10 sec may be enough. After first time TL acquisition, if you rerun the sample, you will get background profile, which will also indicate if there is some residual TL. For Teflon embedded / coated discs, recommended profile is "C (4)" and it is essential to clamp it for longer duration of the order of 40 to 60 sec. {Profile region {1-2}}. Linear heating region (0-1) may be about 60 sec and total run time can be about 150 sec to include some cooling region.
i. The best way to require for background is after the TL glow curve acquisition, once again acquire for back ground and save this file as bdg.gtl (by default). This way if it is done it will indicate whether TL has been fully extracted and what extent of residual TL is remaining in the background.

For better accuracy, at least three measurements are to be taken and averaged.

The TL reproducibility of phosphor is found to be ± 2 %. The thermoluminescence glow curve reader consists of a specimen holder along with heater, a temperature programmer, a photomultiplier tube as detector, a high voltage unit, a .D.C. amplifier and a suitable displaying or recording device, as shown in Fig. 3.13. Also Fig.3.12

presents the TL detection head and Sr-90 beta source. The TL recorder give the data of time, temperature and TL intensity All these data of each samples are imported in our PC from the TL recorder and then after the draw the graph of Temperature verses Intensity of each sample this graph is called TL Glow curve .It is known as TL characteristic of the particular material. The sample of glow curve is given bellow.

3.8 X-Ray Diffractometer

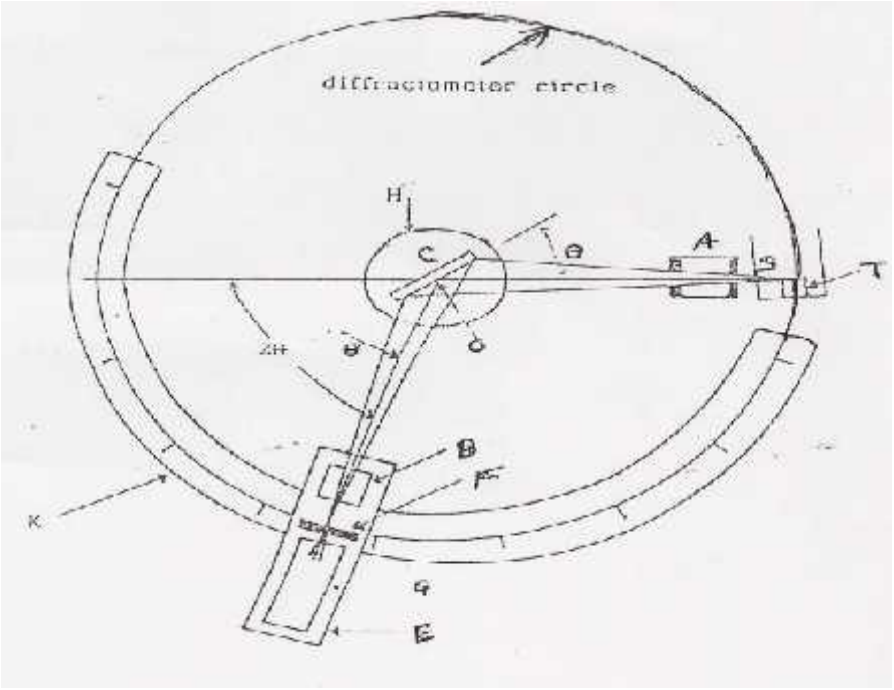

Fig. 3.14: X- ray diffractometer line diagram

This is an easy technique for the characterization of known as well as unknown samples. The simplicity of this technique is due to the specific value of 'd' spacing for a compound. These 'd' values are automatically generated from the computer program. An important feature of diffractometer is its ability to focus into a sharp line, the radiation that is Bragg reflected from an extended specimen area. In this instrument, essentially monochromatic radiation is used and the X-ray detector is placed on the circumference of a circle centered on the powder specimen. The essential feature of diffractometer is shown in fig.3.14. Powder specimen C, in the form of a flat plate, is supported on a table H, Which can be rotated about an axis O, perpendicular to the plane of the paper. The X-ray source is S the line focal point on the target T of the X-ray tube, S is also normal to the plane of the drawing and therefore parallel to the diffractometer axis θ. X-rays diverge from this source and are

diffracted by the specimen to form a convergent diffracted beam which comes to a focus at the slit F and then enters the counter G .A and B are special slits which define and collimate the incident and diffracted beams.

The receiving slits and counter are supported on the carriage E, which may be rotated about the axis θ and whose angular position 2θ may be read on the graduated scale K or directly on a X-ray recorder. The supports E and H are mechanically coupled so that a rotation counter through 2θ degrees is automatically accompanied by rotation of the specimen through θ degrees. This coupling ensures that the angles of incident on and reflection from, the flat specimen will always be equal to one another and will be equal to half angle of diffraction, an arrangement necessary to preserve focusing conditions. For recording the diffractogram of a powdered specimen, the counter is set near $2\theta = 10^0$ run up to 100^0 and collected to a counting rate meter. The output is connected to a PC the d values are calculated automatically. The counter is then driven at a constant angular velocity through increasing values of 2θ until the whole angular range is scanned. At the same time, the paper chart on the recorder moves at a constant speed' so that the distances along the length of the chart are proportional to 2θ. This gives a record of counts per second versus diffraction angle 2θ.

Fig. 3.15: X-Ray diffractometer Brukker D2 Phaser

In the present study D2 PHASER X-ray diffractometer of Brukker is used to record data. The data, 2θ is recorded from 10^0 to 80^0 ranges in the steps of 0.02^0 per 0.1 second. The Kα line of copper source having wavelength 1.54056$\mathring{A}$ is used.

3.9 Fourier transform infrared spectroscopy (FT-IR):

Fourier transform spectroscopy is a measurement technique whereby spectra are collected based on measurements of the coherence of a radiative source, using time-domain or space-domain measurements of the electromagnetic radiation or other type of radiation. It can be applied to a variety of types of spectroscopy including optical spectroscopy, infrared spectroscopy (FTIR, FT-NIRS), nuclear magnetic resonance (NMR) and magnetic resonance spectroscopic imaging (MRSI), mass spectrometry and electron spin resonance spectroscopy. There are several methods for measuring the temporal coherence of the light (see: field-autocorrelation), including the continuous wave Michelson or Fourier transform spectrometer and the pulsed Fourier transform spectrograph (which is more sensitive and has a much shorter sampling time than conventional spectroscopic techniques, but is only applicable in a laboratory environment).

The term Fourier transform spectroscopy reflects the fact that in all these techniques, a Fourier transform is required to turn the raw data into the actual spectrum, and in many of the cases in optics involving interferometers, is based on the Wiener–Khinchin theorem.

Fourier transform spectroscopy is a less intuitive way to get the same information. Rather than allowing only one wavelength at a time to pass through to the detector, this technique lets through a beam containing many different wavelengths of light at once, and measures the total beam intensity. Next, the beam is modified to contain a different combination of wavelengths, giving a second data point. This process is repeated many times. Afterwards, a computer takes all this data and works backwards to infer how much light there is at each wavelength.

To be more specific, between the light source and the detector, there is a certain configuration of mirrors that allows some wavelengths to pass through but blocks

others (due to wave interference). The beam is modified for each new data point by moving one of the mirrors; this changes the set of wavelengths that can pass through.

As mentioned, computer processing is required to turn the raw data (light intensity for each mirror position) into the desired result (light intensity for each wavelength). The processing required turns out to be a common algorithm called the Fourier transform (hence the name, "Fourier transform spectroscopy"). The raw data is sometimes called an "interferogram".

An "interferogram" from a Fourier transform spectrometer. The horizontal axis is the position of the mirror, and the vertical axis is the amount of light detected. This is the "raw data" which can be Fourier transformed into an actual spectrum.

The method of Fourier transform spectroscopy can also be used for absorption spectroscopy. The primary example is "FTIR Spectroscopy", a common technique in chemistry.

In general, the goal of absorption spectroscopy is to measure how well a sample absorbs or transmits light at each different wavelength. Although absorption spectroscopy and emission spectroscopy are different in principle, they are closely related in practice; any technique for emission spectroscopy can also be used for absorption spectroscopy. First, the emission spectrum of a broadband lamp is measured (this is called the "background spectrum"). Second, the emission spectrum of the same lamp shining through the sample is measured (this is called the "sample spectrum"). The sample will absorb some of the light, causing the spectra to be different. The ratio of the "sample spectrum" to the "background spectrum" is directly related to the sample's absorption spectrum.

Accordingly, the technique of "Fourier transform spectroscopy" can be used both for measuring emission spectra (for example, the emission spectrum of a star), and absorption spectra (for example, the absorption spectrum of a glass of liquid).

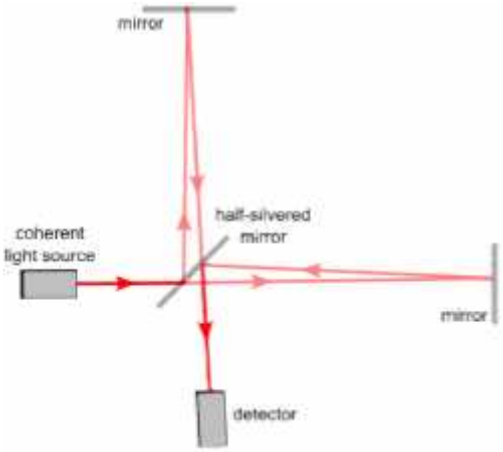

Fig. 3.16: Continuous wave Michelson or Fourier transform spectrograph

The Fourier transform spectrometer is just a Michelson interferometer but one of the two fully-reflecting mirrors is movable, allowing a variable delay (in the travel-time of the light) to be included in one of the beams.

The Michelson spectrograph is similar to the instrument used in the Michelson-Morley experiment. Light from the source is split into two beams by a half-silvered mirror, one is reflected off a fixed mirror and one off a moving mirror which introduces a time delay—the Fourier transform spectrometer is just a Michelson interferometer with a movable mirror. The beams interfere, allowing the temporal coherence of the light to be measured at each different time delay setting, effectively converting the time domain into a spatial coordinate. By making measurements of the signal at many discrete positions of the moving mirror, the spectrum can be reconstructed using a Fourier transform of the temporal coherence of the light. Michelson spectrographs are capable of very high spectral resolution observations of very bright sources. The Michelson or Fourier transform spectrograph was popular for infra-red applications at a time when infra-red astronomy only had single pixel detectors. Imaging Michelson spectrometers are a possibility, but in general have been supplanted by imaging Fabry–Pérot instruments which are easier to construct.

Extracting the spectrum

The intensity as a function of the path length difference in the interferometer p and wave number $\tilde{\nu} = 1/\lambda$

is

$$I(p,\tilde{\nu}) = I(\tilde{\nu})[1+\cos(2\pi\tilde{\nu}p)],$$

where $I(\tilde{\nu})$ is the spectrum to be determined. Note that it is not necessary for $I(\tilde{\nu})$ to be modulated by the sample before the interferometer. In fact, most FTIR spectrometers place the sample after the interferometer in the optical path. The total intensity at the detector is

$$I(p) = \int_0^\infty I(p,\tilde{\nu})d\tilde{\nu} = \int_0^\infty I(\tilde{\nu})[1+\cos(2\pi\tilde{\nu}p)]d\tilde{\nu}.$$

This is just a Fourier cosine transform. The inverse gives us our desired result in terms of the measured quantity I(p):

$$I(\tilde{\nu}) = 4\int_0^\infty [I(p) - \tfrac{1}{2}I(p=0)]\cos(2\pi\tilde{\nu}p)dp.$$

Fig. 3.17: Fourier transform infrared spectrometer Thermo Nicolet 6700

Infrared Spectroscopy (FTIR) Analytical Capabilities

- Identifies chemical bond functional groups by the absorption of infrared radiation which excites vibrational modes in the bond
- May be used in transmission mode

- In attenuated total reflectance (ATR) mode, the detection depth is generally 1-2μm deep, but can be much more or less dependent upon the material. Black, absorbing materials tend to be less
- Especially capable of identifying the chemical bonds of organic materials
- Detects and Identifies organic contaminants
- Identifies water, phosphates, sulfates, nitrates, nitrites, and ammonium ions
- Detection limits vary greatly, but are sometimes $<10^{13}$ bonds/cm^3 or sometimes sub monolayer
- Useful with solids, liquids, or gases

As a general rule of thumb, if it's big enough to see with a microscope, it's big enough to get a spectrum of and hopefully to identify. So don't think your unknown contaminant is too small to work with! Micro-FTIR is therefore uniquely suited to the microelectronic industry as well, where the progressive miniaturization of integrated components on silicon wafers necessitates the capability of analyzing micro-contaminants.

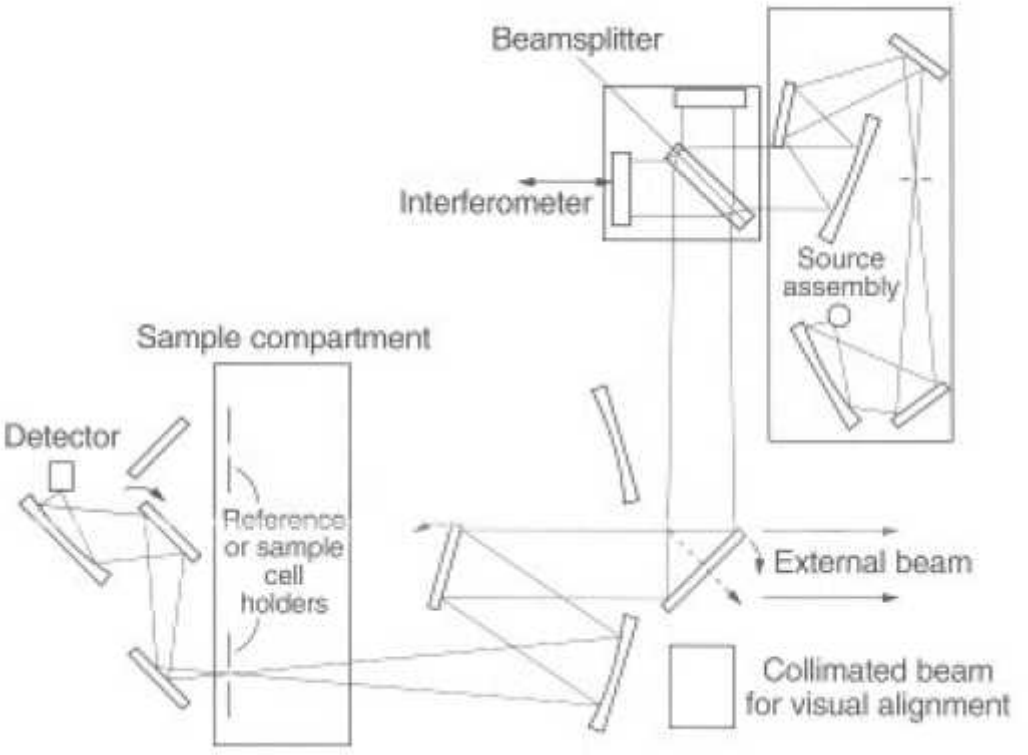

Fig. 3.18: Optical diagram of an FTIR spectrometer

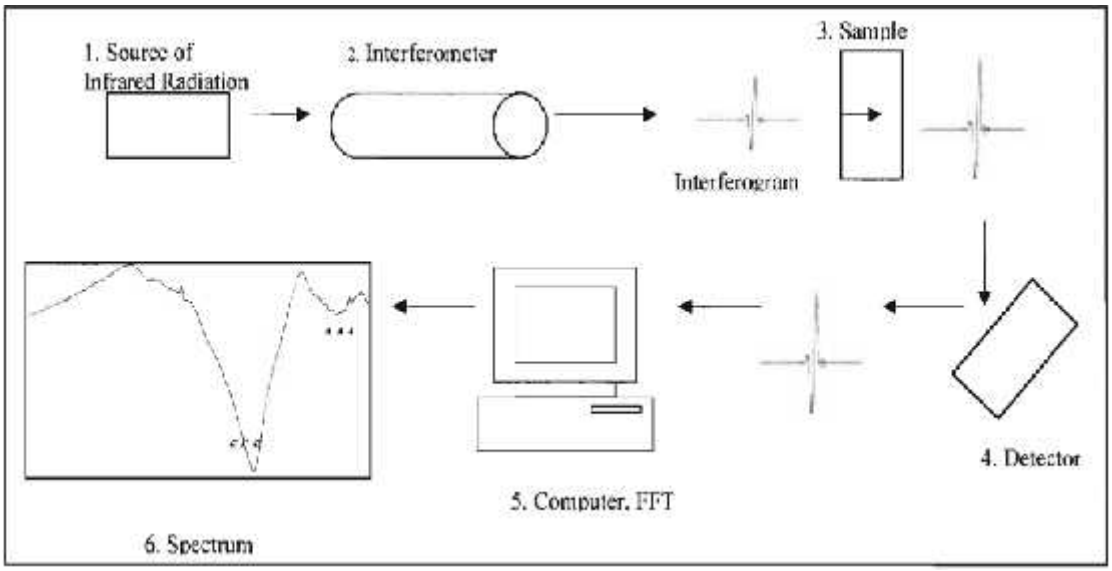

Infrared spectroscopy has been a workhorse technique for materials analysis in the laboratory for over seventy years. An infrared spectrum represents a finger print of a sample with absorption peaks which correspond to the frequencies of vibrations between the bonds of the atoms making up the material. Because each different material is a unique combination of atoms, no two compounds produce the exact same infrared spectrum. Therefore, infrared spectroscopy can result in a positive **identification** (qualitative analysis) of every different kind of material. In addition, the size of the peaks in the spectrum is a direct indication of the **amount** of material present. With modern software algorithms, infrared is an excellent tool for quantitative analysis.

Application of FTIR

Fourier Transform Infrared Spectroscopy is a well-established analytical technique used for analysis of solids, liquids and gases. This technique is routinely used for research and development, as well as quality control/quality assurance in many industries including pharmaceutical, paper and pulp, and polymers and plastics. FTIR was primarily developed for analysis of organic matters based on their chemical bonding characteristics, but more and more, this technique is finding its applications in the analysis of inorganic matters like oxides, nitrides, etc. Relatively weaker chemical bonds in organic matters excite easier than stronger bonds between a metallic element like iron and oxygen; however, chemical bonding in many oxides

including CaO and oxide-hydroxide such as $Ca(OH)_2$ are weak enough to generate a vibration spectrum that could be used for analytical purposes.

Working Principle:

FTIR involves the twisting, rotating, bending, and vibration of the chemical bonding (Figure 3.19). Let incident infrared radiation intensity be I_0 and I be the intensity of the beam after it interacts with the sample. The ratio of intensities I/I_0, as a function of frequency of light gives a spectrum, which can be in three formats: as transmittance, reflectance, and absorbance. The multiplicity of vibrations occurring simultaneously produces a highly complex absorption spectrum, which is a unique characteristic of the functional groups comprising the molecule, and also the configuration of the atoms. A detector is used to read out the intensity of light after it interacts with the sample.

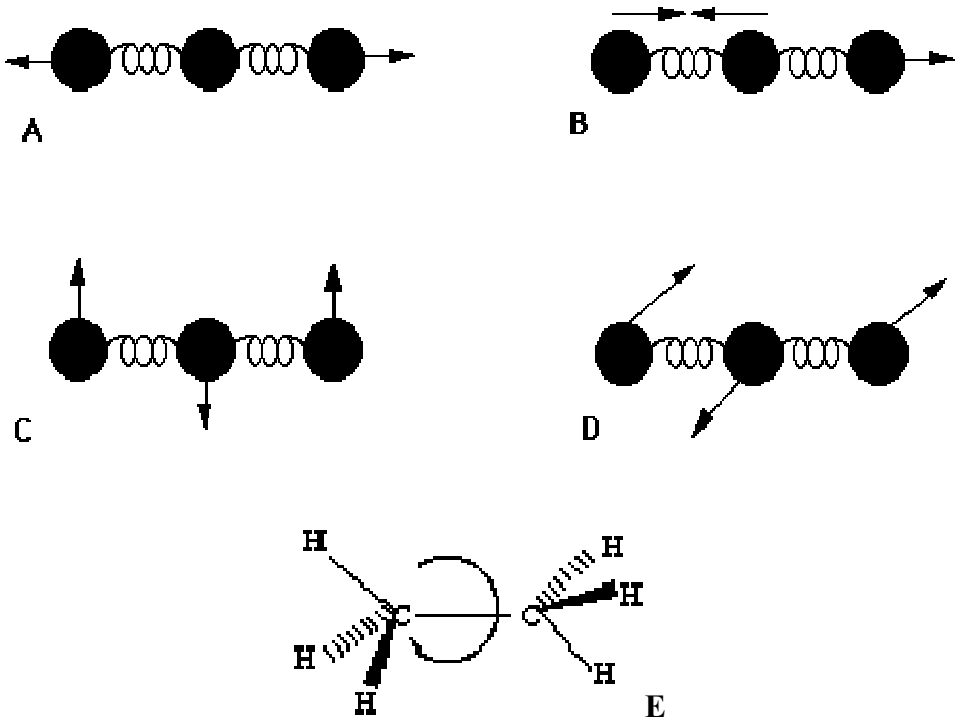

Fig. 3.19: Different vibrational modes. (A) Symmetric stretching (B) Asymmetric Vibration (C and D) in plane and Out of Plane bending (E) torsional Mode

The FT-IR data of collected samples is taken by the Nicolet 6700 of Thermoscientific

3.10 Thermo gravimetric analyzer (TGA):

Thermo gravimetric Analysis (TGA) measures weight changes in a material as a function of temperature (or time) under a controlled atmosphere. Its principal uses include measurement of a material's thermal stability and composition. Thermo gravimetric Analysis instruments are routinely used in all phases of research, quality control and production operations

Thermo gravimetric analysis or thermal gravimetric analysis (TGA) is a type of testing that is performed on samples to determine changes in weight in relation to change in temperature. Such analysis relies on a high degree of precision in three measurements: weight, temperature, and temperature change. As many weight loss curves look similar, the weight loss curve may require transformation before results may be interpreted. A derivative weight loss curve can be used to tell the point at which weight loss is most apparent. Again, interpretation is limited without further modifications and deconvolution of the overlapping peaks may be required.

TGA is commonly employed in research and testing to determine characteristics of materials such as polymers, to determine degradation temperatures, absorbed moisture content of materials, the level of inorganic and organic components in materials, decomposition points of explosives, and solvent residues. It is also often used to estimate the corrosion kinetics in high temperature oxidation.

Simultaneous TGA-DTA/DSC measures both heat flow and weight changes (TGA) in a material as a function of temperature or time in a controlled atmosphere. Simultaneous measurement of these two material properties not only improves productivity but also simplifies interpretation of the results. The complementary information obtained allows differentiation between endothermic and exothermic events which have no associated weight loss (e.g., melting and crystallization) and those which involve a weight loss (e.g., degradation).

The analyzer usually consists of a high-precision balance with a pan (generally platinum) loaded with the sample. The pan is placed in a small electrically heated oven with a thermocouple to accurately measure the temperature. The atmosphere

may be purged with an inert gas to prevent oxidation or other undesired reactions. A computer is used to control the instrument.

Analysis is carried out by raising the temperature gradually and plotting weight (percentage) against temperature. The temperature in many testing methods routinely reaches 1000°C or greater, but the oven is so greatly insulated that an operator would not be aware of any change in temperature even if standing directly in front of the device. After the data are obtained, curve smoothing and other operations may be done such as to find the exact points of inflection.

Fig. 3.20: Mettler Toledo TGA instrument

The above figure shows the Mettler Toledo TGA instrument used to record the TGA data.

3.11 Scanning Electron Microscopy (SEM):

Introduction:

Electron Microscopes are scientific instruments that use a beam of highly energetic electrons to examine objects on a very fine scale. This examination can yield information about the topography (surface features of an object), morphology (shape and size of the particles making up the object), composition (the elements and compounds that the object is composed of and the relative amounts of them) and crystallographic information (how the atoms are arranged in the object).

The first Scanning Electron Microscope (SEM) debuted in 1942 with the first commercial instruments around 1965. Its late development was due to the electronics involved in "scanning" the beam of electrons across the sample.

Electron Microscopes (EMs) function exactly as their optical counterparts except that they use a focused beam of electrons instead of light to "image" the specimen and gain information as to its structure and composition. The basic steps involved in all Ems are the following: A stream of electrons is formed in high vacuum (by electron guns). This stream is accelerated towards the specimen (with a positive electrical potential) while is confined and focused using metal apertures and magnetic lenses into a thin, focused, monochromatic beam. The sample is irradiated by the beam and interactions occur inside the irradiated sample, affecting the electron beam. These interactions and effects are detected and transformed into an image.

Electron Gun:

The first and basic part of the microscopes is the source of electrons. It is usually a V-shaped filament made of LaB_6 or W (tungsten) that is wreathed with Wehnelt electrode (Wehnelt Cap). Due to negative potential of the electrode, the electrons are emitted from a small area of the filament (point source). A point source is important because it emits monochromatic electrons (with similar energy). The two usual types of electron guns are the conventional electron guns and the field emission guns (FEG). Figure 3.21 illustrates the geometry of an electron gun.

In conventional electron guns, a positive electrical potential is applied to the anode, and the filament (cathode) is heated until a stream of electrons is produced. The electrons are accelerated by the positive potential down the column, and because of the negative potential of cap, all electrons are repelled toward the optic axis. A collection of electrons occurs in the space between the filament tip and Cap, which is called a space charge. Those electrons at the bottom of the space charge (nearest to the anode) can exit the gun area through the small (<1 mm) hole in the Whenelt Cap and then move down the column to be later used in imaging.

A field emission gun consists of a sharply pointed tungsten tip held at several kilovolts negative potential relative to a nearby electrode, so that there is a very high potential gradient at the surface of the tungsten tip. The result of this is that the potential energy of an electron as a function of distance from the metal surface has a sharp peak (from the work function), then drops off quickly (due to electron charge traveling through an electric field). Because electrons are quantum particles and have a probability distribution to their location, a certain number of electrons that are nominally at the metal surface will find themselves at some distance from the surface, such that they can reduce their energy by moving further away from the surface. This transport-via-delocalization is called 'tunneling', and is the basis for the field emission effect. FEGs produce much higher source brightness than in conventional guns (electron current > 1000 times), better monochromaticity, but requires a very good vacuum (~10^{-7} Pa).

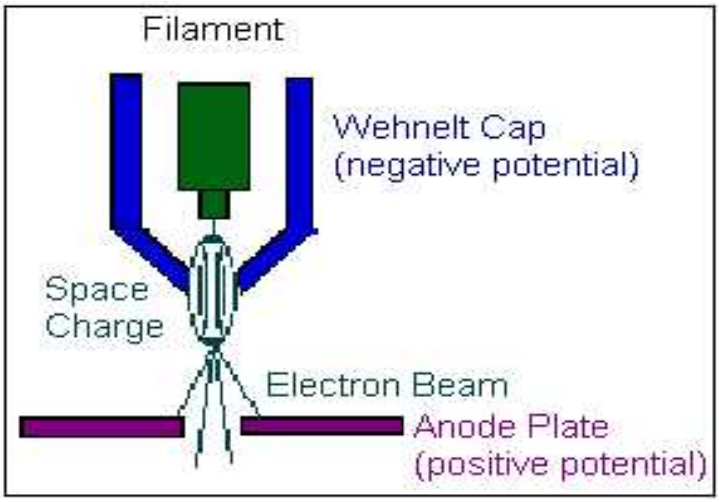

Fig. 3.21: Illustration of the electron gun

Electron-specimen interactions

When an electron beam interacts with the atoms in a sample, individual incident electrons undergo two types of scattering - elastic and inelastic (Figure 3.22). In the former, only the trajectory changes and the kinetic energy and velocity remain constant. In the case of inelastic scattering, some incident electrons will actually collide with and displace electrons from their orbits (shells) around nuclei of atoms comprising the sample. This interaction places the atom in an excited (unstable) state. Specimen interaction is what makes Electron Microscopy possible.

The interactions (inelastic) noted on the top side of the diagram are utilized when examining thick or bulk specimens (Scanning Electron Microscopy, SEM) while on the bottom side are those examined in thin or foil specimens (Transmission Electron Microscopy, TEM).

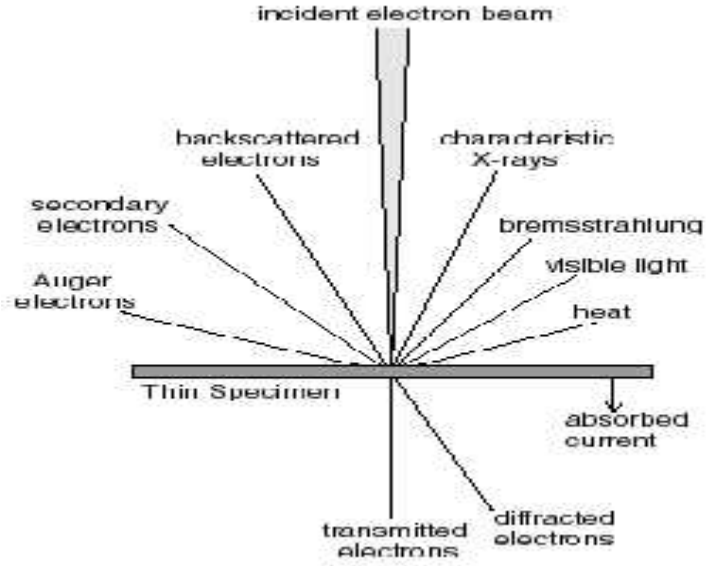

Fig. 3.22:. Effects produced by electron bombardment of a material

Reactions Exploited In SEM

Secondary Electrons:

When a sample is bombarded with electrons, the strongest region of the electron energy spectrum is due to secondary electrons. The secondary electron yield depends on many factors, and is generally higher for high atomic number targets, and at higher angles of incidence. Secondary electrons are produced when an incident electron excites an electron in the sample and loses most of its energy in the process. The excited electron moves towards the surface of the sample undergoing elastic and inelastic collisions until it reaches the surface, where it can escape if it still has sufficient energy.

Production of secondary electrons is very topography related. Due to their low energy (5eV) only secondaries that are very near the surface (<10 nm) can exit the

sample and be examined. Any changes in topography in the sample that are larger than this sampling depth will change the yield of secondaries due to collection efficiencies. Collection of these electrons is aided by using a "collector" in conjunction with the secondary electron detector. Figure 3.23 presents two secondary electron images from SEM.

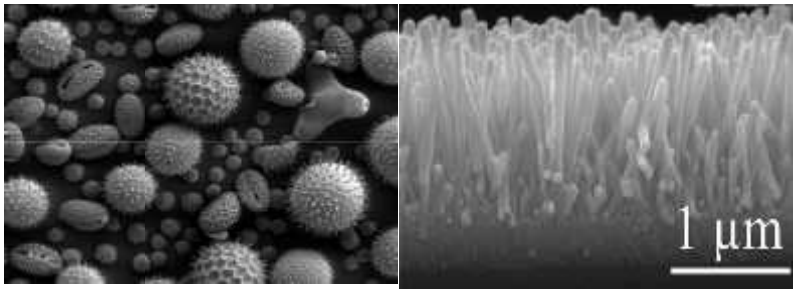

(A) (B)

Fig. 3.23: SEM secondary electron image. A) Pollen - various types B) ZnO Nanorods (side view)

Backscattered Electrons:

Backscattered electrons consist of high-energy electrons originating in the electron beam, that are reflected or back-scattered out of the specimen interaction volume. The production of backscattered electrons varies directly with the specimen's atomic number. This differing production rates causes higher atomic number elements to appear brighter than lower atomic number elements. This interaction is utilized to differentiate parts of the specimen that have different average atomic number.

Relaxation of excited atoms:

As was mentioned above, inelastic scattering, places the atom in an excited (unstable) state. The atom “wants” to return to a ground or unexcited state. Therefore, at a later time the atoms will relax giving off the excess energy. X- Rays, cathodoluminescence and Auger electrons are three ways of relaxation. The relaxation energy is the fingerprint of each element.

When the sample is bombarded by the electron beam of the SEM, electrons are ejected from the atoms on the specimen's surface. A resulting electron vacancy is filled by an electron from a higher shell, and an X-ray is emitted to balance the energy difference between the two electrons. The EDS X-ray detector (also called EDS or EDX) measures the number of emitted x-rays versus their energy. The energy of the x-ray is characteristic of the element from which the x-ray was emitted.

In practice, EDS (or EDX) is most often used for qualitative elemental analysis, simply to determine which elements are present and their relative abundance. In some instances, however, the area of interest is simply too small and must be analyzed by TEM (where EDS is the only option) or high resolution SEM (where the low beam currents used preclude WDS-Wavelength X-ray Dispersive Spectroscopy-, making EDS the only option).

Cathodoluminescence (CL) is the emission of photons of characteristic wavelengths from a material that is under high-energy electron bombardment. The electron beam is typically produced in an electron microprobe (EPMA) or scanning electron microscope (SEM-CL)

Auger electrons are electrons ejected by radiation less excitation of a target atom by the incident electron beam. When an electron from the L shell drops to fill a vacancy formed by K-shell ionization, the resulting X-ray photon with energy $E_K - E_L$ may not be emitted from the atom. If this photon strikes a lower energy electron (e.g.an M-shell electron), this outer electron may be ejected as a low- energy Auger electron. Auger electrons are characteristic of the fine structure of the atom and have energies between 280 eV (carbon) and 2.1 keV (sulfur). By discriminating between Auger electrons of various energies, a chemical analysis of the specimen surface can be made. Auger electrons are exploited in Auger Electron Spectroscopy tools (AES)

The volume inside the specimen in which interactions occur while being struck with an electron beam is called specimen interaction volume. Figure 3.25, illustrates the interaction volumes for secondary and backscattered electrons, as well as X-Rays.

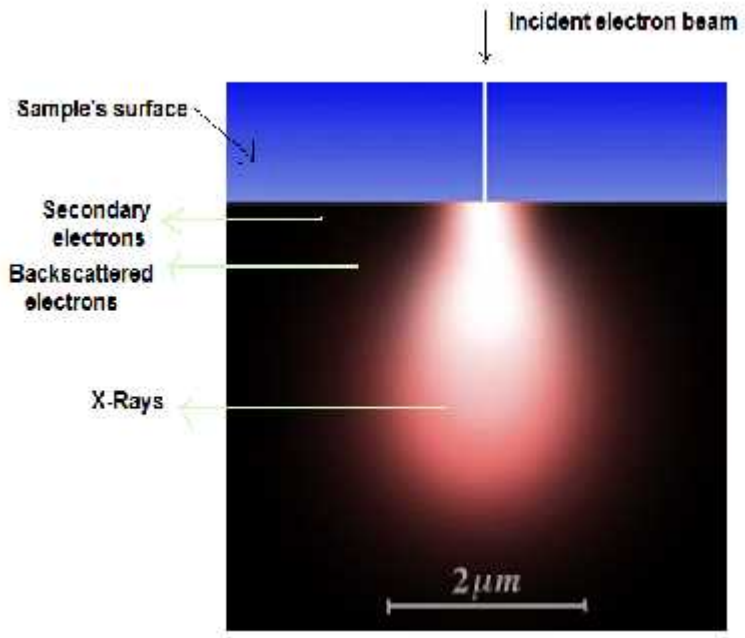

Fig. 3.25:. Generalized illustration of interaction volumes for various electron-specimen interactions

Operation:

In SEM, a source of electrons is focused in vacuum into a fine probe that is rastered over the surface of the specimen. The electron beam passes through scan coils and objective lens that deflect horizontally and vertically so that the beam scans the surface of the sample (Figure 3.26).

As the electrons penetrate the surface, a number of interactions occur that can result in the emission of electrons or photons from or through the surface. A reasonable fraction of the electrons emitted can be collected by appropriate detectors, and the output can be used to modulate the brightness of a cathode ray tube (CRT) whose x- and y- inputs are driven in synchronism with the x-y voltages rastering the electron beam. In this way an image is produced on the CRT; every point that the beam strikes on the sample is mapped directly onto a corresponding point on the screen. As a result, the magnification system is simple and linear magnification is calculated by the equation:

$$M=L/l$$

where L is the raster's length of the CRT monitor and l the raster's length on the surface of the sample.

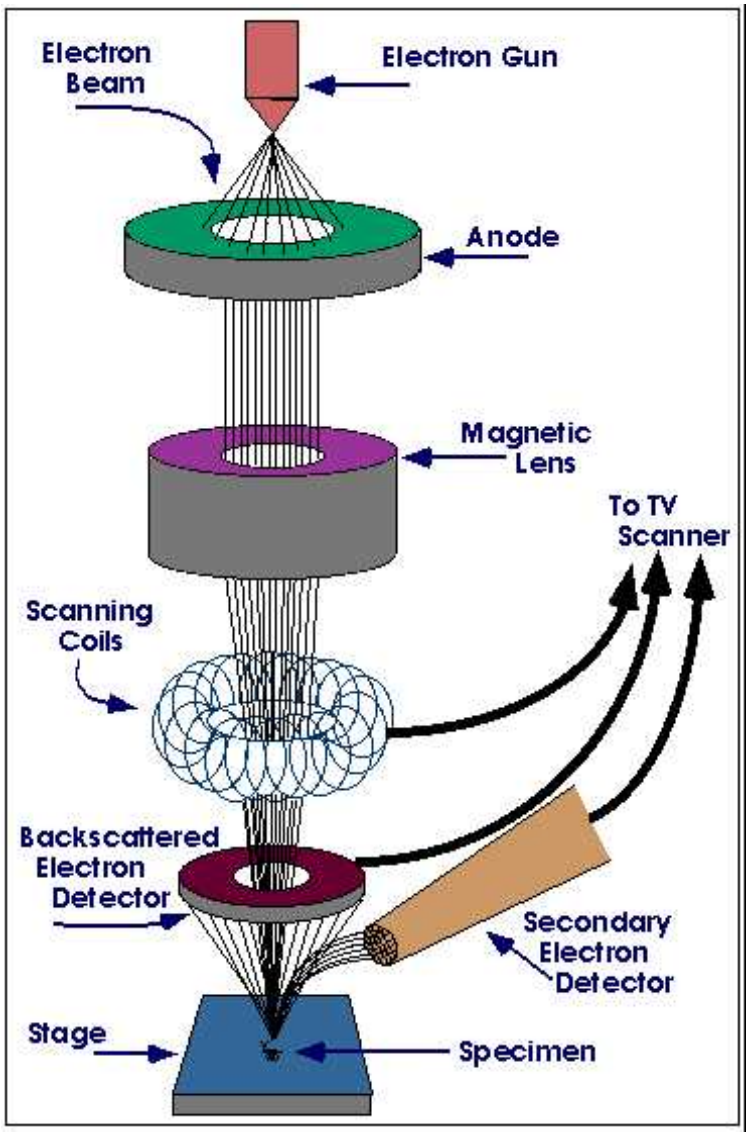

Fig. 3.26: Geometry of SEM

SEM works on a voltage between 2 to 50kV and its beam diameter that scans the specimen is 5nm-2μm. The principle images produced in SEM are of three types: secondary electron images, backscattered electron images and elemental X-ray maps. Secondary and backscattered electrons are conventionally separated according to their energies. When the energy of the emitted electron is less than about 50eV, it is referred as a secondary electron and backscattered electrons are considered to be the electrons that exit the specimen with an energy greater than 50eV. Detectors of each type of electrons are placed in the microscope in proper positions to collect them.

Advantages and Disadvantages

Electrons in scanning electron microscopy penetrate into the sample within a small depth, so that it is suitable for surface topology, for every kind of samples (metals, ceramics, glass, dust, hair, teeth, bones, minerals, wood, paper, plastics, polymers, etc). It can also be used for chemical composition of the sample's surface since the brightness of the image formed by backscattered electrons is increasing with the atomic number of the elements. This means that regions of the sample consisting of light elements (low atomic numbers) appear dark on the screen and heavy elements appear bright. Backscattered are used to form diffraction images, called EBSD, that describe the crystallographic structure of the sample. In SEM, X-rays are collected to contribute in Energy Dispersive X- Ray Analysis (EDX or EDS), which is used to the topography of the chemical composition of the sample.

Consequently, SEM is only used for surface images and both resolution and crystallographic information are limited (because they're only referred to the surface). Other constraints are firstly that the samples must be conductive, so non-conductive materials are carbon-coated and secondly, that materials with atomic number smaller than the carbon are not detected with SEM.

Fig. 3.27: Scanning Electron Microscope

The fig. 3.27 Shows the SEM, Model: LEO s- 440i With OXFORD Energy Dispersive X-Ray Analyzer (EDX) (MODEL : 7060) used for our present study.

3.12 Laser diffraction particle size analyzers

The Mie solution is named after its developer, German physicist Gustav Mie. **Mie theory**, also called **Lorenz–Mie theory** or **Lorenz–Mie–Debye theory**, is an analytical solution of Maxwell's equations for the scattering of electromagnetic radiation by spherical particles (also called **Mie scattering**). For particles much larger or much smaller than the wavelength of the scattered light there are simple and excellent approximations that suffice to describe the behavior of the system. But for objects whose size is similar to the wavelength (e.g., water droplets in the atmosphere, latex particles in paint, droplets in emulsions including milk, and biological cells and cellular components) this more exact approach is necessary.

The formalism allows the calculation of the electric and magnetic fields inside and outside a spherical object and is generally used to calculate either how much light is scattered, the total optical cross section, or where it goes, the form factor. The notable

features of these results are the Mie resonances, sizes that scatter particularly strongly or weakly. This is in contrast to Rayleigh scattering for small particles and Rayleigh-Gans-Debye scattering for large particles. The existence of resonances and other features of Mie scattering, make it a particularly useful formalism when using scattered light to measure particle size.

Using Mie Theory and the Fraunhofer Approximation

When setting up laser diffraction methods, users are faced with the decision as to whether to use Mie Theory or the Fraunhofer Approximation to calculate the particle size distribution results.

The Fraunhofer Approximation represents the easiest model to set-up as, in contrast to Mie Theory, it does not require the user to provide any optical property information. However, its use can lead to significant errors due to the assumptions it makes regarding the nature of the materials being measured. As such, users need to consider the following when selecting the Fraunhofer Model:

- **Particle Absorption** : If the particles show some transparency (absorption < 0.2), then the Fraunhofer approximation will tend to yield inaccurate results below 50µm in size. If the absorption is high (>0.2), good results may be obtained down to 2µm in size, although this does depend on the refractive index.
- **Particle Refractive Index** : If the refractive index different between the particle and the medium which surrounds it is low, then the Fraunhofer model can shown errors, even up to very large particle sizes (>200µm).
- **Particle Size** : If the particle size distribution contains material less than 2 microns in size then the Fraunhofer Approximation will lead to an incorrect assessment of the fine particle fraction.

The nature of the errors observed when using the Fraunhofer Approximation are not always predictable. In most instances an over-estimation of the fine particle fraction is observed, as shown here for a pharmaceutical material. However, it is also possible for the Fraunhofer model to underestimate the fine particle fraction, as is seen for

materials such as calcium carbonate, because it incorrectly predicts the scattering efficiency of these particles.

In the present investigation the Mastersizer Micro system, Version 2.19 was used to find out the particle size. The following are the technical details.

Extensive market research and customer opinion directed the development of the Mastersizer Micro systems. The result is a small footprint, low cost instrument that takes laser diffraction out of the specialist laboratory and into the hands of particle technologists everywhere. The Micro is an instrument system in the clear Malvern tradition – with no compromise on sample handling, Mastersizer Micro performs like a research machine and yet operates like a cost effective QC tool. The wide measuring

range makes it ideal for application in fundamental studies and quality control of production lines in diverse industries such as pharmaceuticals, mining, minerals, clays, food, metal powders, emulsions, ceramics, polymers, pigments, paints and coatings to name a few.

Easy Operation and Maintenance:

Single button operation means that inexperienced users can perform repetitive measurements easily and reproducibly. The stable single lens optics minimizes set up and routine maintenance.

Rapid data acquisition and analysis allows repeatable measurements to be made in less than 4 seconds. A unique "dip-in" probe provides sample agitation, sonication and circulation through the measuring system. By allowing the use of standard laboratory beakers as the sample tank, variable volumes of material can be analyzed.

Superior Software – Complete Control: Malvern software sets an acknowledged world-wide standard for instrument operation, data acquisition and handling, reporting and systems integration.

Set up as easy as ABC: A special "ABC" icon guides the user through a set-up routine ensuring that no parameters are over looked.

Mastersizer Micro's Technical Specifications

Size Range **: Mastersizer Micro:** 0.3um – 300um
Mastersizer Microplus: 0.05um – 550um

Measurement Principle **:** Mie scattering**ime**

Measurement Time **:** < 4 seconds typical – user variable

Light Source **:** HeNe laser of wavelength 632.8nm

Accuracy **:** ± 2.0% on Dv50 on Malvern reference standard

Power **:** 100-240V, 50/60Hz

External Dimensions: 500 (w) x 560 (h) x 325 (d) mm

Weight **:** 32Kg

Easy Mode: a "GO" button runs the complete measurement to pre-selected requirements.

Report Generation: company logos, typestyles and formats can be incorporated into printouts.

Flexible Data Processing: a range of data processing options are available allowing the user to specify the graph format and scale.

Statistical Analysis: reproducibility of results and size trends can be reported using built-in statistical analysis options.

Security Features: four password access levels are available from supervisor down to a level for the infrequent or unskilled user.

LASER DIFFRACTION PARTICLE SIZE ANALYSERS LASER DIFFRACTION PARTICLE SIZE ANALYSERS

Full Mie theory: full Mie theory matrix generator enables compliance with ISO13320.

Advanced features: Malvern BASIC – a powerful set of programming tools enable the user to customize measurement parameters.

Windows operation: all the benefits of the Windows operating system are available to the Mastersizer user. A key feature is the ability to integrate particle size data by "cutting and pasting" into other independent software packages.

Additional features for specific needs: For measurement of solvent based systems, Malvern's QSpec small volume sample dispersion unit can be used, and when only very small amounts of material are available a direct injection small volume flow cell is available.

Laser Diffraction: Laser diffraction particle size analysis is based on the phenomenon that all particles scatter light at a range of angles, which is a characteristic of their size. Large particles scatter at small angles and vice versa.

The Mastersizer Micro comprises a Helium-Neon laser as a light source, which illuminates the dispersed particles in the measuring zone. This is then focused by a Fourier lens to a detector, which consists of a large number of photosensitive elements radiating outward from the centre. A novel property of a Fourier lens is that it collects the scattered light from an ensemble of particles, and overlays the common angles of scattering on the detector array. The intensity of the scattered light is measured and using an optical model (Mie theory) to calculate the scattering pattern and a mathematical deconvolution procedure, a volumetric particle size distribution is calculated that best matches the measured pattern.

The Mastersizer Micro produces volume-based measurements based on the measurement of ensembles of particles sampled at a rate of 500 snaps per second,

simultaneously from all detectors. This means that the system is exceptionally suitable for the detection of rogue coarse particles.

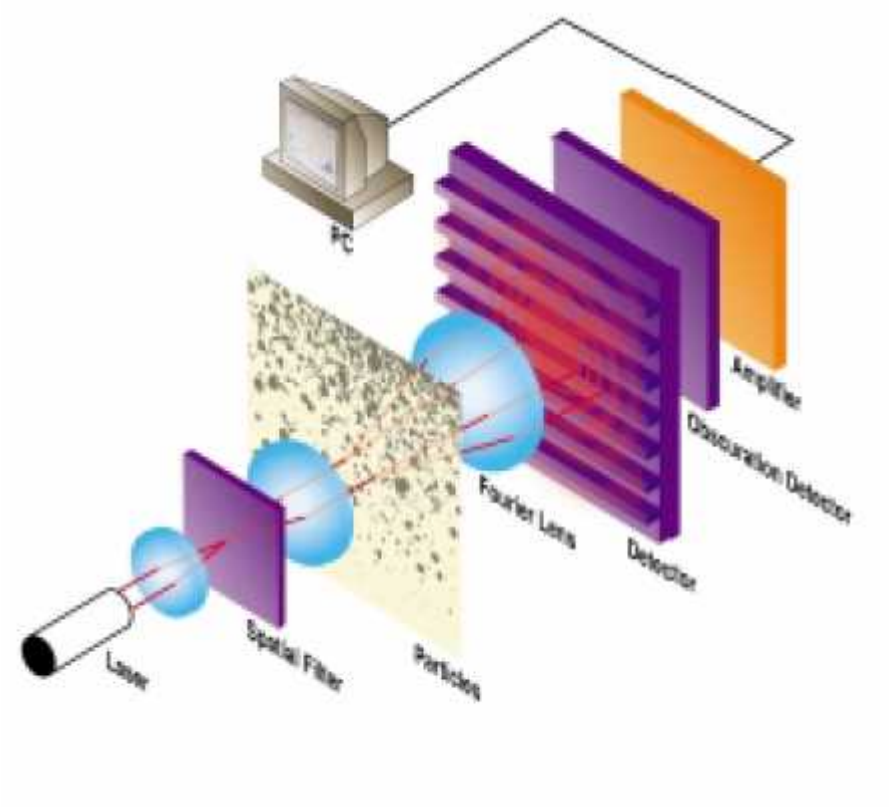

References

1. Nucleonix PC based TL Reader Manual, 2003.
2. B.P.Cullity, Elements of X-ray diffraction, Addison – Wesley Inc., 1978.
3. T.Peng, L. Huajun, H.Yng, C. Yan, Materials Chemistry and Physics 85, 68
4. M. Capron, A. Douy, J. Am. Ceram. Soc., 85, 12, 3036-40, (2002).
5. T.Katsumata, K.Sasajima, T.Nabae,J.Am.Ceram.Soc.81(1998)413.
6. Skoog,Holler and Nieman Principle of instrumental analysis,2005
7. M.T. Postek, K.S. Howard, A.H. Johnson and K.L. McMichael, Scanning Electron Microscopy: A Student's Handbook, (Ladd Research Ind., Inc. Williston, VT., 1980).
8. C.E. Lyman, D.E. Newbury, J.I. Goldstein, D.B. Williams, A.D. Romig, J.T. Armstrong, P. Echlin, C.E. Fiori, D.C. Joy, E. Lifshin and Klaus-Ruediger Peters, Scanning Electron Microscopy, X-Ray Microanalysis and Analytical Electron Microscopy: A Laboratory Workbook, (Plenum Press. New York, N.Y., 1990).
9. J.I. Goldstein, H. Yakowitz, D.E. Newbury, E. Lifshin, J.W. Colby, J.W. Colby and J.R. Coleman, Pratical Scanning Electron Microscopy: Electron and Ion Microprobe Analysis, edited by J.I. Goldstein and H. Yakowitz (Pelnum Press. New York, N.Y.,1975).
10. Benramdane L, Bressolle F, Vallon JJ (1999). "Arsenic speciation in humans and food products: a review". Journal of chromatographic science 37.
11. Ma R, McLeod CW, Tomlinson K, Poole RK (2004). "Speciation of protein-bound trace elements by gel electrophoresis and atomic spectrometry". Electrophoresis 25 (15): 2469–77.
12. Leach, Peter (1991). Shepton Mallet: Romano-Britons and Early Christians in Somerset. Birmingham: Birmingham University Field Archeology Unit. ISBN 0704411296.
13. Savill, Richard (2008-09-18). "'Ancient' Christian amulet declared a fake". Daily Telegraph (London).
14. "New tests challenge age of amulet". BBC News (BBC). 2008-09-18. http://news.bbc.co.uk/1/hi/england/somerset/7622395.stm. Retrieved 2008-09-18.

15. de Bruxelles, Simon (2008-09-16). "Romano-British silver Christian cross may be fake". Times Online (London: The Times).
16. Thermoluminescence, Basic Theory & Applications; -K.V.R Murty J.N. Reddy Feb – 2008.
17. de Boer, G.B. 1987. Laser diffraction spectrometry: Fraunhofer versus Mie scattering. Particle Charac. 4:14–19.
18. Gee, G.W. 1979. Particle-size analysis by hydrometer: A simplified method for routine textural analysis and a sensitivity test of measurement parameters. Soil Sci. Soc. Am. J. 43:1004–1007.
19. Gee, G.W., and J.W. Bauder. 1986. Particle-size analysis. p. 383–411. In A. Klute (ed.) Methods of soil analysis. Part 1. 2nd ed. Agron. Monogr. 9. ASA and SSSA, Madison, WI.
20. Janitzky, P. 1986. Particle-size analysis. p. 11–15. In M.J. Singer and P. Janitzky (ed.) Field and laboratory procedures used in a soil chronosequence study. USGS Bull. 1684. U. S. Gov. Print. Office, Washington, DC.
21. Jonasz, M. 1987. Nonsphericity of suspended marine particles and its influence on light scattering. Limnol. Oceanogr. 32:1059–1065.
22. Jonasz, M. 1991. Size, shape, composition and structure of microparticles from light scattering. p. 143–162. In J.P.M. Syvitske (ed.) Principles, methods, and application of particle size analysis. Cambridge Univ. Press. Cambridge.
23. Konert, M. 1997. Comparison of laser grain size analysis with pipette and sieve analysis: A solution for the underestimation of clay fraction. Sedimentology 44:523–535.
24. Peter Atkins, Julio De Paula. 2006. Physical Chemistry, 8th ed. Oxford University Press: Oxford, UK.
25. William H. Smith U.S. Patent 4,976,542 Digital Array Scanned Interferometer, issued Dec. 11, 1990.
26. Antoine Abragam. 1968. Principles of Nuclear Magnetic Resonance., Cambridge University Press: Cambridge, UK.
27. “Application of FTIR for Quantitative Lime Analysis”, by Seifollah Nasrazadani and Esteban Eureste. Project Report Number 5-9028-01-1, University of North Texas, April,2008.
28. Introduction to Fourier Transform Infrared Spectroscopy, By Thermo Nicolet Corporation. • www.thermonicolet.com

29. I.M. Watt, The Principles and Practice of Electron Microscopy, (Cambridge University Press. Cambridge, England, 1985).
30. The comprehensive reference book on the science and practice of SEM and EDS is: Goldstein J., Newbury D., Joy D., Lyman C., Echlin P., Lifshin E., Sawyer L., and Michael J. "Scanning Electron Microscopy and X-Ray Microanalysis" Kluwer Academic /Plenum Publishers, New York, (2003).

Chapter # 4

Thermoluminescence Study of Dolomite and other minerals

4.1 Introduction

Dolomite is a double carbonate of calcium and magnesium ($CaCO_3.MgCO_3$) which has a theoretical content of 45.7% $MgCO_3$ and 54.3% $CaCO_3$. Dolomite is a mineral commonly occurring in nature and with calcite are main constituents of carbonate rocks. Based on of Tucker classification dolomite rock contain 90 to 100 percent of dolomite mineral. Dolomite formed by dolomitisation process as by replacement of magnesium in calcite. Dolomite in small amounts formed in exist as hydrothermal deposits mainly, associated with fluorite, barite, calcite, siderite, quartz, lead minerals veins, copper and also serpentinic.

Among different practical and industrial application, dolomite is commonly used as a refractory material as well as in the magnesium metal production. Dolomite is a fluxing agent in metallurgical, glass and ceramic industry, filling material in paper, rubber and plastic production. Large amounts of dolomite are also used in building industry and agriculture (dolomite fertilizer). In chemical industry dolomite is first of all a source of magnesium compounds. Dolomite has a large amount of MgO and is an important raw material for refractory industry. As the product properties are considerably influenced by chemical composition of the raw material and operating condition, many researches have been focused on dolomite thermal behavior in recent year.

By considering the industrial applications and availability of the dolomite mineral in Vadodara District of Gujarat, nineteen dolomite minerals are selected for TL study which are presented in Table-4.01

There are nineteen verities of dolomite collected from various mines of Gujarat and other nine minerals from different parts of India, which are studied for ATL and TL.

All samples are annealed and quenched for one hour at different temperatures 200^0C, 400^0C, 600^0C and 800^0C. Now these samples are bagged in zip bags and the appropriate codes are given to the bags. The following are the codes, genesis and chemical formula presenting in Table 4.01.

These samples are then taken for the ATL study, in which the sample is irradiated using the Sr-90 beta source (dose 25Gy) having weight of 5mg. The TL is recorded for these samples and presented in this chapter. After this section some of the samples, which shows good TL, are selected for the TL dosimetric study.

Some abbreviations used in this chapter are as under:

AR : As received (sample)

AQ : Annealed and quenched.

ATL : Artificial thermoluminescence.

TL : Thermoluminescence

NTL : Natural Thermoluminescence.

S. No.	Name of Mineral	Chemical Formula	Location/ Name of mines	Code
1	Dolomite	$CaMg(CO_3)_2$	KhanijMining-1 (Kanawat)	Z03
2	Dolomite	$CaMg(CO_3)_2$	KhanijMining-2 (Kanawat)	Z04
3	Dolomite	$CaMg(CO_3)_2$	Jalaram Mining (Kanawat)	Z05
4	Dolomite	$CaMg(CO_3)_2$	Shreeji Mining (Kanawat)	Z06
5	Dolomite	$CaMg(CO_3)_2$	Bharat Mining (Kanawat)	Z07
6	Dolomite	$CaMg(CO_3)_2$	ChamundaMining (Kanawat)	Z08
7	Dolomite	$CaMg(CO_3)_2$	Aaras Mining (Dadigaam)	Z09
8	Dolomite	$CaMg(CO_3)_2$	Noor Mining (Dadigaam)	Z10
9	Dolomite	$CaMg(CO_3)_2$	Mala Mining (Zair)	Z11
10	Dolomite	$CaMg(CO_3)_2$	Alirajpur (M.P.)	Z12
11	Dolomite	$CaMg(CO_3)_2$	Bachubhai (Bedvi)	Z13
12	Dolomite	$CaMg(CO_3)_2$	Mala Mining (Bedvi)	Z14
13	Dolomite	$CaMg(CO_3)_2$	R.C.Mistry (Bedvi)	Z15
14	Dolomite	$CaMg(CO_3)_2$	Bedvi	Z16
15	Dolomite	$CaMg(CO_3)_2$	Kishanbhai (Bedvi)	Z17
16	Dolomite	$CaMg(CO_3)_2$	Silver Mining (Bedvi)	Z18
17	Dolomite	$CaMg(CO_3)_2$	Nazru sheth (Bedvi)	Z19
18	Dolomite	$CaMg(CO_3)_2$	Madhav (Dhamodi)	Z20
19	Dolomite	$CaMg(CO_3)_2$	Padaliya	Z21
20	Fluorspar	CaF_2	Amba dungar	Z22
21	Appophyllite	$KFCa_4(SiO_5)_4\ 8H_2O$	Jalgaon (M.S.)	Z23
22	Appophyllite	$KFCa_4(SiO_5)_4\ 8H_2O$	Nasik (M.S.)	Z24
23	Appophyllite	$KFCa_4(SiO_5)_4\ 8H_2O$	Mahad (M.S.)	Z25
24	Heulandite	$(Ca, Na_2)Al_2Si_7O_{18}\ 6H_2O$	Nasik (M.S.)	Z26
25	Prehnite	$Ca_2\ Al_2\ Si_3\ O_{10}(OH)_2$	Mumbai (M.S.)	Z27
26	Stilbite	$NaCa_4(Al_4Si_{28}O_{72}]\bullet n(H_2O)$ (n=28-32)	Mahad (M.S.)	Z28
27	Stilbite	$NaCa_4(Al_4Si_{28}O_{72}]\bullet n(H_2O)$ (n=28-32)	Poona (M.S.)	Z29

TABLE- 4.01 Shows mineral codes, chemical formula, and location from where it was collected.

4.2 TL study of dolomite sample Z03 collected from Khanij mining, Kanawant

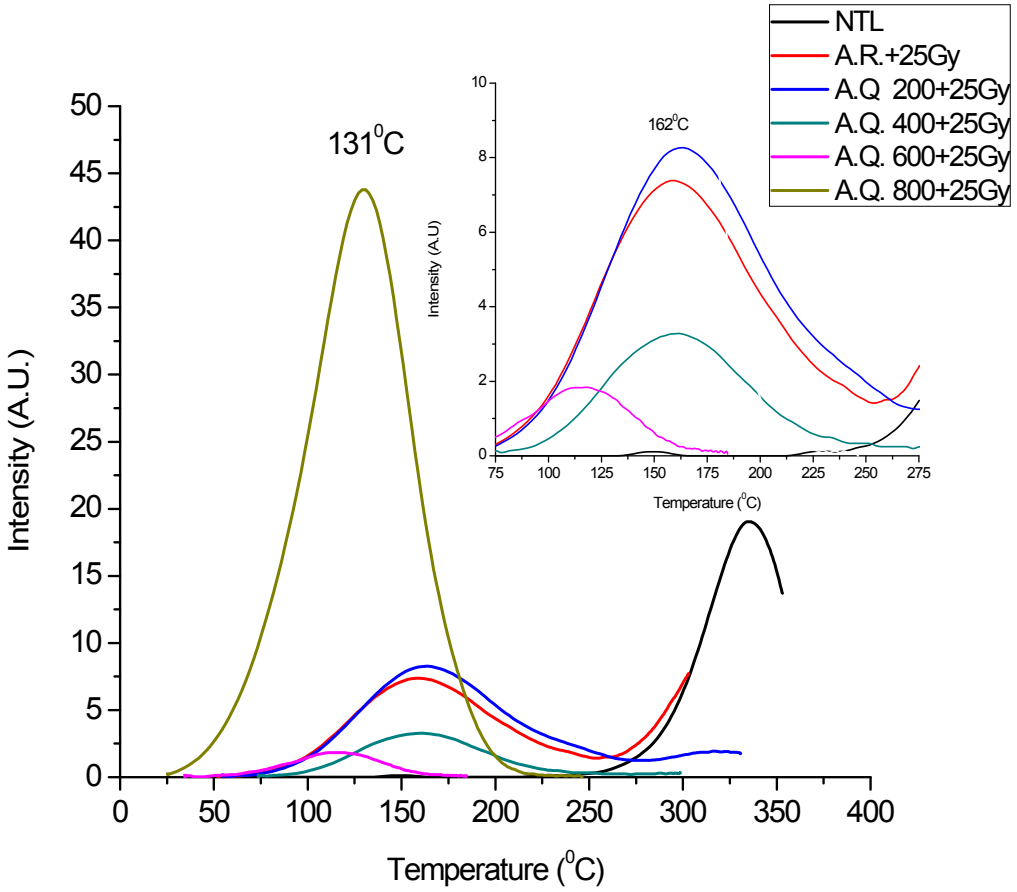

FIG.: 4.01 TL glow curve of as received sample Z03 and also annealed and quenched sample at various temperatures after irradiated using Sr-90 beta source.

The TL glow curve shows a well resolved peak around 131^{0}C for the sample annealed and quenched from 800^{0}C. The sample has shown very low intensity broad TL peak around 164^{0}C, when sample annealed and quenched from 200^{0}C, 400^{0}C and 600^{0}C, which is shown in the inset figure of 4.01. From the TL glow curve it is clear that the TL peak shifts towards lower temperature as the annealing and quenching temperature increases from 200^{0}C to 800^{0}C. The peak temperature and peak Intensity obtained from the glow curve for the Z03 sample are given in table 4.02.

Table- 4.02

S.No.	AQ Temperature (^{0}C)	Peak Temperature (^{0}C)	Peak Intensity (A.U)
1	Natural	149	0.11
2	Beta Irradiated	158	7.38
3	200^{0}C + Beta(25Gy)	164	8.27
4	400^{0}C + Beta(25Gy)	162	3.28
5	600^{0}C + Beta(25Gy)	117	1.84
6	800^{0}C + Beta(25Gy)	131	43.77

The above table shows the peak temperature and peak intensity of sample Z03 annealed and quenched from different temperatures. It is observed from the above table maximum TL peak intensity is obtained for the sample annealed and quenched from 800^{0}C.

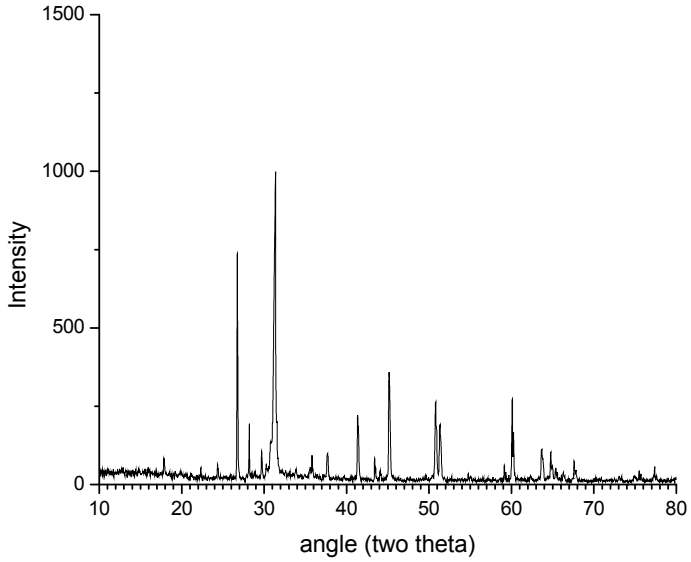

Fig. 4.02 Shows the x-ray diffraction pattern for as received sample Z03.

From the above XRD pattern high intensity peak is observed at 31^0, and low intensity peaks around 27^0, 29^0, 41^0, 45^0, 51^0 and 60^0. The crystallite size is calculated from Scherrer's formula, and is found to be 86.2 nm.

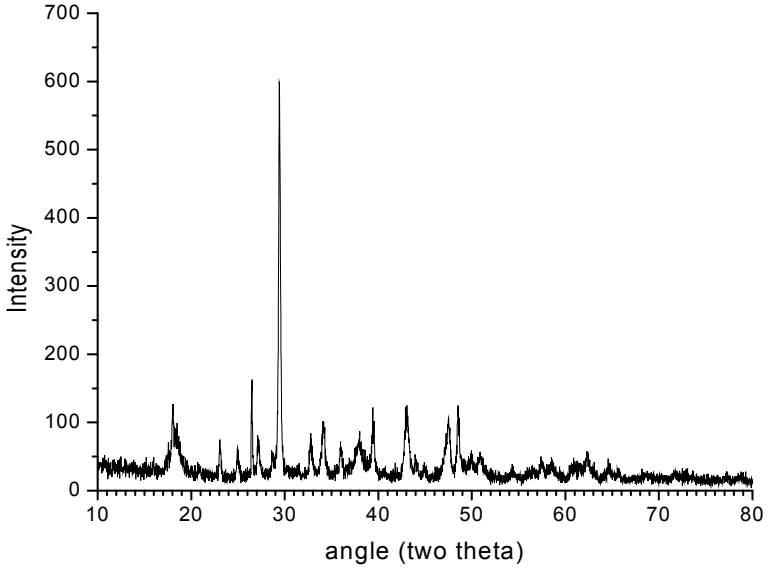

Fig. 4.03 Shows the x-ray diffraction pattern for sample Z03 annealed and quenched from 800^0C.

From the above XRD pattern it is observed that high intensity peak is at 31^0, and low intensity peaks are observed at 26^0, 32^0, 34^0, 38^0, 39^0, 43^0 and 48^0. The crystallite size is calculated from the Scherrer's formula, and is found to be 35.76 nm.

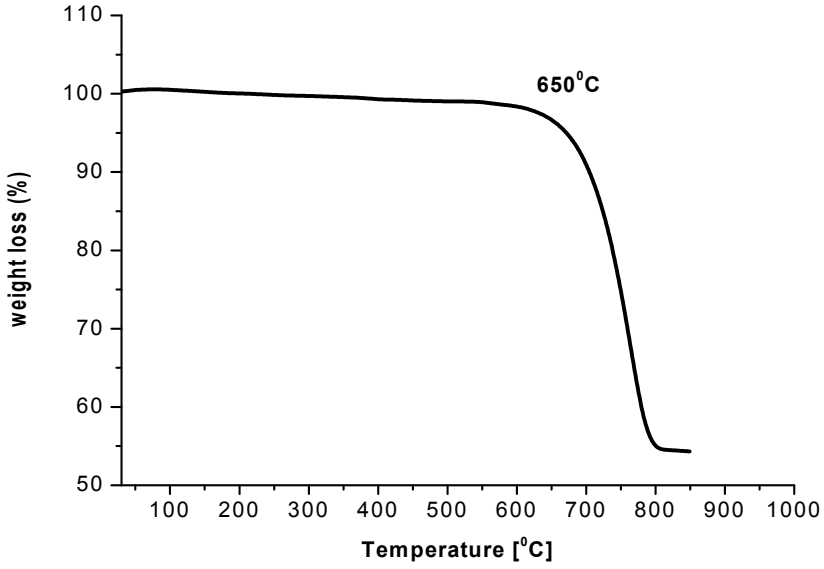

Fig. 4.04 Shows TGA curve for as received sample Z03.

From the above TGA curve it is observed that there is variation in phase in the temperature range of 650^0C to 800^0C. The weight loss is started from 650^0C, and

sample lost its weight by 23% within 750^0C and sample lost its overall 46% weight within 800^0C.

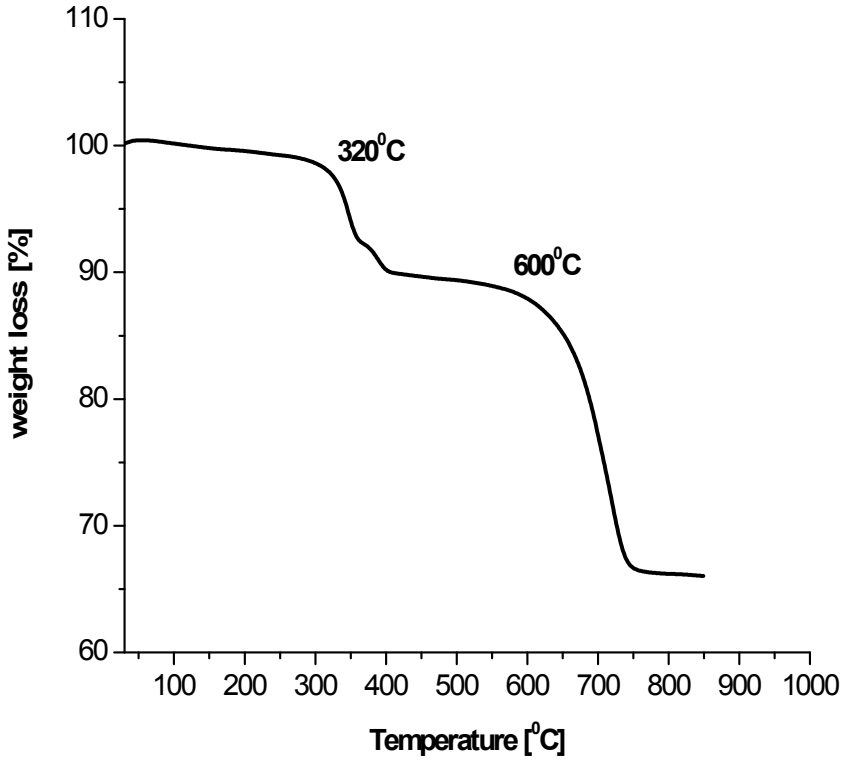

Fig. 4.05 Shows the TGA curve for sample Z03 annealed and quenched from 800^0C.

From the above TGA curve it is observed that the variation in phase occurs in two stages. In the first stage, sample lost its weight by 11% in the temperature range of 320^0C to 400^0C. In the second stage, sample lost its weight by 23% in the temperature range of 600^0C to 760^0C.

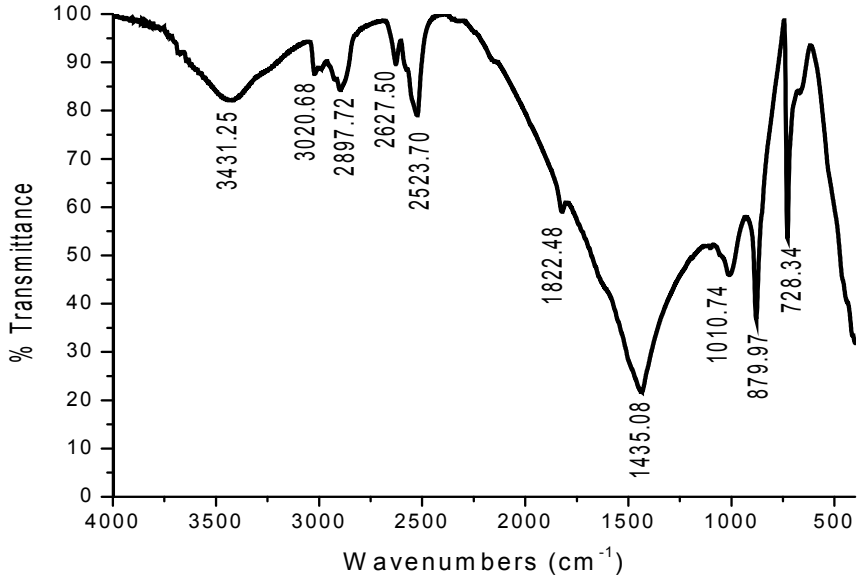

Fig. 4.06 Shows the FTIR absorption spectrum for as received sample Z03.

The FTIR spectra shows a very strong absorption at 1435 cm^{-1} which is attributed to the asymmetric stretching C-O bond, out of plane bending at 880 cm^{-1}, in plane bending at 728 cm^{-1} and OH stretching bond is observed with a broad absorption peak at 3421cm^{-1} which is attributed to the presence of water molecules in the sample.

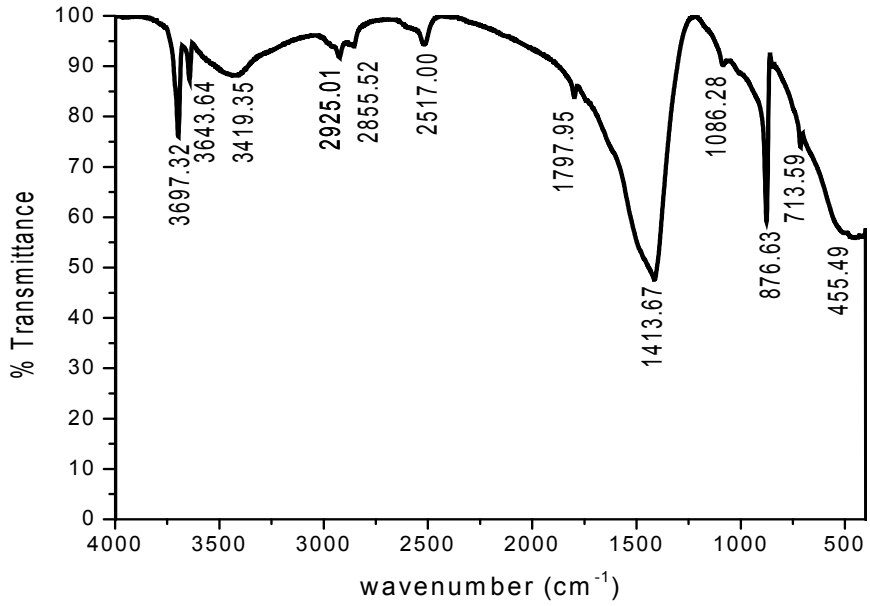

Fig. 4.07 Shows the FTIR absorption spectrum for sample Z03 annealed and quenched from 800^0C.

The FTIR spectra shows the out of plane bending at 877 cm^{-1}, the asymmetric stretching at 1413 cm^{-1}, in plane bending at 714 cm^{-1} having very low absorption and OH stretching bond is observed with a broad absorption peak at 3421cm^{-1} which is attributed to the presence of water molecules in the sample. A sharp absorption peak is observed at 3497cm^{-1} and also a peak at 1086cm^{-1} which are not observed in the as received sample.

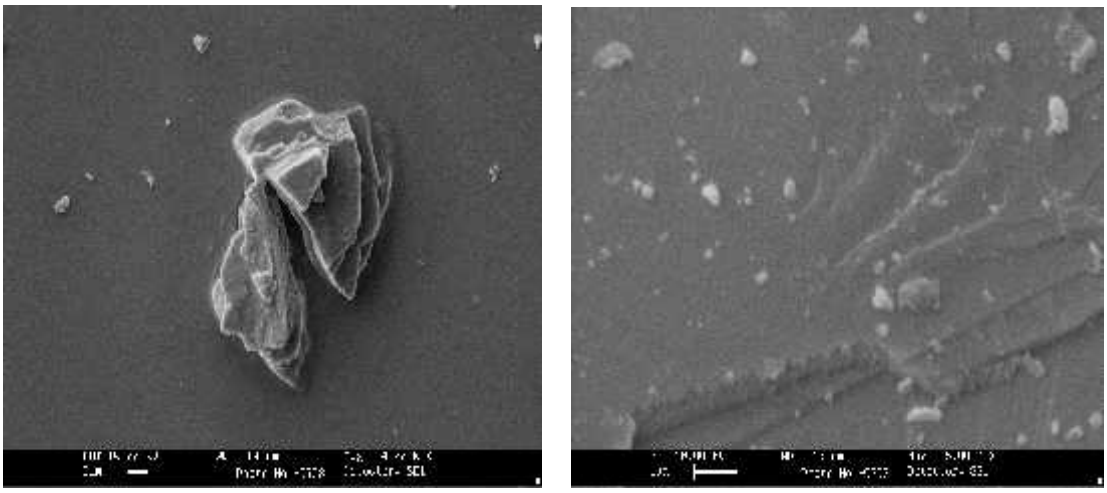

Fig. 4.08 Shows the SEM micrographs of the as received sample Z03.

The above SEM micrographs shows fine layered structure and it is observed that the size of these layers are in nano scale. Surface morphology is clear

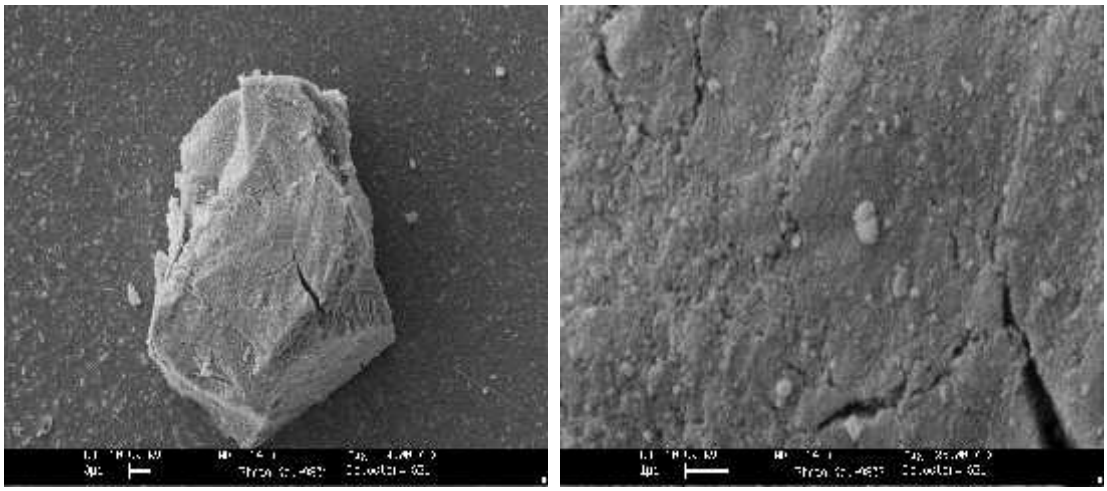

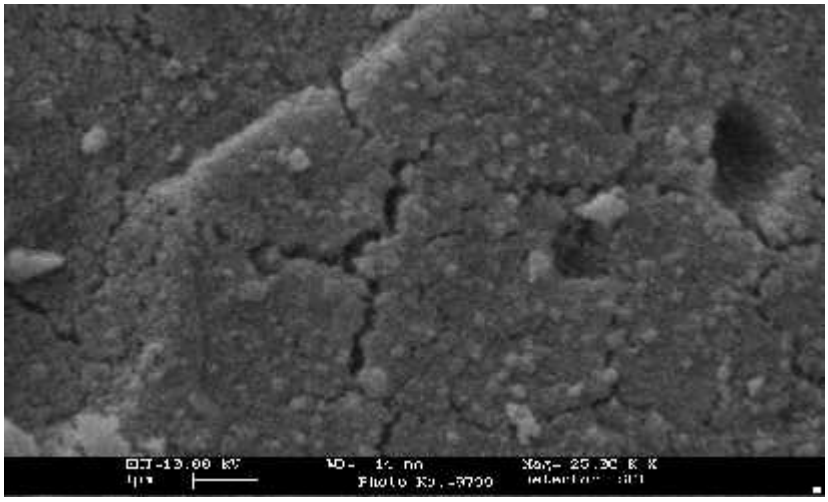

Fig. 4.9 Shows the SEM micrographs of the sample Z03 annealed and quenched from 800^0c.

From the above SEM micrographs it is observed that the sample is having cracks on its surface due to some deformation. This is attributed to the annealing and quenching process and phase change occurred in the mineral Z03 due to annealing at 800^0CAQ.

4.3 TL study of dolomite sample Z04 collected from Khanij mining, Kanawant

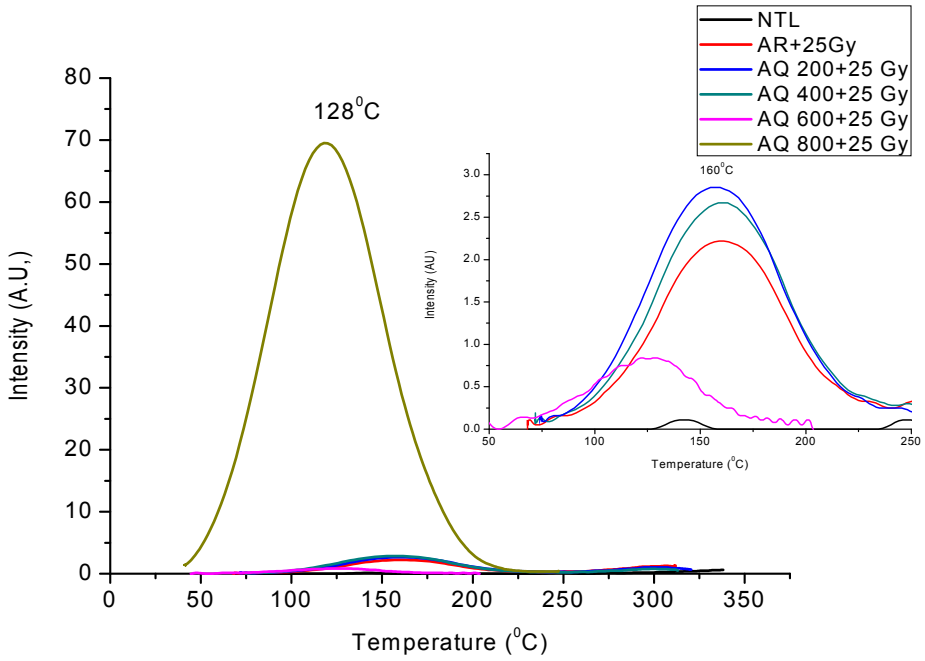

Fig.: 4.10 TL glow curve of as received sample Z04 and also annealed and quenched sample at various temperatures after irradiated using Sr-90 beta source.

The TL glow curve shows a well resolved peak around 128^0C for the sample annealed and quenched from 800^0C. The sample has shown very low intensity broad TL peak around 160^0C, when sample annealed and quenched from 200^0C, 400^0C and 600^0C, which is shown in the inset figure of 4.10. From the TL glow curve it is clear that the TL peak shifts towards lower temperature as the annealing and quenching temperature increases from 200^0C to 800^0C. The peak temperature and peak Intensity obtained from the glow curve for the Z04 sample are given in table 4.03.

Table- 4.03

S.No.	AQ Temperature (^{0}C)	Peak Temperature (^{0}C)	Peak Intensity (A.U.)
1	Natural	142	0.11
2	Beta Irradiated	160	2.22
3	200^0C + Beta(25Gy)	160	2.67
4	400^0C + Beta(25Gy)	157	2.85
5	600^0C + Beta(25Gy)	128	0.84
6	800^0C + Beta(25Gy)	128	69.5

The above table shows the peak temperature and peak intensity of sample Z04 annealed and quenched from different temperatures. It is observed from the above table maximum TL peak intensity is obtained for the sample annealed and quenched from 800^0C.

4.4 TL study of dolomite sample Z05 collected from Jalaram mining, Kanawant

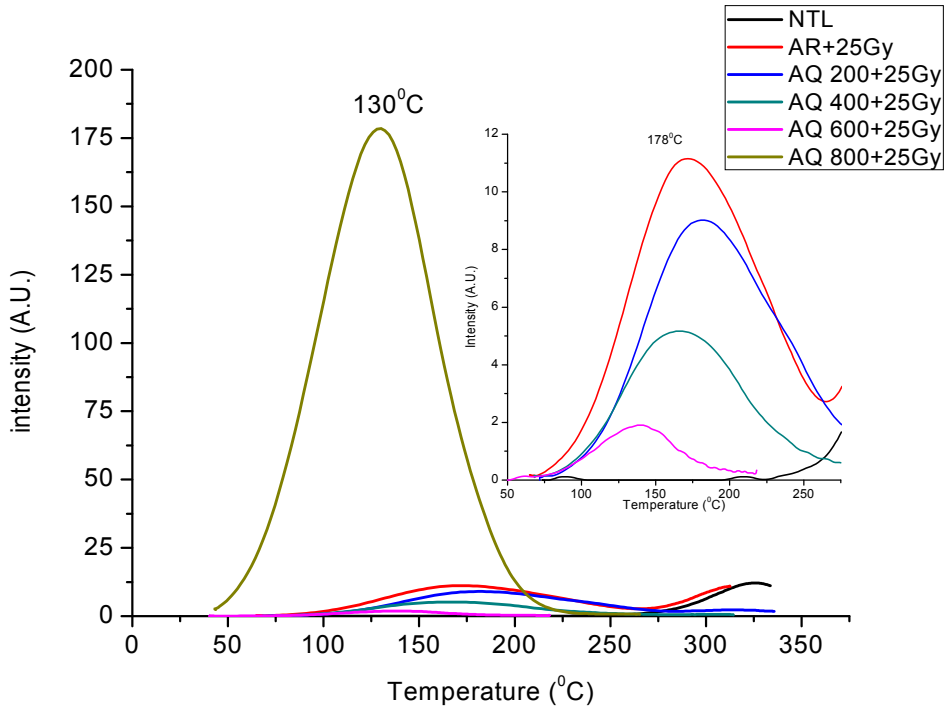

Fig.: 4.11 TL glow curve of as received sample Z05 and also annealed and quenched sample at various temperatures after irradiated using Sr-90 beta source.

The TL glow curve shows a well resolved peak around 130^{0}C for the sample annealed and quenched from 800^{0}C. The sample has shown very low intensity broad TL peak around 160^{0}C, when sample annealed and quenched from 200^{0}C, 400^{0}C and 600^{0}C, which is shown in the inset figure of 4.11. From the TL glow curve it is clear that the TL peak shifts towards lower temperature as the annealing and quenching temperature increases from 200^{0}C to 800^{0}C. The peak temperature and peak Intensity obtained from the glow curve for the Z05 sample are given in table 4.04.

Table- 4.04

S.No.	AQ Temperature (^{0}C)	Peak Temperature (^{0}C)	Peak Intensity (A.U.)
1	Natural	89	0.11
2	Beta Irradiated	172	11.15
3	200^{0}C + Beta(25Gy)	181	9.02
4	400^{0}C + Beta(25Gy)	166	5.17
5	600^{0}C + Beta(25Gy)	140	1.91
6	800^{0}C + Beta(25Gy)	130	178.47

The above table shows the peak temperature and peak intensity of sample Z05 annealed and quenched from different temperatures. It is observed from the above table 4.04 maximum TL peak intensity is obtained for the sample annealed and quenched from 800^{0}C.

4.5 TL study of dolomite sample Z06 collected from Shreeji mining, Kanawant

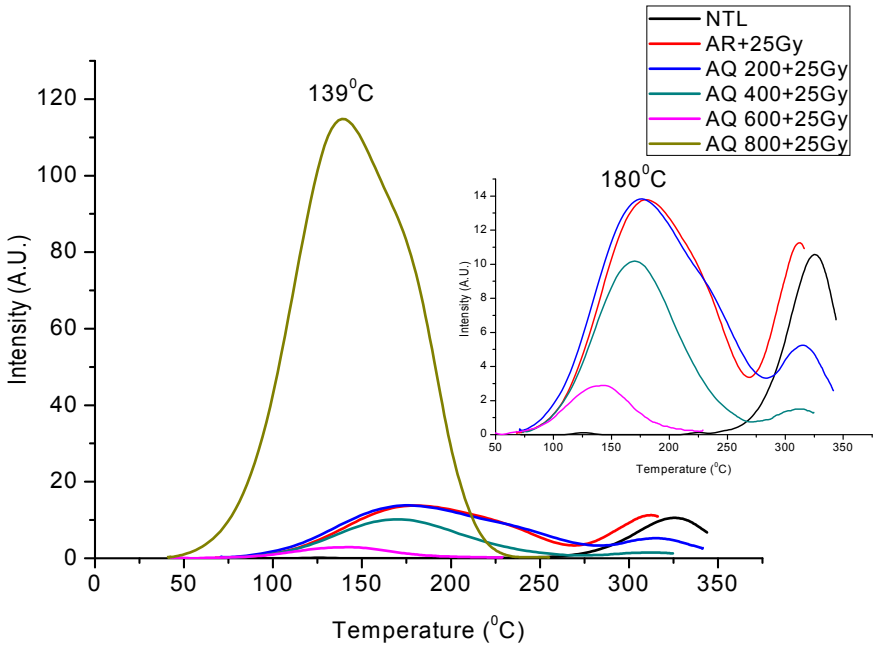

Fig.: 4.12 TL glow curve of as received sample Z06 and also annealed and quenched sample at various temperatures after irradiated using Sr-90 beta source.

The TL glow curve shows a peak around 139^0C for the sample annealed and quenched from 800^0C. There is also a hump observed around 174^0C. The sample has shown very low intensity broad TL peak around 176^0C, when sample annealed and quenched from 200^0C, 400^0C and 600^0C, which is shown in the inset figure of 4.12. From the TL glow curve it is clear that the TL peak shifts towards lower temperature as the annealing and quenching temperature increases from 200^0C to 800^0C. The peak temperature and peak Intensity obtained from the glow curve for the Z06 sample are given in table 4.05.

Table-4.05

S.No.	AQ Temperature (^{0}C)	Peak Temperature (^{0}C)	Peak Intensity (A.U.)
1	Natural	126	0.11
2	Beta Irradiated	180	13.79
3	200^0C + Beta(25Gy)	176	13.83
4	400^0C + Beta(25Gy)	170	10.18
5	600^0C + Beta(25Gy)	142	2.89
6	800^0C + Beta(25Gy)	139	114.83

The above table shows the peak temperature and peak intensity of sample Z06 annealed and quenched from different temperatures. It is observed from the above table 4.05 maximum TL peak intensity is obtained for the sample annealed and quenched from 800^0C.

4.6 TL study of dolomite sample Z07 collected from Bhaarat mining, Kanawant

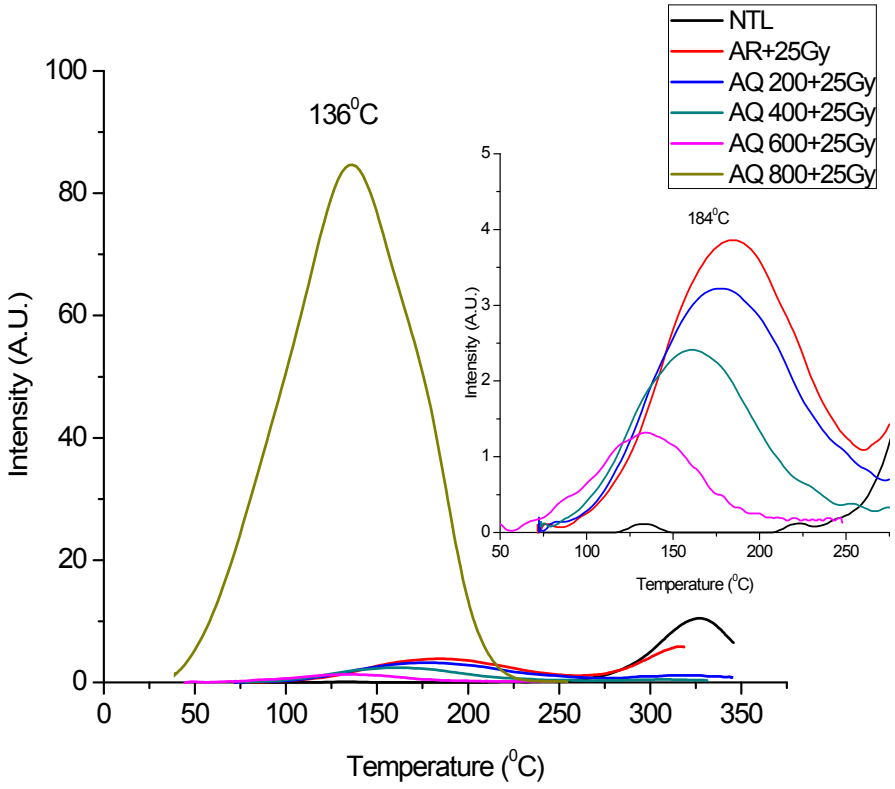

FIG.: 4.13 TL glow curve of as received sample Z07 and also annealed and quenched sample at various temperatures after irradiated using Sr-90 beta source.

The TL glow curve shows a peak around 138^{0}C for the sample annealed and quenched from 800^{0}C. A small hump is also observed around 173^{0}C. The sample has shown very low intensity broad TL peak around 177^{0}C, when sample annealed and quenched from 200^{0}C, 400^{0}C and 600^{0}C, which is shown in the inset figure of 4.13. From the TL glow curve it is clear that the TL peak shifts towards lower temperature as the annealing and quenching temperature increases from 200^{0}C to 800^{0}C. The peak temperature and peak Intensity obtained from the glow curve for the Z07 sample are given in Table 4.06.

Table-4.06

S.No.	AQ Temperature (^{0}C)	Peak Temperature (^{0}C)	Peak Intensity (A.U.)
1	Natural	133	0.11
2	Beta Irradiated	184	3.86
3	200^{0}C + Beta(25Gy)	177	3.22
4	400^{0}C + Beta(25Gy)	160	2.41
5	600^{0}C + Beta(25Gy)	133	1.32
6	800^{0}C + Beta(25Gy)	136	84.68

The above table shows the peak temperature and peak intensity of sample Z07 annealed and quenched from different temperatures. It is observed from the above table 4.06 maximum TL peak intensity is obtained for the sample annealed and quenched from 800^{0}C.

4.7 TL study of dolomite sample Z08 collected from Chamunda mining, Kanawant

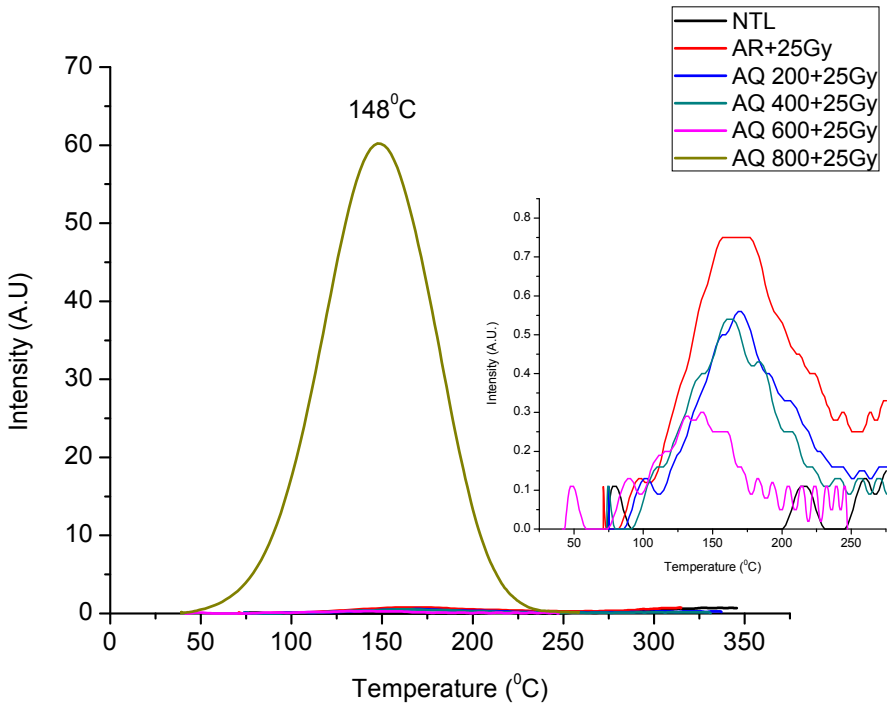

Fig.: 4.14 TL glow curve of as received sample Z08 and also annealed and quenched sample at various temperatures after irradiated using Sr-90 beta source.

The TL glow curve shows a well resolved peak around 148^0C for the sample annealed and quenched from 800^0C. The sample has shown very low intensity broad TL peak with kinks around 168^0C for NTL, ATL for as received sample and for the sample annealed from 200^0C, 400^0C and 600^0C, which is shown in the inset figure of 4.14. From the TL glow curve it is clear that the TL peak shifts towards lower temperature as the annealing and quenching temperature increases from 200^0C to 800^0C. The peak temperature and peak Intensity obtained from the glow curve for the Z07 sample are given in Table 4.07.

Table-4.07

S.No.	AQ Temperature (^{0}C)	Peak Temperature (^{0}C)	Peak Intensity (A.U.)
1	Natural	80	0.11
2	Beta Irradiated	168	0.75
3	200^0C + Beta(25Gy)	168	0.56
4	400^0C + Beta(25Gy)	162	0.54
5	600^0C + Beta(25Gy)	142	0.3
6	800^0C + Beta(25Gy)	148	60.2

The above table shows the peak temperature and peak intensity of sample Z08 annealed and quenched from different temperatures. It is observed from the above table 4.07 maximum TL peak intensity is obtained for the sample annealed and quenched from 800^0C.

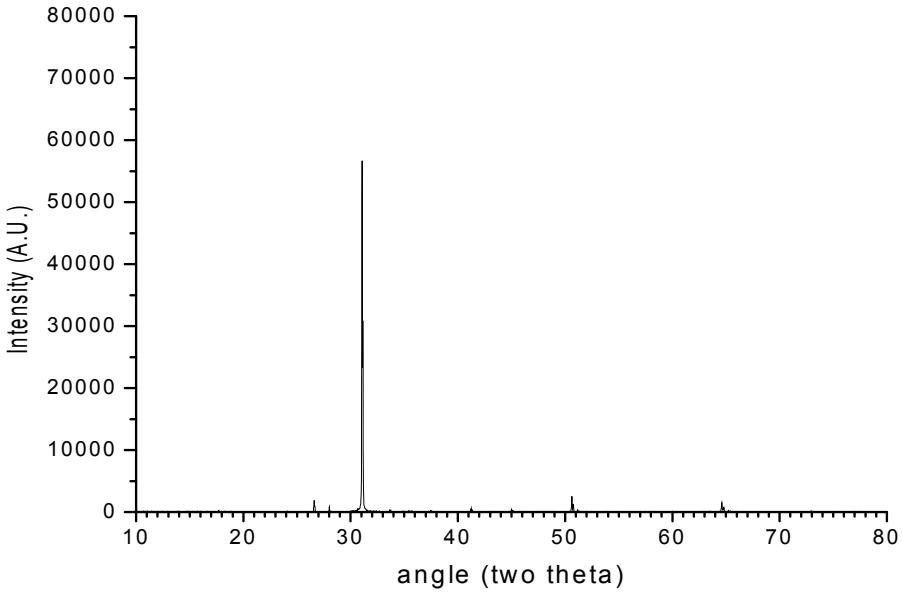

FIG. 4.15 Shows the x-ray diffraction pattern for as received sample Z08.

From the above XRD pattern high intensity peak is observed at 31^0, and low intensity peaks are observed around 17^0, 26^0, 28^0, 41^0, 45^0, 51^0 and 64^0. The crystallite size is calculated from Scherrer's formula, and is found to be 61.54 nm.

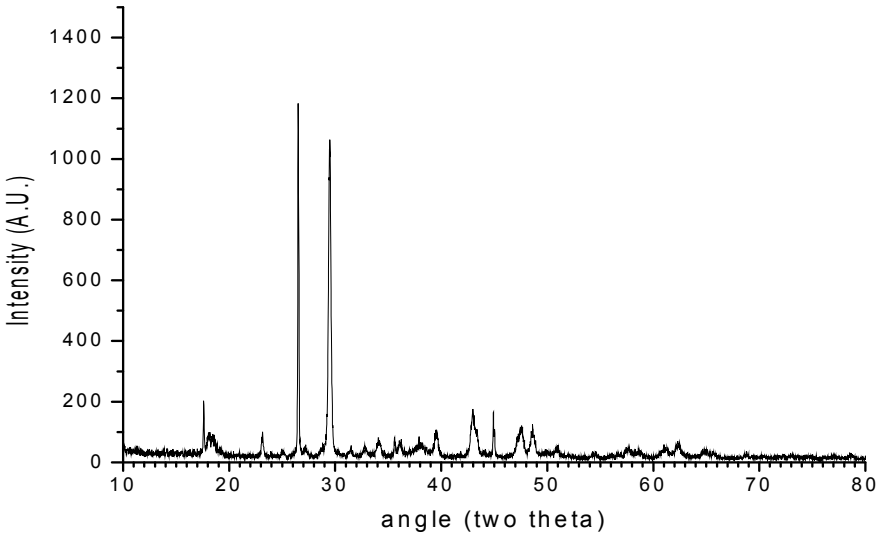

FIG. 4.16 Shows the x-ray diffraction pattern for sample Z08 annealed and quenched from 800^0C.

From the above XRD pattern high intensity peak is observed at 29^0, and low intensity peaks are observed around 17^0, 26^0, 32^0, 34^0, 36^0, 38^0, 40^0, 43^0, 48^0, 51^0 and 62^0. The

crystallite size is calculated from Scherrer's formula, and is found to be 71.07nm.

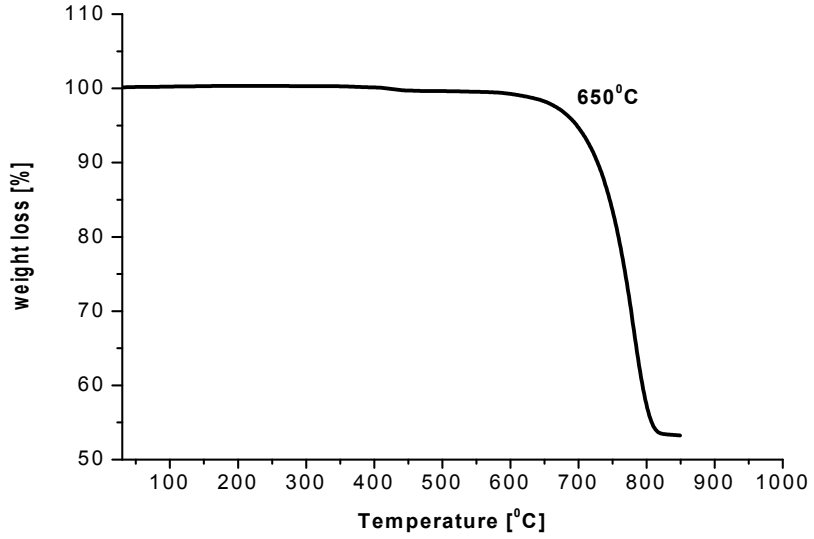

Fig. 4.17 shows TGA curve for as received sample Z08.

It is observed from the above TGA figure that, there is a variation in phase in the temperature range from 650^0C to 800^0C. The weight loss is started from 650^0C, and the sample lost its weight by 23% within 750^0C and the sample lost its overall 46% weight within 800^0C.

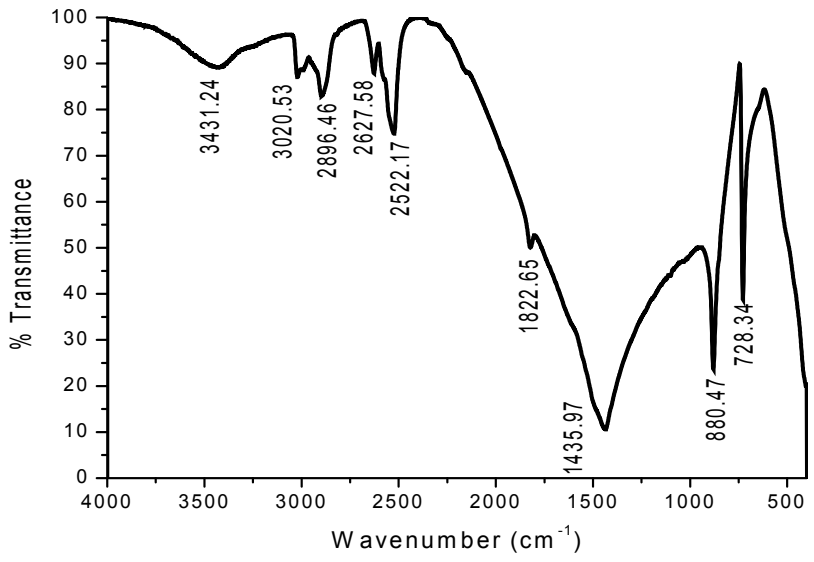

Fig. 4.18 Shows the FTIR absorption spectrum for as received sample Z08.

The FTIR spectra shows the out of plane bending at 880 cm^{-1}, the asymmetric stretching at 1436 cm^{-1}, in plane bending at 728 cm^{-1}, and also (OH) stretching bond

is observed with broad peak at 3421cm^{-1}. This may be due to absorption of water molecules.

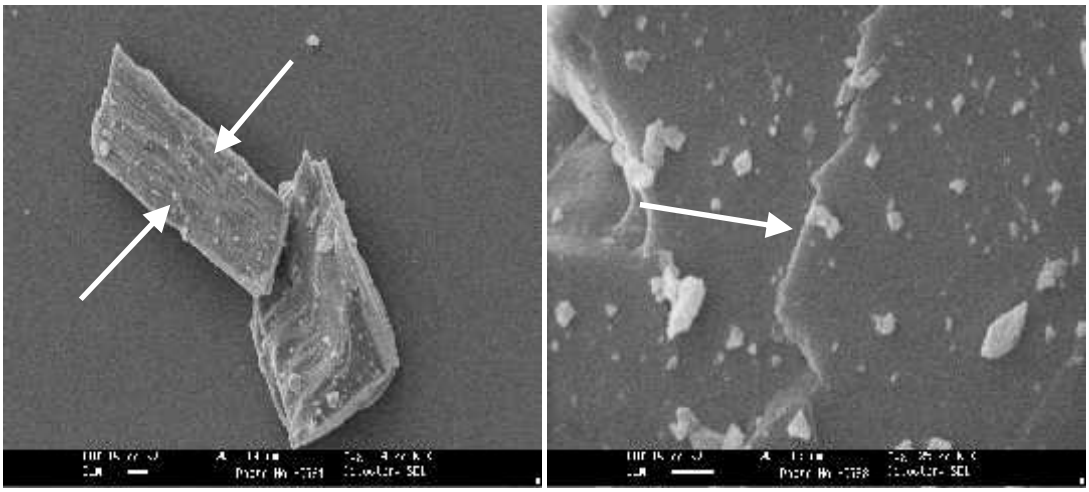

Fig. 4.19 Shows the SEM micrographs of the as received sample Z08.

Above SEM photographs shows fine layered structure and it is observed that, the size of these layers are in nano scale. Surface morphology is clear.

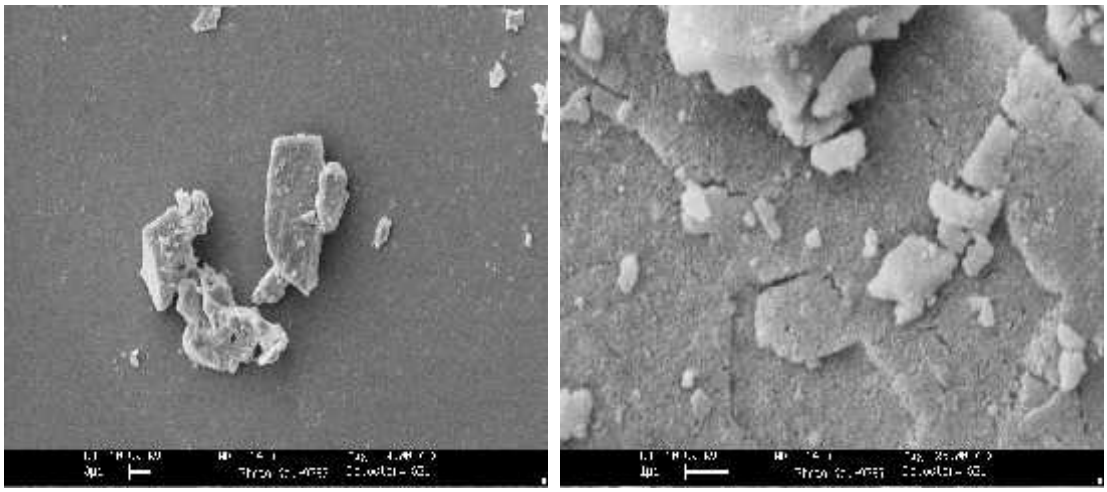

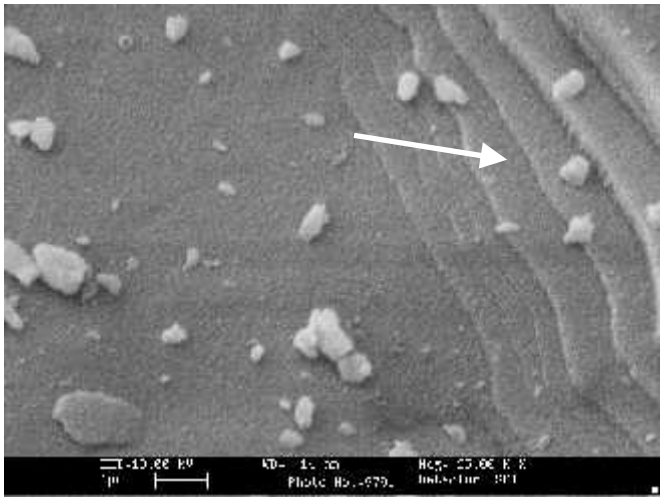

Fig. 4.20 shows the SEM micrographs of the sample Z08 annealed and quenched from 800^0C.

From the above SEM micrographs it seems the sample is having cracks on its surface due to some deformation. This is attributed to the annealing and quenching process.

4.8 TL study of dolomite sample Z09 collected from Aaras mining, Dadigaam

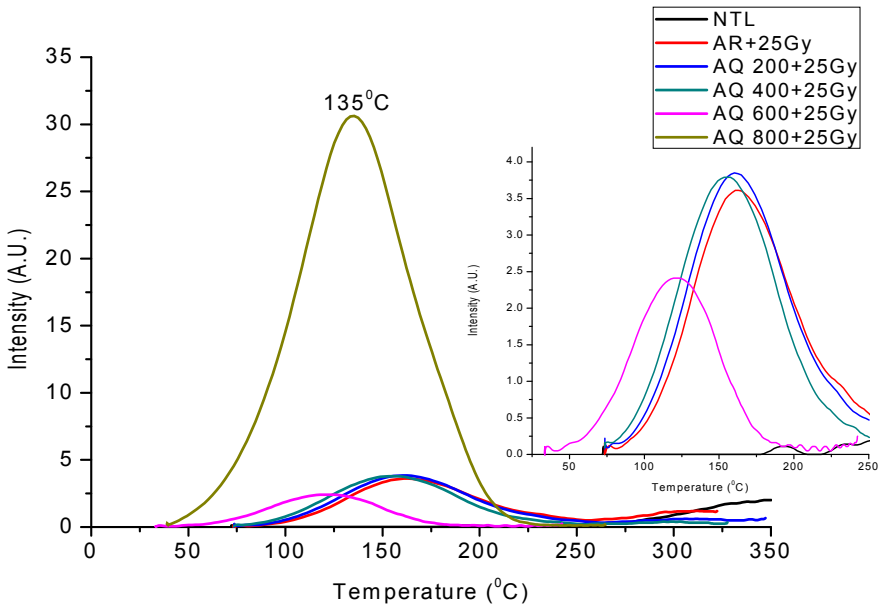

Fig.: 4.21 TL glow curve of as received sample Z09 and also annealed and quenched sample at various temperatures after irradiated using Sr-90 beta source.

The TL glow curve shows a peak around 135^0C for the sample annealed and quenched from 800^0C. The sample has shown very low intensity broad TL peak around 160^0C, when sample annealed and quenched from 200^0C, 400^0C and 600^0C, which is shown in the inset figure of 4.21. From the TL glow curve it is clear that the TL peak shifts towards lower temperature as the annealing and quenching temperature increases from 200^0C to 800^0C. The peak temperature and peak Intensity obtained from the glow curve for the Z09 sample are given in Table 4.08.

Table-4.08

S.No.	AQ Temperature (^{0}C)	Peak Temperature (^{0}C)	Peak Intensity (A.U.)
1	Natural	193	0.11
2	Beta Irradiated	161	3.61
3	200^0C + Beta(25Gy)	160	3.85
4	400^0C + Beta(25Gy)	153	3.79
5	600^0C + Beta(25Gy)	119	2.41
6	800^0C + Beta(25Gy)	135	30.68

The above table shows the peak temperature and peak intensity of sample Z09 annealed and quenched from different temperatures. It is observed from the above table 4.08 maximum TL peak intensity is obtained for the sample annealed and quenched from 800^0C.

4.9 TL study of dolomite sample Z10 collected from Noor mining, Dadigaam

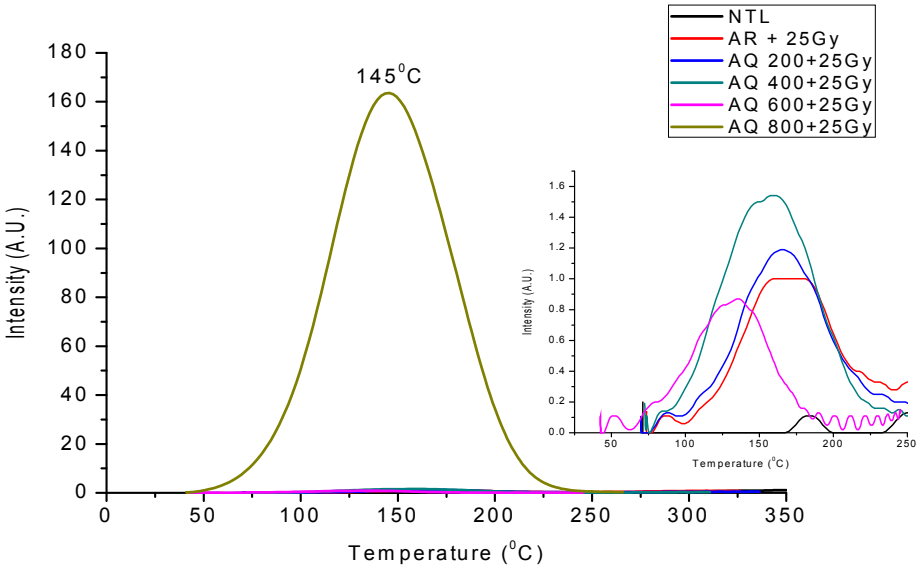

Fig.: 4.22 TL glow curve of as received sample Z10 and also annealed and quenched sample at various temperatures after irradiated using Sr-90 beta source.

The TL glow curve shows a well resolved peak around 145^{0}C for the sample annealed and quenched from 800^{0}C. The sample has shown very low intensity broad TL peak around 170^{0}C, when sample annealed and quenched from 200^{0}C, 400^{0}C and 600^{0}C, which is shown in the inset figure of 4.22. From the TL glow curve it is clear that the TL peak shifts towards lower temperature as the annealing and quenching temperature increases from 200^{0}C to 800^{0}C. The peak temperature and peak Intensity obtained from the glow curve for the Z10 sample are given in Table 4.09.

Table 4.09

S.No.	AQ Temperature (^{0}C)	Peak Temperature (^{0}C)	Peak Intensity (A.U.)
1	Natural	183	0.11
2	Beta Irradiated	170	1
3	200^{0}C + Beta(25Gy)	165	1.19
4	400^{0}C + Beta(25Gy)	157	1.54
5	600^{0}C + Beta(25Gy)	135	0.87
6	800^{0}C + Beta(25Gy)	146	163.58

The above table shows the peak temperature and peak intensity of sample Z10 annealed and quenched from different temperatures. It is observed from the above table 4.09 maximum TL peak intensity is obtained for the sample annealed and quenched from 800^0C.

4.10 TL study of dolomite sample Z11 collected from Mala mining, Zair

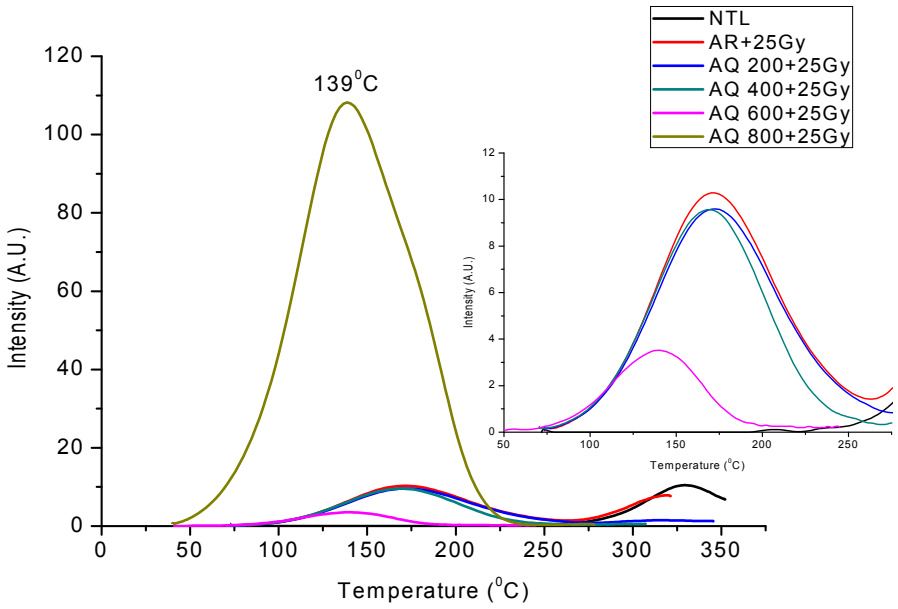

Fig.: 4.23 TL glow curve of as received sample Z11 and also annealed and quenched sample at various temperatures after irradiated using Sr-90 beta source.

The TL glow curve shows a peak around 139^0C for the sample annealed and quenched from 800^0C. A small hump is also observed around 177^0C. The sample has shown very low intensity broad TL peak around 171^0C, when sample annealed and quenched from 200^0C, 400^0C and 600^0C, which is shown in the inset figure of 4.23. From the TL glow curve it is clear that the TL peak shifts towards lower temperature as the annealing and quenching temperature increases from 200^0C to 800^0C. The peak temperature and peak Intensity obtained from the glow curve for the Z11 sample are given in Table 4.10.

Table- 4.10

S.No.	AQ Temperature (^{0}C)	Peak Temperature (^{0}C)	Peak Intensity (A.U.)
1	Natural	75	0.11
2	Beta Irradiated	171	10.29
3	200^{0}C + Beta(25Gy)	173	9.6
4	400^{0}C + Beta(25Gy)	168	9.56
5	600^{0}C + Beta(25Gy)	139	3.52
6	800^{0}C + Beta(25Gy)	139	108.19

The above table shows the peak temperature and peak intensity of sample Z11 annealed and quenched from different temperatures. It is observed from the above table 4.10 maximum TL peak intensity is obtained for the sample annealed and quenched from 800^{0}C.

4.11 TL study of dolomite sample Z12 collected from Alirajpur, Madhya Pradesh

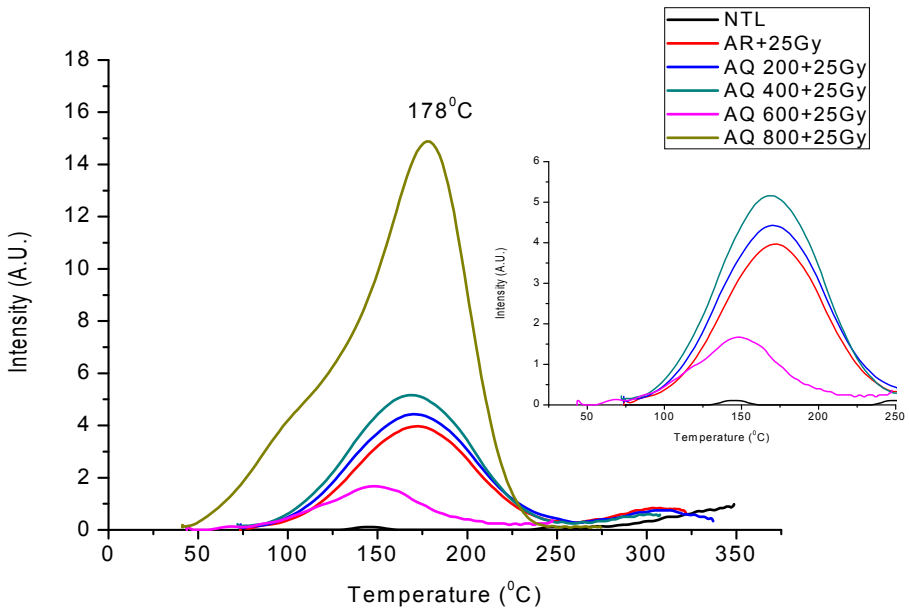

Fig.: 4.24 TL glow curve of as received sample Z12 and also annealed and quenched sample at various temperatures after irradiated using Sr-90 beta source.

The TL glow curve shows a peak around 178^0C for the sample annealed and quenched from 800^0C. A small hump is also observed around 100^0C. The sample has shown very low intensity broad TL peak around 170^0C, when sample annealed and quenched from 200^0C, 400^0C and 600^0C, which is shown in the inset figure of 4.24. From the TL glow curve it is clear that the TL peak shifts towards lower temperature as the annealing and quenching temperature increases from 200^0C to 600^0C. The peak temperature and peak Intensity obtained from the glow curve for the Z12 sample are given in Table 4.11.

Table- 4.11

S.No.	AQ Temperature (^{0}C)	Peak Temperature ^{0}C	Peak Intensity (A.U.)
1	Natural	145	0.11
2	Beta Irradiated	172	3.97
3	200^0C + Beta(25Gy)	170	4.43
4	400^0C + Beta(25Gy)	167	5.16
5	600^0C + Beta(25Gy)	147	1.67
6	800^0C + Beta(25Gy)	178	14.88

The above table shows the peak temperature and peak intensity of sample Z12 annealed and quenched from different temperatures. It is observed from the above table 4.11 maximum TL peak intensity is obtained for the sample annealed and quenched from 800^0C.

4.12 TL study of dolomite sample Z13 collected from Bachu mining, Bedvi

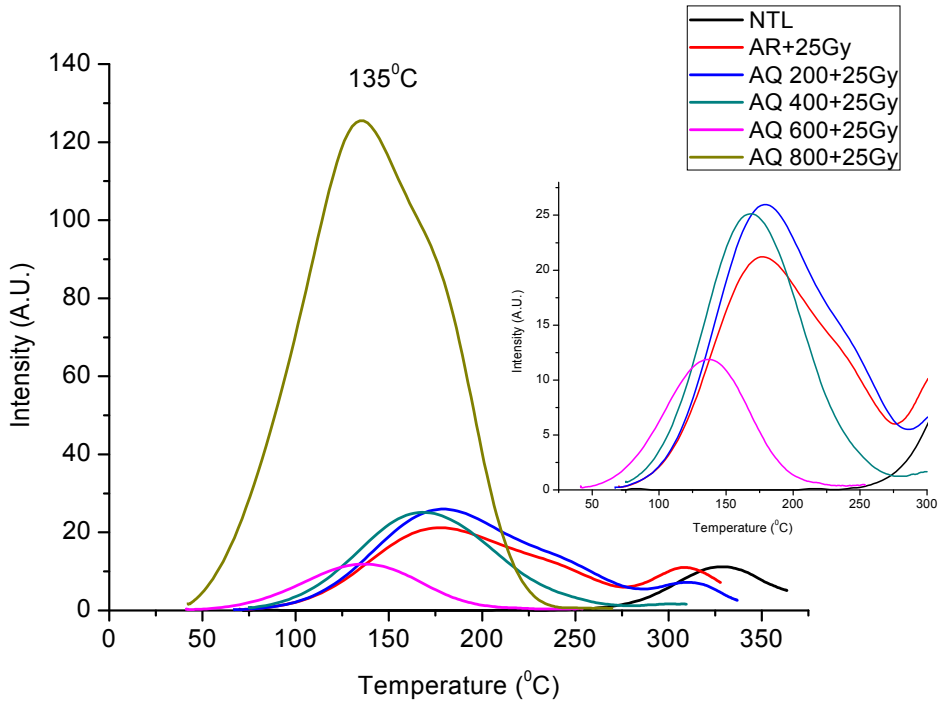

Fig.: 4.25 TL glow curve of as received sample Z13 and also annealed and quenched sample at various temperatures after irradiated using Sr-90 beta source.

The TL glow curve shows a peak around 135^{0}C for the sample annealed and quenched from 800^{0}C. A small hump is also observed at 174^{0}C. The sample has shown very low intensity broad TL peak around 178^{0}C, when sample annealed and quenched from 200^{0}C, 400^{0}C and 600^{0}C, which is shown in the inset figure of 4.25. From the TL glow curve it is clear that the TL peak shifts towards lower temperature as the annealing and quenching temperature increases from 200^{0}C to 800^{0}C. The peak temperature and peak Intensity obtained from the glow curve for the Z13 sample are given in Table 4.12.

Table-4.12

S.No.	AQ Temperature (^{0}C)	Peak Temperature (^{0}C)	Peak Intensity (A.U.)
1	Natural	-	-
2	Beta Irradiated	178	21.21
3	200^{0}C + Beta(25Gy)	178	25.96
4	400^{0}C + Beta(25Gy)	168	25.13
5	600^{0}C + Beta(25Gy)	138	11.88
6	800^{0}C + Beta(25Gy)	134	125.5

The above table shows the peak temperature and peak intensity of sample Z13 annealed and quenched from different temperatures. It is observed from the above table 4.12 maximum TL peak intensity is obtained for the sample annealed and quenched from 800^{0}C.

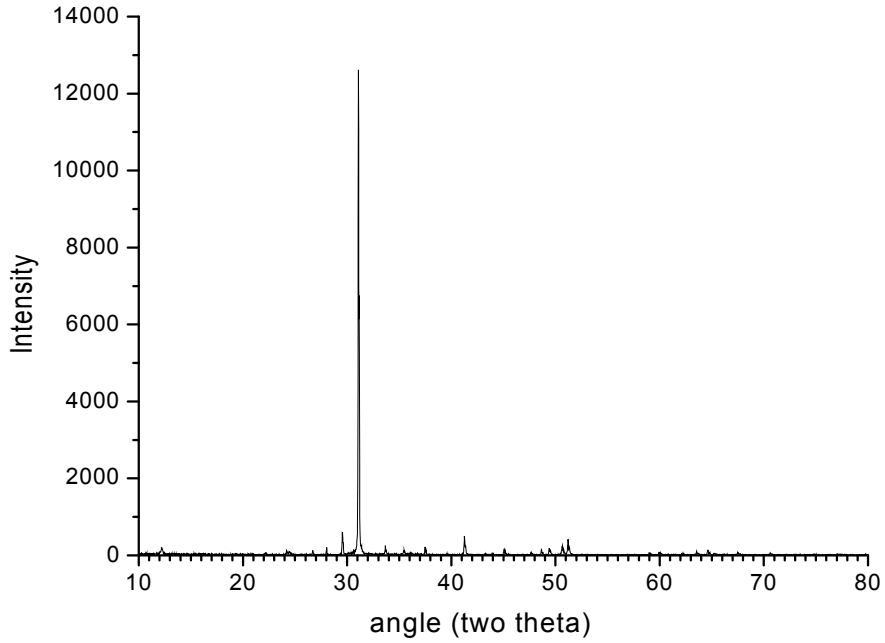

Fig. 4.26 Shows the x-ray diffraction pattern for as received sample Z13.

From the above XRD pattern high intensity peak is observed at 31^0, and low intensity peaks are observed around 12^0, 26^0, 29^0, 34^0, 37^0, 41^0, 45^0 and 51^0. The crystallite size is calculated from Scherrer's formula, and is found to be 86.16 nm.

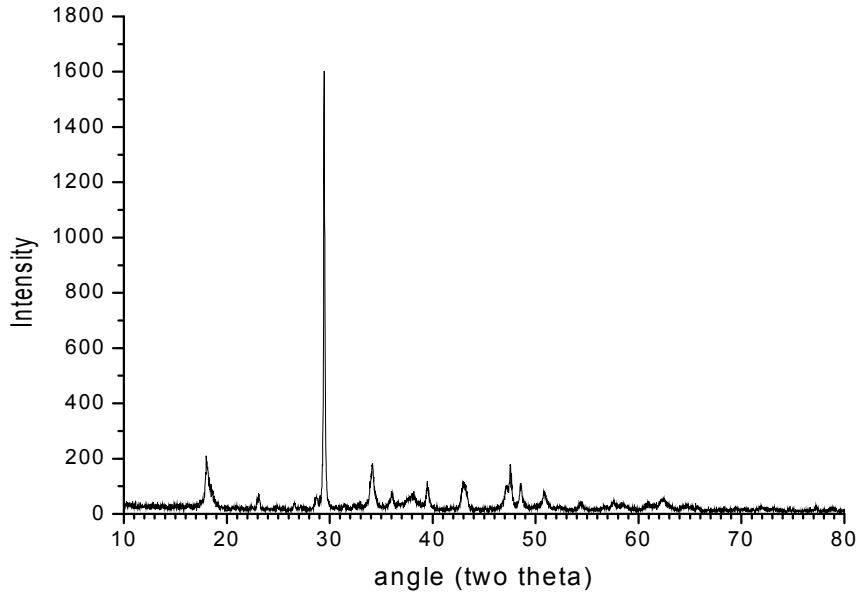

Fig. 4.27 Shows the x-ray diffraction pattern for sample Z13 annealed and quenched from 800^0C.

From the above XRD pattern high intensity peak is observed at 29^0, and low intensity peaks are observed around 18^0 23^0, 34^0, 36^0, 38^0, 39^0, 43^0 and 48^0. The crystallite size is calculated from Scherrer's formula, and is found to be 53.66nm.

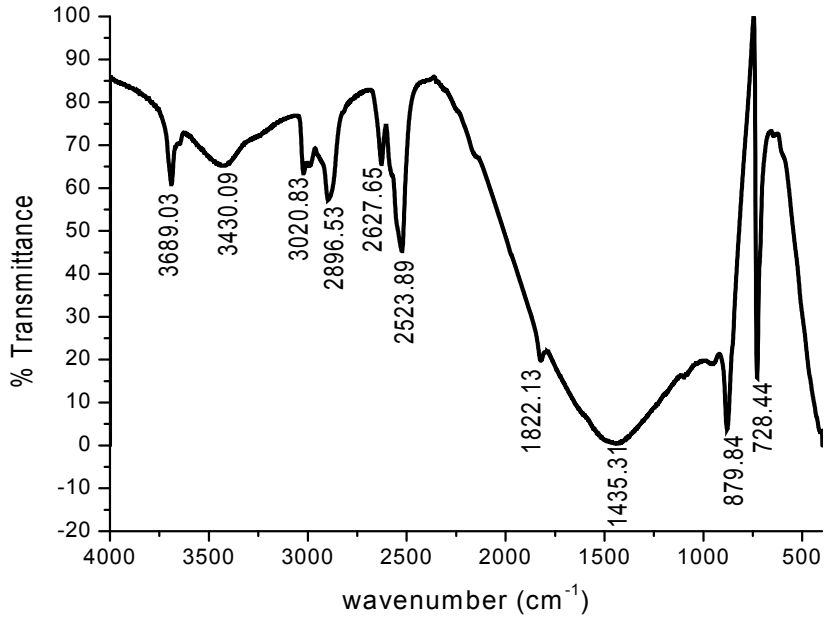

Fig. 4.28 Shows the FTIR absorption spectrum for as received sample Z13.

The FTIR spectra show the out of plane bending at 880 cm^{-1}, the asymmetric stretching at 1435 $cm^{-1}$and in plane bending at 728 cm^{-1}. A OH stretching bond is observed with broad peak at 3430cm^{-1}, this may be due to presence of water molecules and also a sharp absorption peak is observed at 3689cm^{-1}.

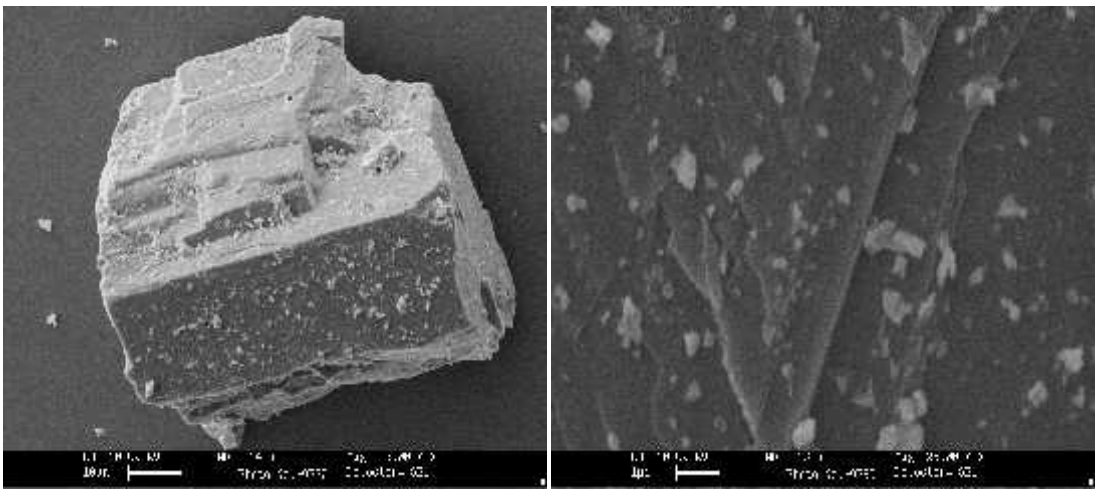

Fig. 4.29 Shows the SEM micrographs of the as received sample Z13.

The above SEM micrographs shows fine layered structure and it is observed that, the size of these layers are in nano scale. Surface morphology is clear. Here the white spots are the crystals of silicate mineral (SiO_2) .

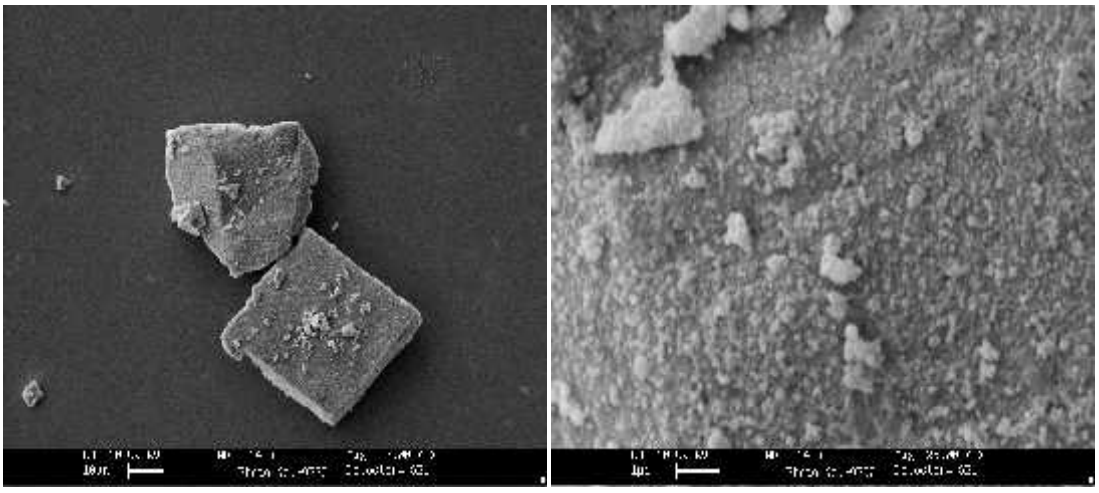

Fig. 4.30 Shows the SEM micrographs of the sample Z13 annealed and quenched from 800^0C.

From the above SEM micrographs it is observed that the sample is having cracks on its surface due to some deformation. This is attributed to the annealing and quenching process.

4.13 TL study of dolomite sample Z14 collected from Mala mining, Bedvi

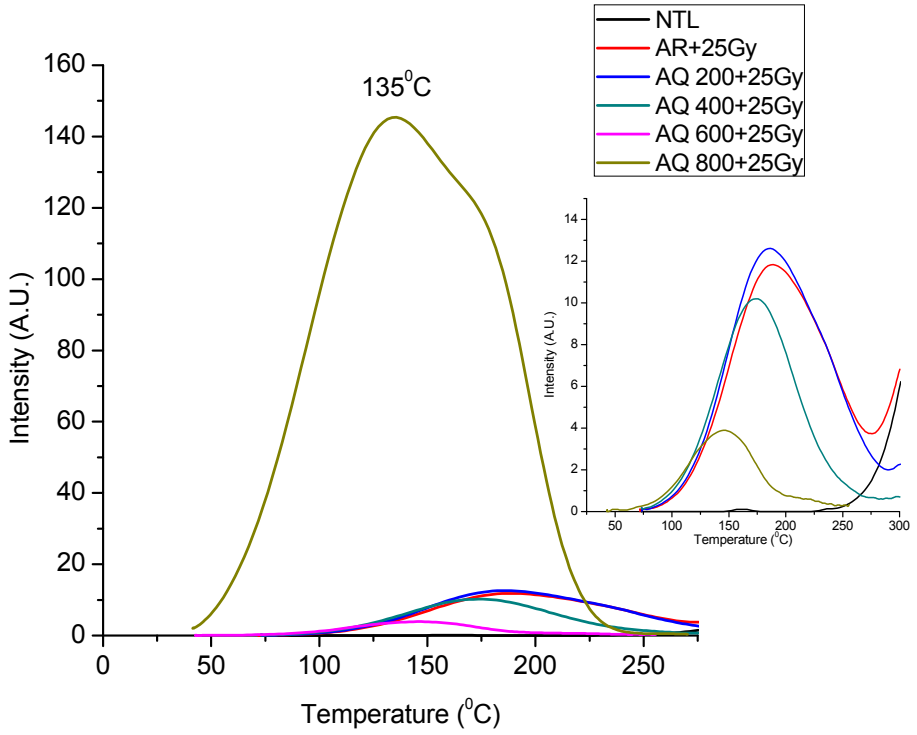

Fig.: 4.31 TL glow curve of as received sample Z14 and also annealed and quenched sample at various temperatures after irradiated using Sr-90 beta source.

The TL glow curve shows a peak around 135^{0}C for the sample annealed and quenched from 800^{0}C. A small hump is observed at 174^{0}C. The sample has shown very low intensity broad TL peak around 187^{0}C, when sample annealed and quenched from 200^{0}C, 400^{0}C and 600^{0}C, which is shown in the inset figure of 4.31. From the TL glow curve it is clear that the TL peak shifts towards lower temperature as the annealing and quenching temperature increases from 200^{0}C to 800^{0}C. The peak temperature and peak Intensity obtained from the glow curve for the Z14 sample are given in Table 4.13.

Table- 4.13

S.No.	AQ Temperature (^{0}C)	Peak Temperature (^{0}C)	Peak Intensity (A.U.)
1	Natural	161	0.11
2	Beta Irradiated	189	11.83
3	200^{0}C + Beta(25Gy)	187	12.61
4	400^{0}C + Beta(25Gy)	173	10.20
5	600^{0}C + Beta(25Gy)	145	3.90
6	800^{0}C + Beta(25Gy)	136	145.37

The above table shows the peak temperature and peak intensity of sample Z14 annealed and quenched from different temperatures. It is observed from the above table 4.13 maximum TL peak intensity is obtained for the sample annealed and quenched from 800^{0}C.

4.14 TL study of dolomite sample Z15 collected from R.C.Mistry Mining, Bedvi

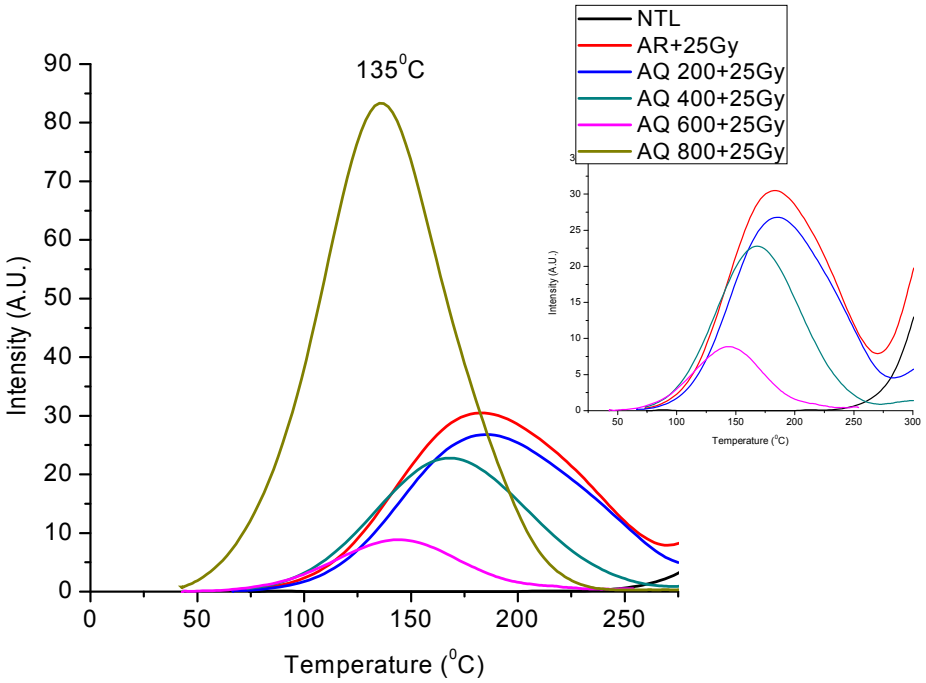

Fig.: 4.32 TL glow curve of as received sample Z15 and also annealed and quenched sample at various temperatures after irradiated using Sr-90 beta source.

The TL glow curve shows a well resolved peak around 135^0C for the sample annealed and quenched from 800^0C. The sample has shown very low intensity broad TL peak around 185^0C, when sample annealed and quenched from 200^0C, 400^0C and 600^0C, which is shown in the inset figure of 4.32. From the TL glow curve it is clear that the TL peak shifts towards lower temperature as the annealing and quenching temperature increases from 200^0C to 800^0C. The peak temperature and peak Intensity obtained from the glow curve for the Z15 sample are given in Table 4.14.

Table-4.14

S.No.	AQ Temperature (^{0}C)	Peak Temperature (^{0}C)	Peak Intensity (A.U.)
1	Natural	-	-
2	Beta Irradiated	182	30.49
3	200^0C + Beta(25Gy)	185	26.79
4	400^0C + Beta(25Gy)	168	22.78
5	600^0C + Beta(25Gy)	144	8.87
6	800^0C + Beta(25Gy)	136	83.32

The above table shows the peak temperature and peak intensity of sample Z15 annealed and quenched from different temperatures. It is observed from the above table 4.14 maximum TL peak intensity is obtained for the sample annealed and quenched from 800^0C.

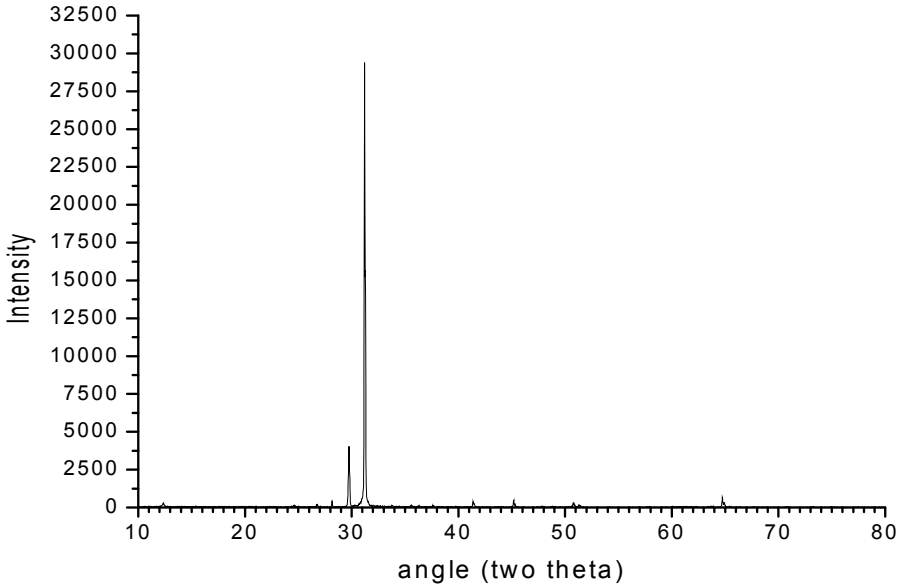

Fig. 4.33 Shows the x-ray diffraction pattern for as received sample Z15.

From the above XRD pattern high intensity peak is observed at 31^0, and low intensity peaks are observed around 12^0, 24^0, 26^0, 29^0, 34^0, 37^0, 41^0, 45^0, 51^0 and 65^0. The crystallite size is calculated from Scherrer's formula, and is found to be 61.56 nm.

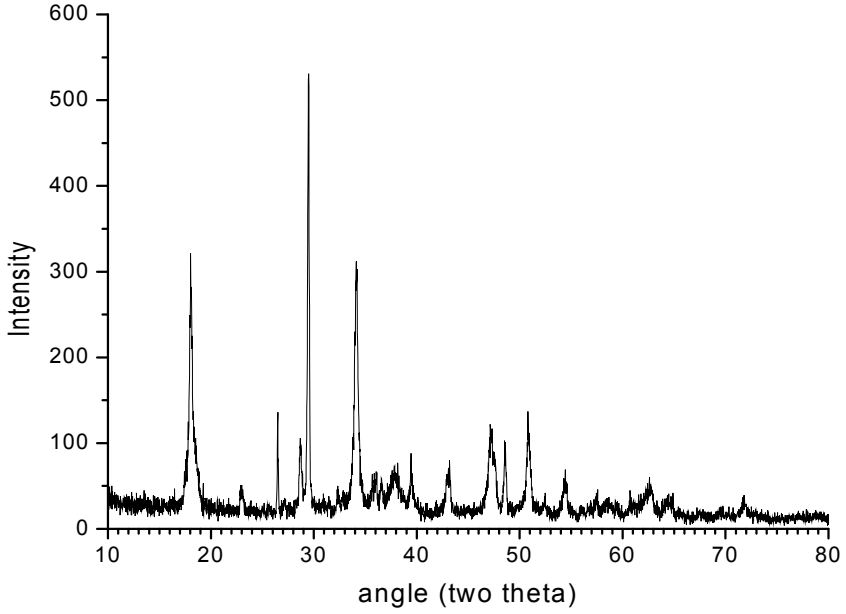

FIG. 4.34 Shows the x-ray diffraction pattern for sample Z15 annealed and quenched from 800^0C.

From the above XRD pattern high intensity peak is observed at 29^0, and low intensity peaks are observed around 18^0, 23^0, 26^0, 28^0, 34^0, 36^0, 39^0, 43^0, 47^0, 48^0, 51^0 and 63^0. The crystallite size is calculated from Scherrer's formula, and is found to be 42.92nm.

4.15 TL study of dolomite sample Z16 collected from Bedvi

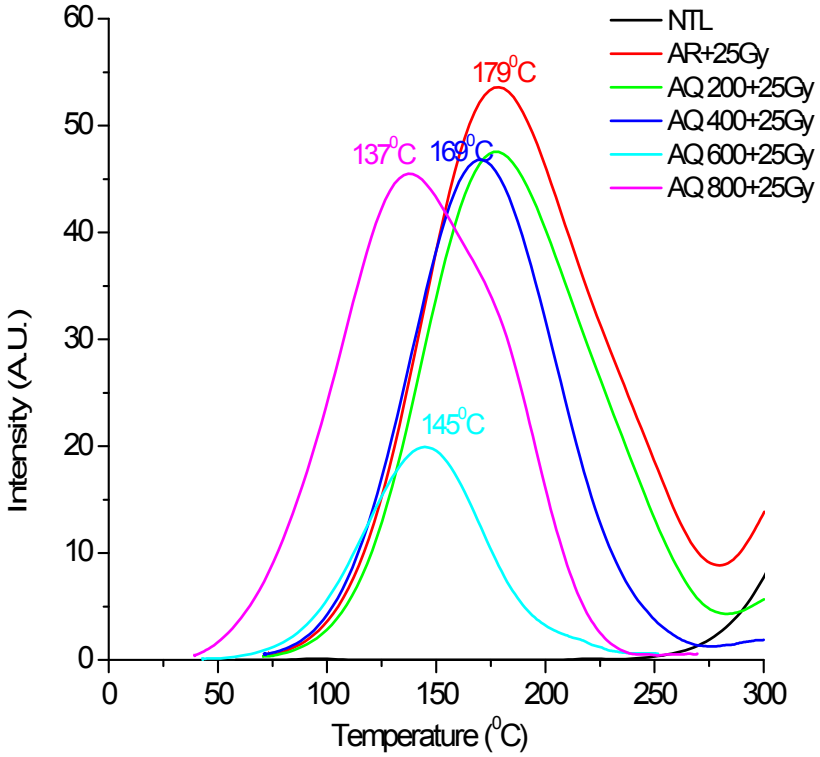

Fig.: 4.35 TL glow curve of as received sample Z16 and also annealed and quenched sample at various temperatures after irradiated using Sr-90 beta source.

The ATL glow curve for as received sample and annealed and quenched from 200^0C, shows a well resolved peak around 179^0. A small hump is observed at 177^0 for the sample annealed and quenched from 800^0C. The variation in intensity is negligible for entire ATL glow curves. From the TL glow curve it is clear that the TL peak shifts towards lower temperature as the annealing and quenching temperature increases from 200^0C to 800^0C. The peak temperature and peak Intensity obtained from the glow curve for the Z16 sample are given in Table 4.15.

Table- 4.15

S.No.	AQ Temperature (^{0}C)	Peak Temperature (^{0}C)	Peak Intensity (A.U.)
1	Natural	-	-
2	Beta Irradiated	179	53.60
3	200^{0}C + Beta(25Gy)	176	47.53
4	400^{0}C + Beta(25Gy)	171	46.79
5	600^{0}C + Beta(25Gy)	145	19.93
6	800^{0}C + Beta(25Gy)	137	45.49

The above table shows the peak temperature and peak intensity of sample Z16 annealed and quenched from different temperatures. It is observed from the above table 4.15 maximum TL peak intensity is obtained for the sample annealed and quenched from 800^{0}C.

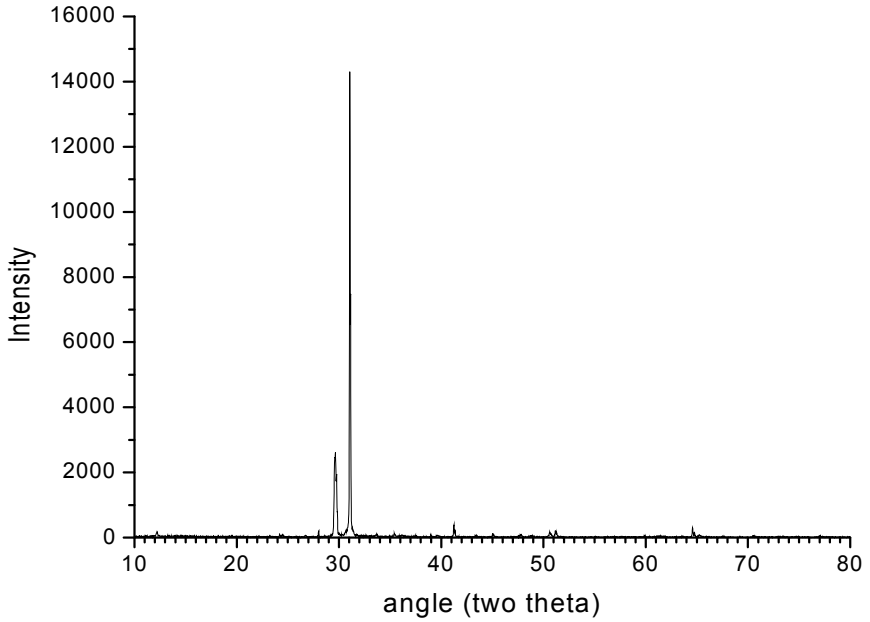

Fig. 4.36 Shows the x-ray diffraction pattern for as received sample Z16.

From the above XRD pattern high intensity peak is observed at 31^0 and low intensity peaks are observed around 12^0, 28^0, 29^0, 35^0, 41^0, 45^0, 51^0 and 65^0. The crystallite size is calculated from Scherrer's formula, and is found to be 71.80 nm.

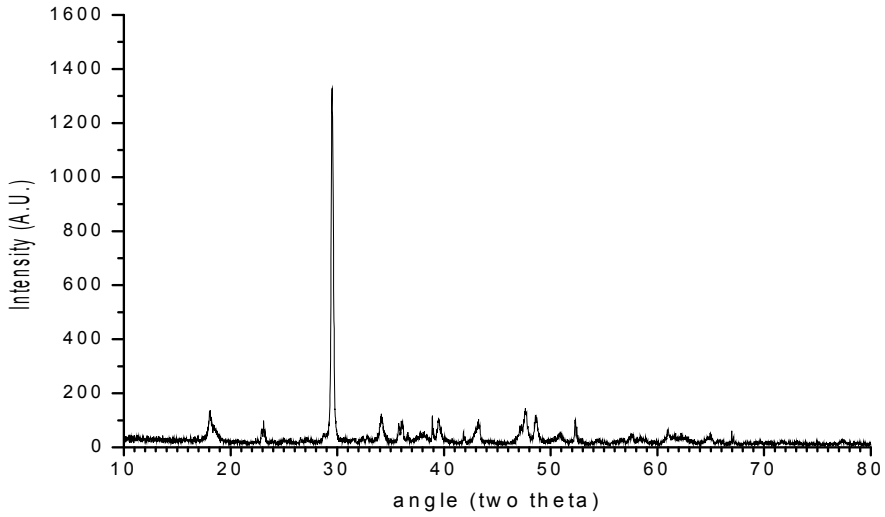

Fig. 4.37 Shows the x-ray diffraction pattern for sample Z16 annealed and quenched from 800^0C.

From the above XRD pattern high intensity peak is observed at 29^0 and low intensity peaks are observed around 18^0, 23^0, 34^0, 36^0, 39^0, 43^0, 47^0, 48^0, 52^0 and 61^0. The crystallite size is calculated from Scherrer's formula, and is found to be 39.02nm.

4.16 TL study of dolomite sample Z17 collected from Kishan Mining, Bedvi

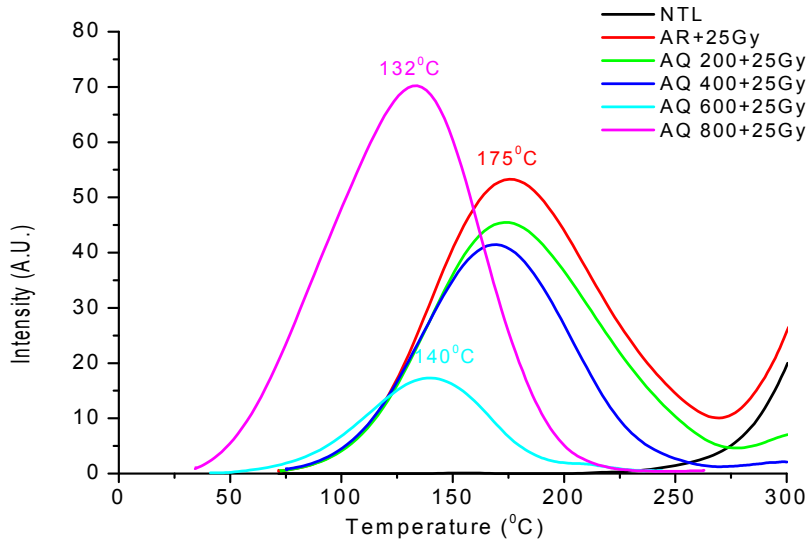

Fig.: 4.38 TL glow curve of as received sample Z17 and also annealed and quenched sample at various temperatures after irradiated using Sr-90 beta source.

From the TL glow curve high intensity well resolved peak is observed at 132^0C for the sample annealed and quenched from 800^0C. The ATL glow curve for as received sample and annealed and quenched from 200^0C shows a well resolved peak around 175^0. The variation in intensity is negligible for entire ATL glow curves. From the TL glow curve it is clear that the TL peak shifts towards lower temperature as the annealing and quenching temperature increases from 200^0C to 800^0C. The peak temperature and peak Intensity obtained from the glow curve for the Z17 sample are given in Table 4.16.

Table-4.16

S.No.	AQ Temperature (^{0}C)	Peak Temperature (^{0}C)	Peak Intensity (A.U.)
1	Natural	155	0.11
2	Beta Irradiated	175	53.28
3	200^0C + Beta(25Gy)	173	45.48
4	400^0C + Beta(25Gy)	170	41.45
5	600^0C + Beta(25Gy)	140	17.31
6	800^0C + Beta(25Gy)	132	70.21

The above table shows the peak temperature and peak intensity of sample Z17 annealed and quenched from different temperatures. It is observed from the above table 4.16 maximum TL peak intensity is obtained for the sample annealed and quenched from 800^0C.

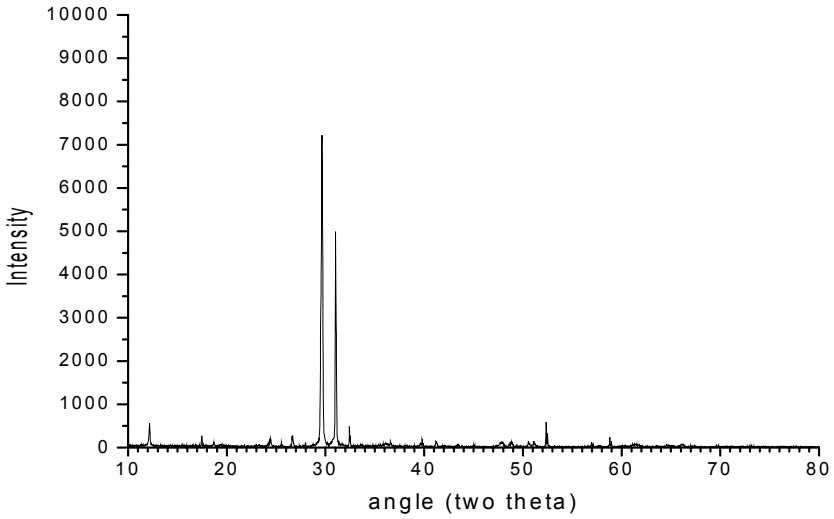

Fig. 4.39 Shows the x-ray diffraction pattern for as received sample Z17.

From the above XRD pattern high intensity peak is observed at 29^0, and low intensity peaks are observed around 12^0, 17^0, 18^0, 24^0, 25^0, 26^0, 27^0, 31^0, 32^0, 36^0,390, 41^0, 47^0, 49^0, 51^0, 520, 57^0 and 59^0. The crystallite size is calculated from Scherrer's formula, and is found to be 47.40 nm.

4.17 TL study of dolomite sample Z18 collected from Silver Mining, Bedvi

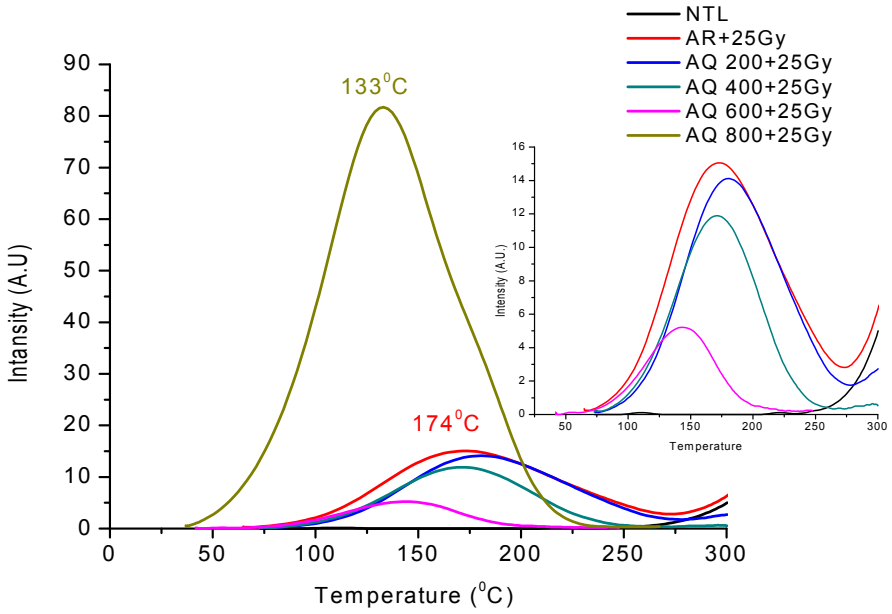

Fig.: 4.40 TL glow curve of as received sample Z18 and also annealed and quenched sample at various temperatures after irradiated using Sr-90 beta source.

The TL glow curve shows a peak around 133^0C for the sample annealed and quenched from 800^0C. A small hump is also observed around 174^0C. The sample has shown very low intensity broad TL peak around 171^0C, when sample annealed and quenched from 200^0C, 400^0C and 600^0C, which is shown in the inset figure of 4.40. From the TL glow curve it is clear that the TL peak shifts towards lower temperature as the annealing and quenching temperature increases from 200^0C to 800^0C. The peak temperature and peak Intensity obtained from the glow curve for the Z18 sample are given in Table 4.17.

Table- 4.17

S.No.	AQ Temperature (^{0}C)	Peak Temperature (^{0}C)	Peak Intensity (A.U.)
1	Natural	-	-
2	Beta Irradiated	174	15.06
3	200^0C + Beta(25Gy)	181	14.12
4	400^0C + Beta(25Gy)	171	11.89
5	600^0C + Beta(25Gy)	144	5.22
6	800^0C + Beta(25Gy)	133	81.69

The above table shows the peak temperature and peak intensity of sample Z18 annealed and quenched from different temperatures. It is observed from the above table 4.17maximum TL peak intensity is obtained for the sample annealed and quenched from 800^0C.

4.18 TL study of dolomite sample Z19 collected from Nazru sheth, Bedvi

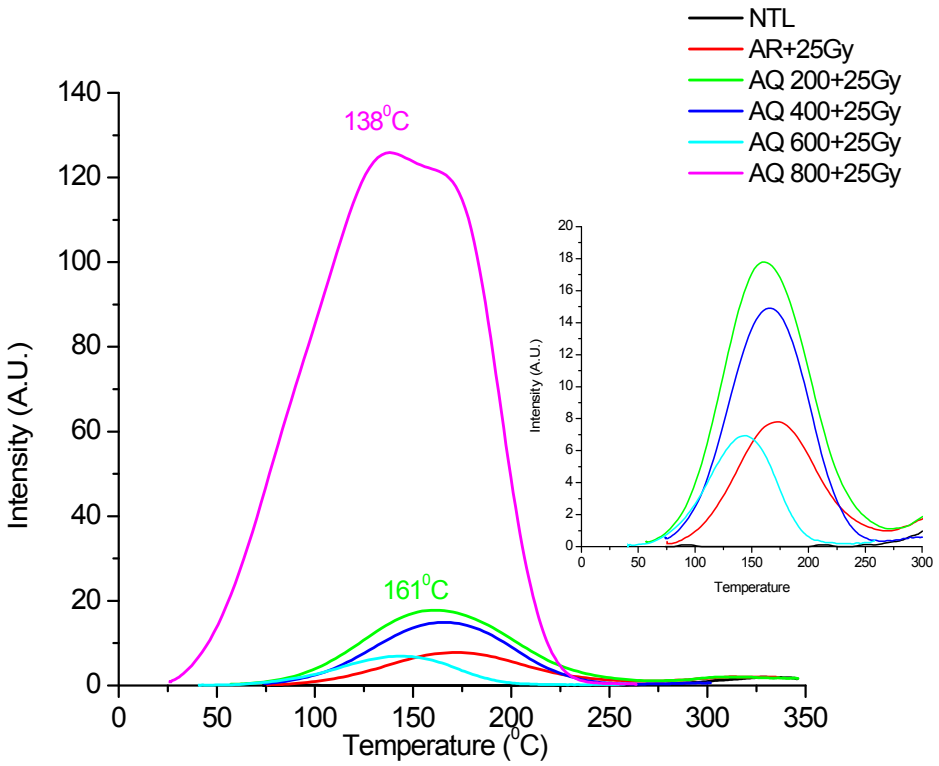

Fig.: 4.41 TL glow curve of as received sample Z19 and also annealed and quenched sample at various temperatures after irradiated using Sr-90 beta source.

The TL glow curve shows a peak around 135^{0}C for the sample annealed and quenched from 800^{0}C and also a small hump is observed at 165^{0}C. The sample has shown very low intensity broad TL peak around 161^{0}C, when sample annealed and quenched from 200^{0}C, 400^{0}C and 600^{0}C, which is shown in the inset figure of 4.41. From the TL glow curve it is clear that the TL peak shifts towards lower temperature as the annealing and quenching temperature increases from 200^{0}C to 800^{0}C. The peak temperature and peak Intensity obtained from the glow curve for the Z19 sample are given in Table 4.18.

Table-4.18

S.No.	AQ Temperature (^{0}C)	Peak Temperature (^{0}C)	Peak Intensity (A.U.)
1	Natural	-	-
2	Beta Irradiated	172	7.80
3	200^{0}C + Beta(25Gy)	161	17.79
4	400^{0}C + Beta(25Gy)	165	14.90
5	600^{0}C + Beta(25Gy)	144	6.94
6	800^{0}C + Beta(25Gy)	138	125.87

The above table shows the peak temperature and peak intensity of sample Z19 annealed and quenched from different temperatures. It is observed from the above table 4.18 maximum TL peak intensity is obtained for the sample annealed and quenched from 800^{0}C.

4.19 TL study of dolomite sample Z20 collected from Madhav mining, Bedvi

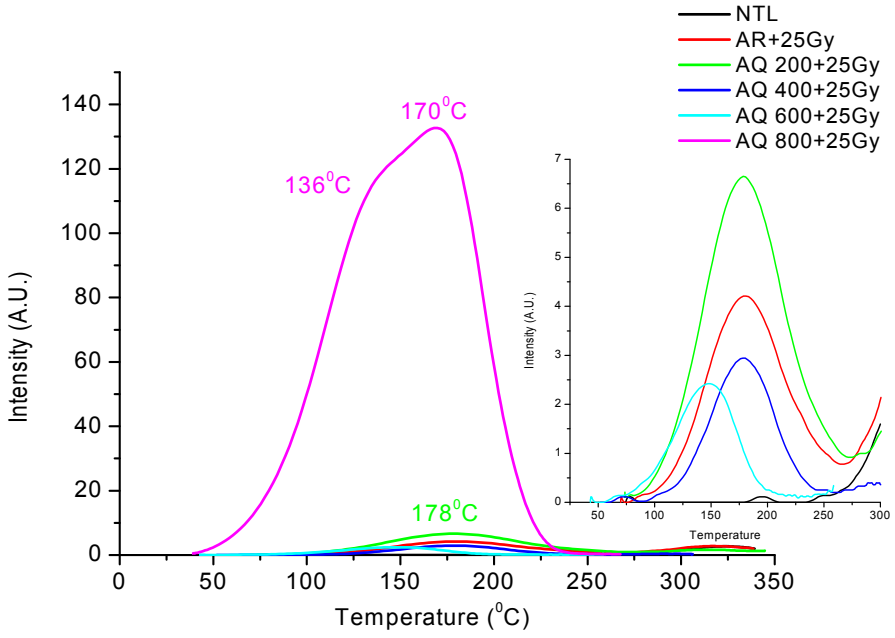

Fig.: 4.42 TL glow curve of as received sample Z20 and also annealed and quenched sample at various temperatures after irradiated using Sr-90 beta source.

The TL glow curve shows a peak around 170^0C for the sample annealed and quenched from 800^0C and also a small hump is observed at 136^0C. The sample has shown very low intensity broad TL peak around 178^0C when sample annealed and quenched from 200^0C, 400^0C and 600^0C, which is shown in the inset figure of 4.42. The peak temperature and peak Intensity obtained from the glow curve for the Z20 sample are given in Table 4.19.

Table- 4.19

S.No.	AQ Temperature (^{0}C)	Peak Temperature (^{0}C)	Peak Intensity (A.U.)
1	Natural	-	-
2	Beta Irradiated	178	4.21
3	200^0C + Beta(25Gy)	178	6.65
4	400^0C + Beta(25Gy)	178	2.94
5	600^0C + Beta(25Gy)	147	2.42
6	800^0C + Beta(25Gy)	170	132.69

The above table shows the peak temperature and peak intensity of sample Z20 annealed and quenched from different temperatures. It is observed from the above table 4.19 maximum TL peak intensity is obtained for the sample annealed and quenched from 800^0C.

4.20 TL study of dolomite sample Z21 collected from Padaliya

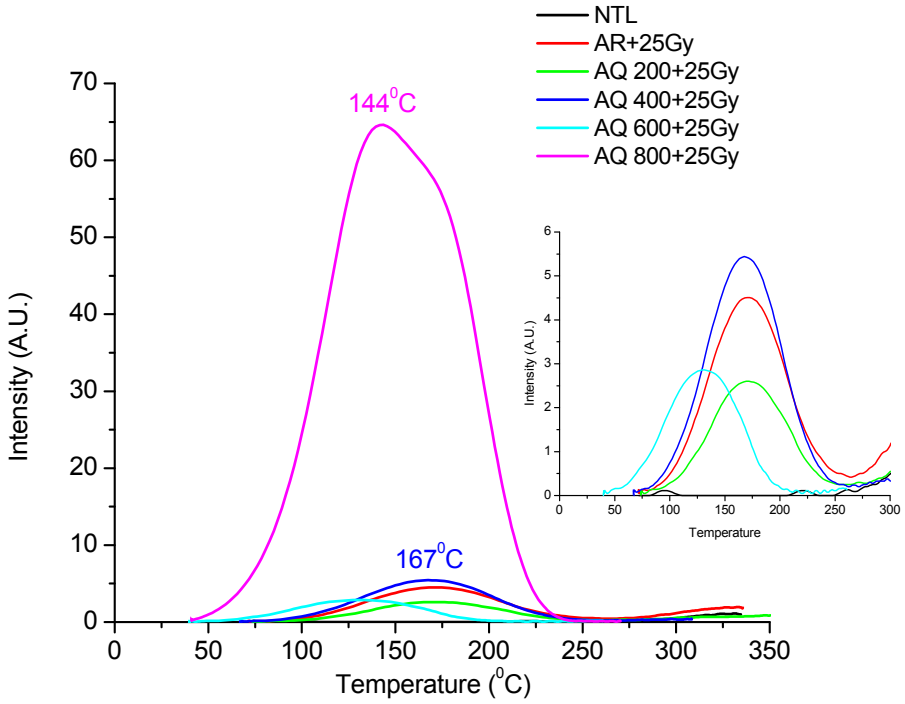

Fig.: 4.43 TL glow curve of as received sample Z21 and also annealed and quenched sample at various temperatures after irradiated using Sr-90 beta source.

The TL glow curve shows a peak with hump around 144^{0}C for the sample annealed and quenched from 800^{0}C and also a small hump is observed at 175^{0}C. The sample has shown very low intensity broad TL peak around 170^{0}C when sample annealed and quenched from 200^{0}C, 400^{0}C and 600^{0}C, which is shown in the inset figure of 4.43. From the TL glow curve it is clear that the TL peak shifts towards lower temperature as the annealing and quenching temperature increases from 200^{0}C to 800^{0}C. The peak temperature and peak Intensity obtained from the glow curve for the Z21 sample are given in Table 4.20.

Table- 4.20

S.No.	AQ Temperature (^{0}C)	Peak Temperature (^{0}C)	Peak Intensity (A.U.)
1	Natural	95	0.11
2	Beta Irradiated	170	4.51
3	200^{0}C + Beta(25Gy)	170	2.6
4	400^{0}C + Beta(25Gy)	167	5.44
5	600^{0}C + Beta(25Gy)	130	2.86
6	800^{0}C + Beta(25Gy)	144	64.61

The above table shows the peak temperature and peak intensity of sample Z21 annealed and quenched from different temperatures. It is observed from the above table 4.20 maximum TL peak intensity is obtained for the sample annealed and quenched from 800^{0}C.

4.21 TL study of Fluorspar sample Z22 collected from Amba dungar, Kadipani

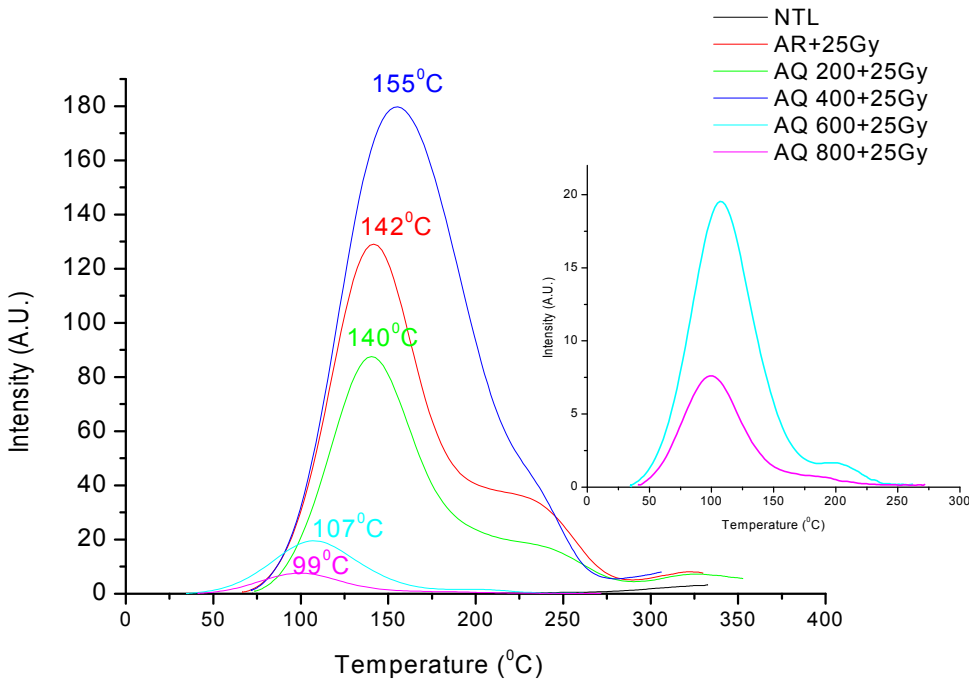

Fig.: 4.44 TL glow curve of as received sample Z22 and also annealed and quenched sample at various temperatures after irradiated using Sr-90 beta source.

The TL glow curve shows a high intensity peak around 155^0C for the sample annealed and quenched from 400^0C and also a small hump is observed at 225^0C. It is observed that the TL peak intensity increases as the annealing and quenching temperature increases from 200^0C to 400^0C and also this Peak shifts towards higher temperature. It is also observed that TL peak intensity drastically falls down as annealing and quenching temperature increases from 400^0C to 800^0C.From the TL glow curve it is observed that the TL peak and hump shifts towards lower temperature as the annealing and quenching temperature increases from 400^0C to 800^0C and also intensity drastically falls down. The peak temperature and peak Intensity obtained from the glow curve for the Z22 sample are given in Table 4.21.

Table- 4.21

S.No.	AQ Temperature (^{0}C)	Peak Temperature (^{0}C)	Peak Intensity (A.U.)
1	Natural	165	0.11
2	Beta Irradiated	142, 225	129.09, 36.73
3	200^0C + Beta(25Gy)	140, 225	87.55, 19.02
4	400^0C + Beta(25Gy)	155, 225	179.71, 49.69
5	600^0C + Beta(25Gy)	107, 200	19.53, 1.67
6	800^0C + Beta(25Gy)	99, 185	7.6, 0.73

The above table shows the peak temperature and peak intensity of sample Z22 annealed and quenched from different temperatures. It is observed from the above table 4.21 maximum TL peak intensity is obtained for the sample annealed and quenched from 400^0C. It is interesting to note as the annealing and quenching temperature increases the TL peak intensity increases and reduced to 7.6a.u. when annealed and quenched from 800^0C. It may be due to decomposition of the mineral at various temperature.

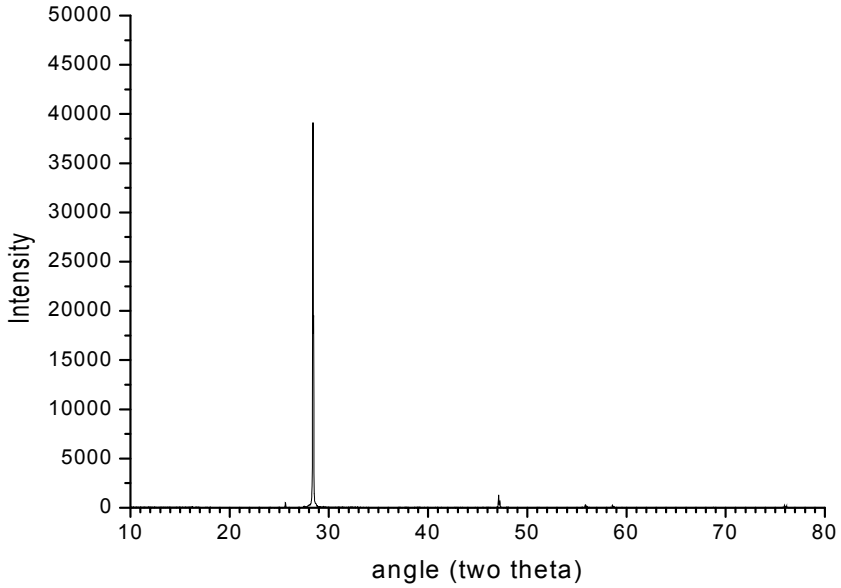

Fig. 4.45 Shows the x-ray diffraction pattern for as received sample Z22.

From the above XRD pattern high intensity peak is observed at 28^0 and low intensity peaks are observed at 26^0, 47^0, 56^0, 59^0 and 76^0. The crystallite size is calculated from Scherrer's formula, and is found to be 71.33 nm.

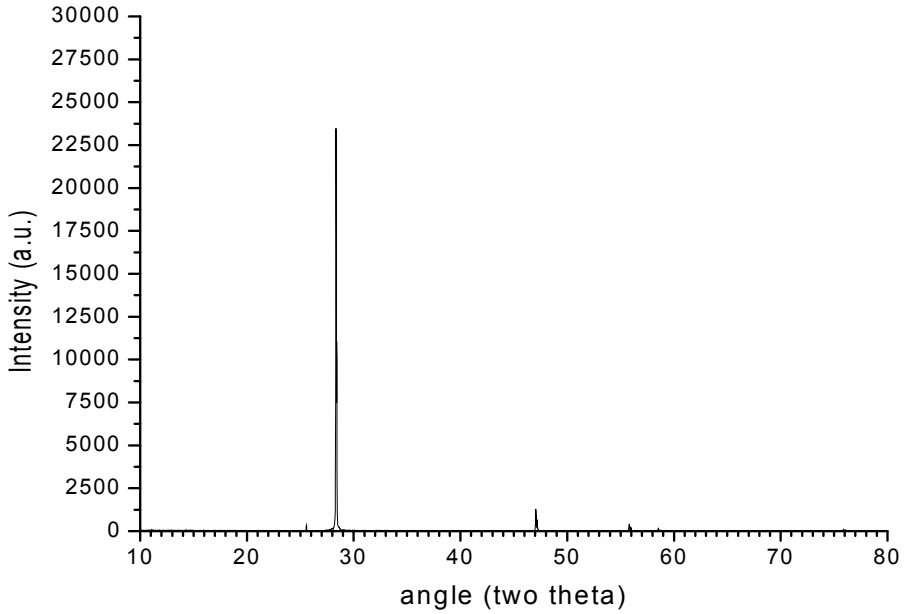

Fig. 4.46 Shows the x-ray diffraction pattern for the sample Z22 annealed and quenched from 800^0C.

From the above XRD pattern high intensity peak is observed at 28^0 and low intensity peaks are observed at 26^0, 47^0, 56^0, 59^0 and 76^0. The crystallite size is calculated from Scherrer's formula, and is found to be 85.61 nm.

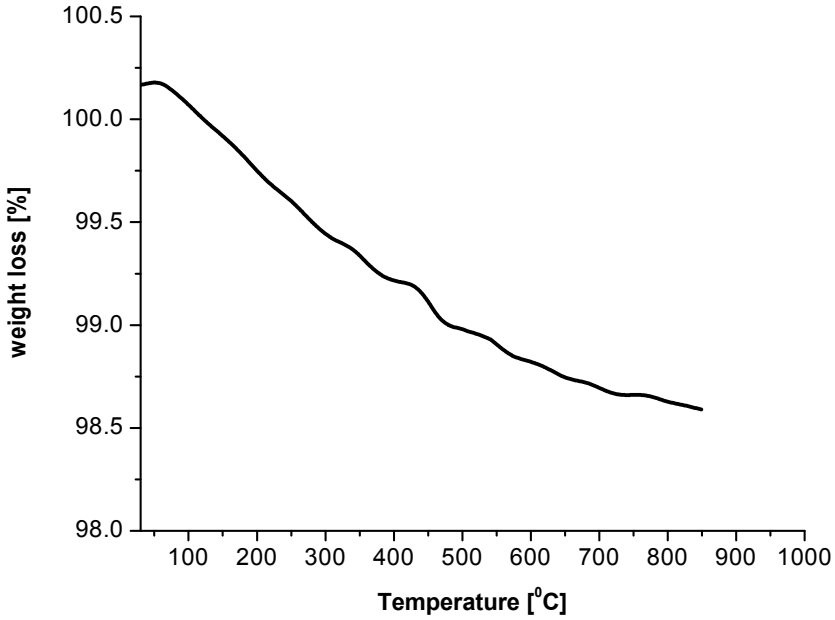

Fig. 4.47 Shows TGA curve for the as received sample Z22.

From the above TGA curve it is observed that the sample lost its weight by 1.5% within 800^0C. This weight loss is attributed to the loss of water molecules from the sample. A small hump is also observed at 400^0C.

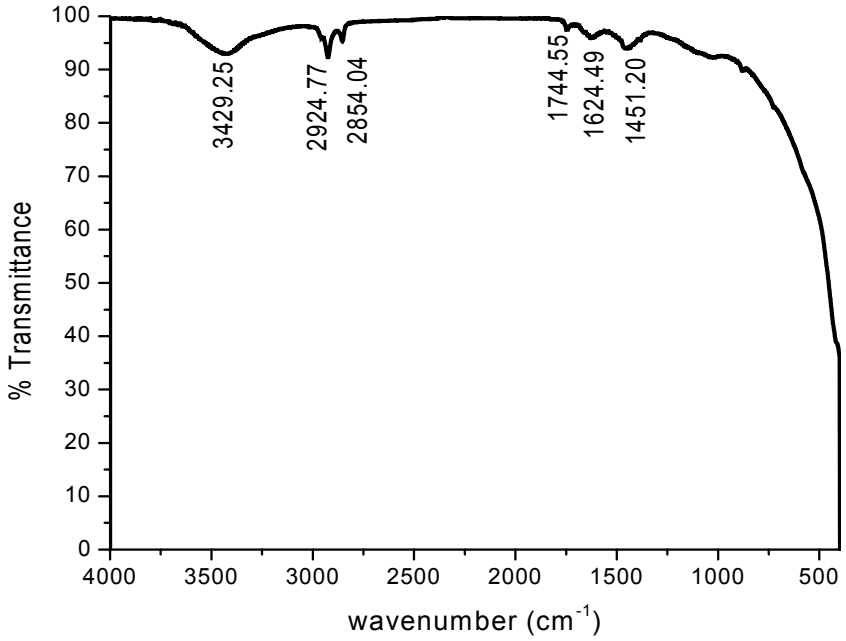

Fig. 4.48 Shows the FTIR absorption spectrum for as received sample Z22

The above FTIR spectra shows a small amount of absorption due to asymmetric stretching around 1451 cm^{-1} and (OH) stretching bond is observed with broad peak at 3429cm^{-1}. This may be due to presence of water molecules.

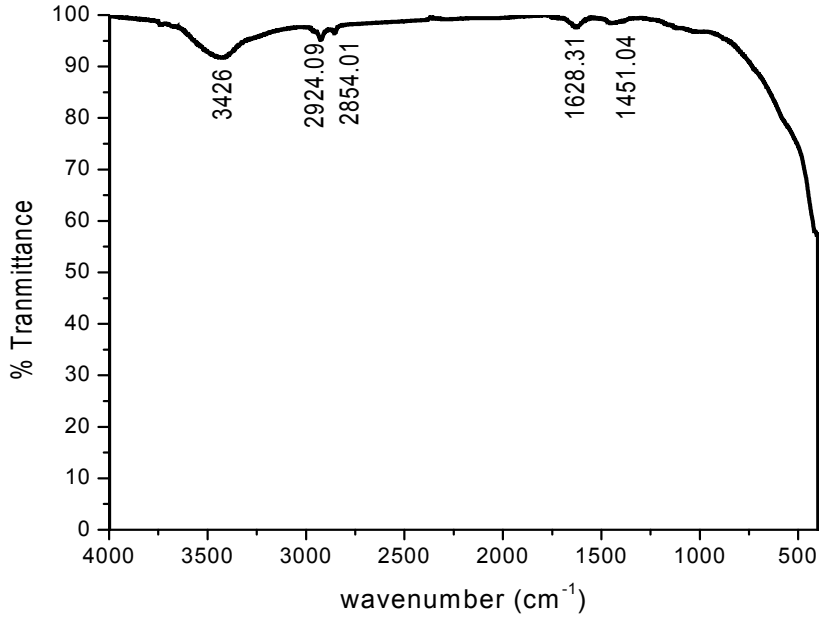

Fig. 4.49 Shows the FTIR absorption spectrum for as received sample Z22.

The FTIR spectra shows a small amount of absorption due to asymmetric stretching around 1451 cm^{-1} and (OH) stretching bond is observed with broad peak at 3426cm^{-1}. This may be due to presence of water molecules.

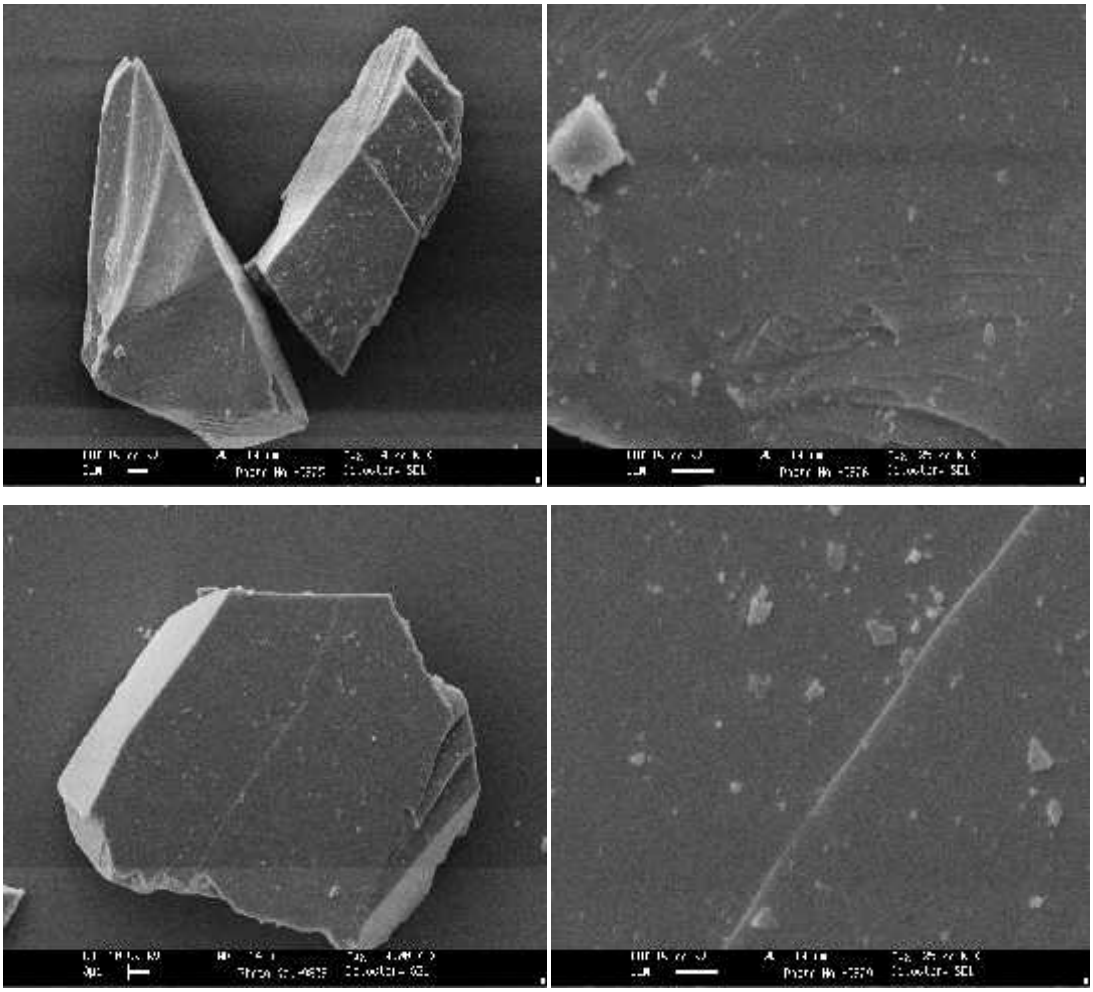

Fig. 4.50 Shows the SEM micrographs of the as received sample Z22.

SEM photographs shows fine layered structure and it is observed that, the size of these layers are in nano scale. Surface morphology is clear

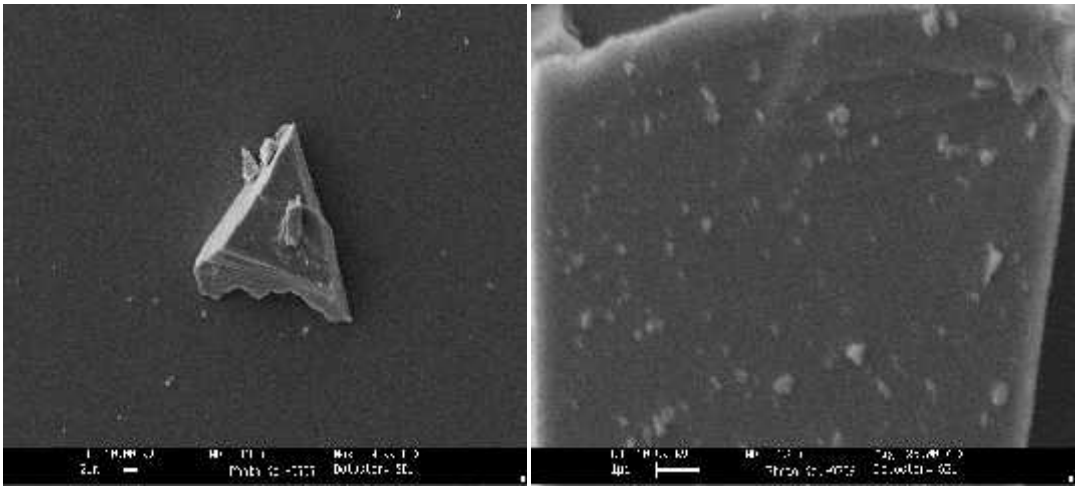

Fig. 4.51 Shows the SEM micrographs of the sample Z03 annealed and quenched from 800^0C.

There is no change observed in layered structure and on the surface when compared to as received sample.

4.22 TL study of Appophyllite sample Z23 collected from Jalgaon (M.S.)

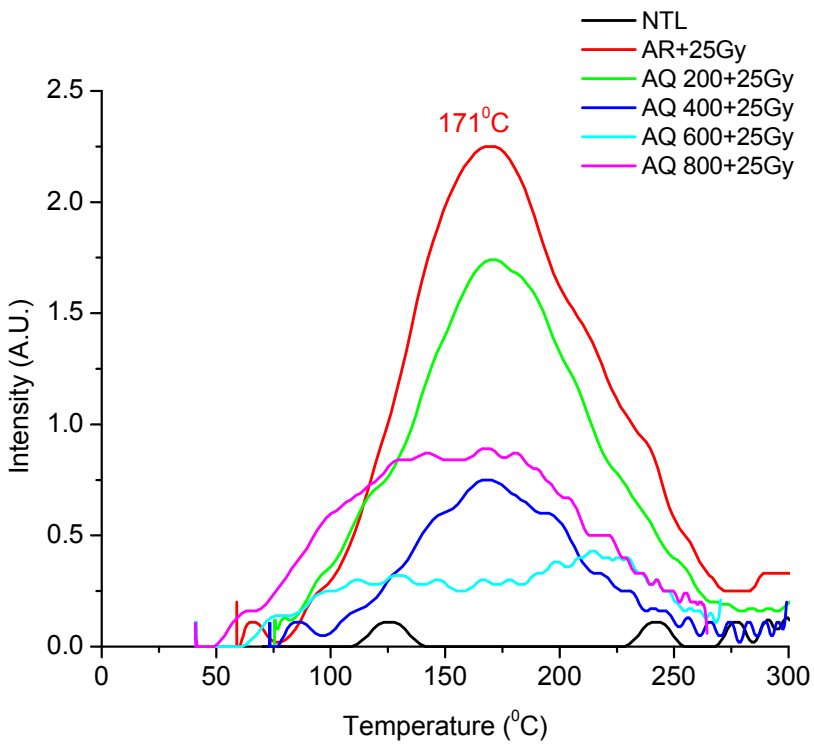

Fig.: 4.52 TL glow curve of as received sample Z23 and also annealed and quenched sample at various temperatures after irradiated using Sr-90 beta source.

The TL glow curve shows a peak with kinks around 171^0C for the as received sample, annealed and quenched from 200^0C and 400^0C. There is no good TL observed for the remaining sample which are annealed and quenched from 600^0C and 800^0C. TL peak temperature and peak intensity obtained from the glow curve of sample Z23 is given in the table 4.22.

Table- 4.22

S.No.	AQ Temperature (^{0}C)	Peak Temperature (^{0}C)	Peak Intensity (A.U.)
1	Natural	126	0.11
2	Beta Irradiated	169	2.25
3	200^0C + Beta(25Gy)	170	1.74
4	400^0C + Beta(25Gy)	169	0.75
5	600^0C + Beta(25Gy)	129	0.32
6	800^0C + Beta(25Gy)	168	0.89

The above table shows the peak temperature and peak intensity of sample Z23 annealed and quenched from different temperatures. It is observed from the above table 4.22 maximum TL peak intensity is obtained for the as received sample irradiated by Sr-90

4.23 TL study of Appophyllite sample Z24 collected from Nasik (M.S.)

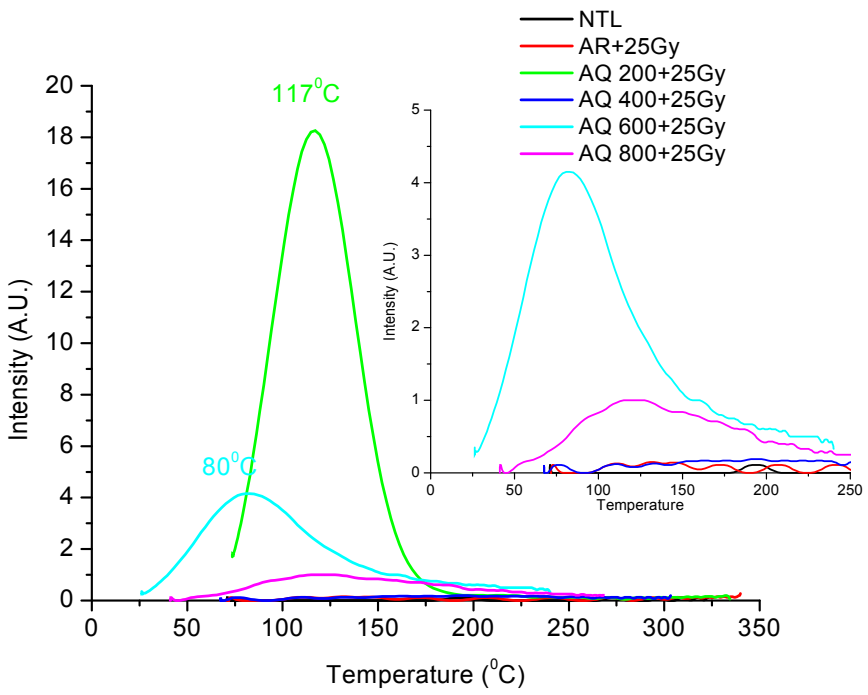

Fig.: 4.53 TL glow curve of as received sample Z24 and also annealed and quenched sample at various temperatures after irradiated using Sr-90 beta source.

The TL glow curve shows a well resolved high intensity peak around 117^{0}C for the sample annealed and quenched from 200^{0}C. This peak shifts at 80^{0}C for the sample annealed and quenched from 600^{0}C. There is no good TL observed for as received, annealed and quenched from 400^{0}C and 800^{0}C. TL peak temperature and peak intensity obtained from the glow curve of sample Z24 is given in the table 4.23.

Table- 4.23

S.No.	AQ Temperature (^{0}C)	Peak Temperature (^{0}C)	Peak Intensity (A.U.)
1	Natural	-	-
2	Beta Irradiated	-	-
3	200^{0}C + Beta(25Gy)	117	18.26
4	400^{0}C + Beta(25Gy)	-	-
5	600^{0}C + Beta(25Gy)	81	4.15
6	800^{0}C + Beta(25Gy)	121	1

The above table shows the peak temperature and peak intensity of sample Z24 annealed and quenched from different temperatures. It is observed from the above table 4.23 maximum TL peak intensity is obtained for the sample annealed and quenched from 200^{0}C.

4.24 TL study of Appophyllite sample Z25 collected from Mahad (M.S.)

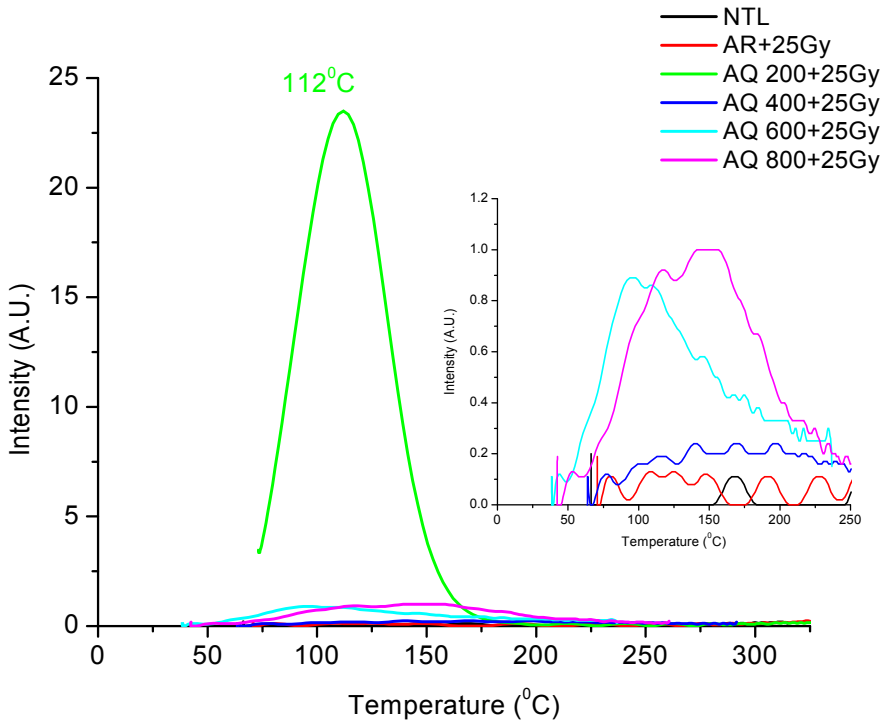

Fig.: 4.54 TL glow curve of as received sample Z25 and also annealed and quenched sample at various temperatures after irradiated using Sr-90 beta source.

The TL glow curve shows a well resolved high intensity peak around 112^0C for the sample annealed and quenched from 200^0C. There is no good TL observed for as received sample and sample annealed quenched from 400^0C, 600^0C and 800^0C. TL peak temperature and peak intensity obtained from the glow curve of sample Z25 is given in the table 4.24.

Table- 4.24

S.No.	AQ Temperature (^{0}C)	Peak Temperature (^{0}C)	Peak Intensity (A.U.)
1	Natural	-	-
2	Beta Irradiated	-	-
3	200^0C + Beta(25Gy)	112	23.49
4	400^0C + Beta(25Gy)	-	-
5	600^0C + Beta(25Gy)	96	0.89
6	800^0C + Beta(25Gy)	149	1

The above table shows the peak temperature and peak intensity of sample Z25 annealed and quenched from different temperatures. It is observed from the above table 4.24 maximum TL peak intensity is obtained for the sample annealed and quenched from 200^0C.

4.25 TL study of Heulandite sample Z26 collected from Nasik (M.S.)

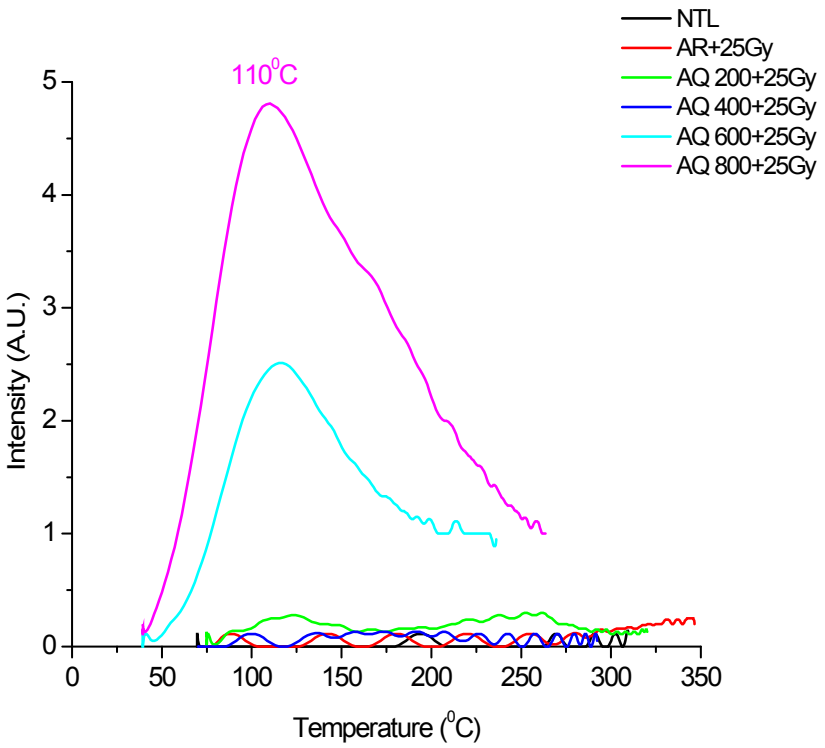

Fig.: 4.55 TL glow curve of as received sample Z26 and also annealed and quenched sample at various temperatures after irradiated using Sr-90 beta source.

The TL glow curve shows a broad peak around 110^{0}C for the sample annealed and quenched from 800^{0}C and 600^{0}C. There is no good TL observed for as received sample and sample annealed and quenched from 200^{0}C and 400^{0}C. TL Peak temperature and peak intensity obtained from the TL glow curve of sample Z26 is given in the table 4.25.

Table- 4.25

S.No.	AQ Temperature (^{0}C)	Peak Temperature (^{0}C)	Peak Intensity (A.U.)
1	Natural	-	-
2	Beta Irradiated	-	-
3	200^{0}C + Beta(25Gy)	-	-
4	400^{0}C + Beta(25Gy)	-	-
5	600^{0}C + Beta(25Gy)	110	2.51
6	800^{0}C + Beta(25Gy)	110	4.81

The above table shows the peak temperature and peak intensity of sample Z26 at different annealing and quenching temperature irradiated with beta source Sr-90. From the table 4.25 it is observed that the peak intensity is maximum for sample annealed and quenched from 800^{0}C. Not much TL was observed in heulandite collected from Nasik. Here the peak at 110^{0}C is noting but originated from SiO_2 of the mineral.

4.26 TL study of Prehnite sample Z27 collected from Mumbai (M.S.)

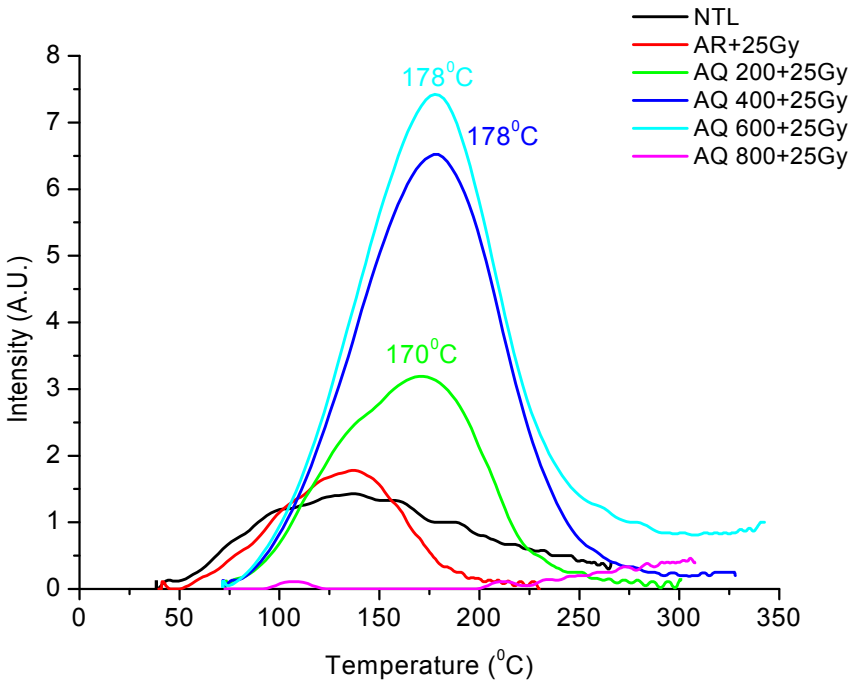

Fig.: 4.56 TL glow curve of as received sample Z27 and also annealed and quenched sample at various temperatures after irradiated using Sr-90 beta source.

The TL glow curve shows a well resolved high intensity peak around 178^0C for the sample annealed and quenched from 600^0C. From the TL glow curve it is observed that NTL and ATL for as received sample exhibits a broad peak having kinks. A small hump is also observed around 140^0C for the sample annealed and quenched from 200^0C. There is no good TL is observed for the sample annealed and quenched from 800^0C. It is also observed from the TL glow curve that the peak position shifts towards higher temperature and also peak intensity increases as the annealing and quenching temperature increases from 200^0C to 400^0C. The peak temperature and peak Intensity obtained from the glow curve for the sample Z27 is given in the table 4.26.

Table- 4.26

S.No.	AQ Temperature (^{0}C)	Peak Temperature (^{0}C)	Peak Intensity (A.U.)
1	Natural	136	1.43
2	Beta Irradiated	136	1.78
3	200^0C + Beta(25Gy)	170	3.19
4	400^0C + Beta(25Gy)	177	6.52
5	600^0C + Beta(25Gy)	178	7.42
6	800^0C + Beta(25Gy)	-	-

The above table shows the peak temperature and peak intensity of sample Z27 at different annealing and quenching temperature irradiated with beta source Sr-90. From the table 4.26 it is observed that the high intensity peak is obtained from the sample annealed and quenched from 600^0C

4.27 TL study of Prehnite sample Z28 collected from Mahad (M.S.)

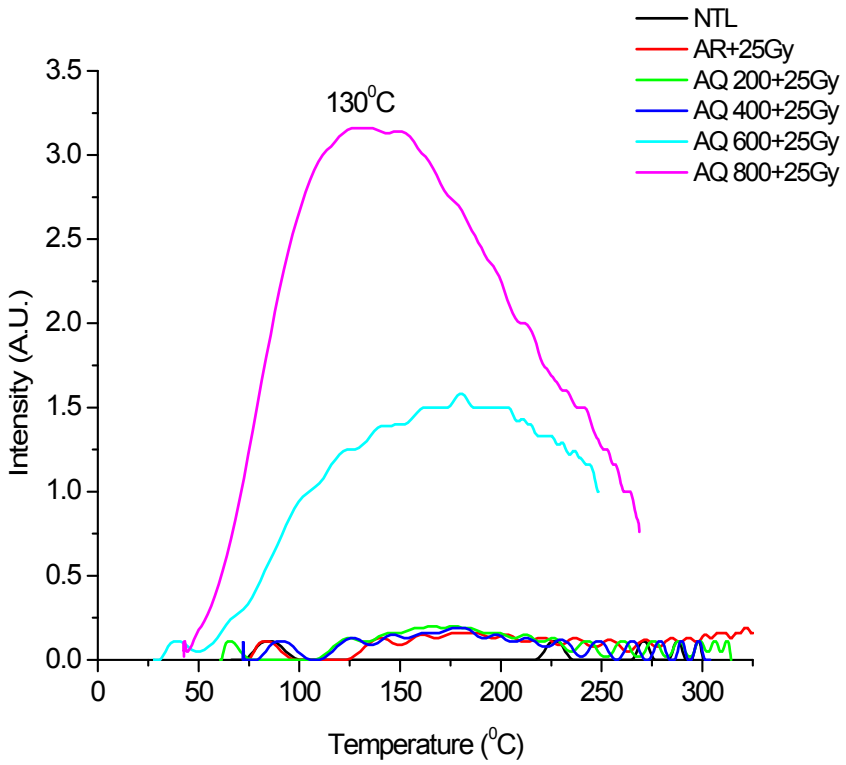

Fig.: 4.57 TL glow curve of as received sample Z28and also annealed and quenched sample at various temperatures after irradiated using Sr-90 beta source.

The TL glow curve shows a broad peak around 130^{0}C for the sample annealed and quenched from 800^{0}C. A hump and kinks are also observed in the TL glow curve. There is no good TL observed from NTL, ATL for as received sample and sample annealed and quenched from 200^{0}C, 400^{0}C and 600^{0}C. TL peak temperature and peak intensity obtained from the above TL glow curve of sample Z28 is given in the table-4.27.

Table- 4.27

S.No.	AQ Temperature (^{0}C)	Peak Temperature (^{0}C)	Peak Intensity (A.U.)
1	Natural	-	-
2	Beta Irradiated	-	-
3	200^{0}C + Beta(25Gy)	-	-
4	400^{0}C + Beta(25Gy)	-	-
5	600^{0}C + Beta(25Gy)	180	1.58
6	800^{0}C + Beta(25Gy)	130	3.16

The above table shows the peak temperature and peak intensity of sample Z28 at different annealing and quenching temperature irradiated with beta source Sr-90. From the table 4.27 it is observed that the maximum intensity is obtained for the sample annealed and quenched from 800^{0}C.

4.28 TL study of Stilbite sample Z29 collected from Poona (M.S.)

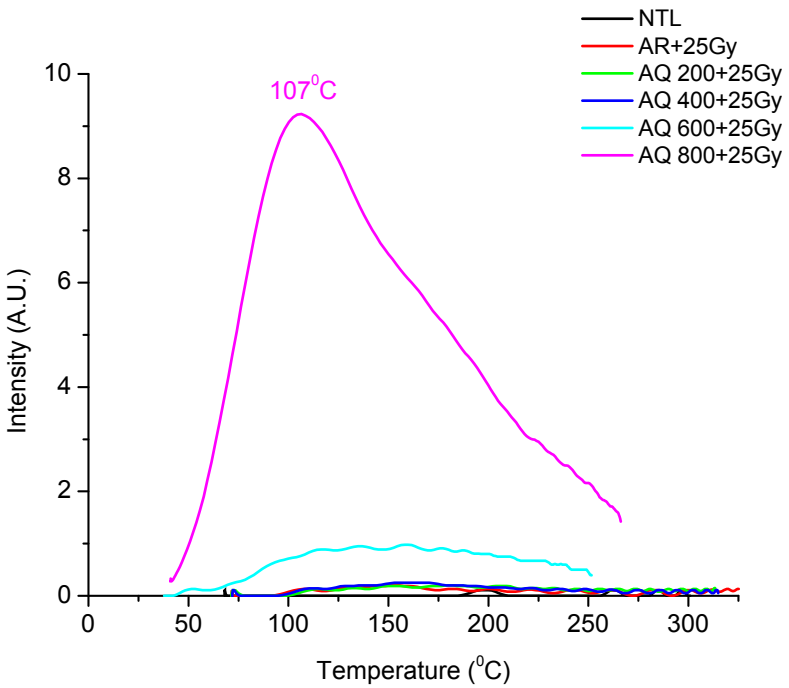

Fig.: 4.58 TL glow curve of as received sample Z29 and also annealed and quenched sample at various temperatures after irradiated using Sr-90 beta source.

The TL glow curve shows a broad peak around 107^0C for the sample annealed and quenched from 800^0C. Two humps are also observed in the TL glow curve. There is no good TL observed from NTL, ATL for as received sample and sample annealed and quenched from 200^0C, 400^0C and 600^0C. TL peak temperature and peak intensity obtained from the above TL glow curve is given in the table- 4.28.

Table- 4.28

S.No.	AQ Temperature (^{0}C)	Peak Temperature (^{0}C)	Peak Intensity (A.U.)
1	Natural	68	0.11
2	Beta Irradiated	153	0.20
3	200^0C + Beta(25Gy)	180	0.2
4	400^0C + Beta(25Gy)	162	0.25
5	600^0C + Beta(25Gy)	158	0.98
6	800^0C + Beta(25Gy)	107	9.23

The above table shows the peak temperature and peak intensity of sample Z29 at different annealing and quenching temperature irradiated with beta source Sr-90. From the above table 4.28 maximum TL peak intensity is observed for the sample annealed and quenched from 800^0C.

4.29 Particle Size Analysis (PSA):

Fig. 4.P. 1, 2, 3, 4 are the particle size histograms of as received sample Z03, Z17 annealed and quenched from 800°C, Z13 as received and 800°CAQ.

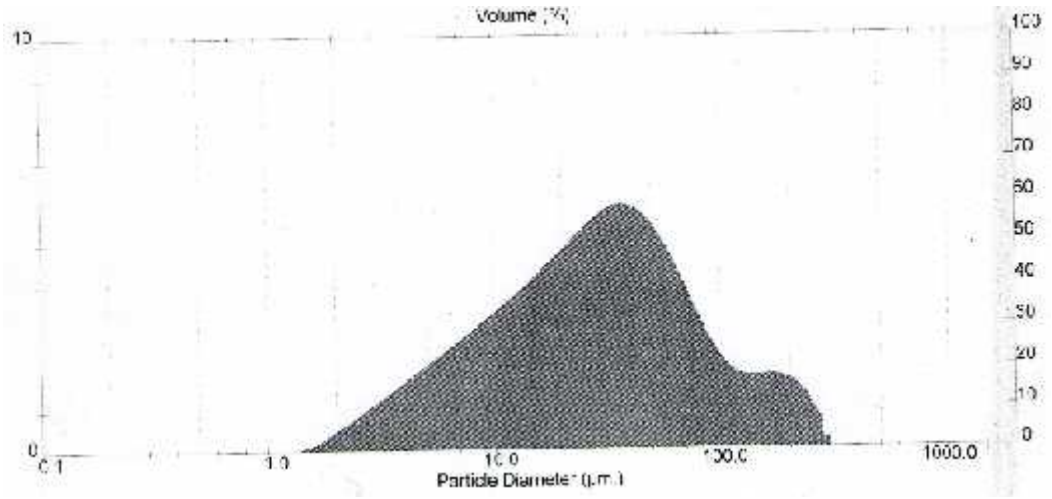

Fig.4.P.1: The PSA of as received Z03 sample.

From PSA of the mineral dolomite it is observed that various sized particles having sizes of 45 µm and very small amount of 110 µm are present. From the data the average surface area of the phosphor particles of 1 Gram was found to be 0.4103m^2. Therefore it was concluded that, more grindings of the material is required to get uniform size.

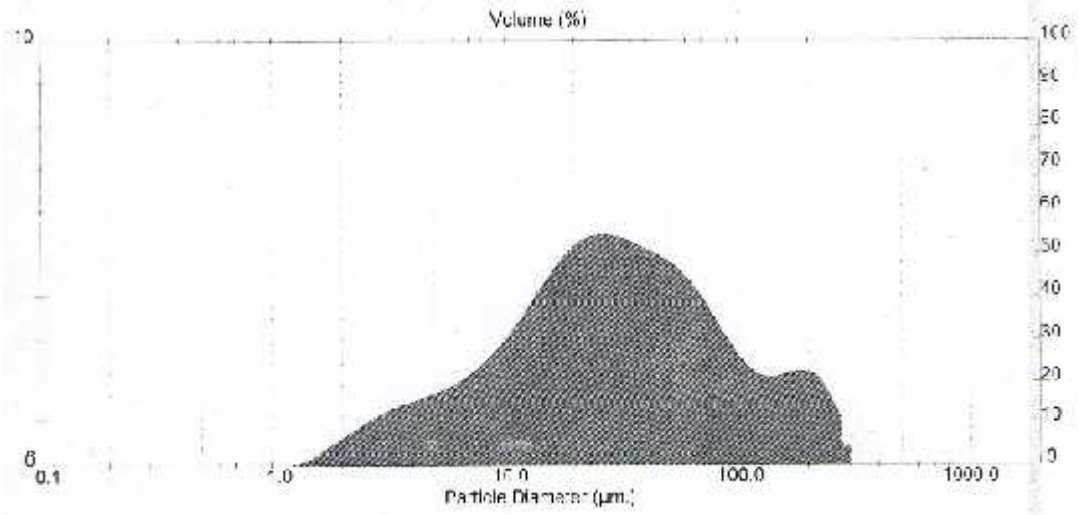

Fig.4.P.2:The PSA of Z17 annealed and quenched from 800°C.

From Fig.4.P.2 it is observed that various sized particles having sizes of 28 µm and very small amount of 3 µm, and 110 µm are present. From the data the average surface area of the phosphor particles of 1 Gram was found to be 0.4049m^2. The surface area is reduced by 0.03m^2

This may be due to agglomeration of the particles due to heating the mineral at 800^{o}C.

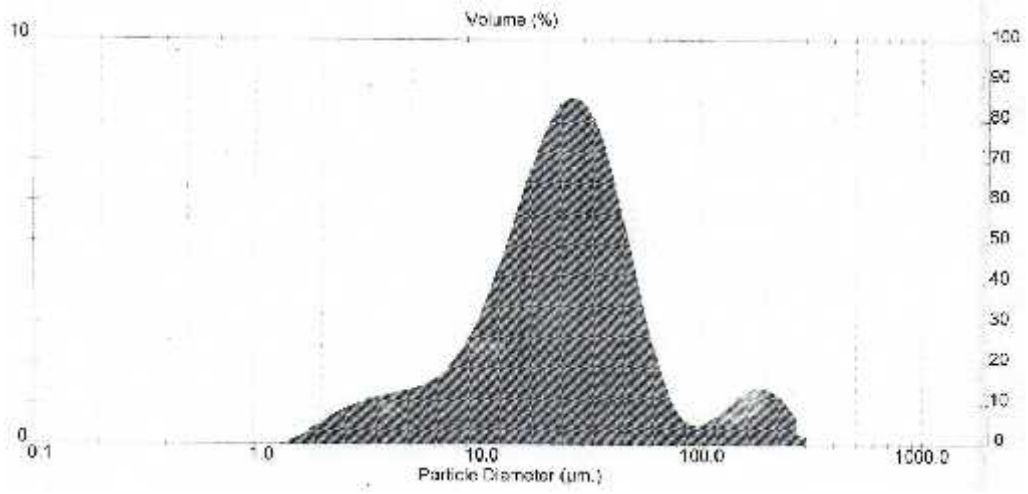

Fig.4.P.3: The PSA of as received Z13 sample.

From PSA of the mineral dolomite it is observed that various sized particles having sizes of 36 µm and very small amount of 3 µm, and 110 µm are present. From the data the average surface area of the phosphor particles of 1 Gram was found to be 0.4103m^2. Therefore it was concluded that, more grindings of the material is required to get uniform size.

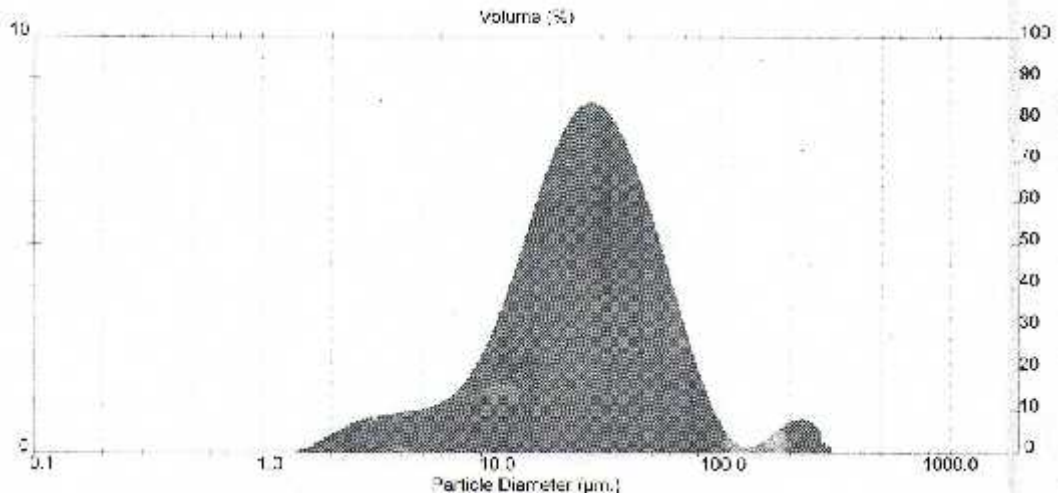

Fig.4.P.4: The PSA of Z13 annealed and quenched from 800^{o}C.

From Fig.4.P.4 it is observed that various sized particles having sizes of 35 µm and very small amount of 3 µm, and 110 µm are present. From the data the average surface area of the phosphor particles of 1 Gram was found to be 0.3737 m^2. The surface area is reduced by 0.031m^2 . This may be due to agglomeration of the particles due to heating the mineral at 800^{o}C.

4.30 Discussion:

Nineteen varieties of dolomite mineral collected from various mines of Chhotaudepur, Gujarat and studied for their TL characteristics in as received as well as annealed and quenched from different temperatures. Appophyllite [$KFCa_4(SiO_5)_4\ 8H_2O$] from three different origins are collected and studied for TL characteristics. Fluorspar [CaF_2] from Amba dungar is also studied for TL characteristics. Heulandite, Prehnite and Stilbite from two different geneses are also studied for thermoluminescence.

For minerals mention above which shows good TL are subjected to the following characterization, these are XRD, SEM, FTIR, particle size analysis and TGA.

Upon 19 dolomite mineral studied, Z08 collected from mines of Kanawant did not show any TL. It is also interesting to note the crystallite size of as received sample is calculated from Scherrer's formula for XRD is 61.57nm. When annealed and quenched same mineral the calculated crystallite size is 71.07nm, which is more than 15% when compared to the crystallite size of as received sample.

From XRD studies, it is found well isolated peaks which may be due to the minerals studied are in pure form. The crystallite size 0f Z03 is 86.20nm, when it is annealed and quenched from 800^0C the crystallite size is reduced by 58% which is around 35.77nm. From XRD studies of Z13 the crystallite size calculated from Scherrer's formula is 86.16nm and when annealed and quenched from 800^0C it is 53.65nm, which is less than 38% of as received sample. From XRD studies of Z15 the crystallite size calculated from Scherrer's formula is 61.57nm and when annealed and quenched from 800^0C it is 42.92nm, which is less than 30% of as received sample. Calculate crystallite size of Z16 is 71.80nm when annealed and quenched from 800^0C it is 39.02nm, which is about 45% less than as received sample. The crystallite size of Z22 which is fluorspar from Amba dungar is around 71.36nm, when annealed and quenched from 800^0C the crystallite size increases by 20% is found around 85.62nm

It is naturally observed phenomena that crystallite size always decreases when annealed and quenched from higher temperature. This may be due to released of trapped gas molecules, structural water and deformation under partial collapse of the

crystal when annealed and quenched from higher temperature. It is interesting to note that the crystallite size of the two minerals (1) dolomite Z08 and (2) fluorspar Z22 increased by 20% when annealed and quenched from 800^0C, this may be due o rearranging the bonds. The annealing may lead to increase the crystallite size and also may be due to change in the positions of elements. It is also noted here the main XRD peak which is selected for calculation of crystallite size did not much change its position (from 31^0 to 29^0) when annealed and quenched from 800^0C.

SEM:

From SEM studies of Z03 sample, the white spots found on the surface may be due to clusters of SiO_2, nearly in nano scale (<1μm). It is also found fine layers of dolomite minerals, these layers mostly are in nano layered structure. When mineral annealed and quenched from 800^0C, here the surface developed cracks and also agglomeration of particles due to deformation is observed.

From SEM studies of Z03 sample, the white spots found on the surface may be due to clusters of SiO_2, nearly in nano scale (<1nm). It is also found fine layers of dolomite minerals, these layers mostly are in nano layered structure. From the SEM of dolomite sample Z08 annealed and quenched from 800^0C, the surface morphology we can clearly see various layers may be around 500nm thick and also SiO_2 clusters are found.

Fig.4.29 is SEM of Z13 dolomite mineral. We can clearly see the clusters of SiO_2, layers thickness are in different size. Fig 4.30 shows the SEM for the sample Z13 annealed and quenched from 800^0C and we can found nano scale clusters of irregular shape of SiO_2 are seen.

SEM for Fluorspar minerals are presented in fig.4.50 and 4.51, the surface is clear for as received and annealed and quenched from 800^0C. We can find layered surface in both the cases. Nano clusters of other impurities are found on the surface.

TGA

Thermal decomposition of dolomite was studied by TGA from room temperature to

800ºC in nitrogen atmosphere. The typical TGA curve of dolomite as received sample Z03 is presented in Fig.4.04. The measured weight loss was 1.33% below 600ºC and between 600ºC and 800ºC reached to 46%. The weight loss of dolomite is attributed to the decomposition of carbonates. The dolomite sample Z03 annealed and quenched from 800^0C shows two decomposition bands one is from 300^0C to 400^0C and the other is from 600^0C to 750^0C which is presented in fig.4.05. It is observed from the first decomposition band the sample lost weight by 11% which may be due to retained water during the recrystallisation of mineral when it is stored after annealed and quenched from 800^0C. In the second decomposition band sample lost weight by 23% which may be due to regain of CO_2 either from $CaCO_3$ or $MgCO_3$. So it is concluded that after annealing and quenching process in the air $CaMg(CO_3)_2$ converted in to $CaMg(OH)_2CO_3$.

FTIR

The typical transmittance FTIR spectra of the dolomite mineral Z03 is shown in figure 4.06. In the room temperature FTIR spectra of the samples, the out-of-plane bending (ν2) at 880cm^{-1}, the asymmetric stretching (ν3) at 1435cm^{-1}, and the in-plane bending (ν4) at 728cm^{-1} modes of the carbonate group are found to be active. Besides the internal modes, the ν2 + ν4 combination mode has also been observed at 2524 cm^{-1}. Additionally peaks due to silicates (1011 cm^{-1}) and H-bonded water (at 3431 cm^{-1}) are visible. The characteristic dolomite bands are shifted to 877, 714 and 1414cm^{-1}, in addition, the weak band due to quartz (456 cm^{-1}) is also visible in the FTIR spectra of 800°C heat-treated dolomite (figure 4.07) demonstrating the structural transformation of dolomite to calcite. It is also observed that the transmittance of peak at 1414cm^{-1} is almost double when compared to the FTIR spectra of as received sample Z03 due to release of CO_2 from 50% of carbonate group and the sample partially converted in to hydroxide i.e. $CaMg(OH)_2CO_3$. Hence a sharp band observed due to this hydroxyl group (3697cm^{-1}). The characteristic absorption peak for dolomite at 2627cm^{-1} differentiates it from calcite, which is not observed in the calcite. This clearly indicates the structural transformation of dolomite to calcite.

X-ray diffraction analysis shows that dolomite is the dominant mineral in samples and amount of calcite and quartz are low. The room temperature XRD pattern of sample

displays sharp diffractions that can attributed to dolomite (JCPDS files card 79-1342;2000).

The X- ray diffraction results are compared with heat treatment of 800^0C. The original reflection disappeared completely and new lines are developed at the asymmetric position of (104) and (202) reflections. At 800^0C dolomite transformed to calcite and MgO and dolomite peaks disappeared.

The hydration degree of dolomite was increased by increasing the calcinations temperature. X-ray diffraction analysis of heat treated samples up to 800^0C indicates that calcite transformed into MgO which on reaction with atmospheric water $Mg(OH)_2$ was formed. Quantitative XRD analysis showed formation of $CaCO_3$, MgO and CaO in air condition between 550 and 750^0C though CaO content is less than 2%.

In order to evaluate the heating time effect on formed phases, the pure dolomite sub samples and subsamples from a sample with the highest impurity content are studied at 800^0C AQ. The quantitative XRD analyses of formed phases are indicating that CaO is insignificant phase and major phases are MgO, calcite and dolomite, and calcite formed prior to CaO formation.

TGA curve shows that at 758.2ºC weight loss due to dolomite decomposition is 20.77% which is indicated by formation of calcite and periclase and CO_2 releases. At 836.4ºC weight loss is 25.43% and the total weight loss for decomposition of dolomite is 46.2%. The thermal decomposition of dolomite shows a peculiar characteristic depending on the experiments atmosphere. Decomposition of dolomite in air occurs in single step and can be depicted by reaction (I).Quantitative XRD showed formation of $CaCO_3$, MgO and CaO in air condition between550 and 750ºC but amount of CaO is less than 2%. By increasing heating temperatures between 750 and 950 ºC calcite was totally decomposed to CaO and CO_2.

Reaction (I):

$MgCa(CO_3)2 \rightarrow MgO + CaO + CaCO_3 + CO_2$

At 800ºC, dolomite structure is changed to calcite which is confirmed by presence of calcite characteristic peak at 714, 877 and 1420 cm^{-1} in FTIR spectra..

By increasing residence time in furnace, dolomite decomposes at lower temperature. The residence time increase compensate the higher temperature required for dolomite decomposition.

Identification of dolomite with an FTIR

The carbonates in the samples were demonstrated by the strong absorption bands between 3050 and 2850 cm^{-1}, 2650 and 2500 cm^{-1}; 1790 and 1820 cm^{-1}; 1400 and 1500 cm^{-1}, and at 877 cm^{-1}, 730 $cm^{-1}$and 710 cm^{-1}. Compared to calcite, dolomite displays characteristic FTIR absorptions at 3020 cm^{-1},2626 $cm^{-1}$and 730 cm^{-1}, and the presence of these bands in the sample confirms the presence of dolomite. The FTIR bands detected at 3020 $cm^{-1}$and 2626 $cm^{-1}$are combination frequencies (Nguyen et al., 1991), and the band at 730 cm^{-1} is assigned to the in plane bending (v4) mode of CO_3^{2-} in the dolomite structure (Farmer, 1974). These three FTIR bands were used to trace changes in dolomite concentration in the samples studied. The appearance of both the 2626 cm^{-1} and 730 cm^{-1} absorption bands in a sample is especially useful for indicating the presence of dolomite.

Quantification of dolomite with an FTIR

It is noted that the absorption feature at 2626 cm^{-1} is a shoulder band associated with the main carbonate absorption at 2520 cm^{-1} (Fig. 2) in the dolomite FTIR spectrum, but it enables calcite/dolomite discrimination (Nguyen et al., 1991) and shows little interference from other minerals and, compared to 730 cm^{-1} band, has a Y intercept closer to zero and a lower slope thereby making estimates potentially more accurate.

Conclusions

TL of nineteen natural dolomite minerals is studied. All the nineteen minerals showed natural thermoluminescence around 120^0C to 150^0C with less intensity. However in Z07 and Z08 there is no TL observed up to 600^0C, when annealed and quenched from 800^0C and given beta dose of 25Gy a well resolved and isolated peak around 148^0C appeared. This may be due to partial collapse of the mineral led to majority content of

CaO. From literature it is found when calcite decomposes it releases carbon dioxide and forms as CaO.

All nineteen samples of dolomite when annealed and quenched from 600^0C the TL intensity is reduced by 60 to 80% and in some cases almost nil.
All the samples annealed and quenched from 200^0C, 400^0C and 800^0C are compared for TL, it is found the intensity increases and TL peak temperature variations are observed.

The sudden reduction of TL intensity of all dolomite samples annealed and quenched from 600^0C may be due to various phases of MgO, CaO, $CaMg(CO_3)_2$, $CaMgCO_3(OH)_2$ and also the electric dipole and magnetic dipole did not allowed to form traps during irradiation. Unstable traps must have been formed due to crystal field effects of various constituents of minerals mixture at 600^0C, leads the TL intensity reduced drastically.

The dolomite sample Z07 and Z08 did not yield much TL up to 600^0C annealing and quenching this may be due to the presence of ferrite ions in the mineral matrix, normally up to 0.5% of Fe_2O_3 are present in few dolomite samples. This leads to less TL output from the samples, since Fe ion is a killer center of luminescence.

All the annealed and quenched dolomite samples shows very well resolved peak with moderate to very high intensity around 125^0C to 150^0C. This may be due to the formation of CaO as well as agglomeration of SiO_2 in the 800^0C AQ dolomite samples.

Fluorspar is nothing but calcium fluoride (CaF_2) mineral which is recognized as natural thermoluminescent dosimeter. From the TL study it s concluded that the natural fluorspar sample displayed a well resolved peak at 155^0C and a hump at 225^0C with very high intensity. So this natural fluorspar considered as Thermoluminescent dosimeter.

The Appophyllite [$KFCa_4(SiO_5)_4$ $8H_2O$] mineral did not yield any considerable TL even after annealed and quenched from various temperatures followed by beta

irradiation. This may be due to the perfect crystal structure or electro negativity of crystal.

The prehnite and stilbite which are calcium alumino silicates called zeolites contains water molecules in the channel leads the mineral at high electro negativity. This leads no thermoluminescence or very less TL emissions are observed.

By considering good TL characteristics, the following minerals are selected for thermoluminescence dosimetry. They are Z03, Z13, Z15, Z16, Z17, Z22.

References

1. Mckeever S.W.S, "Thermoluminescence in solids", Cambridge University Press, Cambridge, 1985.
2. D.K.Banerjee, Mineral Resources of India-The World press Pvt. Ltd, Kolkatta, 1992.
3. Indian Minerals Hand Book,- Indian Bureau of Mines , 1998 &1999.
4. Nina – Keegan – Industrial Mineral Directory ,4th Edition, Industrial minerals information Ltd, U.K. 1999.
5. M.J.Aitken – Thermoluminescence Dating ,1985.
6. P.L.Soni, Mohan Katyal – Text Book of Inorganic Chemistry, 2007.
7. K.V.R.Murthy, L.H.H.Prasad, T.R.Joshi –Thermoluminescence and it 's Applications, Tata Mccrraw – Hill Publishing Company Limited New Delhi, 1992.
8. K.V.R.Murthy, V.Natarajan, M.D.Shastri - Lumilnscence & it 's Applications February, 2009.
9. R.Debnath, H.K.Kundu, M.D.Shastri, K.V.R.Murthy – Luminscence & it 's Applications February -21-2009.
10. K.Mahesh, P.S.Weng – C.Furetta – Thermmoluminescence, India Solids And It 's Application , 1971.
11. D.J.Mc Dougall – Thermoluminescence of Geological Materials, Academic press , London & New York , 1984.
12. Thermoluminescence, Basic Theory & Applications -K.V.R.Murty, J.N.Reddy. Feb, 2008.
13. Alien M.Alper, High temperature Oxides-part -1 – academic press, new York, 1970.
14. F.H Nortion, refractories, 3rd Edn.- Megraw Hill Book Co. Inc., 1949.
15. Kirk – Othmer, Encyclopedia of chemical technology – 3rd Edn. Vols 3, 12, 14, 15, 19, 22, & 24 Wiley – Inter – Science Publication , John Wilely & sons, New York.
16. P.P.Budnikon The technology of ceramics & Refractories Translation of Scripta Techniqa, Edward Arnold (publishing) – Ltd London, 1964.
17. S.K.Guha, Ceramic raw Materials of India – A Directory, Indian, Institute of Ceramics, 1928.

18. A.V.Sankaran, K.S.V.Nambi & C.M.Sunta– progress of Thermonluminescence reasearch on Geological Materials – 7th September, 1982.
19. Amin Y.M, Bull R.K. & Durrani S.A. (1982) Effect of radiation damage on T.L properties of crystals, Third specialities Meeting on T.L & ESR dating, Helslinger Counc, Eur, PACt J,9 159.
20. J.P Patel, G.H. Upadhayay – Material Science , Atul Parakashan, 20007.
21. Material Science – S.L Kakani – New Age Int. Pub. 2006.
22. Saxena Gupta saxena – Solid State Physics – 1985.
23. H.V. Keer – Sollid State Physics – Wiley Eastern Ltd. 1993.
24. Azaroff – Introduction to Solid ,1977
25. Skoog, Holler, Nieman – Parinciples of Instrumental Analysis, 5th Edition 2005.
26. Y.H Gandhi, "Thermoluminescence and allied studies of synthetic quartz and its application", Ph.D. Thesis, pp83, 1995.
27. A.G. Wintle, "Luminescence dating: Laboratory procedure and protocols". Radiation Measurements. vol-27 No-5/6, pp769-817, 1997.
28. P.R.Vyas, "TL of synthetic quartz and practical utility in high level gamma dosimetry", Ph.D. Thesis, pp74-75, 1997.
29. Martini et.al, "Defects dynamics in as grown and electro diffused quartz: An interpretation of the pre-dose effect", J.App.Phy, 61(7), 1st April 1987.
30. Mckeever and Yang, "Point defects and the pre-dose effect in quartz", Radiation Protection Dosimetry, vol-33, No 1/4, pp27-30, 1990. 160
31. Botter-Jenson et al., "Luminescence sensitivity changes in quartz as a result of annealing", Radiation Measurements, No-4, pp535-541, 1995.
32. Mckeever et al., "Effect of thermal cycling on the TL and RL of quartz", PACT-9, pp123-132, 1983.
33. Randell H. et al., "Thermal treatment and emission spectra of TL from quartz", Radiation Measurements, 23, pp441-119, 1994.
34. Wintle et al., "Factor controlling the shape of the OSL decay curve in quartz", Radiation Measurements, vol-29, No-1, pp65-79, 1998.
35. B. W. Smith et al., "Partial bleaching and the decay form characteristic of quartz OSL" Radiation Measurements, vol-27, No-2, pp123-136, 1997.

36. R.Chen and Mckeever, “Sensitization of TL in synthetic quartz- heat treatment and radiation effects”, Journal of Luminescence, 48 and 49, pp 833-837, 1991.
37. R.Chen, “TL characteristic of the 375^0C electron trap in quartz”, Physical Review letters: B., vol 46, No 13, pp8036-8084, 1992.
38. Mckeever, “Point defects and pre-dose effect in natural quartz”.Radiation Measurements. vol-10, No 4-6, pp489-495, 1985.
39. Mckeever, “TL in quartz and silica”, Radiation Protection Dosimetry, vol 8, No 1/2, pp 81-89, 1984.
40. Chen, “The strongly supralinear dose dependence of TL in synthetic quartz”, J.Phy.D: App.Phy, 21,1452-1457, 1988.
41. Rink and Odam, “ Natural alpha recoil practical radiation and ionizing radiation sensitization in quartz detected with EPR: Implication for geochronometry”, Radiation Measurements, 18, pp163-173, 1994.
42. Ranjbar A.H., “ESR and TL in powder form of clear fused quartz: effect of grinding”, Radiation Measurements, 30, pp73-81, 1999.
43. M.R.Kribetschek et al., “Spectral information from minerals relevant for luminescence dating”, Radiation Measurements, vol 27, No 5/6, pp695-746, 1997.
44. Franklin et al., “The mechanism of TL in an Australian sedimentary quartz”, Journal of Luminescence, vol-63, pp317-326, 1995.
45. R.B.Galloway et al., “A substantially improved green light emitting diodes system for luminescence stimulation”, Meas. Sci. Technol., 8, pp267-271, 1997.
46. Mckeever et al., “Temperature dependence of OSL decay curve: experimental and theoretical aspects”, Radiation Measurements, vol 27, No-2, pp161-170, 1997.
47. Morris et al., “Computer simulation of optical bleaching TL and OSL signals”, Radiation Measurements, vol-23, pp301-306, 1994.
48. Englermark W. Santana, M.L. Mittleman and D. Balazs, The Rigaku Jurnal, 5 (1988) 2.
49. M.E. Tucker, A n introduction to the origin of sedimentary rocks, Blackwell, 1991, p.228.
50. L. Xu, D. Min, Cement and Concrete Research, 35 (2005) 1480.

51. F. Garcia–Labiano, A. Abad, Chemical Engineering Science, 57 (2002) 2381.
52. D.N. Todor, Thermal Analysis of Minerals, Abacus Press, 1stedition, 1976, p.171.
53. J.M. Criado and A. Ortega. Thermochim. Acta, 195 (1992) 163.
54. H.H. Horowitz and G. Metzge, Anal. Chem. 35 (1993) 1464.
55. JCPDS Files card nos.86-2334 and 79-1342 (2000).
56. R. Ozao, A. Yamazaki, M. Ochiai, R. Otsuka, Thermochimica Acta, 183 (1991) 183.
57. H.G. F. Wilsdrf and R.A.W Haul, Nature, 167 (1951) 945.
58. S. Gunasekaran, G. Anbalagan, Spectrochimica Acta, Part A, 69 (2008) 1246.
59. H. Chester, Refractories, Production and Properties, The Iron and Steel Institute, London, 1stedition, 1973, p.189.
60. E. Kristof, A. Juhasz, Thermochimica Acta, 342 (1999) 105.
61. S. Maitra, A. Choudhury, H.S. Das, J. Pramanik, Journal of Materials Science, 40 (2005) 4749.
62. B.V. Lvov, V.L. Ugolkov, Thermochem. Acta, 401 (2003) 139.
63. P.S. Keeling, Trans.Br.Ceram.Soc.(GB) 62 (1963) 549.
64. S. Gunasekaran, G. Anbalagan, Indian Academy of Sciences, 30 (2007) 339.
65. J.A. Gasden, Infrared Spectra of Minerals and Related Inorganic Compounds, Butterworths, London, 1975, p.277.
66. B.K. Shahraki, B. Mehrabi and R. Dabiri, Journal of Mining and Metallurgy 45 B (1) (2009) 35 – 44
67. J.F. Lima, P. Trzesniak, E.M. Yoshimura, E. Okuno, Radiat. Prot. Dosimet. 33 (1990) 143.
68. B. Engin, D. Güven, Radiat. Meas. 32 (2000) 253.
69. J.F. Lima, M.E.G. Valerio, E. Okuno, Phys. Rev. B 64 (2001) 014105.
70. K. Koike, M. Nakagawa, C. Koike, M. Okada, H.Chihara, A. and A. 390 (2002) 1133.

Chapter # 5

Thermoluminescence Dosimetric Study of Dolomite and other Minerals

5.1 Introduction

In the present scientific world, ionizing radiations have been found very useful in engineering, medicine, science and technology. Professionals used them at every walk of life. In all the applications, the exact amount of absorption of radiation energy in the exposed material is important factor to get the desired results. The better use can be achieved mostly by accurate determination of energy absorbed from the radiation field and it possible the distribution of this absorbed energy within the material. Measurements of these quantities form the basis of radiation dosimetry and systems used for this purpose are referred as dosimeters.

In TSL dosimetry the relationship between the TSL signal and the absorbed dose to be measured must be determined by an appropriate calibration. Thermoluminescence Dosimeters (TLD) has found increasing applications with the progress made in the development of solid thermoluminescence dosimeters and instrumentation for reading them. Many TLD based systems are now commercially available, and are widely used in routine personal dosimetry, environmental monitoring and clinical radiation dosimetry. The extreme sensitivity of TSL for detecting the presence of defects, as few as 10^9 within a specimen is beneficial for detecting low radiation levels which are encountered in personal and environmental monitoring.

The application potential of TL-dosimeters is very high. They have been found very useful in many fields on account of several favorable characteristics such as high sensitivity, small size, ability to cover wide range of exposure / dose, reusability, insensitive to environmental conditions. In the past professionals had used the film budge technique in real practice. Later on they found that TLD technique is better for many reasons. And hence during last three to four decades they have developed and established the TLD technique. This is became popular now-a-days prominent applications of thermoluminescence dosimetry and radiation protection. The dosimeters have been widely used for in-phantom and in-vivo dosimetry, in medical applications. Another area, where thermoluminescence dosimeters have found use is personal monitoring of radiation workers.

This chapter deals with the Thermoluminescence (TL) dosimetry of minerals under study. They are Z03, Z13, Z15, Z16, Z17, Z22.This chapter is divided in to two parts (1) TL Growth (2) TL Decay. The first part deals with the comparative TL growth study and discussion of glow curves of as received minerals and also treated with annealing and quenching from 800^0C followed by applying different beta radiation dose as 25Gy, 50Gy, 100Gy, 150Gy and 250Gy from Sr-90 beta source. The tables indicating TL peak temperatures and TL peak intensities also furnish. Second part deals with the comparative TL decay study and discussion of glow curve of as received samples and also treated with annealing and quenching from 800^0C with fixed dose 25Gy from Sr-90 beta source. The TL of above samples are recorded at different hours as immediately after irradiation and after storage of 24hrs, 48hrs, 100hrs, 150hrs and 280hrs. The tables indicating TL peak temperatures and TL peak intensities will also furnished for better understanding.

The following characteristic are required for phosphors used in TL dosimeters:

1) High concentration of electron or hole traps
2) High emission efficiency of electrons or holes thermally released from the trap.
3) Large trap depth and small frequency factor.
4) Trap depth distribution to have a small energy range.
5) Thermal emission spectrum that is in a relatively short wavelength region.
6) Trap luminescence center and crystalline lattice that are not damaged or otherwise changed by radiation.

The dose response glow curve shape, super linearity, fading and sensitivity are some of the properties to be examined for practical uses of the dosimeters.

5.2 TL Growth of Sample z03 AQ at 800^{0}C

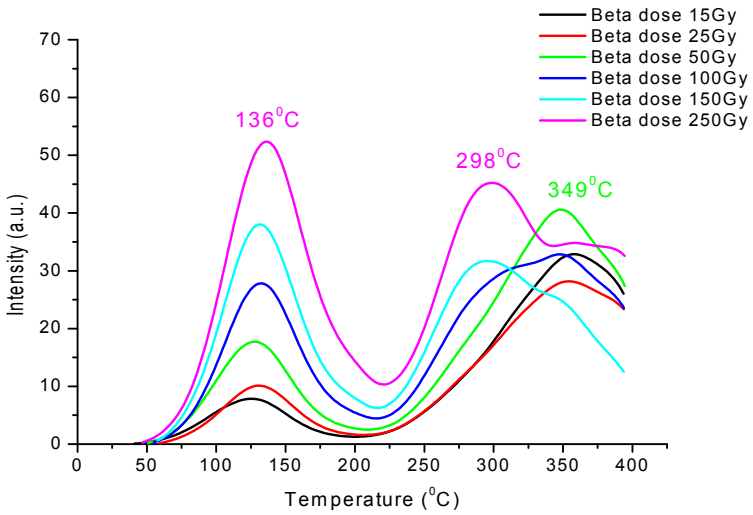

Fig. 5.01: TL glow curves for the sample Z03 annealed and quenched from 800^{0}C exposed to various amount of Sr-90 beta doses.

The TL glow curve shows a well resolved peak around 136^{0}C. The peak intensity increases as the dose increases. There are two more peaks observed at 298^{0}C and 349^{0}C, in which the peak at 298^{0}C is observed only when the amount of beta dose exceeds the 150Gy. TL peak temperature and intensity for various amounts of beta doses are listed in the table 5.01

Table- 5.01

S.No.	Amount of Beta Dose (Gy)	Peak Temperature (^{0}C)	Peak Intensity (A.U.)
1	15	125, 358	8, 33
2	25	131, 354	10, 28
3	50	127, 349	18, 41
4	100	133, 347	28, 33
5	150	136, 296, 354	38, 32, 24
6	250	136, 298, 358	52, 45, 34

Table 5.01 shows the TL Peak temperature and intensity for the sample annealed and quenched from 800^{0}C exposed to various amount of Sr-90 beta doses.

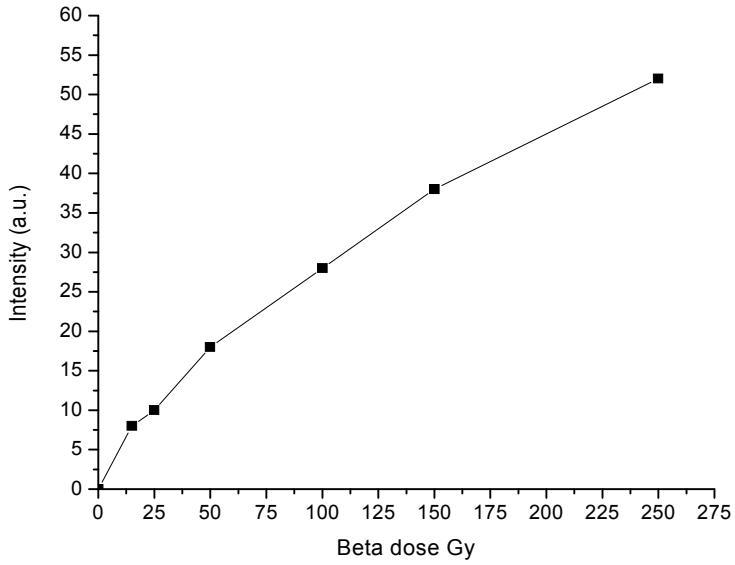

Fig. 5.02: Dose response curve for the sample Z03 annealed and quenched from 800^0C.

The dose response curve shows that the TL Peak intensity is linearly increases as the amount of beta dose increases from 50Gy to 250Gy.

5.3 TL Growth of sample Z13

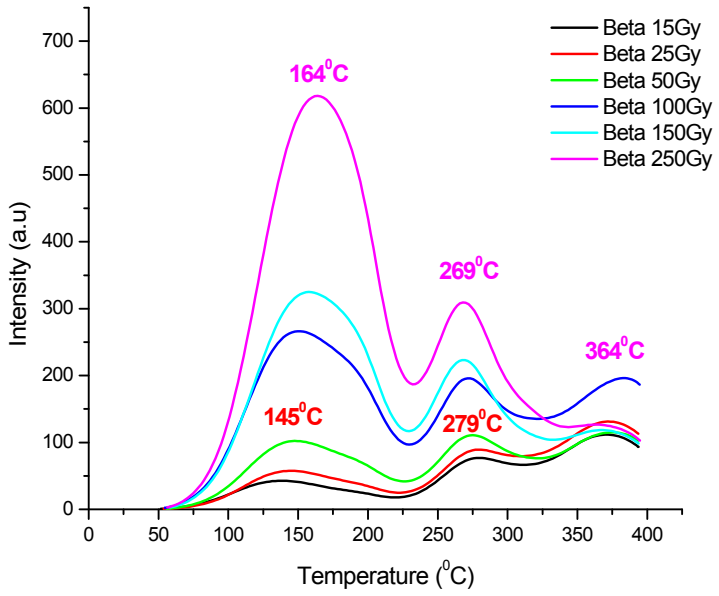

Fig. 5.03: TL glow curves for the as received sample Z13 exposed to various amount of Sr-90 beta doses.

The TL glow curve shows three peaks around 138^0C, 280^0C and 370^0C. A hump is also observed at 190^0C with the 138^0C peak. The 138^0C peak becomes an isolated broad peak and shifts at 164^0C for 250Gy dose. It is observed from the figure that low temperature peak shifts towards higher temperature and both high temperature peaks shifts towards lower temperature as the amount of beta dose increases. Intensity of 138^0C peak and hump is increases as the amount of dose increases whereas 370^0C peak doesn't affected by amount of beta dose. TL peak temperature and intensity for various amounts of beta doses are listed in the table 5.02 given below.

Table- 5.02

S.No.	Amount Beta Dose (Gy)	Peak Temperature (^{0}C)	Peak Intensity (A.U.)
1	15	138, 280, 370	43, 77, 112
2	25	145, 279, 372	58, 89, 131
3	50	147, 275, 374	102, 111, 115
4	100	150, 271, 382	266, 196, 196
5	150	158, 269, 366	325, 223, 119
6	250	164, 269, 364	618, 310, 127

Table 5.02 shows TL peak temperature and intensity for the as received sample z13 exposed to various amount of Sr-90 beta doses.

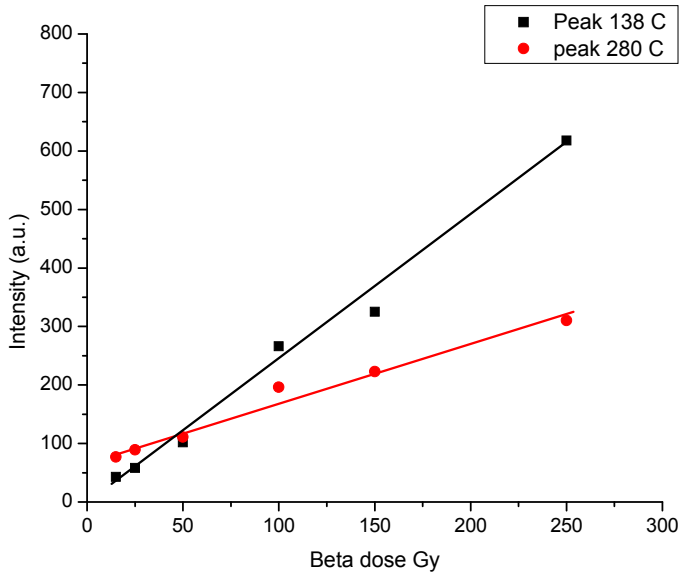

Fig. 5.04: Dose response curve for the as received sample z13.

The dose response curve shows that the TL Peak intensity of both peaks at are linearly increases as the amount of beta dose increases.

5.4 TL Growth in sample z13 AQ 800^{0}C

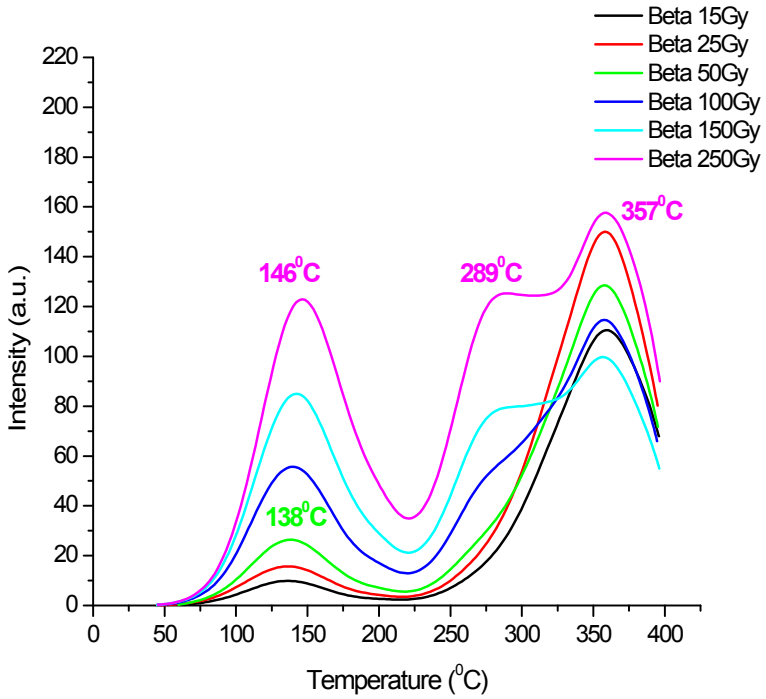

Fig. 5.05: TL glow curves for the sample Z13 annealed and quenched from 800^{0}C exposed to various amount of Sr-90 beta doses.

The TL glow curve shows two well resolved peaks, the first is around 138^{0}C and the second is around 357^{0}C. It is observed from the above figure 5.05 that the intensity of the 137^{0}C peak is increases as the amount of dose increases and also this peak shifts towards the higher temperature from 137^{0}C to 146^{0}C. A hump is observed at 290^{0}C with the 357^{0}C peak when the amount of dose exceeds 100Gy and also the intensity of this hump is increases as the amount of applied dose is increases. TL peak temperature and intensity for various amounts of beta doses are listed in the table 5.03.

Table: 5.03

S.No.	Amount of Beta dose (Gy)	Peak Temperature (^{0}C)	Peak Intensity (A.U.)
1	15	137, 359	10, 111
2	25	137, 358	16, 150
3	50	138, 357	26, 128
4	100	139, 357	56, 115
5	150	142, 357	85, 100
6	250	146, 289, 357	123, 125, 158

Table 5.03 shows the peak temperature and peak intensity of the sample Z13 annealed and quenched from 800^0 and irradiated with different amount of beta dose using Sr-90. It is observed from the above table that the peak intensity is increases as the amount of applied dose is increases.

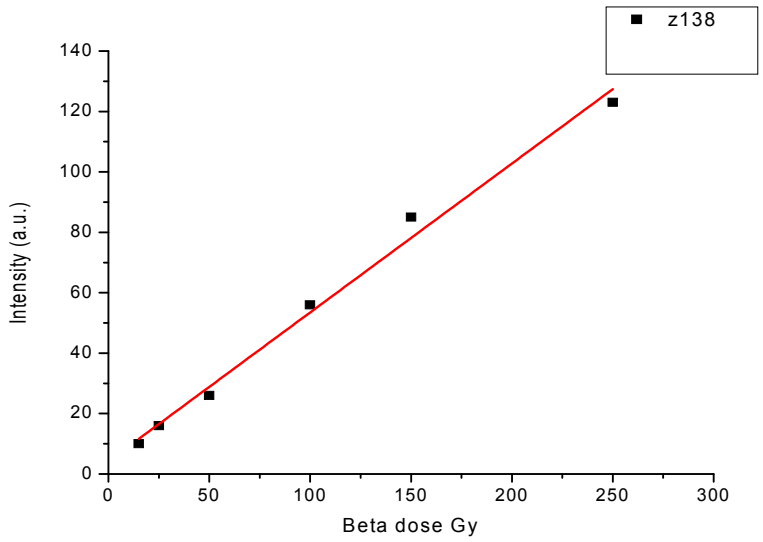

Fig. 5.06: Dose response curve for the sample Z13 annealed and quenched from 800^0C.

The above curve shows that the peak intensity linearly increases as the amount of dose increases within dose range of 15Gy to 250Gy.

5.5 TL Growth of as received sample-Z15

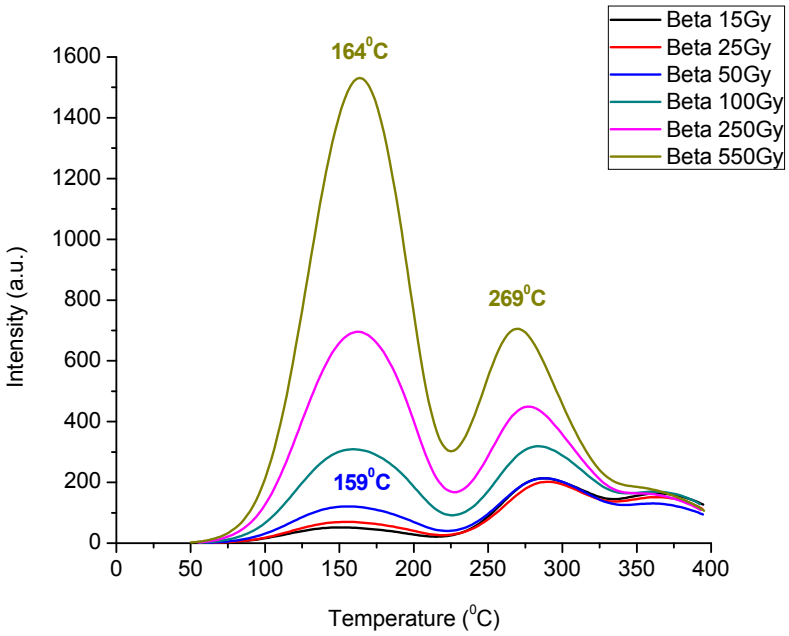

Fig. 5.07: TL glow curves for the as received sample Z15 exposed to various amount of Sr-90 beta doses.

The TL glow curve shows two well resolved and isolated peaks around 150^{0}C and 290^{0}C. It is observed from the above glow curve that the 150^{0}C peak shifts towards higher temperature and 290^{0}C peak shifts towards lower temperature as the amount of dose increases. Also the intensities of both peaks are increases with the amount of dose. TL peak temperature and intensity for various amounts of beta doses are listed in the table 5.04

Table: 5.04

S.No.	Amount of Beta dose (Gy)	Peak Temperature (^{0}C)	Peak Intensity (A.U.)
1	15	151, 288, 362	52, 214, 164
2	25	156, 289, 363	70, 202, 152
3	50	156, 288, 361	121, 214, 130
4	100	159, 284, 361	309, 319, 170
5	250	163, 276	695, 449
6	550	164, 269	1531, 706

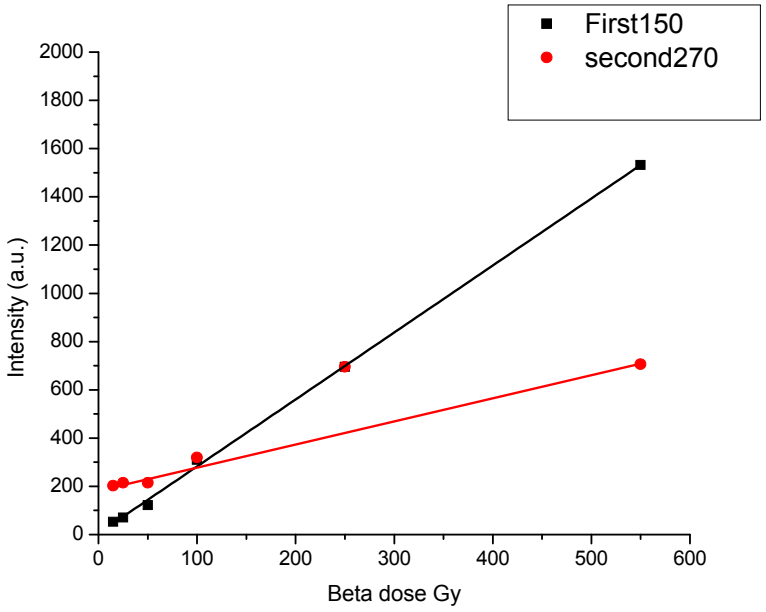

Fig. 5.08: Dose response curve for the as received sample Z15.

From the above figure the intensity of both peaks gradually increases with the amount of dose increases. The TL dose response of beta irradiated peak at 150^{0}C increases with good intensity.

5.6 TL Growth in sample Z15 AQ 800^{0}C

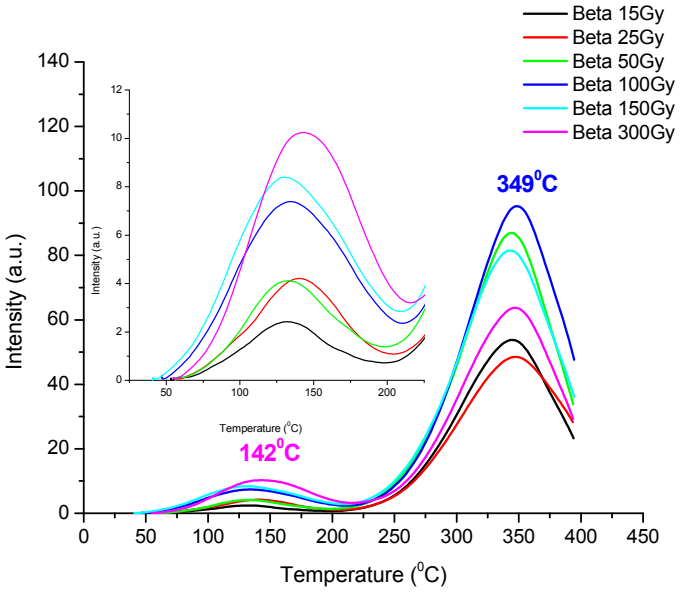

Fig. 5.09: TL glow curves for the sample Z15 annealed and quenched from 800^{0}C exposed to various amount of Sr-90 beta doses.

The TL glow curve shows two isolated peaks around 130^{0}C and 350^{0}C. It is observed from the inset figure 5.09 that the 130^{0}C peak shifts towards higher temperature and also intensity increases as the amount of dose increases. TL peak temperature and intensity for various amounts of beta doses are listed in the table 5.05.

Table: 5.05

S.No.	Amount of Beta dose (Gy)	Peak Temperature (^{0}C)	Peak Intensity (A.U.)
1	15	131, 345	2.42, 54
2	25	141, 348	4.1, 49
3	50	133, 345	4.2, 87
4	100	133, 349	7.4, 95
5	150	129, 343	8.4, 82
6	250	142, 348	10.2, 64

Table -05 show the peak temperature and peak intensity of the z15 sample treated with annealing and quenching at 800^{0}C and irradiated with different dose of beta source by Sr-90.

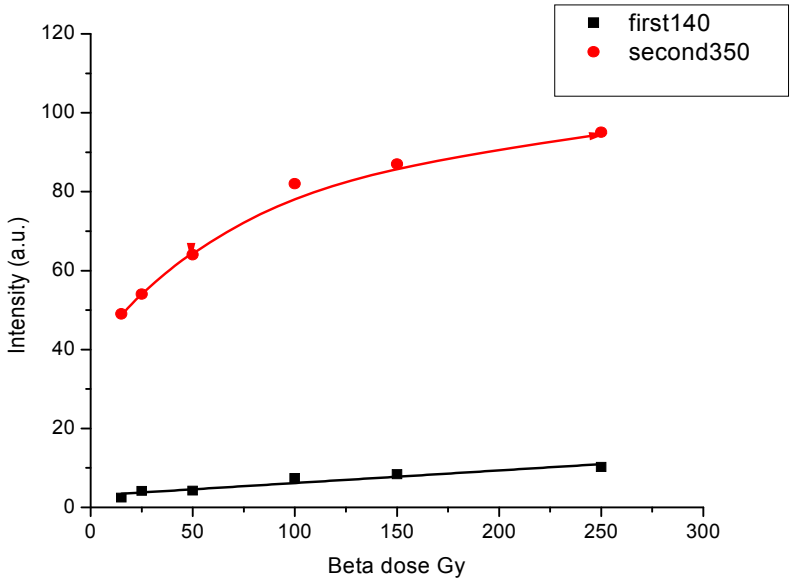

Fig. 5.10: Dose response curve for the sample Z15 annealed and quenched from 800^0C.

From the above figure it is observed that the intensity of the 130^0C peak is gradually increases as the amount of dose increases.

5.7 TL Growth of as received sample z16

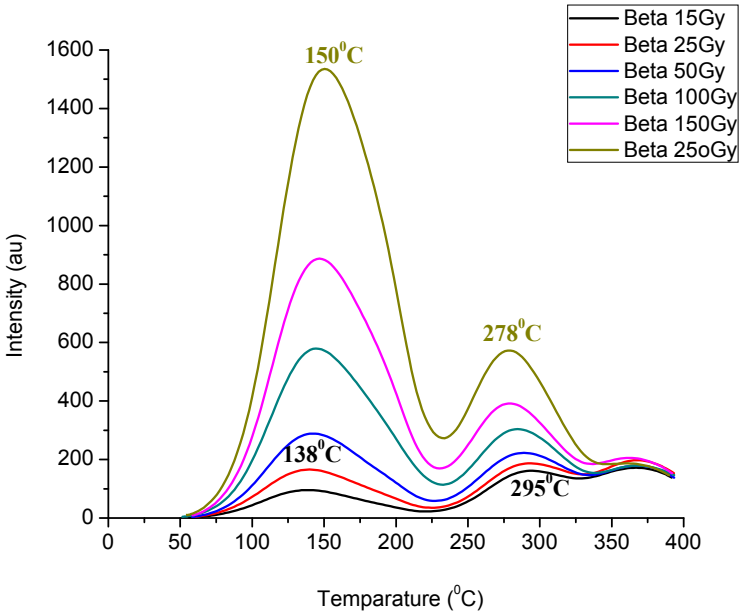

Fig. 5.11: TL glow curves for the as received sample Z16 exposed to various amount of Sr-90 beta doses.

The TL curve shows three TL peaks around 138^{0}C, 295^{0}C and 363^{0}C. The higher temperature peak at 363^{0}C doesn't affected by the radiation. It is observed from the above glow curve that the 138^{0}C peak shifts towards higher temperature i.e. from 138^{0}C to 150^{0}C and 295^{0}C peak shifts towards lower temperature i.e. from 295^{0}C to 278^{0}C as the amount of dose increases. Also the intensities of both peaks are increases with the amount of dose. TL peak temperature and intensity for various amounts of beta doses are listed in the table 5.06.

Table: 5.06

S.No.	Amount of Beta dose (Gy)	Peak Temperature (^{0}C)	Peak Intensity (A.U.)
1	15	138, 295, 367	96, 161, 172
2	25	140, 294, 367	166, 187, 198
3	50	142, 289, 368	289, 223, 179
4	100	144, 285, 368	579, 304, 179
5	150	147, 278, 363	887, 392, 205
6	250	150, 278, 361	1536, 573, 187

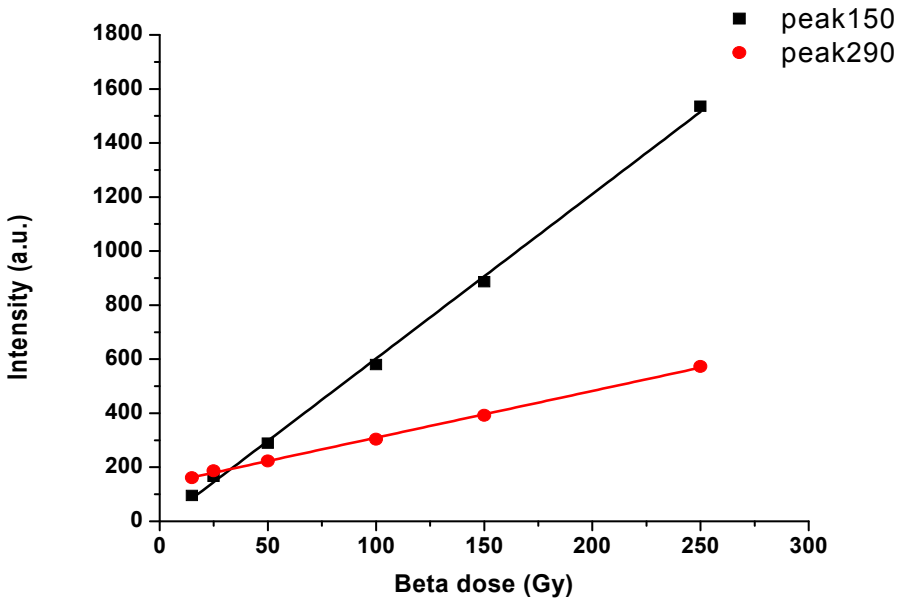

Fig. 5.12: Dose response curve for the as received sample Z16.

It is observed from the above figure that intensity of peaks at 150^{0}C and 290^{0}C linearly as the amount of beta dose is increases. Low temperature peak has good dose

response with respect to the second peak at 290^{0}C. However both peaks have good TL response with respect to beta dose.

5.8 TL Growth in sample z16 AQ 800^{0}C

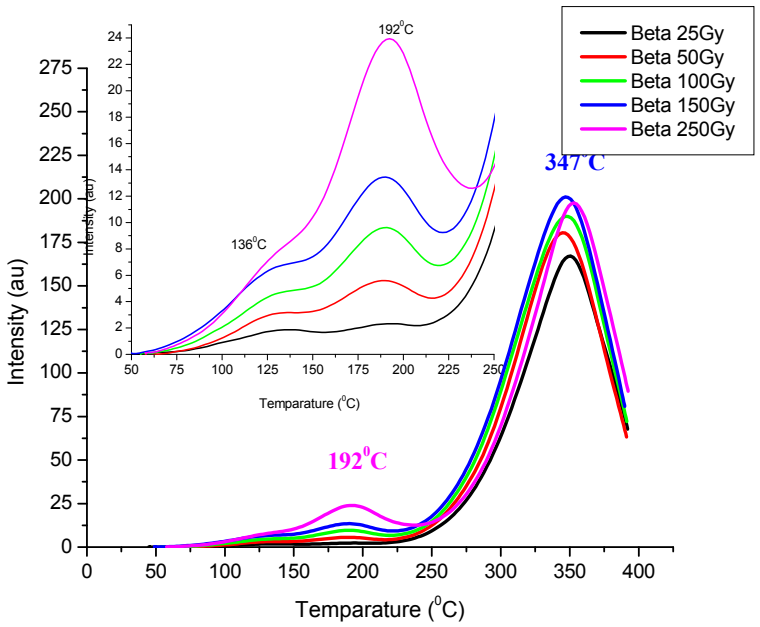

Fig. 5.13: TL glow curves for the sample Z16 annealed and quenched from 800^{0}C exposed to various amount of Sr-90 beta doses.

It is observed from the above figure that the sample Z16 annealed and quenched from 800^{0}C exhibits two peaks at 192^{0}C and 347^{0}C. A small hump is observed from the inset figure 5.13 at 136^{0}C with the peak at 192^{0}C and the intensities of this peak and hump also increases as the amount of dose increases. TL peak temperature and intensity for various amounts of beta doses are listed in the table 5.07.

Table: 5.07

S.No.	Amount of Beta dose (Gy)	Peak Temperature (^{0}C)	Peak Intensity (A.U.)
1	25	136, 193, 351	1.87, 2.3, 167
2	50	136, 190, 345	3.1, 5.6, 181
3	100	191, 347	10, 190
4	150	190, 347	13, 201
5	250	192, 353	24, 198

From the above table intensity increases from 167a.u. to 198a.u. as the amount of beta dose increases for the peak at 347^{0}C.

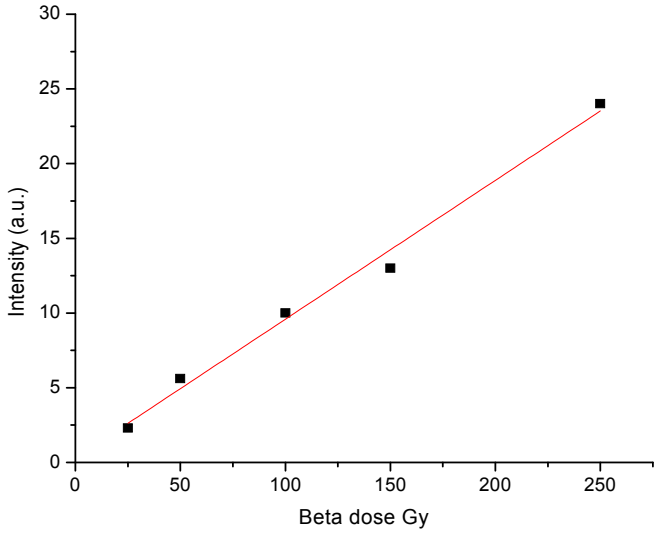

Fig. 5.14: Dose response curve for the sample Z16 annealed and quenched from 800^{0}C.

The above figure shows that the intensity of peak at 192^{0}C linearly increases as the amount of beta dose increases. The TL response is very week when compared to other dolomite samples.

5.9 TL Growth of as received sample z17

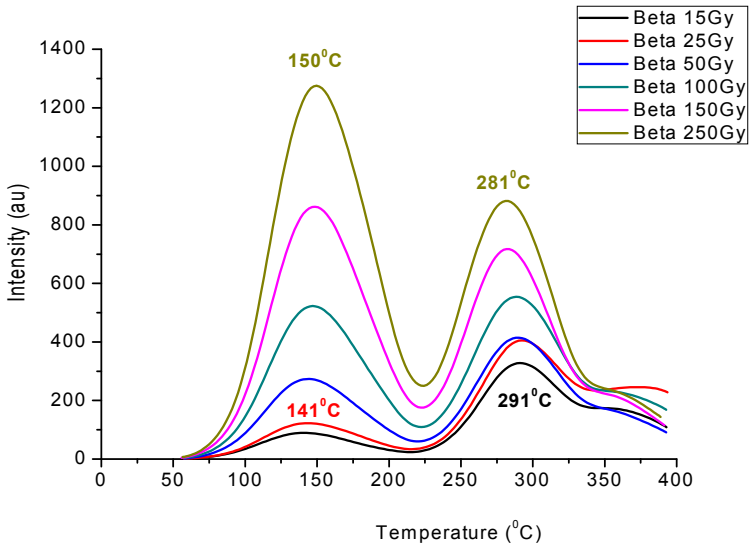

Fig. 5.15: TL glow curves for the as received sample Z17 exposed to various amount of Sr-90 beta doses.

The TL glow curve shows two well resolved and isolated peaks around 141^0C and 291^0C. It is observed from the above glow curve that the 141^0C peak shifts towards higher temperature from 141^0C to 150^0C and 291^0C peak shifts towards lower temperature from 291^0C to 281^0C as the amount of dose increases. Also the intensities of both peaks are increases with the amount of dose. TL peak temperature and intensity for various amounts of beta doses are listed in the table 5.08

Table: 5.08

S.No.	Amount of Beta dose (Gy)	Peak Temperature (^{0}C)	Peak Intensity (A.U.)
1	15	141, 291	89, 328
2	25	144, 292	123, 405
3	50	145, 290	274, 414
4	100	147, 288	523, 554
5	150	149, 282	862, 717
6	250	150, 281	1275, 882

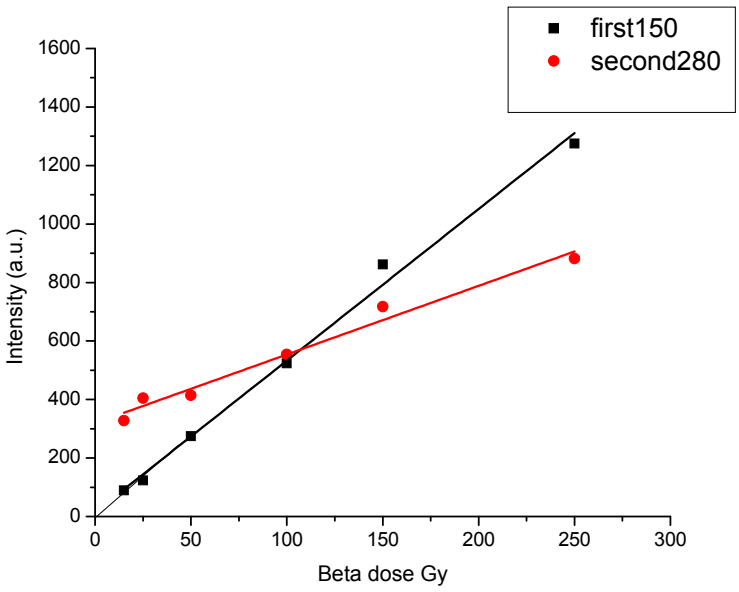

Fig. 5.16: Dose response curve for the as received sample Z17.

It is observed from the above figure that intensity of both peaks linearly increases as the amount of beta dose increases. TL response with beta dose is also good.

5.10 TL Growth of as received sample z22

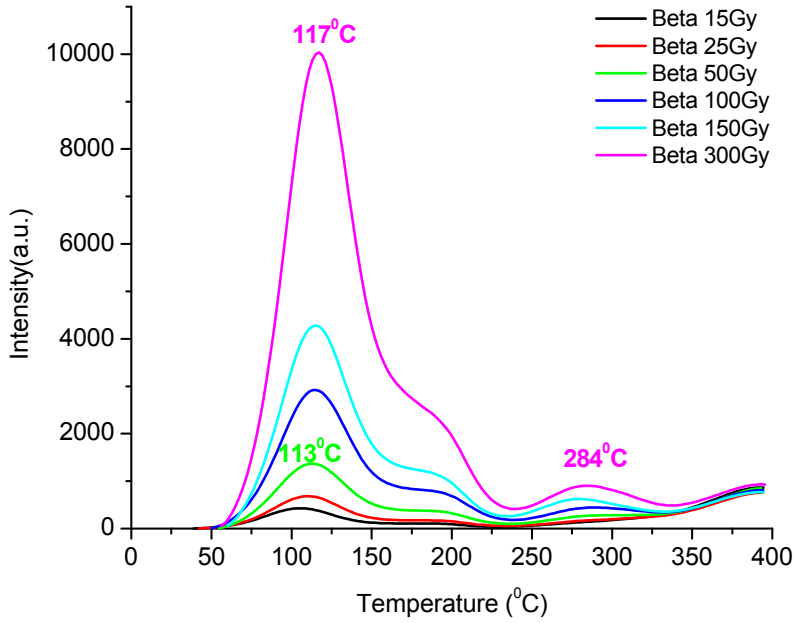

Fig. 5.17: TL glow curves for the as received sample Z22 exposed to various amount of Sr-90 beta doses.

The TL glow curve shows two peaks at 105^0C and 284^0C. A hump also observed around 190^0 with the peak at 105^0C. Intensity of this hump and peak increases with the amount of dose and also the peak shifts from 105^0C to 117^0C. It is interesting point to note that the colour of the sample changes to cyan when the amount of beta dose exceeds 100Gy. The TL emission studies of 117^0C peak may reveal the change of colour of the specimen. TL peak temperature and intensity for various amounts of beta doses are listed in the table 5.09

Table: 5.09

S.No.	Amount of Beta dose (Gy)	Peak Temperature (^{0}C)	Peak Intensity (A.U.)
1	15	105	428
2	25	111	682
3	50	113	1371
4	100	115, 287	2924, 444
5	150	115, 285	4221, 623
6	250	117, 284	10037, 903

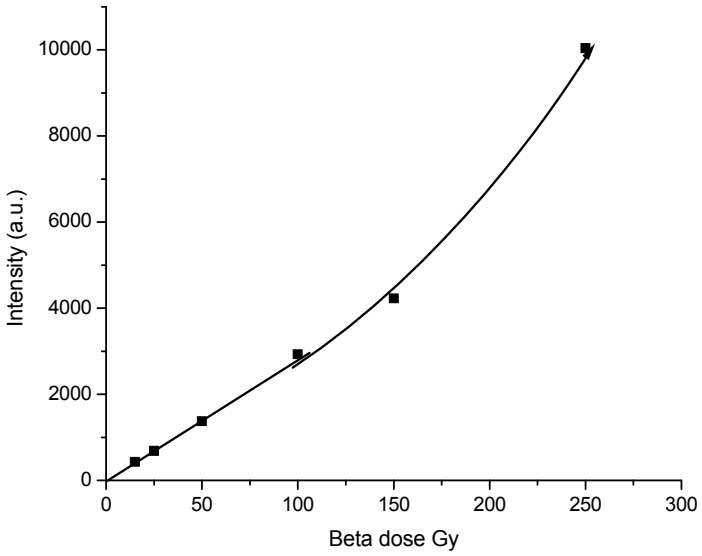

Fig. 5.18: Dose response curve for the as received sample Z03.

It is observed from above the figure that intensity of the TL peak at 105^0Cis gradually increases with the amount of dose.

5.11 TL decay of the sample z03 annealed and quenched from 800^0C.

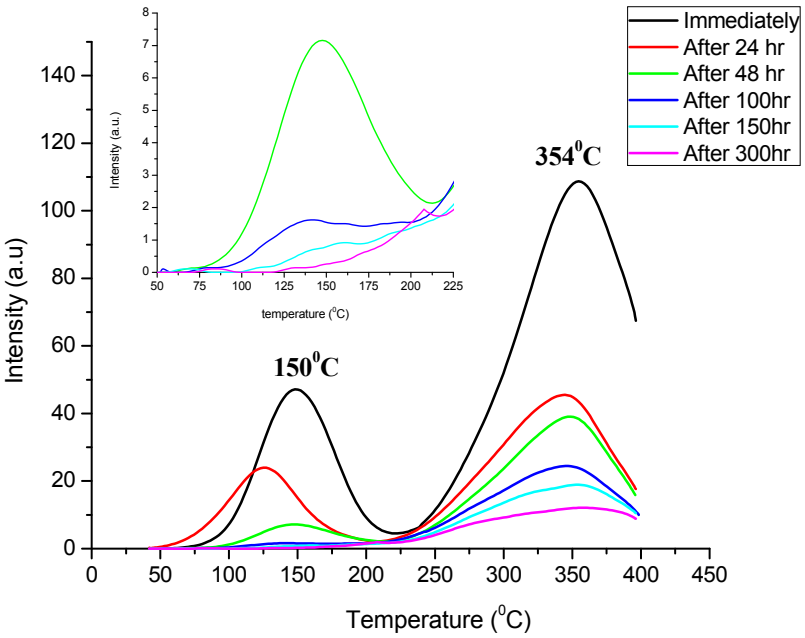

Fig. 5.19: TL glow curve recorded at different time after the exposure of Sr-90 to the sample Z03 annealed and quenched from 800^0C.

TL glow curve shows two peaks around150^{0}C and 354^{0}C. From the TL glow curve it observed that the intensity of both peaks is decreases gradually as the time of storage increases. There is no good TL peak observed for the peak 150^{0}C after 100hr of storage. After exposure to beta dose, TL peak temperature and intensity recorded at different times are listed in the table 5.10

Table- 5.10

S.No.	Time of Storage after Irradiation (hrs)	TL Peak Temperature (^{0}C)	TL Peak Intensity (A.U.)
1	Immediately	150, 354	47, 109
2	24	125, 345	24, 45
3	48	150, 350	7, 39
4	100	150, 345	1, 39
5	150	160, 349	0.9, 24
6	300	348	12

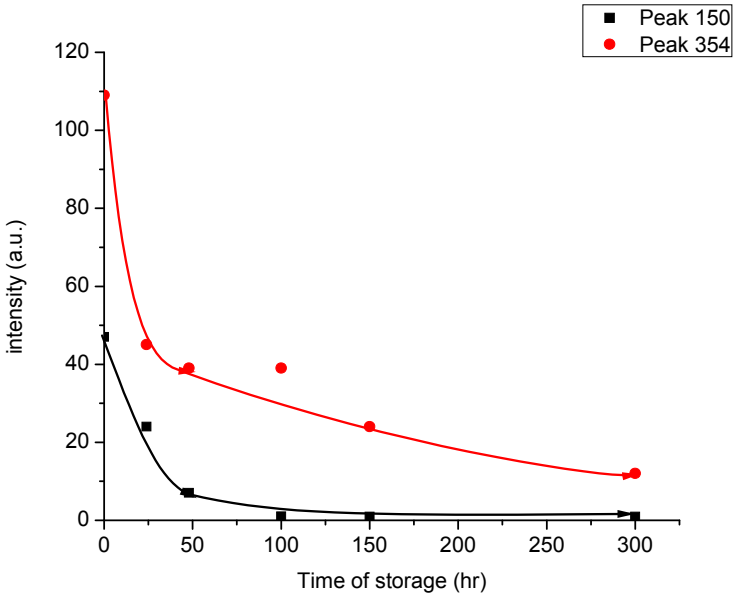

Fig. 5.20: TL decay curve for the sample Z03 annealed and quenched from 800^{0}C.

It is observed from the above figure that the intensity is gradually decreases as the time of storage increases and reduced by 90% of its original value. There is not good TLD material.

5.12 TL decay of the as received sample z13.

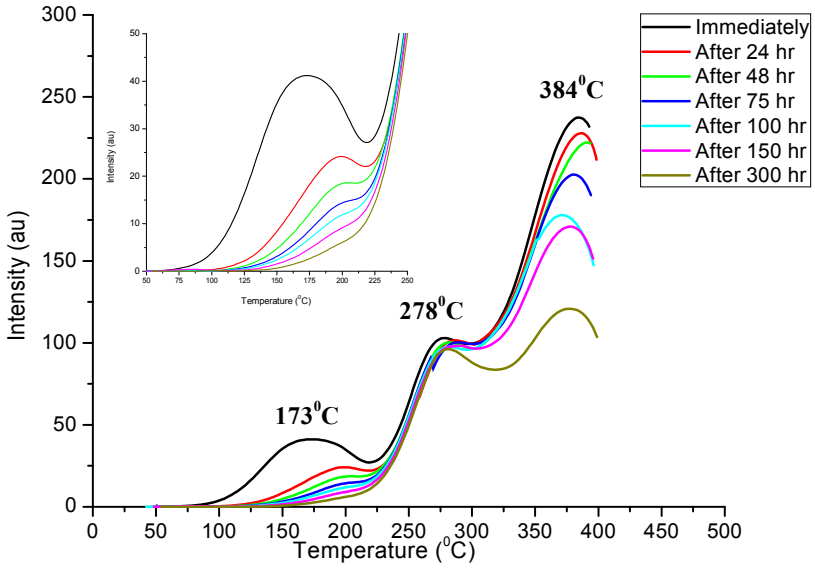

Fig. 5.21: TL glow curve for the as received sample Z13 at different time after beta dose irradiation.

The TL glow curve shows a peak around 173^{0}C with a hump around 278^{0}C. From the TL glow curve it is observed that the intensity of the peak at 173^{0}C gradually decreases as the time of storage increases and vanishes after 150hr storage. After exposure to beta dose, TL peak temperature and intensity on different times are listed in the table 5.11

Table- 5.11

S.No.	Time of Storage after Irradiation (hrs)	TL Peak Temperature (^{0}C)	TL Peak Intensity (A.U.)
1	Immediately	176, 281, 378	41, 96, 237
2	24	198, 281, 371	24, 103, 228
3	48	198, 282, 379	18, 100, 222
4	75	198, 283, 380	15, 102, 203
5	100	198, 283, 390	12, 98, 178
6	150	198, 284, 387	10, 98, 171
7	300	198, 286, 384	7, 100, 121

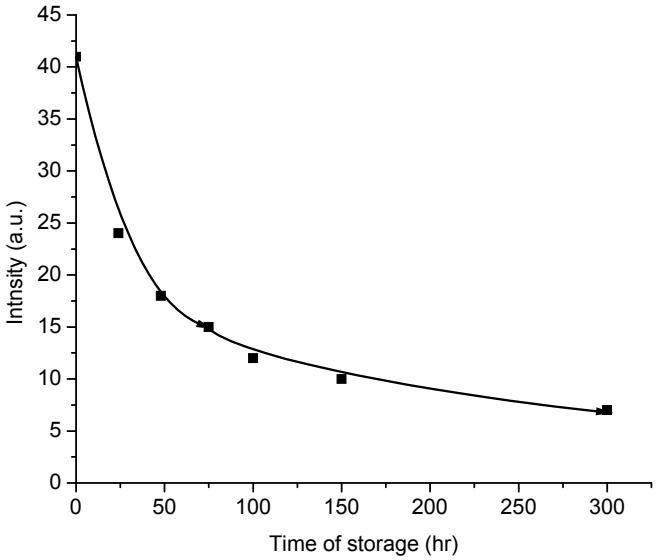

Fig. 5.22: TL decay curve for the as received sample Z13.

It is observed from the graph that the intensity gradually decreases as the time of storage increases. Here, intensity of the peak at 175^{0}C is reduced by 85% of its original intensity. This is not good TLD material.

5.13 TL Decay of sample Z13 AQ 800^{0}C

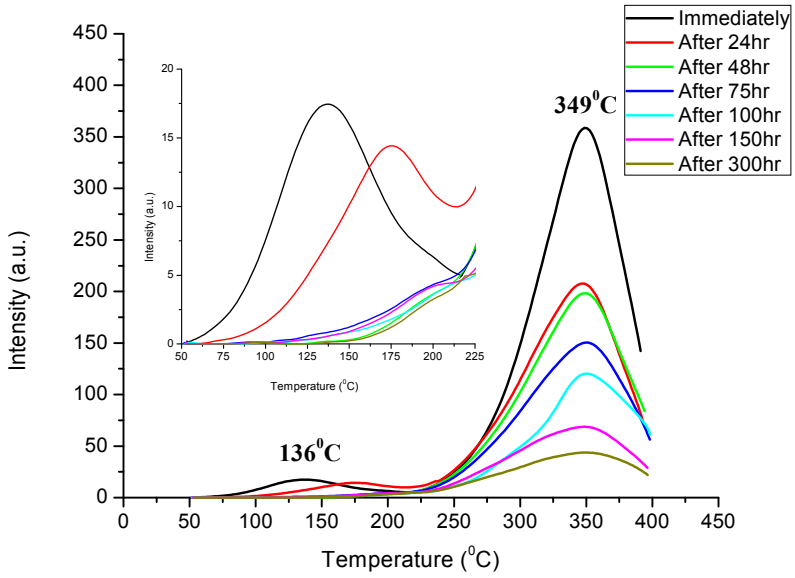

Fig. 5.23: TL glow curve recorded at different time after the exposure of Sr-90 to the sample Z13 annealed and quenched from 800^{0}C.

The TL glow curves shows two peaks around 136^0C and 349^0C. The above figure shows that there is no good TL peak observed at 136^0C after storage of 24hr. After exposure to beta dose, TL peak temperature and intensity on different times are listed in the table 5.12

Table: 5.12

S.No.	Time of Storage after Irradiation (hrs)	TL Peak Temperature (^{0}C)	TL Peak Intensity (A.U.)
1	Immediately	136, 349	17, 359
2	24	349	208
3	48	347	198
4	75	187, 389	14, 150
5	100	349	120
6	150	349	69
7	300	349	44

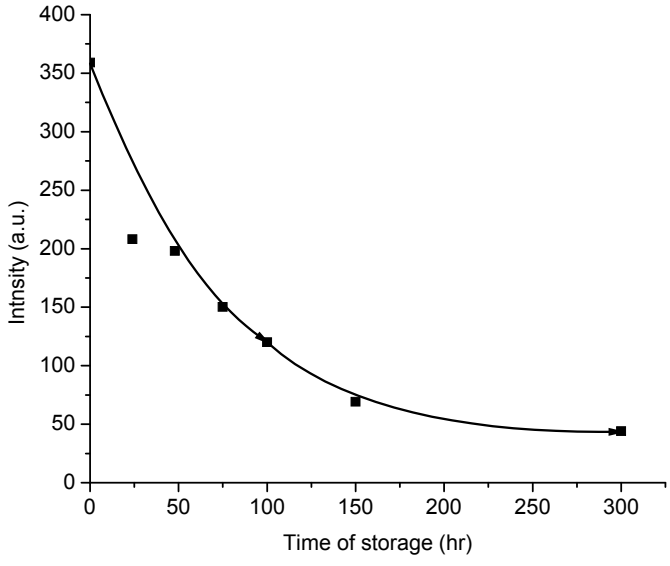

Fig. 5.24: TL decay curve for the sample Z13 annealed and quenched from 800^0C.

It is observed from the above figure that the intensity of the peak at 349^0C gradually decreases as the time of storage increases. The intensity is reduced by 85% of its original intensity after 300hr.this is not good TLD material.

5.14 TL Decay of as received sample z15

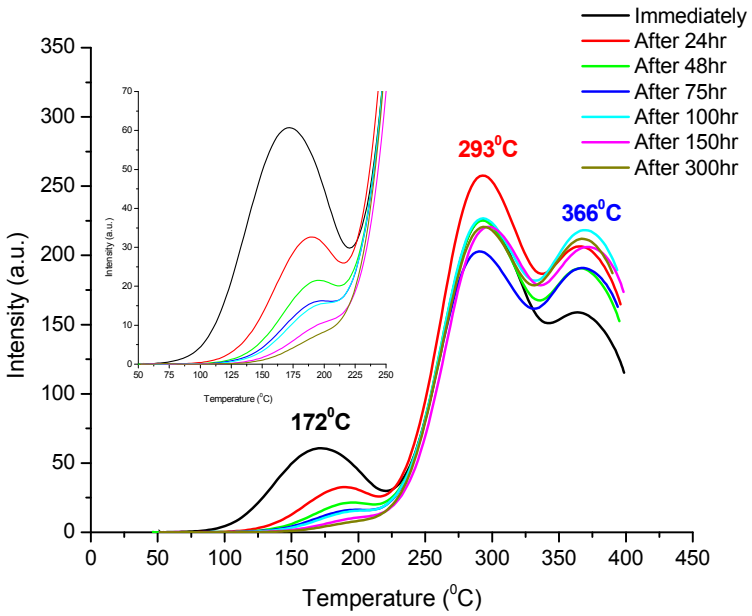

Fig. 5.25: TL glow curve for the as received sample Z15 at different time after beta dose irradiation.

The TL glow curve shows two peaks around 172^{0}C and 293^{0}C. After 48hr of storage time, there is no good TL peak observed at 172^{0}C. From the TL glow curve it is clear that the intensity of the low temperature peaks is decreases gradually as the time of storage increases. After exposure to beta dose, TL peak temperature and intensity on different times are listed in the table 5.13

Table: 5.13

S.No.	Time of Storage after Irradiation (hrs)	TL Peak Temperature (^{0}C)	TL Peak Intensity (A.U.)
1	Immediately	172, 293, 364	61, 258, 159
2	24	190, 293, 365	33, 226, 206
3	48	196, 293, 366	22, 225, 191
4	75	199, 290, 367	18, 220, 191
5	100	199, 293, 370	16, 220, 218
6	150	199, 297, 371	11, 220, 206
7	300	199, 293, 367	10, 220, 212

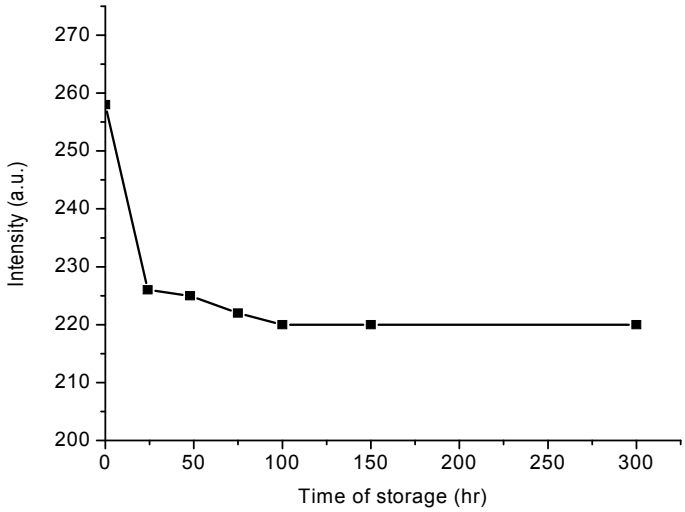

Fig. 5.26: TL decay curve for the as received sample Z15.

The TL decay curve shows that the intensity decrease gradually during 24hr of storage time and is reduced by 15% of its original intensity after 300hr of storage time.

5.15 TL Decay of sample z 15 AQ at 800^{0}C

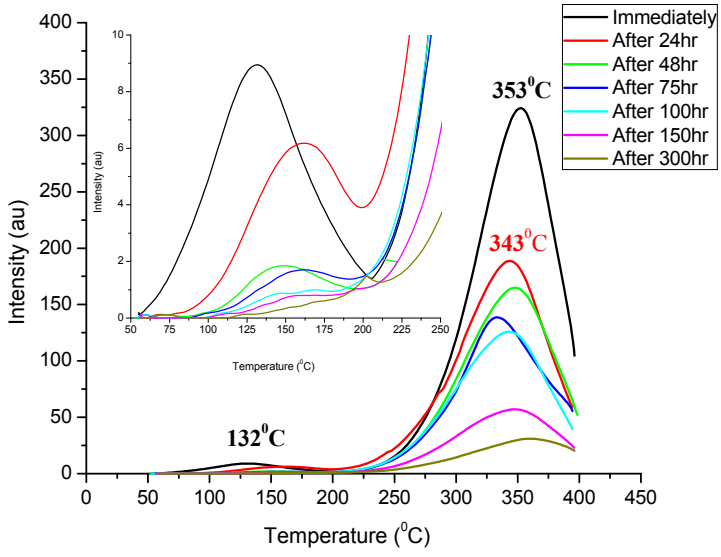

Fig. 5.27: TL glow curve recorded at different time after the exposure of Sr-90 to the sample Z15 annealed and quenched from 800^{0}C.

The TL glow curves shows two peaks around 132^0C and 359^0C. The above figure shows that there is no good TL peak observed at 132^0C after storage of 48hr. After exposure to beta dose, TL peak temperature and intensity on different times are listed in the table 5.14

Table: 5.14

S.No.	Time of Storage after Irradiation (hrs)	TL Peak Temperature (^{0}C)	TL Peak Intensity (A.U.)
1	Immediately	132, 359	9, 31
2	24	148, 348	6, 57
3	48	168, 342	1.9, 126
4	75	168, 389	1.7, 139
5	100	168, 347	1.7, 165
6	150	168, 345	0.8, 189
7	300	346	324

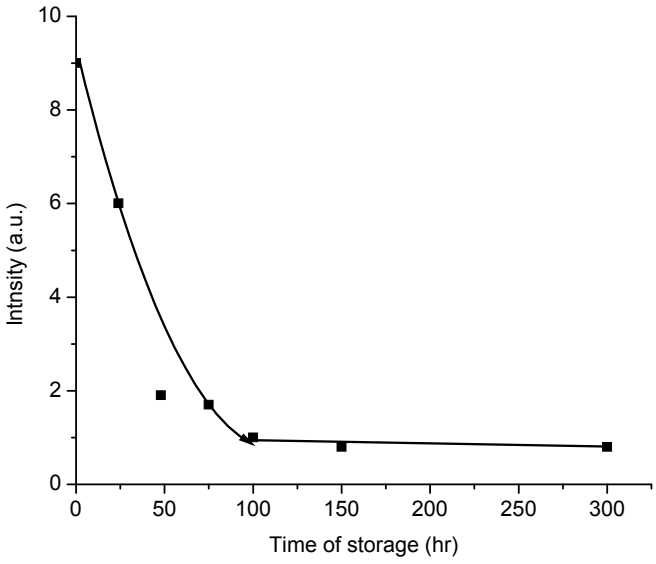

Fig. 5.28 TL decay curve for the sample Z15 annealed and quenched from 800^0C.

From the graph it observed that the intensity is gradually decreases as the time for storage increases and reduced by 90% of its original intensity after 300hr.

5.16 TL Decay of as received sample Z16

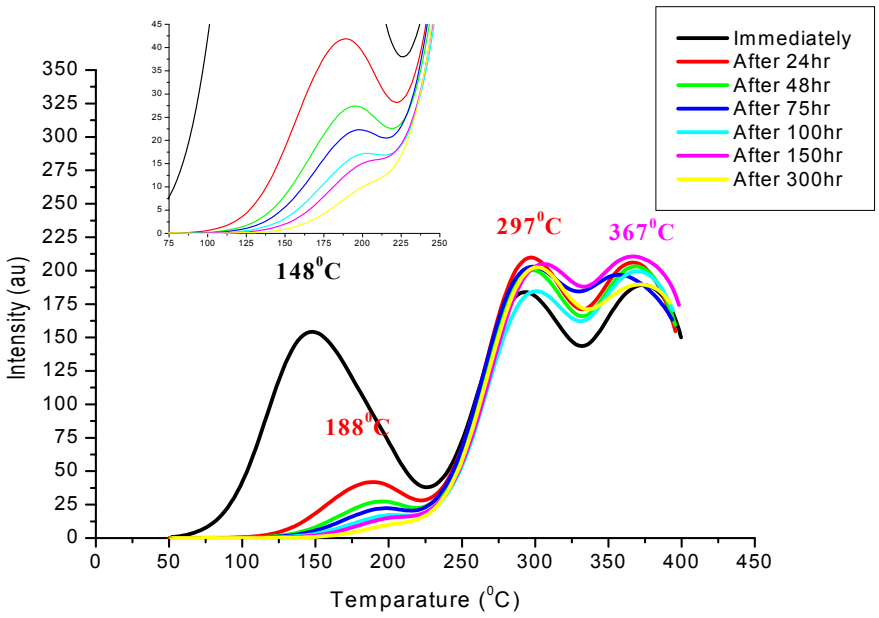

Fig. 5.29: TL glow curve for the as received sample Z16 at different time after beta dose irradiation.

The TL glow curve shows two peaks around 148^{0}C and 293^{0}C. After 48hr of storage time, there is no good TL peak observed at 148^{0}C. From the TL glow curve it is clear that the intensity of the low temperature peaks is decreases gradually as the time of storage increases. After exposure to beta dose, TL peak temperature and intensity on different times are listed in the table 5.15

Table: 15 TL Decay of as received sample z16

S.No.	Time of Storage after Irradiation (hrs)	TL Peak Temperature (^{0}C)	TL Peak Intensity (A.U.)
1	Immediately	148, 293, 373	154, 184, 190
2	24	188, 297, 367	42, 210, 206
3	48	196, 299, 368	27, 200, 203
4	75	198, 298, 357	22, 203, 197
5	100	203, 300, 371	17, 185, 200
6	150	203, 307, 367	15, 205, 211
7	300	203, 301, 371	11, 202, 190

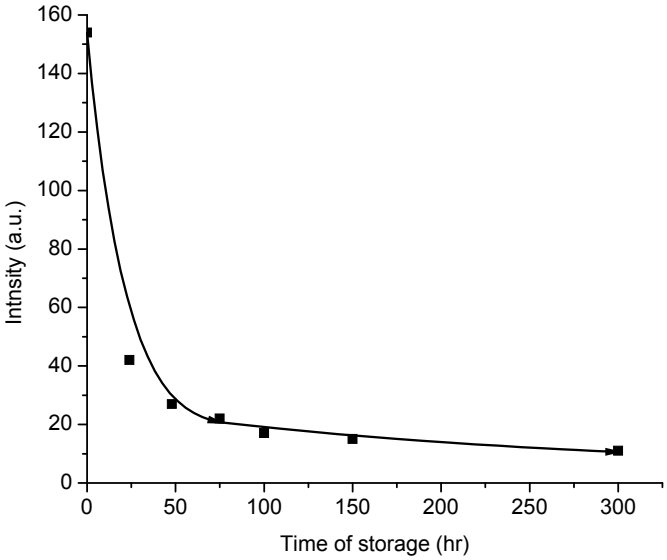

Fig. 5.30: TL decay curve for the as received sample Z16.

5.17 TL Decay of sample Z16 AQ 800^{0}C

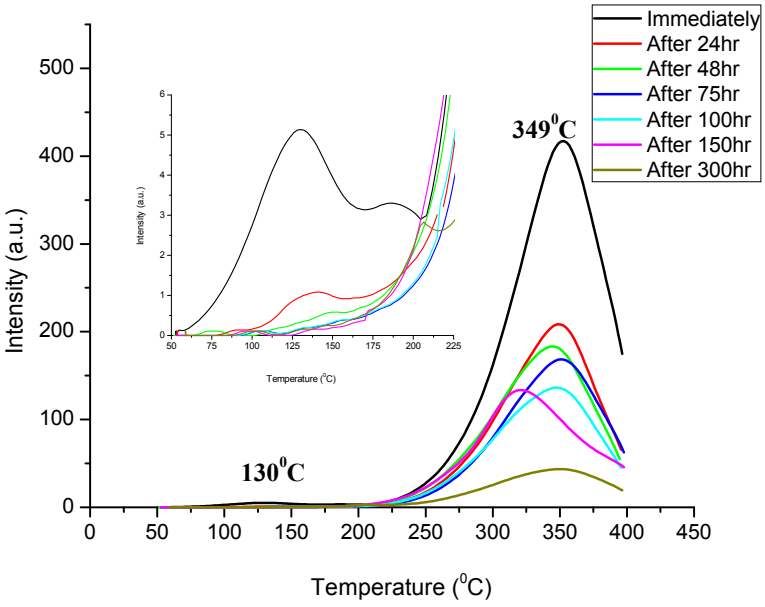

Fig. 5.31: TL glow curve recorded at different time after the exposure of Sr-90 to the sample Z16 annealed and quenched from 800^{0}C.

The TL glow curves shows two peaks around 130^{0}C and 349^{0}C. The above figure shows that there is no good TL peak observed at 130^{0}C after storage of 24hr. After

exposure to beta dose, TL peak temperature and intensity on different times are listed in the table 5.16

Table: 16 TL Decay of sample z16 AQ 800^{0}C

S.No.	Time of Storage after Irradiation (hrs)	TL Peak Temperature (^{0}C)	TL Peak Intensity (A.U.)
1	Immediately	130, 349	5.1, 44
2	24	140, 348	1.1, 136
3	48	345	183
4	75	389	133
5	100	351	169
6	150	348	208
7	300	349	417

5.18 TL Decay of as received sample Z17

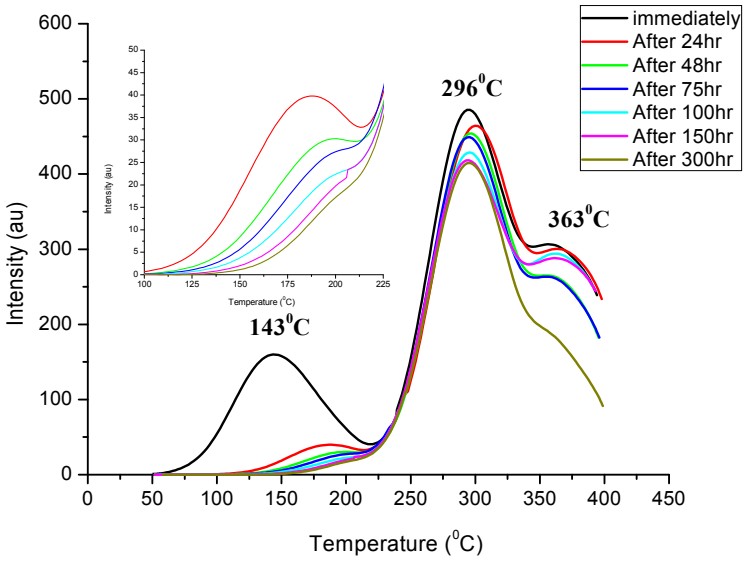

Fig. 5.29: TL glow curve for the as received sample Z17 at different time after beta dose irradiation.

The TL glow curve shows two peaks around 143^{0}C and 296^{0}C. After 48hr of storage time, there is no good TL peak observed at 143^{0}C. From the TL glow curve it is clear that the intensity of the low temperature peaks is decreases gradually as the time of

storage increases. After exposure to beta dose, TL peak temperature and intensity on different times are listed in the table 5.17

Table: 17

S.No.	Time of Storage after Irradiation (hrs)	TL Peak Temperature (^{0}C)	TL Peak Intensity (A.U.)
1	Immediately	143, 296	160, 485
2	24	189, 296	40, 454
3	48	200, 297	30, 449
4	75	200, 296	27, 435
5	100	200, 296	24, 425
6	150	200, 299, 363	18, 420, 300
7	300	200, 296, 362	18, 419, 294

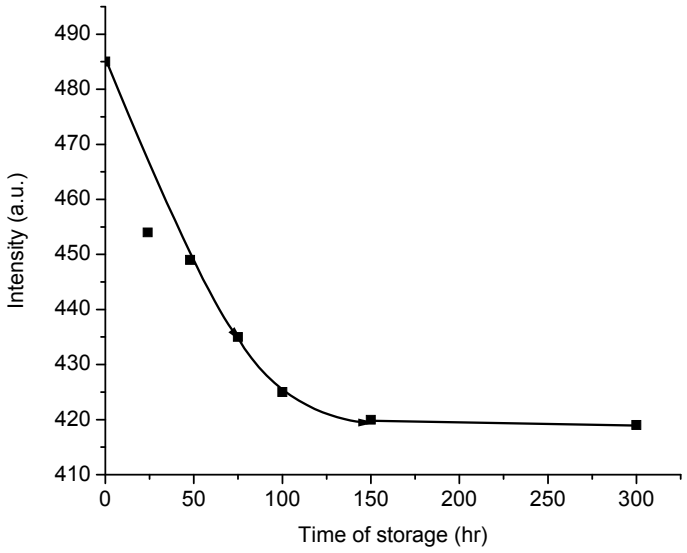

Fig. 5.34 TL decay curve for the as received sample Z17.

From the above decay curve it is observed that peak intensity of the 296^{0}C gradually decreases as the time for the storage increases and is reduced by 13% of its original peak intensity.

5.19 TL Decay of as received sample Z22

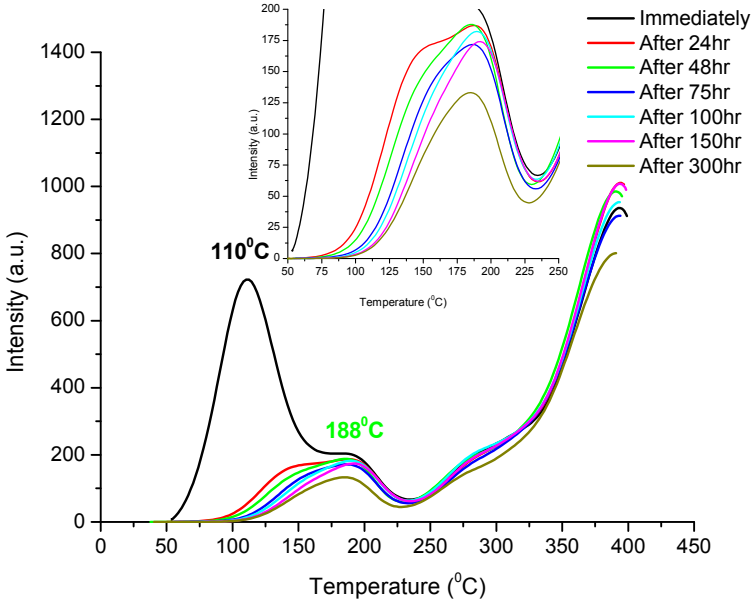

Fig. 5.35 TL glow curve recorded at different time after the exposure of Sr-90 to the as received sample Z22.

The TL glow curve shows the TL peak at 110^0C with a hump around 188^0C. Intensity of the peak at 110^0C reduced by 75% of its original intensity after 24hr time of storage. After 24hr, there is a broad TL peak observed in place of a hump, because of the fall down of peak at 110^0C. After exposure to beta dose, TL peak temperature and intensity on different times are listed in the table 5.18.

Table: 5.18

S.No.	Time of Storage after Irradiation (hrs)	TL Peak Temperature (^{0}C)	TL Peak Intensity (A.U.)
1	Immediately	110, 188	723, 193
2	24	188	187
3	48	188	184
4	75	188	180
5	100	189	170
6	150	187	160
7	300	185	140

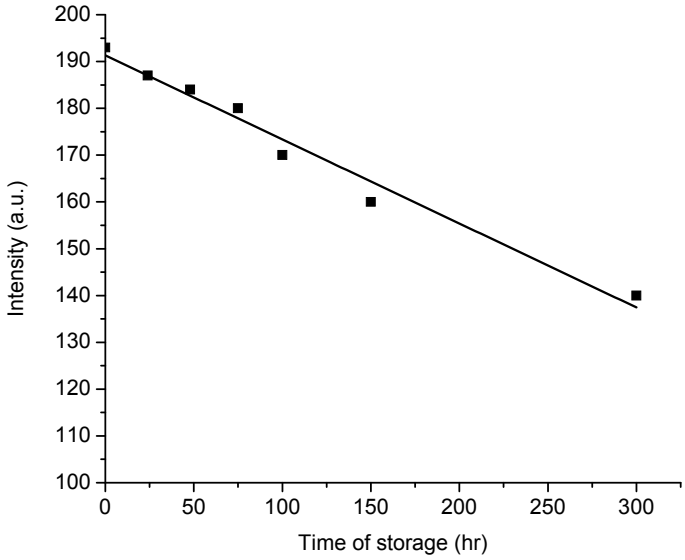

Fig. 5.36 shows the TL Decay with the time of storage in the as received sample z22. From the above figure it is clear that the intensity of hump gradually decreases.

References

1. W.L. Medlin, J. Opt. Soc. Am. 53 (1963) 1276.
2. D. Lapraz, P. Iacconi, Phys. Stat. Sol. (a) 36 (1976) 603.
3. W.L. Medlin, in: D.J. McDougall (Ed.), Thermoluminescence of Geological Materials, Academic Press, New York, 1968, Chapter 4.
4. J.S. Down, R. Flower, J.A. Strain, P.D. Townsend, Nucl.Tracks Radiat. Meas. 10 (1985) 581.
5. T. Calderon, P-D. Townsend, P. Beneitez, J. GarciaGuinea, A. Millau, H.M. Rendell, A. Tookey, M. Urbina, R.A. Wood, Radiat. Meas. 26 (1996) 719.
6. B. Engin, O. Güven, F. Köksal, Appl. Radiat. Isotopes 51 (1999) 729.
7. A.D. Franklin, W.F. Hornyak, V. Pagonis, N. Kristianpoller, Nucl. Tracks Radiat. Meas. 17 (1990) 517.
8. W.L. Medlin, Phys. Rev. 122 (1961) 837.
9. W.L. Medlin, Phys. Rev. 123 (1961) 502.
10. V.P. Pagonis, E. Allman, A. Wooten, Radiat. Meas. 26 (1996) 265.
11. R. Visocekas, T. Ceva, C. Marti, F. Lefaucheux, M.C.Robert, Phys. Stat. Sol. (a) 35 (1976) 315.
12. http://www.findarticles.com.
13. H. Anderle, Detection of food irradiation with luminescence methods, Ph.D. Thesis, University of Vienna, 1997.
14. R. Coy-Yll, T. Calderon, M. Aguilar, Min. Petr. 39 (1988) 39.
15. P.D. Townsend, B.J. Luff, R.A. Wood, Radiat. Meas. 23 (1994) 433.
16. M.J. Aitken, Physics and Archaeology, Clarendon Press, Oxford, 1974, p. 119.
17. E. Mische, S.W.S. Mckeever, Radiat. Prot. Dosim. 29 (1989) 159.
18. V. Pagonis, C. Michael, Radiat. Meas. 23 (1994) 131.
19. P.A. Clark, R.H. Templer, Archaeometry 30 (1988)19.
20. K.V.R.Murthy, L.H.H.Prasad, T.R.Joshi –Thermoluminescence and it‘s Applications, Tata Mccrraw – Hill Publishing Company Limited New Delhi, 1992.
21. K.V.R.Murthy, V.Natarajan, M.D.Shastri - Lumilnscence & it ‘s Applications February, 2009.
22. R.Debnath, H.K.Kundu, M.D.Shastri, K.V.R.Murthy – Luminscence & it ‘s Applications February -21-2009.

23. K.Mahesh, P.S.Weng – C.Furetta – Thermmoluminescence, India Solids And It ‘s Application , 1971.
24. D.J.Mc Dougall – Thermoluminescence of Geological Materials, Academic press , London & New York , 1984.
25. Thermoluminescence, Basic Theory & Applications -K.V.R.Murty, J.N.Reddy. Feb, 2008.
26. A.V.Sankaran, K.S.V.Nambi & C.M.Sunta– progress of Thermonluminescence reasearch on Geological Materials – 7th September, 1982.
27. Amin Y.M, Bull R.K. & Durrani S.A. (1982) Effect of radiation damage on T.L properties of crystals, Third specialities Meeting on T.L & ESR dating, Helslinger Counc, Eur, PACt J,9 159.
28. J.P Patel, G.H. Upadhayay – Material Science , Atul Parakashan, 20007.
29. Material Science – S.L Kakani – New Age Int. Pub. 2006.
30. Saxena Gupta saxena – Solid State Physics – 1985.
31. H.V. Keer – Sollid State Physics – Wiley Eastern Ltd. 1993.
32. Azaroff – Introduction to Solid ,1977
33. Mckeever S.W.S, “Thermoluminescence in solids”, Cambridge University Press, Cambridge, 1985.
34. M.J.Aitken – Thermoluminescence Dating ,1985.
35. J.F. Lima, P. Trzesniak, E.M. Yoshimura, E. Okuno, Radiat. Prot. Dosimet. 33 (1990) 143.
36. B. Engin, D. Güven, Radiat. Meas. 32 (2000) 253.
37. J.F. Lima, M.E.G. Valerio, E. Okuno, Phys. Rev. B 64 (2001) 014105.
38. K. Koike, M. Nakagawa, C. Koike, M. Okada, H.Chihara, A. and A. 390 (2002) 1133.

Chapter # 6

Conclusions

Conclusions

From the results and discussions of Chapter-IV and V the following conclusions are drawn.

1. The dolomite mineral Z03 did not shown much TLD characteristics even though the TL growth and decay are in good agreement for better TLD. Only disadvantage is TL peak intensity which is around 50 units when 25Gy beta dose was given.

2. The TL study of mineral dolomite sample Z03 treated with 800^0C and irradiated with beta source given a dose of 25Gy by Sr-90, did not give considerable TL peak which in turn can be considered for TL dosimetry. Therefore the Z03 sample can not be considered in any form as TLD material.

3. The dolomite mineral Z13 did show good TL with two isolated, well resolved with high intensity at 164 and 269^{o}C. The TL growth and decay are well acceptable for TLD application. This natural mineral dolomite Z13 is a good TL dosimeter for accidental dosimeter in natural form.

4. The Z15 however is a good TLD material in natural form, when annealed and quenched from 800^{o}C, its TL pattern entirely changed, no high intensity peak as well as resolved one are found Fig.5.25 and 5.27. Therefore the dolomite mineral Z15 when annealed and quenched from 800^{o}C can not be considered as TLD material in any application.

5. The natural dolomite mineral Z16 did t show good TLD characteristics with high TL intensity and two well resolved peaks at 150 and 278^{o}C. These two peaks are well resolved with high intensity leads us to study for TLD characteristics. The growth and decay are in good agreement for better TLD. This natural mineral dolomite Z15 is a good TL dosimeter for accidental dosimeter in natural form.

6. The Z16 however is a good TLD material in natural form, when annealed and quenched from 800^{o}C, its TL pattern entirely changed, no high intensity peak as well as resolved one are found Fig.5.31 and 5.33 Therefore the dolomite mineral Z16 when annealed and quenched from 800^{o}C can not be considered as TLD material in any application. Therefore the Z16 sample can not be considered in any form as TLD material.

7. The natural dolomite mineral Z17 did t show good TLD characteristics with high TL intensity and two well resolved peaks at 150 and 281^{o}C. These two peaks are well resolved with high intensity leads us to study for TLD characteristics. The growth and decay are in good agreement for better TLD. This natural mineral dolomite Z17 is a good TL dosimeter for accidental dosimeter in natural form.

8. The Z17 however is a good TLD material in natural form, when annealed and quenched from 800^{o}C, its TL pattern entirely changed, no high intensity peak as well as resolved one are found Fig.5.32, however a mixed TL peak with intensity at 296^{o}C was studied for TLD applications. Therefore the dolomite mineral Z17 when annealed and quenched from 800^{o}C the displayed TL peak with intensity at 296^{o}C can be considered as TLD material in any application. Therefore the Z17sample when annealed and quenched from 800^{o}C can be considered in any form as TLD material for environmental as well as accidental applications.

9. Fig. 5.35 is the TL of feldspar mineral in as received form. The TL peak for 25Gy beta dose generates a well isolated and resolved TL peak at 110^{o}C with a hum at 188^{o}C. When stored for 24hours and above the 110^{o}C peak disappeared and mixed peaks are generated. Therefore this mineral can not be considered as TLD material.

Therefore the mineral dolomite Z13, Z16 and Z17 can be considered as TLD material in environmental as well as accidental applications as TL dosimeter for high dose.

Scope for the further study

1. The systematic study of above studied minerals from various mine can be studied for TL dosimetry.

2. The TL dosimetry of all the dolomite minerals used in industries can be studied by irradiating with gama source for various dose ranges.
3. The same can be repeated with Cyclotron radiation (X ray , UV radiation ,γ-radiation etc..)
4. The chemical analysis using ICP-AES can give better understanding of the minerals and their impurities. This study may help in co-relating the TL output.

List of Research Papers Presented In Seminar/Conference/Workshop/Symposium from 2008 on words

Sr. No.	Title Of Conference/ Seminar	Sponsoring Agency	Title of Paper
1	International conference on Luminescence and its applications 13th to16th Feb, 2008	National physical Laboratory , New Delhi And Luminescence society of India	Attended
2	National conference on Luminescence and its applications CGCRI, Kolkata 19th to 21st Feb, 2009.	Indian association of cultivation of science and Luminescence society of India	Thermoluminescence study of natural minerals used in ceramic tiles industries
3	Fifth national conference on thermo physical properties (NCTP-09) 7th to 9th Oct, 2009.	Applied Physics Department M.S. University of Baroda Baroda.	Thermoluminescence properties of natural dolomite
4	Fifth national conference on thermo physical properties (NCTP-09) 7th to 9th Oct, 2009.	Applied Physics Department M.S. University of Baroda Baroda	Kinetic and trapping parameters of 200^0C TL Dosimetric peak in Kcl:Ba(T)
5	State level seminar on current trends in Physics &Industrial applications 17th Jan, 2010.	M.M. Science College, Morbi, Gujarat	Thermoluminescence properties of natural dolomite

6.	State level seminar on current trends in Physics &Industrial applications 17th Jan, 2010.	M.M. Science College, Morbi, Gujarat	Thermoluminescence characteristics of natural minerals used in ceramic tiles industries
7.	State level seminar on Current Research Areas in Physics and it's applications 5th January, 2011	UGC and Shri C.N.P.F. Arts & D.N. Science College, Dabhoi	Thermoluminescence study of Natural dolomite mineral
8	National conference on Luminescence and its applications 7-9th Feb, 2011.	Physics Department Pt RS University Raipur	Thermoluminescence Studies of Natural Dolomite
9.	4th International conference on luminescence and its Applications. IICT, Hyderabad. 7th to 10th February, 2012.	Rajiv Gandhi University of Knowledge and Technologies, Luminescence Society of India.	Thermoluminescence dosimetry of dolomite mineral

List of Publications in Journal and Proceeding

Sr..No.	Title of the Paper	Name of the Journal	Remark
1.	Thermoluminescence characteristics of natural mineral used in ceramic tiles industries	NCLA-2009 Proceeding.	Published
2.	Thermoluminescence dosimetry of dolomite mineral	ICLA-2012 Proceeding. ISBN: 81-6717-806-5	Published
3.	Thermoluminescence Studies of Natural Dolomite	International Journal Luminescence and Applications ISSNo.2277-6362	Accepted for publication